

Roslan, Rosazra (2014) *Mechanisms of increased arrhythmogenic risk associated with acute regional ischaemia in rabbit: An optical mapping study*. PhD thesis.

<http://theses.gla.ac.uk/5484/>

Copyright and moral rights for this thesis are retained by the author

A copy can be downloaded for personal non-commercial research or study, without prior permission or charge

This thesis cannot be reproduced or quoted extensively from without first obtaining permission in writing from the Author

The content must not be changed in any way or sold commercially in any format or medium without the formal permission of the Author

When referring to this work, full bibliographic details including the author, title, awarding institution and date of the thesis must be given

Mechanisms of increased arrhythmogenic risk
associated with acute regional ischaemia in rabbit:
An optical mapping study

by

Rosazra Roslan

(MBBS, Malaysia)

Submitted in fulfilment of the requirements for the
Degree of Doctor of Philosophy

to

Institute of Cardiovascular & Medical Sciences
College of Medical, Veterinary and Life Sciences
University of Glasgow

August 2014

Abstract

Acute coronary artery occlusion is the most common cause of sudden cardiac death. In some cases an acute myocardial infarction (MI) can immediately lead to lethal arrhythmias, but the factors that determine whether an MI precipitates arrhythmias are uncertain. In this thesis, I compare and contrast the detailed electrophysiology of hearts that develop arrhythmias post MI compared to those that do not using voltage sensitive fluorescent dyes in isolated rabbit hearts.

In an attempt to improve the information from voltage mapping studies, initial work involved attempts to use ratiometric imaging of the fluorescence from the dye RH237. These identified optimal filter settings to collect voltage data at two distinct wavebands that would eliminate movement artefact and permit absolute voltage measurements. But routine implementation of this technique was prevented by additional technical issues related to uneven illumination levels and alignment of the two cameras.

In initial studies the drug E-4031, a selective blocker of the delayed rectifier potassium current (I_{Kr}), was used to assess the contribution of this channel to repolarisation in rabbit ventricle, both in the steady state at a range of physiological and sub-physiological frequencies and in the transition between step frequency changes. The data suggests that I_{Kr} has a small but significant contribution to repolarisation at normal heart rates, 300ms pacing cycle length; a close to maximal concentration of E-4031 ($0.03\mu\text{M}$) increased action potential duration (APD_{90}) by $8.5 \pm 1.7\text{ms}$ ($P<0.01$). This contribution is considerably larger at lower stimulation frequencies; at 1Hz E-4031 increased APD by $73.7 \pm 13.7\text{ms}$ ($P<0.05$). The EC_{50} for E-4031 in this study was $0.01\mu\text{M}$ which is similar to that reported in the literature. The recovery of the channel from inactivation appeared an important determinant of the rate of adaptation of the action potential duration.

In the main experimental section, a novel snare technique was used to produce the acute coronary artery occlusion in the apical region of the left ventricle (LV) free wall. From control experiments ($n=21$), 47.6% of the hearts develop ventricular fibrillation (VF) within 30 minutes of coronary artery occlusion. On average, hearts with intrinsically longer epicardial action potential duration

prior to ischaemia (mean APD₅₀ 168.8 ± 5.5ms) did not develop VF, and those with shorter APD (mean APD₅₀ 141.5 ± 3.5ms) during pre-occlusion period were more prone to VF ($P<0.001$). However, artificially prolonging the APD with the drug E-4031 (0.03μM concentration) prior to coronary artery occlusion did not significantly change the incidence of arrhythmia. Brief and transient exposure to isoprenaline (0.3μM concentration) before the occlusion shortened the average APD prior to occlusion but still did not increase the likelihood of VF. Therefore, I concluded that shorter epicardial APD values prior to ischaemia are associated with a higher incidence of arrhythmia but are not the cause.

To investigate this further, a panoramic optical mapping technique was used to look at the electrophysiological properties across the entire ventricular surface of the hearts. The panoramic optical mapping study confirmed the correlation between shorter APD pre-occlusion and the incidence of VF during occlusion and indicated that the region of the LV exhibiting a shorter APD is confined to the apical half of the LV, and does not include basal LV or RV electrophysiology. Panoramic imaging also revealed a delayed activation time predominantly in the basal aspects of the LV. Both of these events - shorter APD in the apex and longer activation time in the base - were a feature of hearts that developed VF on ligation of the coronary artery. Future work will investigate the cellular/molecular basis for these differences in ventricular electrophysiology.

Table of Contents

Abstract	2
List of Tables	9
List of Figures	10
Acknowledgements	13
Author's declaration	15
Abbreviations	16
Chapter 1: Introduction	20
Aim	21
Cardiac electrophysiology	21
Cardiac action potential	21
Spatial dispersion of APD	23
Refractory period	24
Electrical restitution	26
Electrophysiological changes in regional myocardial ischaemia	27
Electrocardiogram (ECG)	27
ECG in the normal heart	27
ECG in myocardial ischaemia and infarction	29
Animal models of myocardial ischaemia	30
Rabbit model of myocardial ischaemia and infarction	31
Sudden cardiac death	33
Acute myocardial ischaemia and infarction	33
Classification	34
Metabolic consequences of myocardial ischaemia and mechanisms of ischaemia-related arrhythmias	35
Cardiac arrhythmias	37
Mechanisms of ventricular arrhythmias	37
Automaticity	37
Triggered activity	38
Re-entry	38
Premature ventricular contractions (PVCs)	40
T-wave alternans (TWA)	40
Ischaemia-induced ventricular fibrillation	41
Study aims	42
Hypothesis	42
Chapter 2: Methods	43
Introduction	44
Voltage-sensitive dyes	45
Optical mapping set-up	48
Single view optical mapping	48
Panoramic view optical mapping	50
Work involving animals	50
The rabbit coronary artery occlusion during Langendorff perfusion	50
Coronary artery occlusion by using ligation technique	50
Horizontal ligation set-up	53
Vertical ligation set-up	53
Pacing protocols	54
Ventricular pacing (VPACE)	54
Atrial pacing (APACE)	54
Optical data	55
Optical action potentials (OAPs)	55
Optical data analysis	56

ECG data	57
ECG signals recording	57
ECG data analysis	58
Statistical analysis	61
Chapter 3: Use of ratiometric approach to examine membrane potential signals with voltage-sensitive dye	62
Aim	63
Introduction	63
Methods	65
Heart preparation	65
Ratiometric fluorescence emission recording	65
Optical mapping set-up	65
Experimental protocols	66
Background signals recording	66
Signals recording after dye loading	66
Hyperkalaemic induction	67
Coronary artery ligation	67
Spectrophotometry	67
Data analysis	68
Experimental results	70
Spectrophotometric measurement	70
Filter set 1 and Filter set 2	72
Dual-emission wavelength ratiometric measurement	74
Acute regional ischaemia (filter set 1)	74
Hyperkalaemic challenge	77
Simulation of optical action potential	80
1) Ratio value is sensitive to illumination levels	82
2) Ratio AP produces reliable shape even at large movement	84
3) Camera alignment is important for accurate AP shape	86
Discussion	88
Chapter 4: Single view optical mapping - Effect of E-4031 on action potential duration	90
Aim	91
Introduction	91
Methods	92
Preparation of the rabbit hearts	92
Atrioventricular (AV) node ablation	92
Electrophysiological recording and analysis	93
E-4031 drug	93
Pacing protocol	94
Continuous pacing at 500ms cycle length	94
Abrupt rate changes 500ms→300ms→500ms cycle length	94
Range of cycle lengths: 1000ms, 800ms, 700ms, 600ms, 500ms, 400ms, 300ms and 200ms	94
Continuous pacing at 500ms cycle length	94
Electrocardiogram (ECG)	95
Optical data analysis	95
Results	97
Effect of different concentrations of E-4031 on APD ₉₀	97
APD adaptation during rate changes	101
Rate-dependent property of E-4031	103
T-wave alternans (TWA), early afterdepolarisations (EADs) and ventricular tachycardia (VT)	105

Discussion	109
Role of I_{Kr} in repolarisation, rate dependence of APD and adaptation.....	109
E-4031 dose-dependence on isolated channel and whole heart.....	110
E-4031 on adaptation	111
E-4031 and alternans (role of I_{Kr})	111
Early afterdepolarisations (EADs).....	112
Conclusion	112
Chapter 5: Single view optical mapping - Acute regional ischaemia in isolated rabbit hearts	113
Aim.....	114
Introduction	114
Methods	115
Preparation of the rabbit hearts for coronary artery occlusion	115
Experimental protocols.....	116
Dye loading	116
Pre-occlusion	116
Coronary artery occlusion	116
Reperfusion	117
Optical data analysis.....	117
Results.....	118
Incidence.....	118
Premature ventricular contractions (PVCs) and T-wave alternans (TWA) ..	120
Effect of coronary artery occlusion	121
APD ₅₀ (no-VF vs. VF groups).....	124
Activation time (no-VF vs. VF groups)	129
APD ₅₀ vs. heart rate	130
ECG parameters.....	131
Is the behaviour of the epicardial sites homogeneous in terms of APD ₅₀ (no-VF vs. VF groups)	134
Behaviour pre-occlusion	134
Behaviour on occlusion	134
Discussion	137
Shorter APD prior to occlusion predicts tendency to VF.....	137
Decreased APD equates to shorter QT interval.....	138
VF is associated with decreased APD and increased variability of APD.	140
Is there a correlation with area of myocardium that undergoes ischaemic changes in APD?	140
Conclusion	141
Chapter 6: Single view optical mapping during acute regional ischaemia after pharmacological manipulation of action potential duration	142
Part 1: E-4031 experiments.....	144
Experimental protocol	144
Dye loading	144
Pre-occlusion	144
Coronary artery occlusion	145
Reperfusion	145
E-4031 drug.....	145
Results	146
Incidence	146
Effect of coronary artery occlusion.....	146
APD ₅₀ (no-VF vs. VF groups)	147
APD ₅₀ changes (no-VF vs. VF groups)	150
T-wave alternans and EADs	152

Part 2: Isoprenaline experiments	155
Experimental protocol	155
AV node ablation	155
Pacing protocol	155
Dye loading	156
Pre-occlusion	156
Coronary artery occlusion	156
Reperfusion	156
Isoprenaline drug	157
Results	158
Incidence	158
APD ₅₀	158
Discussion	161
Effects of E-4031	161
Effects of transient isoprenaline treatment	163
Conclusion	165
Chapter 7: ECG simulation	166
Aim	167
Introduction	167
ECG during coronary artery occlusion	167
Modelling of ECG	167
Methods	168
Experimental ECG measurement	168
ECGSim software	168
Results	171
Experimental ECG	171
Simulation of ECG	174
Anterior infarction (Site 1)	174
Postero-lateral infarction (Site 2)	177
Discussion	180
Conclusion	181
Chapter 8: Acute coronary artery occlusion - panoramic view optical mapping study	182
Aim:	183
Introduction	183
Methods	184
Preparation of the rabbit hearts	184
Panoramic view optical mapping	184
Rotating chamber	186
Coronary artery occlusion using vertical ligation system	187
Experimental protocol	188
Electrocardiogram (ECG)	189
Optical data analysis	190
Optiq	190
GGobi	192
Results	193
Incidence	193
Electrophysiological parameters	193
APD ₅₀	195
TActM	202
QRS timing in relation to epicardial activation	203
ECG	205
Discussion	207

Correlation of optical signals with phases of the ECG	208
Is the shorter APD in the LV apex an artefact of the experimental procedure?	208
Physiological basis for shorter APD in LV apex	209
Chapter 9: <i>In vivo</i> coronary artery ligation in rabbit - ECG measurements.....	210
Aim	211
Introduction	211
Methods	212
Left coronary artery ligation	212
ECG monitoring and recording	213
ECG analysis	214
Statistical analysis	216
Results.....	217
Discussion	220
Chapter 10: Discussion	222
General discussion	223
Future work	225

List of Tables

Table 1.1 Summary of ECG components.	29
Table 3.1 Dual-wavelength ratiometric values with filter set 2.	79
Table 3.2 Effect of varying illumination level on ratio AP.	83
Table 4.1 Effect of different E-4031 concentrations on rabbit ventricular APD.	99
Table 4.2 T-wave alternans, EADs, and VT.	106
Table 5.1 APD ₅₀ at <i>Pre-occlusion 10min</i> and <i>Pre-occlusion 30min</i>	126
Table 5.2 APD ₅₀ before and during occlusion.	127
Table 5.3 ECG parameters at <i>Pre-occlusion 30min</i>	133
Table 6.1 APD ₅₀ (no-VF vs. VF groups).	150
Table 6.2 Incidence of EADs and TWA.	154
Table 6.3 APD ₅₀ before and after exposure to isoprenaline.	160
Table 6.4 Behaviour of APD ₅₀ prior to coronary artery occlusion.	163
Table 9.1 Beat to beat variation in ECG parameters.	218
Table 9.2 ECG parameters (no-VF vs. VF groups).	218

List of Figures

Figure 1.1 Rabbit ventricular action potential.....	22
Figure 1.2 Spatial dispersion of APD from single cardiac myocytes.	24
Figure 1.3 Restitution curve.....	26
Figure 1.4 Cardiac ventricular AP and ECG in the normal heart.....	28
Figure 1.5 Branching pattern in rabbit coronary artery.	32
Figure 2.1 Voltage-sensitive dyes.	46
Figure 2.2 Spectra of voltage-sensitive dyes used in optical mapping study.	47
Figure 2.3 Diagram of single view optical mapping set-up.	49
Figure 2.4 Photographs of the heart inside the perspex chamber.	49
Figure 2.5 Method to produce acute local ischaemia in isolated rabbit hearts. .	52
Figure 2.6 Definition of TActM, TRepol and APD	57
Figure 2.7 ECG analysis.	59
Figure 2.8 PVCs and TWA	60
Figure 3.1 Voltage-dependent spectral shift.	64
Figure 3.2 Schematic diagram of optical mapping set-up.	65
Figure 3.3 Example of display from Ratio Explorer programme.	69
Figure 3.4 Excitation and emission spectra (filter set 1).	70
Figure 3.5 Excitation and emission spectra (filter set 2).	71
Figure 3.6 Example of signals recording with filter set 1.	72
Figure 3.7 Example of signal recording with filter set 2.	73
Figure 3.8 Fluorescence signal pre-occlusion.	75
Figure 3.9 Fluorescence signal at 10 minutes occlusion.	76
Figure 3.10 Hyperkalaemic induction.	78
Figure 3.11 Fluorescence signal during hyperkalaemic induction.	79
Figure 3.12 SimulateOAP.....	81
Figure 3.13 Effect of varying illumination level on ratio AP.	83
Figure 3.14 Sinusoidal movement trajectories on heart surface.	84
Figure 3.15 Effect of heart movement on ratio AP.	85
Figure 3.16 Effect of camera misalignment and heart movement on ratio AP...	87
Figure 4.1 E-4031 structure.	93
Figure 4.2 Optical data analysis.	96
Figure 4.3 Optical data.	96
Figure 4.4 Full protocol time course at 0.3 μ M E-4031 concentration.	98
Figure 4.5 Effect of E-4031 on action potential.	99
Figure 4.6 Dose-response curve for 4 different concentrations of E-4031.	100
Figure 4.7 APD adaptation during rate changes.	102
Figure 4.8 Mean time constant during abrupt rate changes at 0.03 μ M E-4031 .	103
Figure 4.9 Reverse rate-dependent effect of E-4031.	104
Figure 4.10 EADs and VT in the presence of 0.01 μ M E-4031.....	107
Figure 4.11 EADs and alternans in the presence of 0.03 μ M E-4031.	108
Figure 5.1 Acute regional ischaemia.....	115
Figure 5.2 Experimental protocol for control experiments.....	116
Figure 5.3 Optical data analysis in OPTIQ software.....	117
Figure 5.4 Incidence of VF during acute coronary artery occlusion.....	119
Figure 5.5 PVCs and TWA.	120
Figure 5.6 Effect of coronary artery occlusion.....	122

Figure 5.7 Full protocol time course.....	123
Figure 5.8 APD ₅₀ (no-VF vs. VF groups)	124
Figure 5.9 APD ₅₀ at pre-occlusion period.	125
Figure 5.10 APD ₅₀ before and during occlusion.	126
Figure 5.11 Range of APD ₅₀ before and during occlusion.....	128
Figure 5.12 Activation time before and during occlusion.	129
Figure 5.13 APD ₅₀ vs. heart rate.....	130
Figure 5.14 ECG parameters at <i>Pre-occlusion 30min</i>	132
Figure 5.15 Behaviour of APD ₅₀ on epicardial surface pre-occlusion and during occlusion.	135
Figure 5.16 Absolute shortening of APD ₅₀	136
Figure 6.1 Experimental protocol for E-4031 experiments.	144
Figure 6.2 Incidence of VF during coronary artery occlusion.	146
Figure 6.3 Example of full protocol time course during E-4031 experiment. ...	147
Figure 6.4 APD ₅₀ prior to coronary artery occlusion.	148
Figure 6.5 Effect of E-4031 on APD ₅₀	149
Figure 6.6 Changes in APD ₅₀ before and during occlusion.	151
Figure 6.7 EADs and TWA in heart that developed VF.	153
Figure 6.8 EADs and TWA in heart that did not go into VF.	154
Figure 6.9 Experimental protocol for experiments with 0.3 μ M isoprenaline. ...	155
Figure 6.10 Chemical structure of isoprenaline	157
Figure 6.11 Incidence of no-VF and VF during isoprenaline experiments.	158
Figure 6.12 Full protocol time course for isoprenaline experiment.....	159
Figure 6.13 APD ₅₀ before and after exposure to isoprenaline.....	160
Figure 6.14 Incidence of no-VF and VF in control and E-4031 experiments. ...	161
Figure 6.15 APD ₅₀ in control experiments and E-4031 experiments.....	162
Figure 6.16 APD ₅₀ in control experiments vs. isoprenaline experiments.	164
Figure 7.1 Example of ECGSim display.	169
Figure 7.2 ECG from VF heart.....	172
Figure 7.3 ECG from no-VF heart.....	173
Figure 7.4 Simulation of normal AP at site 1 (indicated by black arrow).	175
Figure 7.5 Simulation of varying severity of infarction.....	176
Figure 7.6 Simulation at site 2.....	178
Figure 7.7 Simulation of varying severity of infarction.....	179
Figure 8.1 Schematic diagram of panoramic optical mapping setup.....	185
Figure 8.2 Images from three different heart surfaces.	185
Figure 8.3 Rotating chamber.	186
Figure 8.4 Vertical ligation set-up.	188
Figure 8.5 Experimental protocol.	189
Figure 8.6 Example of ECG recording with corresponding APs.	189
Figure 8.7 Idealised model of the surface of the heart based on a semi-prolate ellipsoid.....	191
Figure 8.8 Application of exclusion criteria.	191
Figure 8.9 GGobi software display.	192
Figure 8.10 Incidence of VF in panoramic view experiments.	193
Figure 8.11 APD ₅₀ and TActM.....	194
Figure 8.12 APD ₅₀ from three different surfaces of the heart.	196
Figure 8.13 Apex-base difference in APD.	196
Figure 8.14 Range of APD ₅₀ from three different heart surfaces.	197
Figure 8.15 APD ₅₀ prior to coronary artery occlusion.	198

Figure 8.16 Distribution of APD across the heart surface.	199
Figure 8.17 APD ₅₀ distribution during <i>Occlusion 10min</i> (no-VF vs. VF hearts)...	201
Figure 8.18 Activation time pre-occlusion.	202
Figure 8.19 Apex-base difference in activation time.	203
Figure 8.20 QRS timing in relation to epicardial activation.	204
Figure 8.21 ECG from panoramic view optical mapping experiments.	206
Figure 9.1 <i>In vivo</i> ECG data.	213
Figure 9.2 ECG analysis using Chart TM 5 Pro software.	215
Figure 9.3 ECG parameters.	216
Figure 9.4 Incidence of no-VF and VF in <i>in vivo</i> study.....	217
Figure 9.5 Graph showing the relation between RR interval and QT interval. ..	219

Acknowledgements

In the name of ALLAH, the Most Compassionate, the Most Merciful. My thanks and gratitude belong to ALLAH the Lord of all mankind, I ask ALLAH to bless and bestow peace on Prophet Muhammad (SAW), the companions and the messengers, and all who traverse their path.

All the praises and thanks be to ALLAH, for enabling me to continue my PhD journey despite all challenges that I endured throughout the journey. This journey was indeed full of blood, sweat and tears. He instilled high spirit in me and a never ending self-motivation to finish what I started 4 years ago.

First and foremost, I would like to express my heartfelt gratitude and my special thanks to both of my supervisors, Dr Francis L. Burton and Professor Godfrey L. Smith for their guidance, valuable advice, encouragement and a never-ending support throughout my study. I have been very fortunate to have them as my supervisors who always been there in the most beneficial ways. I am very grateful for their patience and commitment and I feel so blessed and honoured to be one of their students.

My special acknowledgement goes to my employer, International Islamic University of Malaysia, in general, and to my Head of Department and Dean of Kulliyyah of Pharmacy, in particular, for approving my study leave and allowing me to pursue my PhD in University of Glasgow together with the financial support, and not to forget my sincere appreciation to Ministry of Education (MoE) Malaysia for the scholarships awarded to fund my study.

My particular thanks to Mrs Aileen Rankin and Mr Michael Dunne for all technical assistances and guidance in the lab. I would also like to acknowledge Mr Andrew Allan for always being there assisting me throughout the panoramic experiments and for giving his technical advice whenever I need help. These special thanks also goes to my lab mate Dr Iffath Ghouri for always being there whenever I need help and for sharing the happy and sad moments together throughout my stay. Not to forget all other lab members; I will definitely miss the time spent in

the lab together and thank you for making it a fun and pleasurable time in the lab.

I would like to convey my heartfelt thanks to my 'big happy family' in Glasgow, Dundee and the United Kingdom elsewhere for their supports, prayers, wonderful friendship and encouragement. Even though I have been far away from my family for the past few years, their presence makes me feel like home. Not to forget, my sincere thanks to my friends and relatives in Malaysia who are always there and giving thought in their prayers for my successful journey.

My wholehearted love and gratitude goes to my beloved mother, Zainab Bt Ab. Majid for her continuous love and prayers, my father, Roslan Bin Saad, my two supportive brothers, Dr Mohd Azrik Bin Roslan and Muhammad Azril Bin Roslan, and my sister-in law, Aadawiyah Bt Abd Razak for their endless love, encouragement, supports and prayers. My special love to my niece, Nurul Iman Bt Mohd Azrik who was born in Glasgow during my third year of PhD; your presence fills my life with joy and love. The same goes to my sister- and brothers in-laws for their love and supports. This accomplishment would not have been possible without them. Special acknowledgement to my late father in-law who passed away during my final year, may ALLAH bless his soul and admit him in Paradise along with the righteous. Ameen.

This thesis is dedicated wholeheartedly to my beloved husband, Dr Che Anuar Bin Che Mohamad who is always being there on my side, day and night despite his busy schedule as a PhD student as well. I am beyond grateful for my amazing husband for taking care of me when I was sick, for giving me hope when I was down, who laugh and cry with me during happy and sad moments. You are a blessing in my life. Thank you so much for being my husband and my best friend.

Last but not least, to all those who have significantly contributed towards the completion of this thesis, directly or indirectly; even though I could not mention each and everyone names here, I am truly grateful to all.

Author's declaration

The coronary artery ligation on rabbit (for *in vivo* ECG study) was carried out by Mr Michael Dunne at the Glasgow Cardiovascular Research Centre (GCRC). All the experimental works contained in this thesis was undertaken by me. Dr Francis Burton assisted in all the single-view optical mapping experiments and Mr Andrew Allan has assisted in all the panoramic view optical mapping experiments. The removal of the heart from the rabbit was carried out by Dr Francis Burton and Mrs Aileen Rankin. The material has not been submitted previously for any other degree.

Abbreviations

AP	Action potential
APACE	Atrial pacing
APD	Action potential duration
APD ₅₀	Action potential duration at 50% repolarisation
APD ₉₀	Action potential duration at 90% repolarisation
ARP	Absolute refractory period
ATP	Adenosine triphosphate
AV	Atrioventricular
Ca ²⁺	Calcium
Ca ²⁺ _i	Intracellular calcium
CHD	Coronary heart disease
DADs	Delayed afterdepolarisations
DI	Diastolic interval
DMSO	Dimethyl sulfoxide
EADs	Early afterdepolarisations
ECG	Electrocardiogram
ERP	Effective refractory period
hERG	Human ether-a-go-go related gene

$I_{Ca,L}$	L-type calcium current
$I_{Ca,T}$	T-type calcium current
$I_{Cl(Ca)}$	Calcium-activated chloride current
I_f	Pacemaker current
I_K	Delayed rectifier potassium current
I_{KATP}	ATP-sensitive potassium current
I_{Kr}	Rapid delayed rectifier potassium current
I_{Ks}	Slow delayed rectifier potassium current
I_{Kur}	Ultra rapid delayed rectifier potassium current
I_{K1}	Inward rectifier potassium current
I_{Na}	Sodium current
I_{NCX}	Sodium-calcium exchanger current
I_{to}	Transient outward current
IU	International unit
KCl	Potassium chloride
LED	Light-emitting diode
LP	Long-pass
LQTS	Long QT syndrome
MI	Myocardial infarction

mV	Millivolts
NA	Numerical aperture
Na ⁺	Sodium
NCX	Sodium/calcium exchanger
OAPs	Optical action potentials
PDA	Photodiode array
pO ₂	Partial pressure of oxygen in the blood
PVCs	Premature ventricular contractions
pVT	Polymorphic ventricular tachycardia
RRP	Relative refractory period
SA	Sinoatrial
SCD	Sudden cardiac death
SEM	Standard error of the mean
SR	Sarcoplasmic reticulum
SQTS	Short QT syndrome
TActM	Activation time (from pacing stimulus to the midpoint of the upstroke of the action potential)
TdP	Torsade de Pointes
TWA	T-wave alternans
VF	Ventricular fibrillation

V _m	Transmembrane potential
VPACE	Ventricular pacing
VPBs	Ventricular premature beats
VSDs	Voltage-sensitive dyes
VT	Ventricular tachycardia
[Ca ²⁺] _o	Extracellular calcium concentration
[K ⁺] _o	Extracellular potassium concentration
[Mg ²⁺] _o	Extracellular magnesium concentration

Chapter 1: Introduction

Aim

The aim of this introduction is to describe basic cardiac electrophysiology and the changes that occur during acute myocardial ischaemia, to provide a general overview of the phenomena of sudden cardiac death related to ventricular fibrillation associated with acute myocardial ischaemia, and to summarize the mechanisms of ventricular arrhythmias which lead to sudden cardiac death.

Cardiac electrophysiology

Cardiac action potential

The cardiac action potential (AP) is a dynamic and phasic change in membrane potential generated by ionic gradients and tightly orchestrated sequence of opening and closing of ion channels. The two general types of cardiac action potential are non-pacemaker and pacemaker action potentials. The non-pacemaker action potential is generated in atrial, ventricular and Purkinje myocytes and the event is triggered by depolarisation of the adjacent connected cells. These action potentials have a stable resting potential, a fast depolarisation phase, and a repolarisation phase as shown in Figure 1.1. In contrast, the electrical activity of pacemaker cells, namely cardiomyocytes in the sinoatrial (SA) and atrioventricular (AV) nodes, display automaticity. In these cells, the diastolic membrane potential is not stable, continuously depolarising to a threshold for the activation of rapid depolarisation. The action potential from non-pacemaker cells is divided into five numbered phases (0 - 4, see Figure 1.1) and the underlying ionic currents responsible for these phases are summarized in Figure 1.1.

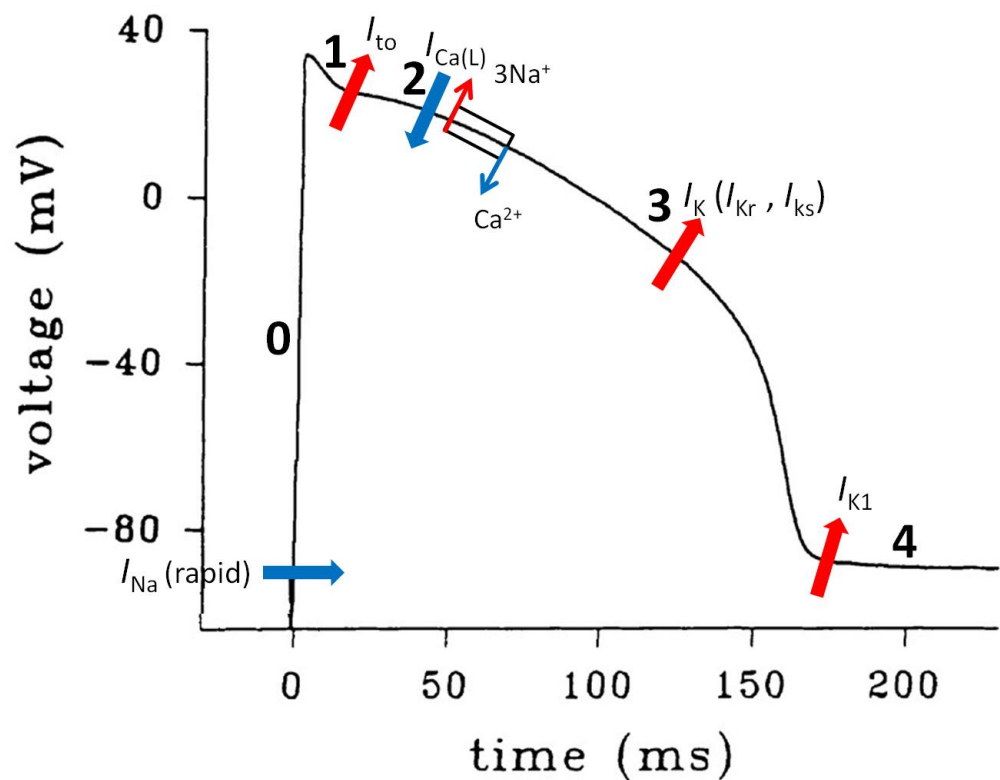


Figure 1.1 Rabbit ventricular action potential.

The number indicates different phases of AP. The arrows indicate the movement of ionic currents into the cell (blue arrows) or leaving the cell (red arrows) which contribute to the generation of AP.

Phase 0 is the rapid depolarisation phase caused by the activation of a fast Na^+ current (I_{Na}) exhibiting very rapid activation and inactivation kinetics. A threshold membrane voltage needs to be reached ($\sim -70mV$) before the fast Na^+ channel start to activate, during this phase the Na^+ conductance is the dominant membrane conductance and therefore the membrane potential is determined by the equilibrium potential for Na^+ ($\sim +30mV$). At these positive potentials, I_{Na} inactivation is accelerated and the Na^+ conductance quickly falls. As the membrane potential depolarises past $\sim -40mV$, inward Ca^{2+} currents are activated namely L-type ($I_{Ca,L}$) and T-type ($I_{Ca,T}$). These currents also inactivate at positive potentials.

Phase 1 is the initial repolarisation phase. This phase is largely due to the activation of a transient outward current (I_{to}) that is rapidly activated during depolarisation alongside the decrease in Na^+ and Ca^{2+} conductance associated with inactivation of I_{Na} and I_{Ca} .

Phase 2 is the plateau phase of the cardiac action potential and contributes to the stability of the action potential duration (APD). During this phase, there is an approximate balance between positive inward and outward currents. The primary inward current is the L-type Ca^{2+} current ($I_{\text{Ca,L}}$), whereas the primary outward current is the delayed rectifier potassium current (I_{K}). The $I_{\text{Ca,L}}$ is the primary link in excitation-contraction coupling in the heart. The influx of calcium ions stimulates calcium release from internal stores and activates the contractile proteins. The electrogenic $\text{Na}^+/\text{Ca}^{2+}$ exchanger (NCX) transiently works in reverse mode to bring the influx of Ca^{2+} into the cell and extract the Na^+ ($3 \text{ Na}^+ : 1 \text{ Ca}^{2+}$) thereby contributing to the net outward current during this plateau phase.

Phase 3 is the repolarisation phase. It is mainly caused by an imbalance of the currents involved in phase 2. $I_{\text{Ca,L}}$ decreases as the channels being inactivated, and I_{K} increases with time due to its slow activation and later becomes the dominant repolarising current. There are several components of I_{K} : a very slow component (I_{Ks}), a rapid component (I_{Kr}), and ultrarapid delayed rectifier K^+ current (I_{Kur}). However, I_{Kur} has only been identified in atrial cells in human (Feng *et al.*, 1998; Wang *et al.*, 1993). Studies show that these different components of I_{K} are carried by different channels (Nerbonne, 2000).

Phase 4 is resting membrane potential which is stable (approximately at -90 mV) that occurs in between AP in non-pacemaker cardiomyocytes. The stable potential during phase 4 is largely due to non-time-dependent background K^+ current termed the inward rectifier current (I_{K1}) which passes the current more readily in the inward direction as compared to the outward direction. This property ensures that when the membrane potential is approximately 0mV during the plateau phase, the outward current carried by I_{K1} is small and does not require large inward currents to maintain a semi-stable phase.

Spatial dispersion of APD

Studies have shown that there is marked heterogeneity in ventricular AP morphology both within and between species. APD is longer at the apex than at the base (Cheng *et al.*, 1999) and shorter in the epicardium as compared to the endocardium (Fedida and Giles, 1991). In larger mammals, the epicardial AP also

shows a distinctive “spike and dome” morphology thought to be due to I_{to} which is more abundant in the epicardium. Study by McIntosh *et al.* (2000) demonstrates that the APD from three different ventricular layers are not uniform (Figure 1.2).

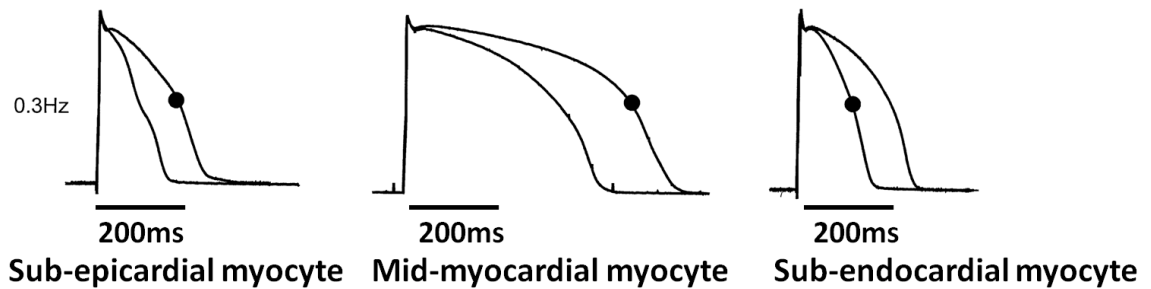


Figure 1.2 Spatial dispersion of APD from single cardiac myocytes.

Spatial dispersion of APD from single cardiac myocyte isolated from three different layers of left ventricle during stimulation at 0.3Hz. The morphology of the AP varies depending on its location. The effect of transmural infarct (•) also displayed in the figure. (Adapted from McIntosh *et al.* (2000))

As shown in Figure 1.2, a third AP type is sometimes seen in midwall of the mammalian ventricle, namely the “M-cell” which has a longer APD than either epicardial or endocardial cells. M-cells have been identified in a range of mammalian species including human, rabbit, guinea pig, canine and pig ventricles (Drouin *et al.*, 1995; McIntosh *et al.*, 2000; Sicouri *et al.*, 1996; Sicouri and Antzelevitch, 1991; Stankovicova *et al.*, 2000). The effect of these cells on the electrophysiology of the ventricle is uncertain (and controversial) since the marked APD prolongation observed in isolated cells is attenuated by the electrical network of cells within the ventricle wall (Yan and Antzelevitch, 1998).

Refractory period

The refractory period in cardiac myocytes can be divided into: 1) absolute refractory period (ARP), 2) relative refractory period (RRP), and 3) effective refractory period (ERP). The refractory period is an important feature of cardiac muscle because it ensures enough time elapses for the heart to fill between contractions before reactivation is possible. During the ARP, no action potential can be triggered regardless of how much inward current is supplied. In this

period, the myocardium is non-excitable because the Na^+ currents are inactivated. In the RRP, the Na^+ channels slowly recover during the final repolarisation of the cell. During this period, myocardial excitability is reduced, conduction is slower, AP amplitude is lower, and the threshold potential is shifted to less positive potentials requiring a greater stimulus. APs can be generated but not propagated during ERP.

Refractory period is a key concept in the understanding of arrhythmogenic mechanisms (Burton and Cobbe, 2001). Ventricular tachycardia is frequently caused by a re-entrant circuit in an area of myocardium leading to continuous self-excitation of an area of myocardium effectively independent of sinus node activity. Normally, self-excitation does not occur because the refractory period is longer than the time taken for this area to be reactivated. But if this time becomes longer than the refractory period, either by an increase in circuit path length or a slower conduction velocity, re-excitation and hence sustained re-entrant ventricular tachycardia is possible. This mechanism is encapsulated in the idea of electrical “wavelength” which is the distance travelled by the AP over the period of a refractory period (Smeets *et al.*, 1986), i.e.:

Electrical wavelength = Refractory period x Conduction velocity.

Conversely anything that causes the refractory period to shorten decreases the wavelength and therefore increases the risk of establishing re-entrant circuits by making space for a re-entrant wave or allowing more waves to be present at one time (Han and Moe, 1964).

Heterogeneity in refractoriness can cause the unidirectional conduction block necessary for the initiation of a re-entrant wave. Under normal circumstances, the heterogeneity in refractoriness is too small to provide a substrate in which re-entry can be induced, but in the presence of pathological abnormality such as acute ischaemia, post-repolarisation refractoriness becomes evident (Opthof *et al.*, 1993; Sutton *et al.*, 2000).

Electrical restitution

Restitution is defined as the relationship between APD and the preceding diastolic interval (Elharrar and Surawicz, 1983). Under normal circumstances, the APD does not vary at a constant cycle length. However, as the cycle length decreases, for example during the higher heart rates associated with exercise, the diastolic interval (DI) reduces and the APD shortens to maintain a minimum diastolic period required for recovery from the refractory state before the next cycle. A restitution curve is derived from a plot of the APD against the diastolic interval. The relationship between the diastolic interval and the APD in human and rabbit is illustrated in Figure 1.3. The slope of the restitution curve is initially steep at the minimum diastolic interval representing a dramatic shortening of APD as the interval between stimuli is decreased. As the diastolic interval is increased (heart rate decreased) the APD increases and the dependence on diastolic interval flattens out as the diastolic interval increases (Franz, 2003). The cellular basis for this relationship is complex and is thought to arise from the time course of the recovery of the main ionic currents that underlie the AP, in particular I_{Na} , $I_{Ca,L}$, I_{Kr} and I_{Ks} (Franz, 2003).

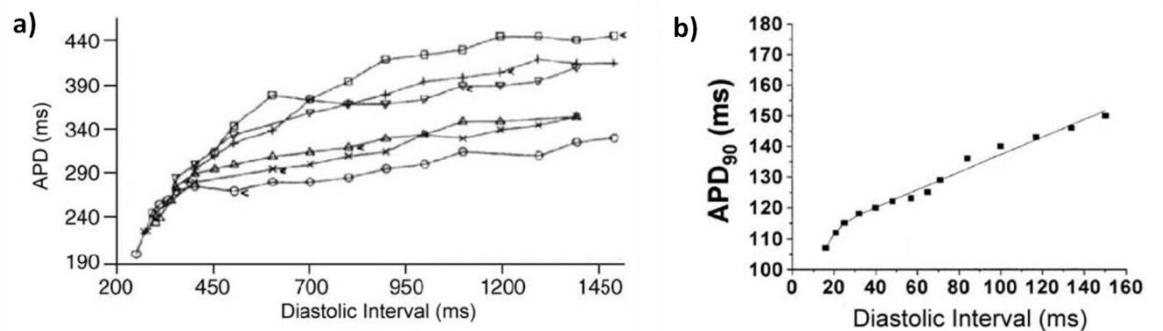


Figure 1.3 Restitution curve.

Comparison between restitution curve in a) human (Morgan *et al.*, 1992), and in b) rabbit (Hayashi *et al.*, 2003).

The shape of the restitution curve has consequences for the stability of the action potential duration at as heart rate changes and for the propensity for arrhythmias. Nolasco and Dahlen (1968) showed that a steep relationship between APD and DI (slope >1) resulted in alternating APD values and increasingly unstable APD. At slopes <1, changes in APD tended to stabilise at one value. Later work on whole hearts showed that arrhythmias and VF were

more frequent when the heart was operating in that part of the restitution curve where slope >1 (Qu *et al.*, 2000; Watanabe *et al.*, 2002).

Electrophysiological changes in regional myocardial ischaemia

After coronary artery ligation, the ischaemic myocardial cells depolarize (Kardesch *et al.*, 1958; Prinzmetal *et al.*, 1961; Samson and Scher, 1960) in parallel with the accumulation of extracellular K^+ released by myocardial cells during acute ischaemia (Hill and Gettes, 1980; Hirche *et al.*, 1980). Kardesch *et al.* (1958) have reported that there was a decrease in amplitude and a marked shortening of the action potential duration a few minutes after occlusion in intact rabbit and canine hearts. Similar observations also seen in ischaemic cells from porcine and canine hearts (Czarnecka *et al.*, 1973; Downar *et al.*, 1977; Kleber *et al.*, 1978) during acute regional ischaemia.

In normal cardiac cells, the time course of recovery of excitability normally follows the repolarisation time course. However, during ischaemia the cell membrane may remain inexcitable even though the membrane has been completely repolarized. This phenomenon is known as “post-repolarisation refractoriness” (Downar *et al.*, 1977; Lazzara *et al.*, 1975). The time course of the change in refractoriness during ischaemia is distinct from that of the changes in APD, as shown by Downar *et al.* (1977); APD shortens after 2 minutes of coronary artery occlusion while post-repolarisation refractoriness develops after approximately 10 minutes.

Electrocardiogram (ECG)

The ECG is a clinically useful tool to assist in diagnosing rhythm abnormality, alteration in electrical conduction, and myocardial ischaemia and infarction.

ECG in the normal heart

Recording of the ECG from the body surface of man was performed for the first time by Waller (1887) by using a Lippmann's capillary electrometer which was composed of a narrow glass capillary half filled with mercury above which was a weak solution of sulphuric acid. This arrangement allowed the recording of small

rapidly changing voltages that could be recorded from the body surface during cardiac depolarisation and repolarisation (Figure 1.4).

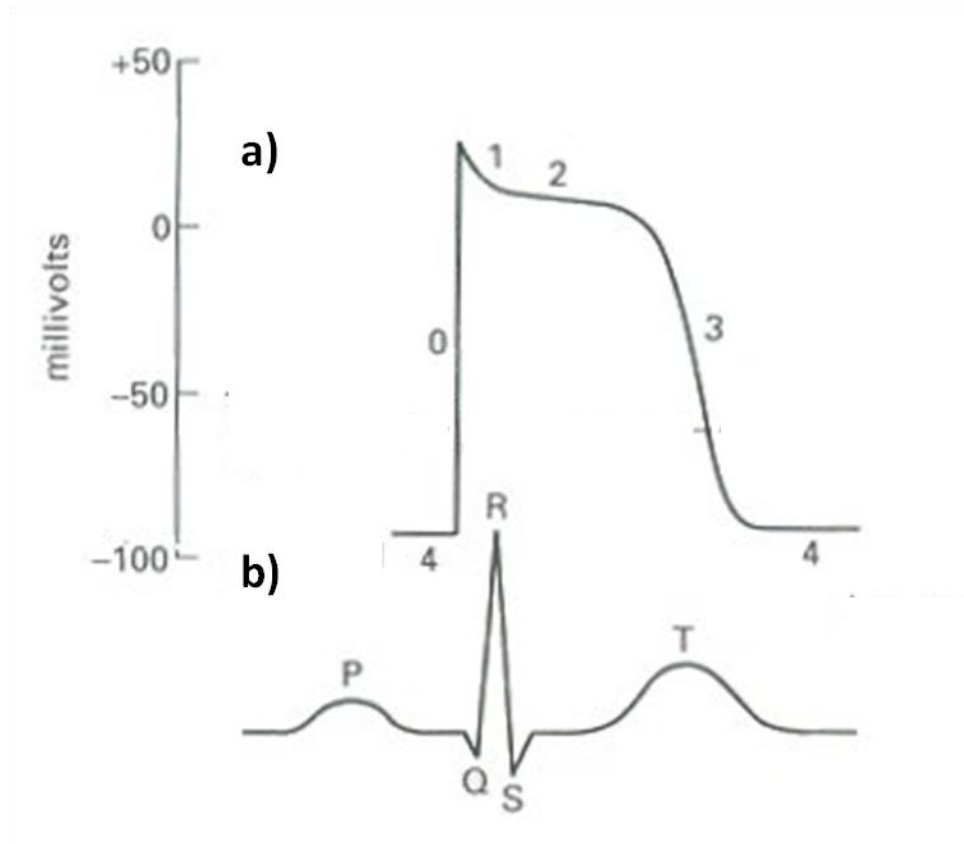


Figure 1.4 Cardiac ventricular AP and ECG in the normal heart.
a) 5 phases of ventricular AP with b) corresponding ECG parameters.

By convention, the first deflection of the ECG is the **P wave**. It indicates the spread of depolarisation from the SA node throughout the atria thereby causing atrial depolarisation. The brief isoelectric period after the P wave corresponds to the time when the impulse is travelling through the AV node and during atrial repolarisation.

The **QRS complex** indicates ventricular depolarisation. Conduction abnormalities such as bundle branch block, or presence of ectopic foci will generally manifest as prolongation of the QRS complex or other changes in its morphology from the normal pattern.

The **ST segment**, an isoelectric period following QRS complex roughly corresponds to the plateau phase of the ventricular action potential in which the entire ventricle is depolarized. This ST segment is particularly important in the

diagnosis of myocardial ischaemia and infarction, where it can become either elevated or depressed, indicative of regional shortening of myocardial action potentials.

The **T wave** indicates ventricular repolarisation and lasts longer than depolarisation.

Q-T interval represents the time for the entire ventricular depolarisation and repolarisation sequence to occur. This interval roughly estimates the duration of ventricular action potentials. Prolonged QT interval is an important diagnostic parameter for the susceptibility of the heart to certain types of arrhythmias.

The duration of each ECG component in human (Klabunde, 2005) and in rabbit (Lord *et al.*, 2010) under normal condition is summarised in Table 1.1.

Table 1.1 Summary of ECG components.

Comparison between the duration in human (at a resting heart rate of 70 bpm) and rabbit (at a resting heart rate of 180bpm).

ECG components	Normal duration (s)	
	Human	Rabbit
P wave	0.08 - 0.10	0.01 - 0.05
QRS complex	0.06 - 0.10	0.02 - 0.06
PR interval	0.12 - 0.20	0.04 - 0.08
QT interval	0.20 - 0.40	0.08 - 0.16

ECG in myocardial ischaemia and infarction

The ECG continues to be an important foundation for the early diagnosis of acute myocardial ischaemia and myocardial infarction (MI). In acute coronary heart disease, the ECG provides useful information about the presence, severity and extent of myocardial ischaemia. During ischaemia, oxygen depletion to the myocardial cell will lead to electrophysiological changes that can alter both rhythm and conduction. Evaluation of the electrical changes by the 12-lead ECG recording can determine the extent, location, and progress of damage to the heart following the ischaemic insult (Klabunde, 2005).

Local myocardial ischaemia normally manifests as a change in the ST segment, either as ST elevation (displacement of the ST segment above the isoelectric baseline) or as ST depression (displacement of ST segment below the isoelectric baseline) on the ECG. This change in ST segment is due to a fall in resting membrane potential and action potential magnitude in ischaemic myocardium. The potential difference between the ischaemic myocytes and surrounding healthy myocardial cells will lead to the flow of an “injury current” during normally isoelectric periods resulting in a shift of the ST segment level and/or ECG baseline. ST segment changes caused by a partial occlusion of the coronary artery may be reversible once the blood supply to the myocardium is restored. However, a full thickness or transmural myocardial infarct will result in permanent changes in ECG parameters. A few hours after infarction, the ECG shows ST segment elevation. Several days later, as ischaemic cells become necrosed and electrically silent, the ST elevation is replaced by pathological Q waves and T wave inversion (Levick R.J, 2010).

Apart from ST segment changes, acute myocardial ischaemia has been shown to modify the duration of QT interval, increase repolarisation heterogeneity (manifested as increase in QT dispersion) and prolong the duration of the maximum electrocardiographic QT interval (Bijl and Verheugt, 1992). The QT interval prolongation secondary to acute myocardial ischaemia has been attributed to several mechanisms: local hypothermia, local conduction delay, neurogenic effect and local hypocalcaemia (Doroghazi and Childers, 1978).

Animal models of myocardial ischaemia

Many ventricular arrhythmias, particularly those associated with acute myocardial ischaemia, are almost impossible to study closely in human patients because of the unpredictable nature of the event and the electrophysiological changes during the event can occur within minutes. Furthermore, in human patients there may be other contributory factors that promote arrhythmia apart from acute ischaemia such as the electrolyte imbalance, presence of a healed infarct, hypertrophy, dilatation or heart failure. Therefore, detailed information on arrhythmogenic mechanisms associated with ischaemia and infarction has to be obtained from experimental animal models. A good model of myocardial ischaemia in experimental animals must accurately reproduce the spectrum of

ischaemic heart disease as seen in human. Animal models of myocardial ischaemia can be achieved either by fully blocking or partially narrowing the coronary artery. A variety of procedures including surgical procedures or drug intervention have been used to occlude coronary arteries, for varying periods, in different species. The simplest method to produce myocardial ischaemia is by ligating a single coronary artery. Another method to produce ischaemia was achieved by introducing air embolism into the coronary arteries (Gunn, 1913, cited in Curtis, 1998). Other method to produce ischaemia is by atherosclerosis induction that closely mimics the human condition (Russell and Proctor, 2006) but this method is rarely used in ischaemia research since the process is slow to develop and variable in outcome.

The severity of the ischaemia induced by coronary artery occlusion depends on the presence or absence of collateral vessels because collateral flow provides an alternative source of blood to the ischaemic field. The animal species that are commonly used to study ventricular arrhythmias include large animals (dogs, pigs, cats) and small animals such as rabbits, rats, and guinea pigs. Warltier *et al.* (1982) demonstrated that the same ligation site on the LAD in dogs can produce varying infarct sizes, due to the variable extent of their collateral development (Estes, Jr. *et al.*, 1966; Jugdutt *et al.*, 1979; Schaper *et al.*, 1967). Studies using pigs (Fedor *et al.*, 1978; Verdouw *et al.*, 1983) produce a consistent infarct size following coronary artery ligation because they possess relatively few collateral vessels. In contrast, ligation of coronary artery in guinea pig produces a minimal infarct because the collaterals are so abundant (Schaper, 1986).

Rabbit model of myocardial ischaemia and infarction

Rabbits are commonly used to produce experimental models that mimic heart failure and myocardial infarction in human. Studies have demonstrated that rabbit myocardium shows important similarities in function to the human heart, in that the force-frequency relation is positive, and calcium removal from the cytosol is 70% by the sarcoplasmic reticulum and 30% by NCX activities (Hasenfuss, 1998; Holubarsch *et al.*, 1991; Pogwizd *et al.*, 2001). According to Miura *et al.* (1989), there are minimal collateral vessels in rabbit hearts. Rabbits can serve as a reliable experimental model in the study of MI related to coronary

artery occlusion (Lee *et al.*, 2002). Rabbits are less costly than dogs and have less variability in terms of distribution, size and length of coronary arteries. Despite a comparatively greater anatomical consistency, variation is nonetheless observed: there is not one constant pattern but two anatomical branching patterns of left coronary artery (LCA) in rabbit hearts, namely bifurcation and trifurcation. In the bifurcation branching pattern, the coronary artery branches into two main divisions: anterior division (AD) and postero-lateral division (PLD). On the other hand, in the trifurcation pattern, the coronary artery branches into three divisions: AD, lateral division (LD), and posterior division (PD) (Lee *et al.*, 2002; Podesser *et al.*, 1997). The difference between the two branching pattern is illustrated in Figure 1.5.

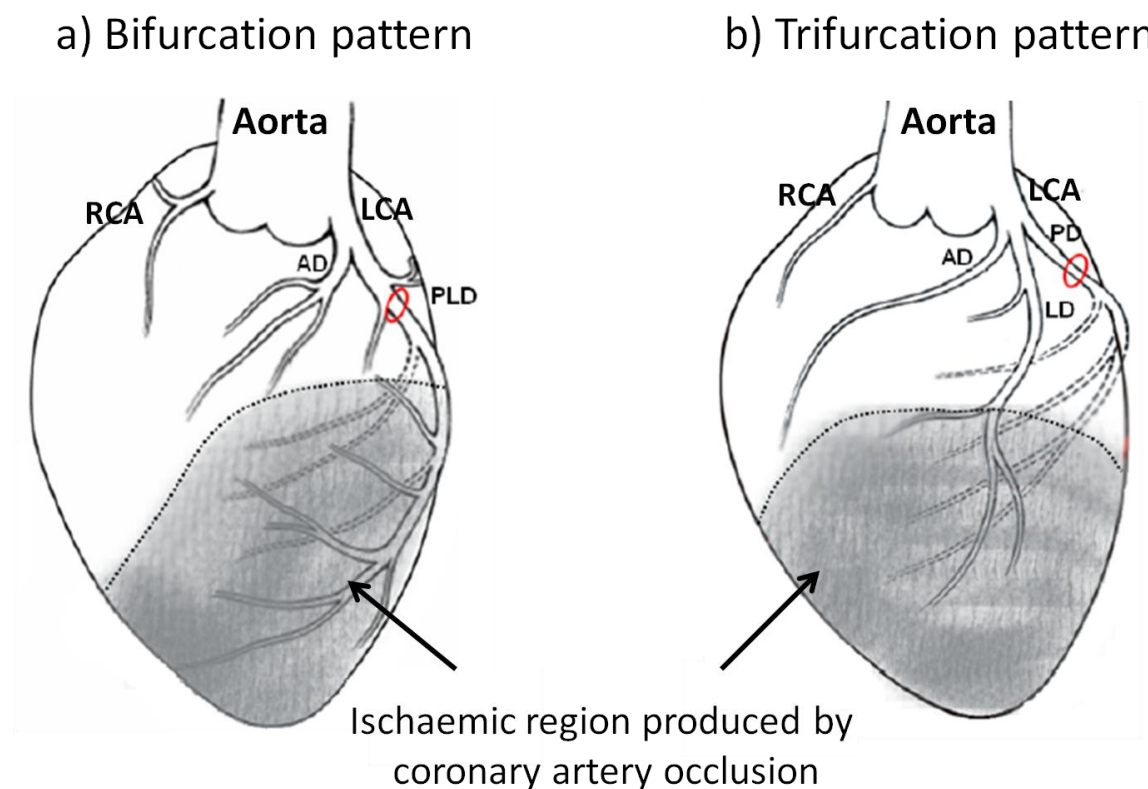


Figure 1.5 Branching pattern in rabbit coronary artery. Illustration of a) bifurcation type of the left coronary artery (LCA) into anterior division (AD) and postero-lateral division (PLD), and b) trifurcation type of the LCA into AD, lateral division (LD) and posterior division (PD). Depending on the type of the branching pattern, the red rings around the PLD and PD in bifurcation and trifurcation patterns, respectively, indicate the ligation site on the respective artery; RCA = right coronary artery (Adapted from Petchdee, 2009).

Sudden cardiac death

Sudden cardiac death (SCD) refers to an unpredictable death in patients with or without pre-existing heart disease. However, in the majority of cases, SCD appears as the first manifestation of a pre-existing, sometimes unrecognized, coronary artery disease. In the majority of cases, SCD is frequently caused by abnormality in the heart rhythm (arrhythmia) including ventricular tachycardia (VT) and ventricular fibrillation (VF) that compromise cardiac pumping which further leads to deprivation of oxygenated blood in vital organs. Most clinical studies define SCD as death that occurred within 1 hour of an acute change in clinical condition, or an unpredictable death occurring within the previous 24 hours (Fishman *et al.*, 2010; Zipes and Rubart, 2006). Clinical case studies by Bayes de Luna *et al.* (1989) reported that ambulatory electrograms from patients who died from sudden cardiac death during the recordings reveal that the most common cause of sudden cardiac death was ventricular tachyarrhythmias (84%) most frequently ventricular fibrillation (VF) secondary to ventricular tachycardia (VT) whereas only 16% was due to bradyarrhythmias. Autopsies performed on the patients suggest that the main cause of sudden cardiac death is acute myocardial ischaemia (Priori *et al.*, 2001).

Acute myocardial ischaemia and infarction

Myocardial ischaemia has been one of the most extensively studied topics in cardiovascular research. According to Mosby's Medical Dictionary, 8th edition (2009), myocardial ischaemia is a condition of insufficient blood flow to the heart muscle via the coronary arteries, often resulting in chest pain (angina pectoris). Saunders Comprehensive Veterinary Dictionary, 3rd edition (2007) defined myocardial ischaemia as deficiency of blood supply to the heart muscle, due to obstruction or constriction of the coronary arteries. However, the most accepted definition of myocardial ischaemia among researchers is an imbalance between the amount of oxygen and substrates supplied to the heart and the amount needed to perform normal function of the heart (Hearse, 1994). Thus, myocardial ischaemia is a condition in which there is an imbalance between supply and demand of the oxygen that lead to anaerobic metabolism and reduced contractile function (Verdouw *et al.*, 1998). Myocardial ischaemia may result from the presence of atherosclerotic disease of the coronary artery

(Brown *et al.*, 1989), or it may occur without a predisposing coronary artery disease, due to perivascular fibrosis (Weber *et al.*, 1993) and a reduction in coronary flow reserve (Scheler *et al.*, 1994; Wallbridge and Cobbe, 1996). Janse and Wit (1989) have stated that dispersion of repolarisation and refractoriness between ischaemic and non-ischaemic myocardial cells as an important pro-arrhythmic mechanism during acute myocardial ischaemia.

Myocardial infarction (MI) which is a major cause of death and disability worldwide may be the first manifestation of coronary artery disease (CAD) or it may occur in patients with established disease. According to the World Health Organisation (WHO), MI can be recognised by clinical symptoms, ECG abnormalities, elevated values of biochemical enzymes (biomarkers) of myocardial necrosis, and by imaging, or it may be defined in pathology as cell death of myocardium due to prolonged ischaemia (Thygesen *et al.*, 2012). Thygesen *et al.* (2012) stated that after the onset of myocardial ischaemia, histological cell death is not immediate but takes at least 20 minutes (or less in some animal models) to develop. Complete myocardial cell necrosis takes several hours (at least 2-4 hours, or longer) before it can be identified by post-mortem examination. The duration depends on several factors such as the presence of collateral circulation to the ischaemic zone, persistent or intermittent coronary arterial occlusion, the sensitivity of the myocytes to ischaemia, pre-conditioning and individual demand of myocardium for oxygen and nutrients.

Classification

Clinically, MI can be classified into 5 types based on universal definition by Thygesen *et al.* (2012):

Type 1: Spontaneous MI related to a coronary plaque rupture, fissuring, or dissection with resulting intraluminal thrombosis

Type 2: MI secondary to myocardial ischaemia resulting from increased oxygen demand or decreased supply

Type 3: MI related to sudden cardiac death usually with symptoms suggestive of myocardial ischaemia associated with new ECG changes in the absence of cardiac biomarkers in the blood

Type 4: MI related to cardiac procedure such as percutaneous coronary intervention (PCI) and stent thrombosis

Type 5: MI related to coronary artery bypass grafting (CABG)

Myocardial ischaemia and myocardial infarction can also be classified into transmural and non-transmural based on morphology and anatomical features. A transmural MI involves the ischaemic cell death across the full thickness of the affected heart muscle, from endocardium to epicardium. Whereas, for the non-transmural MI, the region of the ischaemic cell death only affected part of the myocardial wall (Engblom *et al.*, 2005; Engels *et al.*, 1995; Widimsky *et al.*, 1984). Ryan *et al.* (1996) have documented that the regions which are most vulnerable to ischaemia are in the endocardial and subendocardial zones of the myocardial wall.

Metabolic consequences of myocardial ischaemia and mechanisms of ischaemia-related arrhythmias

The consequences of ischaemia are due to the inadequate myocardial oxygen supply and local accumulation of metabolic waste products. Several studies (Carmeliet, 1999; Ferrero, Jr. *et al.*, 1996; Kagiya *et al.*, 1982; Weiss and Shine, 1982; Weiss *et al.*, 1992) have reported that the most prominent changes in electrophysiological properties in the heart during acute ischaemia include rises of extracellular potassium concentration ($[K^+]_o$), activation of the ATP-sensitive potassium current (I_{KATP}) due to metabolic inhibition, and fall in intracellular pH.

During myocardial ischaemia, aerobic metabolism, i.e. oxidative phosphorylation in the mitochondria is inhibited as the pO_2 within the myocardium falls to below ~1mmHg. Immediately anaerobic glycolysis sustains adenosine triphosphate (ATP) production by breaking down glucose to lactic acid (Elliott *et al.*, 1992). This continues to maintain intracellular ATP for many minutes, but the fall in intracellular pH as a result of lactic acid accumulation inhibits glycolysis (Neely

et al., 1975) and ATP synthesis stops. This results in depletion of intracellular ATP in cardiac myocytes because it cannot be regenerated. Consequently adenosine diphosphate (ADP) and adenosine monophosphate (AMP) accumulate and they are subsequently metabolized into adenosine. Adenosine is a potent vasodilator because it binds to receptors on vascular smooth muscle where it causes a decrease in calcium influx leading to vasodilatation (Naik *et al.*, 2007). ATP depletion within cardiomyocytes inhibits the sodium/potassium (Na^+/K^+) ATPase. In the absence of Na^+/K^+ ATPase, the cells are no longer capable of counterbalancing the Na^+ influx through Na^+ channels, leading to an increase in concentration of intracellular Na^+ .

At the same time, there is also a significant increase in K^+ conductance due to the opening of ATP sensitive K^+ channels (I_{KATP}) as a consequence of the decrease intracellular ATP (Lederer *et al.*, 1989). There is also an increase in extracellular K^+ concentration due to increased intracellular K^+ efflux during ischaemic insult. Regional ischaemia produces a spatial heterogeneity in $[\text{K}^+]_o$, I_{KATP} , and pH resulting in increased dispersion of conduction velocity (Kaplinsky *et al.*, 1979b; Pogwizd and Corr, 1987b), APD (Behrens *et al.*, 1997; Kuo *et al.*, 1983), and effective refractory period (Avitall, 1979; Downar *et al.*, 1977), factors which aggravate the substrate for the initiation and maintenance of re-entry. Gilmour, Jr. and Zipes (1985) have suggested that extracellular K^+ accumulation is responsible for the depolarisation of tissue surrounding the ischaemia area creating an injury current between ischaemic and normal myocardial cells that could initiate ventricular premature beats. In addition, activation of K_{ATP} channels shortens the APD (Kantor *et al.*, 1990; Vanheel and de, 1992; Venkatesh *et al.*, 1991) and increases heterogeneity of APD and dispersion of refractoriness in the ischaemic region, favouring the initiation of re-entrant circuits, and thus ventricular arrhythmias (Billman, 1994; Furukawa *et al.*, 1991). Moreover, increase in extracellular potassium concentration can cause unidirectional block by depolarising the myocardium sufficiently to inactivate the inward Na^+ current. Commonly the central zone of region of ischaemic myocardium becomes inexcitable, while the myocardial cells in the border zone retain a low level of perfusion and therefore remain excitable. The conduction delay associated with the region of block facilitates re-entrant circuit formation (Ettinger *et al.*, 1973) and the development of ventricular tachycardia.

Cardiac arrhythmias

Sudden cardiac death is a disastrous complication of acute myocardial infarction (Huikuri *et al.*, 2001). The reason why certain patients develop lethal ventricular arrhythmia soon after acute myocardial infarction and some patients survive is still poorly understood. A clinical study on the incidence and timing of sudden death or resuscitated cardiac arrest after MI conducted by Solomon *et al.* (2005) showed that the risk of sudden death was highest in the first 30 days after MI in patient with prior left ventricular dysfunction, heart failure, or both.

Mechanisms of ventricular arrhythmias

Normal electrical conduction in the heart involves an AP originating from the sino-atrial (SA) node, conducted through the atria via the atrio-ventricular (AV) node down to the Purkinje fibres and then to the ventricles. Abnormality in the properties of ionic currents can lead to abnormal impulse generation and/or propagation which further leads to electrical disorder in the ventricles.

Three main mechanisms of ventricular tachyarrhythmias are:

- 1) Automaticity
- 2) Triggered activity
- 3) Re-entry

In the case of re-entrant arrhythmias, the first and second mechanisms are potential triggers for the arrhythmia, while re-entry itself maintains the arrhythmia.

Automaticity

Automaticity is a normal feature in the cells in the sino-atrial node. In this case, the electrical behaviour is determined by the expression of channel proteins, including the pacemaker current (I_f), the T-type Ca^{2+} current ($I_{\text{Ca,T}}$), and deactivation of delayed rectifier potassium current (I_{Kr} or I_{Ks}). Under normal conditions in the ventricle and atria, I_f is absent or its activation voltage is too

negative. However, Carmeliet and Vereecke (2002) demonstrated that β -adrenergic stimulation in Purkinje fibres shifts the activation kinetics of I_f in that tissue to a less negative activation potential thus enhancing the diastolic repolarisation. Under these circumstances, Purkinje fibres may be the source of arrhythmic triggers.

Triggered activity

There are two types of triggered activity; early afterdepolarisations (EADs) and delayed afterdepolarisations (DADs). The membrane potential at the onset differentiates between these two types of triggered activity; EADs occur during phase 2 and phase 3 of AP, whereas DADs occur immediately after the membrane potential has returned to the baseline (phase 4). These triggering events (EADs and DADs) are most commonly observed during plasma electrolyte imbalances (low $[K^+]_o$, $[Ca^{2+}]_o$, $[Mg^{2+}]_o$ and pH) and they are more common in heart failure (Pogwizd *et al.*, 2001). Delayed after-depolarisations are caused by spontaneous release of Ca^{2+} from the sarcoplasmic reticulum (SR) of cardiac muscle during diastole (Pogwizd *et al.*, 2001), the raised intracellular Ca^{2+} is extruded mainly by the electrogenic Na^+/Ca^{2+} exchanger and the subsequent inward current can depolarise the cardiac cell sufficiently to activate I_{Na} and a subsequent arrhythmic action potential. These events occur when the SR Ca^{2+} content is higher than normal or when the SR Ca^{2+} release channel is sensitised to cytoplasmic Ca^{2+} .

The mechanism of EADs is less well defined. A common cause of EADs is prolongation of the APD and the extension of the plateau phase sufficiently to allow reactivation of inward currents $I_{Ca,L}$ (Pogwizd *et al.*, 2001). Prolongation of APD can be due to bradycardia or inhibition of repolarising currents, e.g. I_{Kr} .

Re-entry

Botting *et al.* (1985) stated that of the three main mechanisms, only re-entry has been demonstrated as the arrhythmogenic mechanism during acute ischaemia. However, in most of the cases, re-entry is triggered by an ectopic impulse in the context of an abnormal dispersion of refractoriness between the normal and ischaemic myocardium. Experimental studies with animal models have demonstrated that lethal arrhythmias occur most frequently 4-7 minutes

post occlusion (Fleet *et al.*, 1994; Kaplinsky *et al.*, 1979a; Scherlag *et al.*, 1974) due to re-entrant mechanisms (Kaplinsky *et al.*, 1979b; Kuo *et al.*, 1983; Pogwizd & Corr, 1987b). Acute regional myocardial ischaemia in canine right ventricular wedge preparations results in heterogeneous loss of the transient outward potassium current (I_{to})-mediated AP dome across the ischaemic border leading to phase 2 re-entry which is capable of initiating VF by producing R-on-T extrasystoles (Yan *et al.*, 2004).

During acute myocardial ischaemia, shortening of repolarisation by ATP-regulated potassium channel openers (I_{KATP}) has been reported to increase the susceptibility of the heart towards re-entry and fibrillation (Coromilas *et al.*, 2002; Padrini *et al.*, 1992; Uchida *et al.*, 1999). The substrate for initiation and maintenance of ventricular arrhythmia during acute ischaemia has been extensively studied in porcine and canine hearts. Janse *et al.* (1980) showed that during coronary artery occlusion in isolated perfused hearts, the “focal” mechanism occurs at the normal side of the ischaemic border and the macro- and micro-reentry in ischaemic myocardium are responsible for the very early ischaemic arrhythmias. A study by Pogwizd and Corr (1987a) reported that during early ischaemia in canine hearts, the initiation and maintenance of ventricular arrhythmia is due to both intramural re-entry and non-reentrant mechanisms. In both these studies, the arrhythmic event is preceded by ventricular premature beats (VPBs).

Chou *et al.* (2007) have demonstrated that during the subacute phase of myocardial infarction, the dynamic properties of the action potential and Ca^{2+}_i cycling are heterogeneously altered in the peri-infarct zone which may promote ventricular premature beats and increase the incidence of wavebreaks during VF. Several early studies (Harris, 1950; Harris *et al.*, 1954) in canine model of acute ischaemia concluded that ectopic beats were generated near the infarct borders by automatic foci. The authors suggested that these events were triggered by the release of K^+ from ischaemic cells, but given present knowledge of cardiac electrophysiology, this is unlikely to be the cellular mechanism, currently it is uncertain what circumstances in the peri-infarct zone may make premature electrical events more common.

Premature ventricular contractions (PVCs)

Premature ventricular contractions (PVCs) are a form of abnormality of heart rate rhythm in which the heart beat is initiated at ventricular Purkinje fibres rather than by the SA node. Frequently, they occur spontaneously with no known cause. PVCs have been recognized to precede lethal arrhythmia and to identify patients susceptible to sudden death following myocardial infarction. In patients with acute myocardial infarction, tissue injury and cell death has been recognised as a common cause of spontaneous ventricular ectopy associated with the infarct border zone of ischaemic myocardium (Bigger, Jr. *et al.*, 1977; Eldar *et al.*, 1992). Accelerated idioventricular rhythms and ectopic beats may occur during coronary reperfusion. Episodes of spontaneous ventricular ectopy increase the tendency of the heart to develop re-entrant ventricular arrhythmias, particularly along the infarct border zone as a result of non-homogeneous conduction and repolarisation (Cantillon, 2013). Ghuran and Camm (2001) have stated that PVCs are usually asymptomatic and their presence in the peri-infarct zone regardless of frequency and complexity had no relation to mortality or the development of sustained ventricular arrhythmias. In contrast, however, a meta-analysis study conducted by Ataklte *et al.* (2013) to assess the association between PVCs and risk of sudden cardiac death reported that frequent PVCs are associated with increased risk of sudden cardiac death.

T-wave alternans (TWA)

Another phenomenon which is clinically significant in reflecting susceptibility to ventricular arrhythmias in patients is T-wave alternans (TWA). TWA is recognised by regular fluctuations on a beat-to-beat basis in the amplitude, morphology or polarity of the ECG T-wave and is associated with dispersion of repolarisation. It has also been termed repolarisation alternans (Narayan *et al.*, 1999; Narayan and Smith, 2000). Macroscopic TWA was first reported in the early 20th century (Hering, cited by Narayan, 2006). Further observations of macroscopic TWA have noted in association with ischaemia (Kleinfeld and Rozanski, 1977), long QT syndrome (LQTS) (Roden *et al.*, 1996) and with ventricular arrhythmias (Raeder *et al.*, 1992; Verrier *et al.*, 2003). Macroscopic TWA has been observed to occur immediately prior to the onset of ventricular arrhythmia (Armoundas *et al.*, 2000). Previous studies have revealed that TWA indicates spatial or temporal

dispersion of repolarisation that may precede VF (Weiss *et al.*, 1999; Smith and Cohen, 1984). Clinically, TWA can be a good ECG index of sudden cardiac death associated with dispersion of repolarisation and ventricular arrhythmias (Narayan, 2006).

Ischaemia-induced ventricular fibrillation

The ability of ischaemia to induce ventricular fibrillation (VF) in an isolated hearts was first studied by Gunn using rat model (Gunn, 1913, cited in Curtis, 1998). More recently, ischaemia-induced arrhythmias were studied using the left coronary artery ligation technique (Kannengiesser *et al.*, 1975) in which the total coronary flow to the heart was reduced by approximately 27%, but in this report no-VF was observed. In another study using global ischaemia (Bricknell and Opie, 1978) VF incidence was very low despite an 85% reduction in global coronary flow in rats. It was later found out that the global coronary flow would have to be reduced by more than 85% for the heart to routinely develop VF (Wolleben *et al.*, 1989). The relationship between the extent of flow reduction, region involved and tendency to VF was studied in detail by Curtis and Hearse (1989) and Ridley *et al.* (1992). These studies showed that there are several factors that can influence the susceptibility of the hearts to ischaemia-induced VF; (i) variation of K^+ content in the perfusion solution, (ii) the size of the ischaemic region, (iii) the severity of ischaemia and (iv) heart rate. Studies have shown that the K^+ concentration in the perfusion solution can change the incidence of VF from 100% to 0% (Curtis & Hearse, 1989; D'Alonzo *et al.*, 1994) which is similar to the relation between K^+ concentration in blood and incidence of sudden cardiac death seen in human patient (Nordrehaug, 1985; Nordrehaug *et al.*, 1985). Variation in the collateral blood supply to the ischaemic site can determine the tendency of the heart to develop ischaemia-induced VF in which heart with low level of residual flow was found to be more susceptible to VF (Maxwell *et al.*, 1987). Meanwhile, Bernier *et al.* (1989) demonstrated that VF incidence was lower at slow heart rates in rat hearts, an effect suggested to be due to the slower rate of development of ischaemic injury.

In studies involving a variety of experimental animals, the time-course of ischaemia-induced VF is divided into two phases: phase 1 VF which occurs during the first 30 minutes of ischaemia and phase 2 VF which develops after 30

minutes of ischaemia (Curtis, 1998). Kaplinsky *et al.* (1979a) further divided phase 1 VF into *immediate* (occurring 2-10 minutes after ischaemic onset) and *delayed* (between 12-30 minutes of the beginning of ischaemia). Another classification of phase 1 VF was made (Meesman *et al.*, 1978, cited in Curtis, 1998); phase 1a developing before 12 minutes of ischaemia and phase 1b occurring after 12 minutes of onset of ischaemia. However, it is difficult to determine the exact time-course of appearance of ischaemia-induced VF in human, particularly phase 1 VF because the exact time of onset of ischaemia is unknown.

Study aims

Approximately 50% of deaths from cardiac causes are arrhythmic in nature and occur within 1 hour of the onset of symptoms. Pathological examination reveals that in the majority of cases show evidence of acute myocardial infarction but the mechanistic link between ischaemia and lethal arrhythmia is still poorly understood.

The main aims of this thesis were:

- 1) To use the isolated Langendorff-perfused rabbit to reveal the electrophysiological consequences following occlusion of the coronary artery.
- 2) To examine the electrophysiological gradients that develop within 10-30 minutes after an acute myocardial ischaemia and their relationship to the subsequent arrhythmias
- 3) To provide a better understanding of the mechanistic link between ischaemia and arrhythmias, information that will aid the design of therapies that will reduce the incidence of lethal ventricular arrhythmias.

Hypothesis

I hypothesize that an electrophysiological property of the heart, specifically the intrinsic APD prior to coronary artery occlusion, predisposes the heart to VF during acute ischaemic event.

Chapter 2: Methods

Introduction

For over than 100 years, the concept of mapping electrical activity of the hearts has continued to evolve from the first observation of rhythmic muscular contraction around the ring of a jelly fish (Mayer, 1906, cited in Rosenbaum and Jalife, 2001), to the description and mapping of re-entry in the turtle heart by Mines (1913), to the first systematic mapping of sinus rhythm and identification of atrial flutter by Lewis *et al.* in 1920 (cited in Rosenbaum & Jalife, 2001). The technique of activation mapping based on the simultaneous recording from many sites is crucial in order to understand the mechanisms and locations of atrial and ventricular arrhythmias and was originally developed using solid state electrodes placed either on the surface of an exposed heart (Durrer *et al.*, 1970; Ideker *et al.*, 1989) or on the surface of the body. The rapid depolarisation event could be detected as transient electrical event, the timing of which could be used to map the spread of electrical activity throughout the heart (De and Corlan, 2007; Dixit and Callans, 2002; Friedman, 2002; Oster *et al.*, 1998). However, the slower repolarisation event was frequently poorly resolved and details on the plateau phase of the cardiac action potential were not evident.

An alternative approach to map electrical activity in experimental situations is the use of membrane-bound fluorescent voltage-sensitive dyes. This technique has been applied to a variety of tissue preparations from intact heart, to isolated myocardial tissues or cells, to cardiac cells grown in tissue culture (Akar *et al.*, 2001; Lee *et al.*, 2012; Lichtman and Conchello, 2005). It serves as a powerful tool to study cardiac arrhythmias since the optical signal describes the complete time course of the action potential and hence allows mapping of both activation and repolarisation phases. Imaging of the electrical activity with advanced cameras has facilitated the study of the mechanisms of initiation, maintenance, and termination of re-entrant arrhythmias.

Rosenbaum (2001) has described an optical mapping system as consisting of three main components:

- 1) the heart preparation, stained with a voltage-sensitive fluorescence dye;

2) a system of optics, which filters the emitted light and focuses the image onto a photodetector; and

3) a photodetector, which measures the emitted light.

These components will be discussed in detail below.

Voltage-sensitive dyes

Voltage-sensitive dyes are fluorescent molecules which have a high affinity for the membrane of cells and with fluorescent properties that are sensitive to the transmembrane potential. Voltage sensitive dyes are broadly classified into slow and fast types. In cardiac optical mapping, fast electrochromic dyes have been the dye of choice because of their very rapid response time. In the case of di-4- or di-8-ANEPPS, the fluorescence properties change within a few microseconds of the change in voltage (Loew, 2010). With this property, changes in membrane potential can be represented accurately by changes in dye fluorescence (Morad and Salama, 1979).

The principle by which voltage-sensitive dyes translate cardiac membrane potential into light intensity has been described by Rosenbaum (2001) and is shown in Figure 2.1. During rapid upstroke of the action potential, a depolarisation of the cell from its resting transmembrane potential of $V_m = -80\text{mV}$ toward less negative voltage, e.g. $V_m = -40\text{mV}$ and 0mV , causes the fluorescence emission spectrum of the dye to shift to the left (shorter wavelengths), producing an inverted action potential signal. The shaded region under each spectrum corresponds to the amount of light that passes through the emission filter (represented by the vertical line) and is measured by the light detector.

Ideally, voltage-sensitive dyes should be non-toxic with minimal photo bleaching and minimal pharmacologic (e.g. vasoconstrictive) effect and have a large spectral shift with membrane potential. The choice of dye in a particular experiment is often decided based on the excitation and emission spectra of the dye. The main voltage-sensitive dyes used in this study were RH237 and Di-4-ANEPPS. RH237 was used in single view optical mapping experiments (Chapter 4,

5, and 6) whereas Di-4-ANEPPS was used in the panoramic view optical mapping experiments (Chapter 8). Both are styryl dyes developed by Loew *et al.* (1985). Comparison of the excitation and emission spectra between these dyes is shown in Figure 2.2.

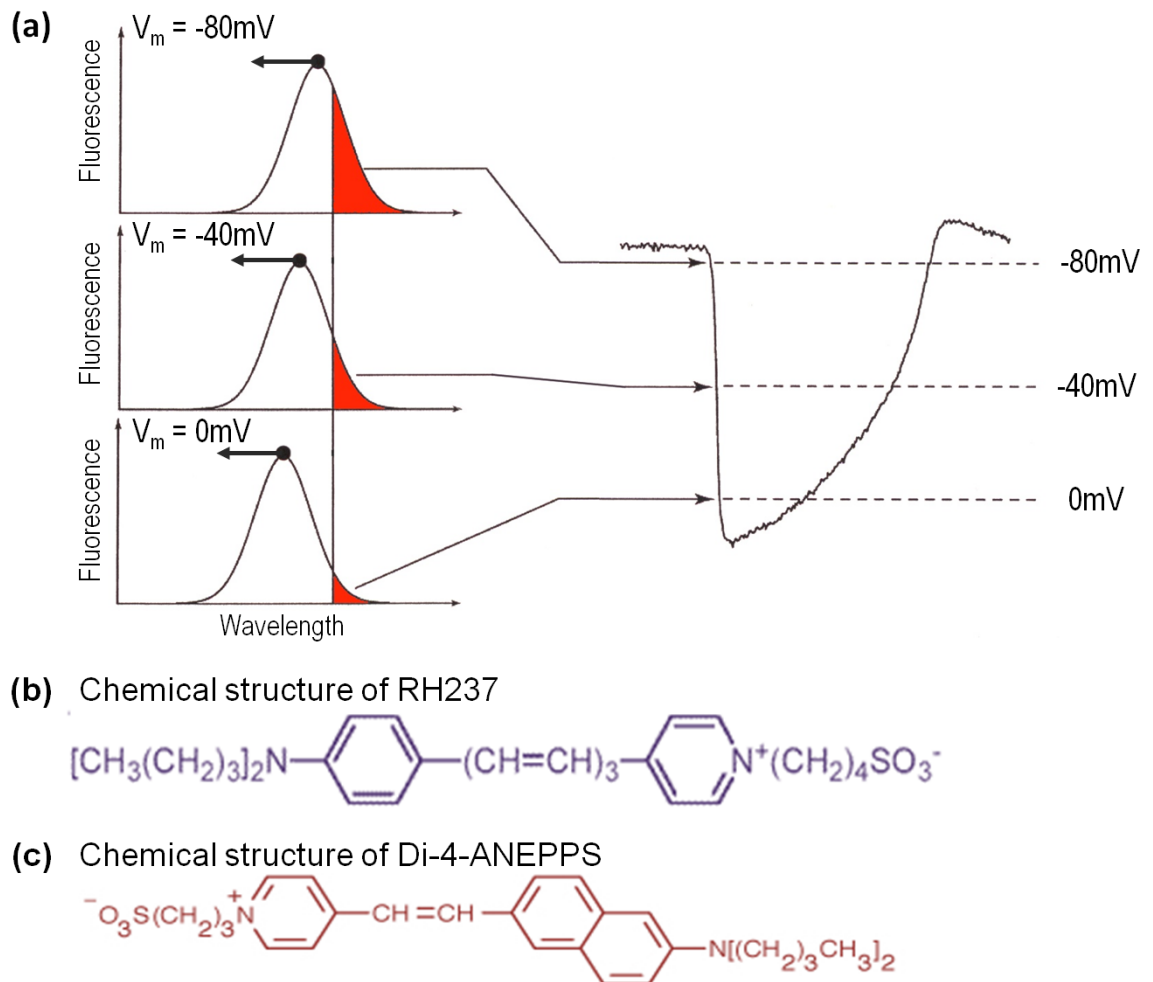


Figure 2.1 Voltage-sensitive dyes.

(a) Schematic diagram of the principle of voltage-sensitive fluorescence, and chemical structure of (b) RH237 and (c) Di-4-ANEPPS. Adapted from Rosenbaum (2001).

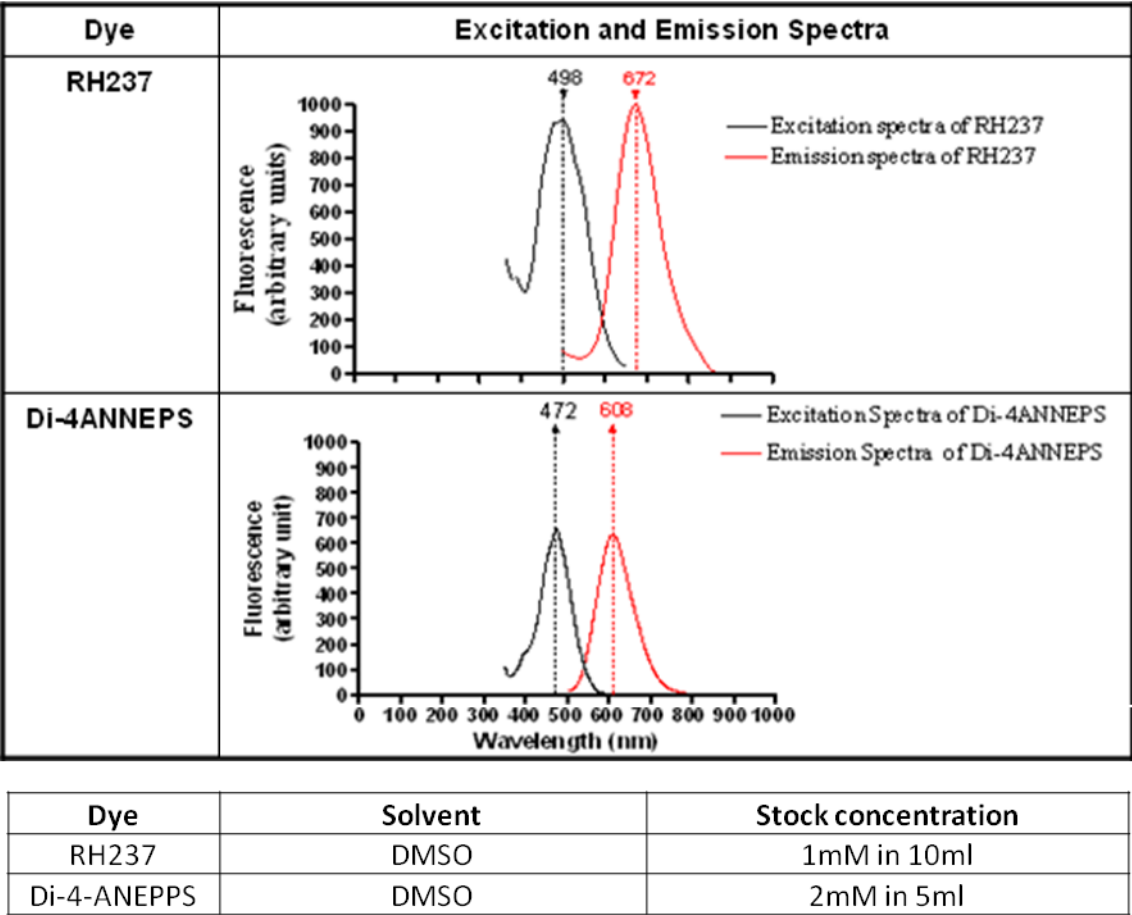


Figure 2.2 Spectra of voltage-sensitive dyes used in optical mapping study.

Optical mapping set-up

In this study, two sets of optical mapping set-ups were used; 1) single view optical mapping that allows us to map electrical activity on a specific site on the hearts surface and 2) panoramic view optical mapping from the whole epicardial surface of the hearts.

Single view optical mapping

Epicardial membrane potentials from the anterior surface of the hearts were recorded using an optical mapping array (Figure 2.3). The isolated Langendorff-perfused heart was placed into custom-made perspex chamber (Figure 2.4a) to physically reduce motion artefact and maintain the temperature of the heart at 37°C by filling the chamber with thermostat-controlled heated solution. Motion artefact was reduced further during optical recordings by sliding forward the back piston against the heart to gently compress the heart against the front-wall of the chamber (Figure 2.4b). Further reduction of motion artefact was achieved by using 10 μ M Blebbistatin (Enzo[®] Life Sciences) in Tyrode's solution (Fedorov *et al.*, 2007). Blebbistatin specifically inhibits myosin II ATPase in the actin detached state (Allingham *et al.*, 2005; Straight *et al.*, 2003).

The heart was loaded with 100 μ L bolus of the voltage-sensitive styryl dye RH237 (Molecular Probes) dissolved in dimethyl sulfoxide (DMSO) (1mg/ml). The dye was made up into stock solution by adding 1ml of DMSO into 5mg RH237 and aliquoted into small Eppendorf tubes. The aliquots were stored at -20°C, wrapped in aluminium foil to protect from the light. Aliquots were thawed on the day of the experiment just prior to use. The bolus of dye was administered by slow injection into the coronary circulation over 1 minute through an injection port in a bubble trap in line with the aortic cannula. Bolus injection of RH237 was repeated throughout the experiment when necessary.

The dye was excited by blue-green LED light at 505nm wavelength. Fluorescent light emitted from the anterior epicardial surface was collected by a camera lens (Nikon 85mm, f/1.4) passed through a 695nm long-pass (LP) filter, and the image was focused onto a 256 (16 x 16) photodiode array (PDA) (Hamamatsu Photonics). During optical recordings, two corner channels of the PDA were

reserved for recording the ECG and pacing stimuli traces. In the single view optical mapping experiments, the CCD camera (Dalsa) was used to acquire high resolution plain images of the heart surface but it was not directly involved during the optical action potential recordings.

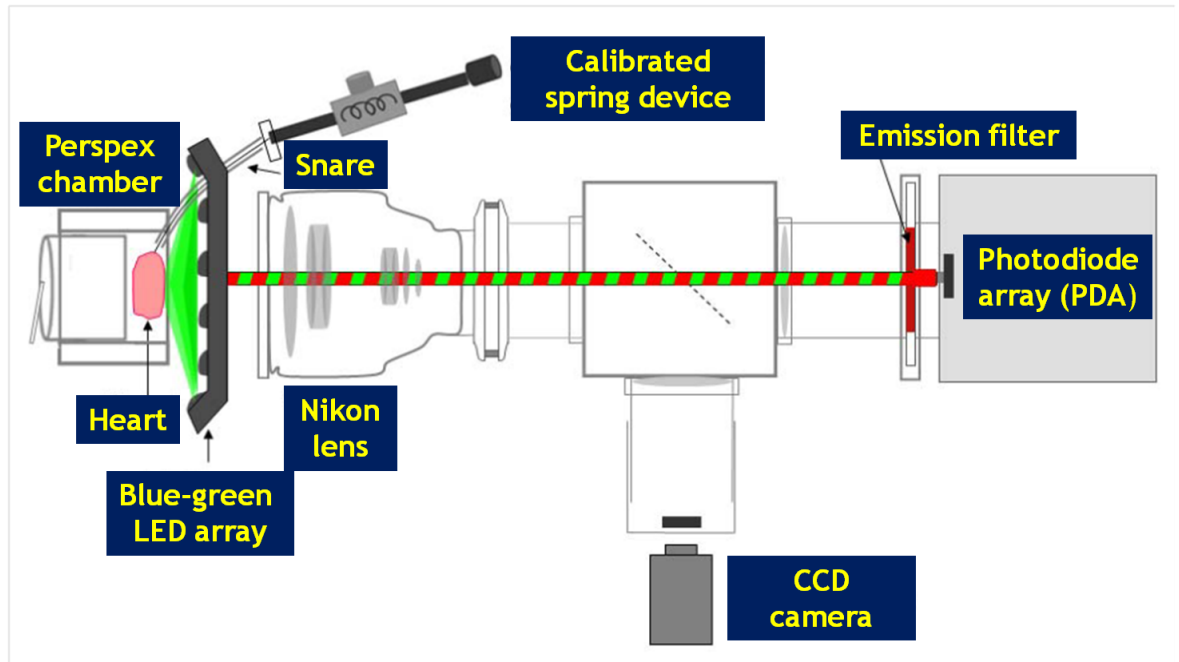
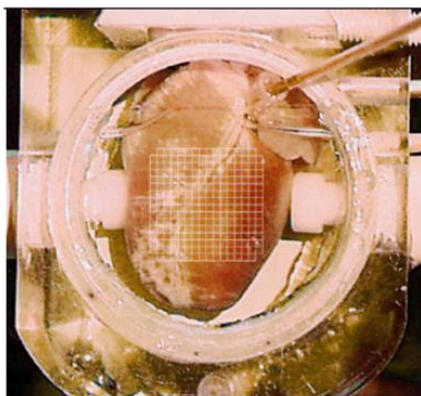
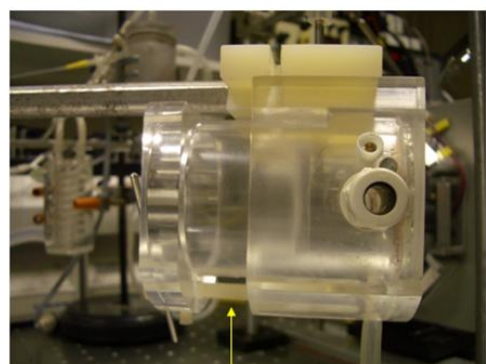


Figure 2.3 Diagram of single view optical mapping set-up.

(a)



(b)



Back piston

Figure 2.4 Photographs of the heart inside the perspex chamber. (a) Front view of the chamber. (b) Side view of the chamber showing the back piston which can produce a gentle compression of the heart when pressed against the front plate.

Panoramic view optical mapping

The methodology relating to panoramic mapping will be described in detail in Chapter 8.

Work involving animals

Altogether in this study, a total of 91 rabbits were used of which 79 rabbits were used for *in vitro* experiments (Chapter 3, 4, 5, 6 and 8) and 12 rabbits were used for *in vivo* experiments (Chapter 9). All procedures involving animals were performed in accordance with the UK Animals (Scientific Procedures) Act 1986 and complying with the Guide for the Care and Use of Laboratory Animals published by the US National Institutes of Health (NIH Publication No. 85-23, revised 1996).

The rabbit coronary artery occlusion during Langendorff perfusion

This study used a model of acute coronary artery occlusion during the experiment to study the relation between acute myocardial ischaemia and its link to ventricular arrhythmia.

Coronary artery occlusion by using ligation technique

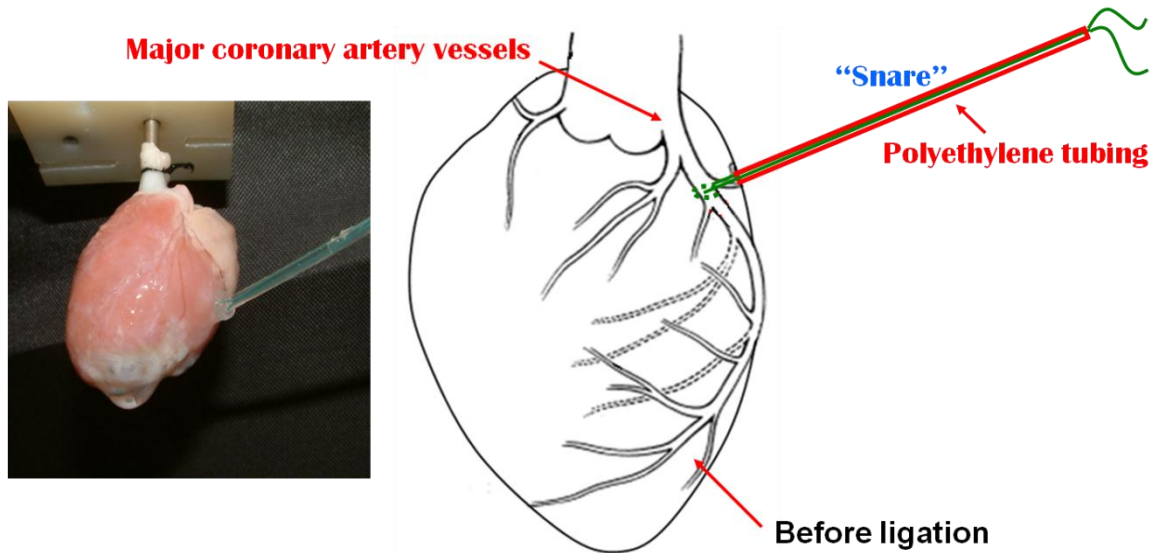
The ligation technique to occlude the coronary artery during experiment has been developed in our lab by a previous PhD student, (Petchdee, 2009). Adult male New Zealand White rabbits (2.5 - 3.5 kg) were sacrificed by terminal anaesthesia using intravenous injection of 0.5ml/kg Euthatal (sodium pentobarbitone 200mg/kg, Merial) mixed with 1000 IU of heparin injected through the left marginal ear vein. The heart was rapidly excised, immersed in chilled Tyrode's solution to temporarily stop the heart contraction. The heart was then retrogradely perfused (Langendorff mode) at a rate of 20 ml/min (Gilson Minipuls peristaltic pump) with chilled Tyrode's solution of the following composition (in mmol/L: Na^+ 134.5, K^+ 5.0, Ca^{2+} 1.9, Mg^{2+} 1.0, Cl^- 101.8, SO_4^{2-} 1.0, H_2PO_4^- 0.7, HCO_3^- 20, acetate 20 and glucose 25) for vessel visualization. With the help from an external light source, the coronary artery was identified and differentiated from the superficial coronary vein. Once the coronary artery

was identified, a 4-0 polyester suture (Ethibond™) was used to ligate the proximal part of the left postero-lateral division (PLD) of the rabbit coronary artery (Podesser *et al.*, 1997). The suture was then threaded through a short piece of 2mm diameter polyethylene tubing forming a snare (Figure 2.5). This procedure took approximately 3 - 5 minutes.

The snared heart was subsequently transferred to the optical mapping set-up. The heart then mounted onto an aortic cannula of the Langendorff system and perfused with Tyrode's solution, filtered through a 5µm filter (Millipore) before the experiment started. The pH of the solution was maintained at 7.4 by continuous bubbling with 95% oxygen (O₂) / 5% carbon dioxide (CO₂) medical gas mixture (BOC Gas, UK). The perfusing solution as well as the solution surrounding the heart inside the chamber was maintained at 37°C by a glass-column heat exchanger connected to a thermostat-controlled water bath.

Langendorff perfusion was by a constant flow rather than constant pressure method. A constant flow of 30 ml/min was used throughout the experiment. Perfusion pressure was continuously monitored with a transducer connected to the aortic cannula. The initial perfusion pressures from all the experiments normally ranged from 20-30 mmHg. Pressures would typically increase by 20-30 mmHg throughout the experiments (2-3 hours). Perfusion pressures were closely monitored and recorded at a regular interval over the course of the experiments.

(a) Before ligation



(b) During ligation

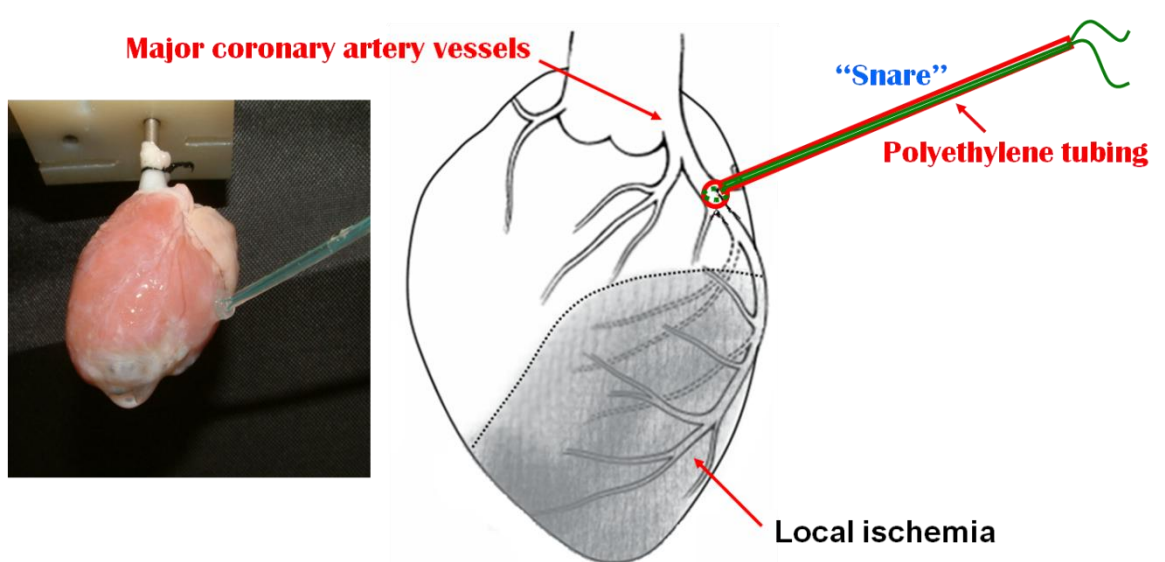


Figure 2.5 Method to produce acute local ischaemia in isolated rabbit hearts.

(a) Before ligation. (b) During ligation, the left postero-lateral division (PLD) of the coronary artery was occluded with a suture using a short piece of polyethylene tubing to form a snare. The ligature was connected to a calibrated spring device. To produce a local ischaemia, the snare was tightened for 30 minutes. In this example, the heart had a bifurcation branching pattern (see Figure 1.5 – page 32 on rabbit coronary artery distribution).

To produce a local ischaemia during the experiments, two different set-ups for the acute ligation system were used:

Horizontal ligation set-up

In the single view optical mapping experiments (described in Chapter 3) the ligature from the snare was passed through a small hole at the left side of the perspex chamber and connected to a calibrated spring device. This device was calibrated in a way to apply a minimum force on the snare required to produce a reversible coronary artery occlusion (Petchdee, 2009). During the experiments, the spring was tightened for 30 minutes to occlude the vessel and produce a local ischaemia. After 30 minutes of occlusion, the snare was released to allow reperfusion of the previously ischaemic region.

Vertical ligation set-up

The vertical ligation set up was used to produce acute regional ischaemia in the panoramic optical mapping experiments (see Chapter 8). This method is described in detail in Chapter 8.

Pacing protocols

To investigate the epicardial electrical conduction, two types of pacing method were used in this study.

Ventricular pacing (VPACE)

Ventricular stimulation was the main pacing method used in single view optical mapping experiments involving the drug E-4031 (Chapter 4) and isoprenaline experiments (Chapter 6) with the aim to pace the hearts at the required cycle length. In these experiments, the hearts were subjected to AV node ablation in order to be able to pace the hearts slower than the intrinsic rate; hence VPACE was used instead of APACE. Custom made bipolar platinum stimulating electrodes were used to produce point stimulation on the ventricular epicardial surface. Most of the time, the stimulating electrodes were placed over the base of the right ventricular area. The electrodes were inserted via a 1mm hole in front of the perspex chamber.

Atrial pacing (APACE)

The atrial pacing method was mainly used in the panoramic view optical mapping experiments (refer Chapter 8). In this set of experiment, the heart was paced at a fixed rate 350ms cycle length. Atrial pacing was used to get an activation pattern as close as possible to the pattern *in vivo*. Pairs of platinum hook electrodes were placed in the right atrium.

For each pacing method, a constant voltage source (Digitimer DS2A-MKII stimulator) which provided a square pulses with width 2ms was used throughout. The stimulus threshold was measured and the voltage set at twice that required to capture the myocardium. Timing of the pulse was computer-controlled using a locally developed program written by Dr Francis Burton, University of Glasgow. Details of the pacing protocol will be given in respective chapters.

Optical data

Optical action potentials (OAPs)

Optical imaging with voltage-sensitive dyes allows simultaneous recording of action potentials from hundreds of sites over a range of scales from single cell to whole heart. These optical action potential signals are produced from a group of membrane-bound dye molecules within a volume of tissue. This volume depends on: (i) the optical magnification of the imaging system (ii) the depth of focus of the optics (ii) the pixel density of the camera sensor.

Optical signals were obtained from a 16x16 array yielding 252 useable pixels (4 pixels in each corner being reserved for ECG and pacing signals). Each pixel had a sensing area of 0.95mm x 0.95mm and the distance between the centres of neighbouring recording pixels was 1.1mm. With an optical magnification of x1.2, each pixel detected light from an epicardial area of 0.8mm x 0.8mm. The depth of field can be calculated from the equation obtained from the optics used in this thesis:

$$\begin{aligned}
 \text{Depth of field} &= 1000\mu\text{m} / [(7 \times \text{NA} \times \text{magnification}) + \lambda_{\text{ex}} / 2(\text{NA})^2] \\
 &= 1000 / [(7 \times 1.4 \times 1.2) + 0.535 / 2 \times 1.4^2] \\
 &= 90\mu\text{m}
 \end{aligned}$$

(NA = Numerical Aperture, λ_{ex} = emission wavelength)

From this calculation, the optical signal in this study originates from the tissue within 90 μm of the epicardial surface, corresponding to approximately 6 cell diameters.

Optical data analysis

The optical signals obtained from this study were analysed using custom analysis programme, OPTIQ (locally developed by Dr FL Burton, University of Glasgow). The optical action potentials (OAPs) were averaged and spatially filtered with a Gaussian filter. Further temporal filtering was done by using Medians + Boxcar filter. Several parameters such as action potential duration at 50%, 75% and 90% of repolarisation (APD_{50} , APD_{75} , and APD_{90} , respectively), the activation time (T_{ActM}), the repolarisation time (T_{Repol}) and colour maps for these parameters were generated using this software. OPTIQ could also generate a movie-like display of the activation spread across the mapped region on the ventricular epicardial surface.

In this study, activation time was defined as the midpoint of the upstroke (T_{ActM}). Another way to define activation time was based on the time at the first derivative (i.e. the fastest rate of rise during the AP upstroke). Repolarisation time (T_{Repol}) was defined as the time at return to baseline from the peak. In this study, the time at 50% repolarisation was used to calculate the APD at 50% repolarisation (APD_{50}) and the time at 90% repolarisation was used to determine the APD at 90% repolarisation (APD_{90}). APD was defined as $T_{Repol_{50}}$ minus T_{ActM} (for APD_{50}) or $T_{Repol_{90}}$ minus T_{ActM} (for APD_{90}). In this study, APD_{50} and APD_{90} were chosen for analysis in different sets of experiments. The definition of T_{ActM} , T_{Repol} and APD were illustrated in Figure 2.6.

For analysis purposes, APD_{90} was chosen in experiment involving E-4031 in Chapter 4 because the maximal effect of E-4031 is during the later part of the repolarisation (Phase 3 of AP). Therefore, APD_{90} would give a better indication of the effect of E-4031 on APD. APD_{50} was chosen for analysis in experimental work involving acute coronary artery occlusion (Chapter 5, 6, and 8) because during ischaemia, there was triangulation of the ventricular AP. Therefore, the effect was much clearer at APD_{50} as compared to APD_{90} .

Action potential

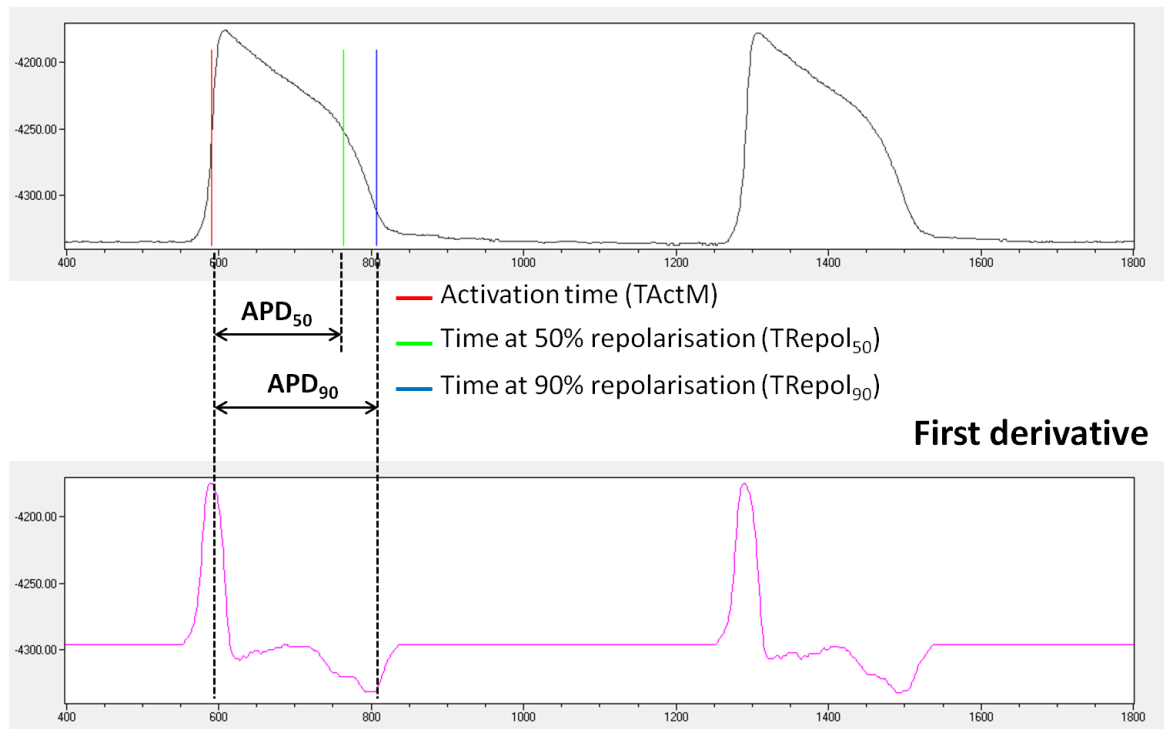


Figure 2.6 Definition of TActM, TRepol and APD

Illustration on the definition of activation time (TActM) and time at 50% and 90% repolarisation (TRepol₅₀ and TRepol₉₀, respectively) based on analysis of the optical action potentials and first derivative in OPTIQ software. APD₅₀ was calculated based on the difference between TRepol₅₀ and TActM and APD₉₀ was determined by the difference between TRepol₉₀ and TActM.

ECG data

ECG signals recording

In single view optical mapping experiments, simultaneous pseudo-ECG recording was obtained by using pairs of silver chloride disc electrodes inserted into both sides of the chamber. For panoramic view optical mapping experiments, the ECG electrodes were the vertical structural bars in the rotating chamber. Signals from these electrodes were amplified with an isolated amplifier (custom built by Medical Electronics, University of Glasgow) and displayed on oscilloscope (Nicolet Instrument Corporation, Wisconsin, USA) to allow real time viewing. During optical recordings, the 2 corner channels of the PDA were used to store the ECG and pacing stimuli traces. Continuous pseudo-ECG signals were also recorded onto a laptop computer using a USB compatible digitizer (DI-158U, Dataq Instruments Inc).

ECG data analysis

ECG provides a non-invasive assessment of the electrical activity of the heart and can be measured with equal facility in *in vivo* and *in vitro* preparations. In *in vitro*, changes in ECG parameters may be correlated with changes in action potential produced by experimental interventions. ECG recordings from the experiments were analysed using ChartTM 5 Pro (ADInstruments) software (Figure 2.7). The main ECG parameters extracted using this software were RR, PR, QRS and QT intervals (P, R and T amplitude information was available but not used). The software works in a semi-automated way; the computer assigns a cursor at certain points on each of the ECG beat, but may be manually overridden. The landmarks for the cursors are P start, P peak, QRS start, QRS end, T peak and T end (Figure 2.7b); the results can be displayed in a table form (Figure 2.7c). Reliability of the data depends on the quality of the ECG recordings, a limitation explained further in Chapter 9.

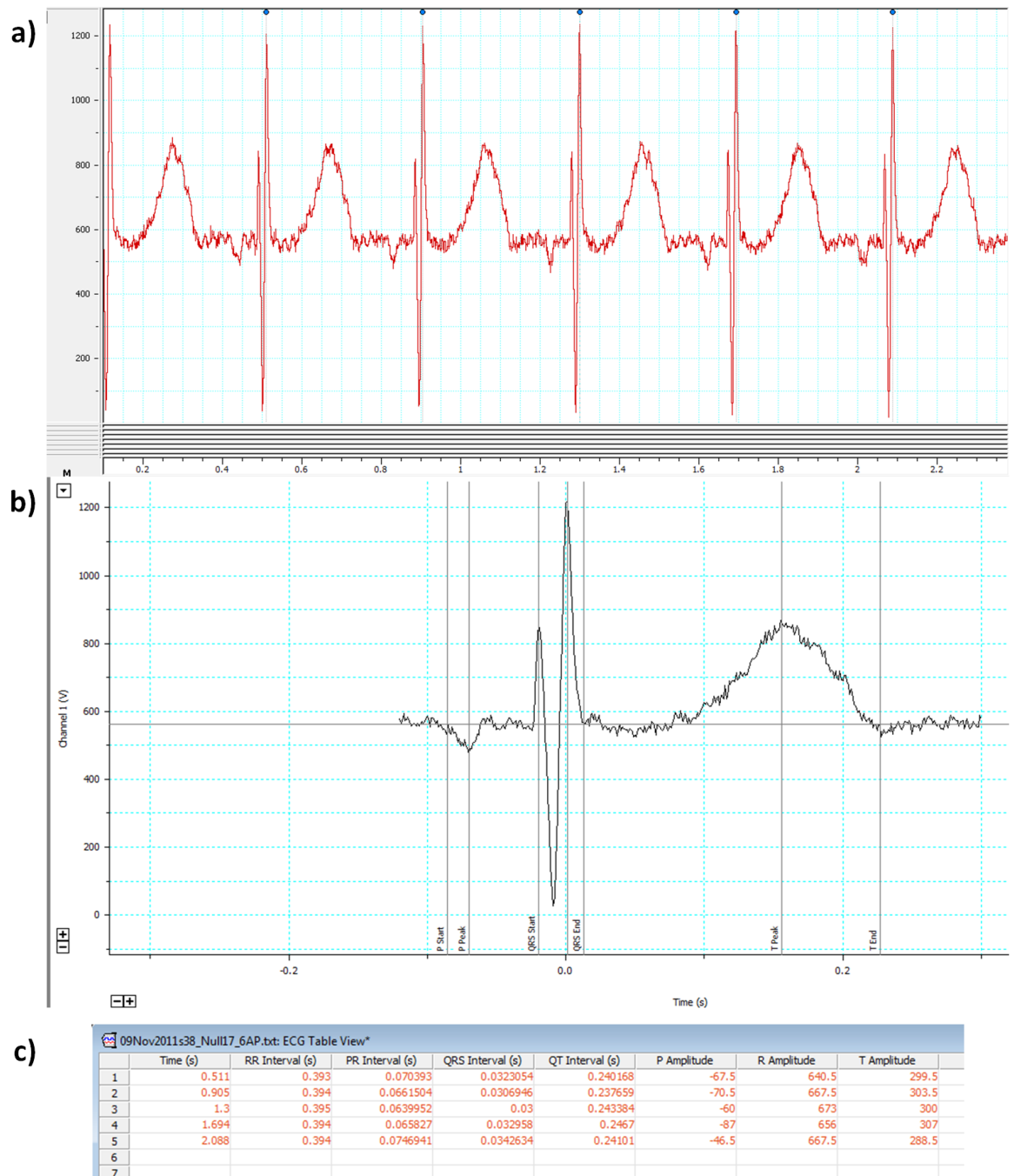


Figure 2.7 ECG analysis.

Example of display from software ChartTM5 Pro showing a) typical ECG traces from acute coronary artery ligation experiments, b) the averaged view indicating the placement of cursors to analyze the ECG, and c) the table view showing the results of ECG analysis.

In this study, some instances of PVCs and TWA were observed. For the analysis purposes, PVCs were defined based on the findings of the simultaneous ECG recording in which the PVCs was characterized by premature and broad QRS complexes not preceded by a P wave, and its direction is opposite the major deflection of the normal QRS (Figure 2.8a). As for the T wave alternans, it was defined by a periodic beat-to-beat variation in the amplitude and/or shape of the T wave on the ECG (Figure 2.8b).

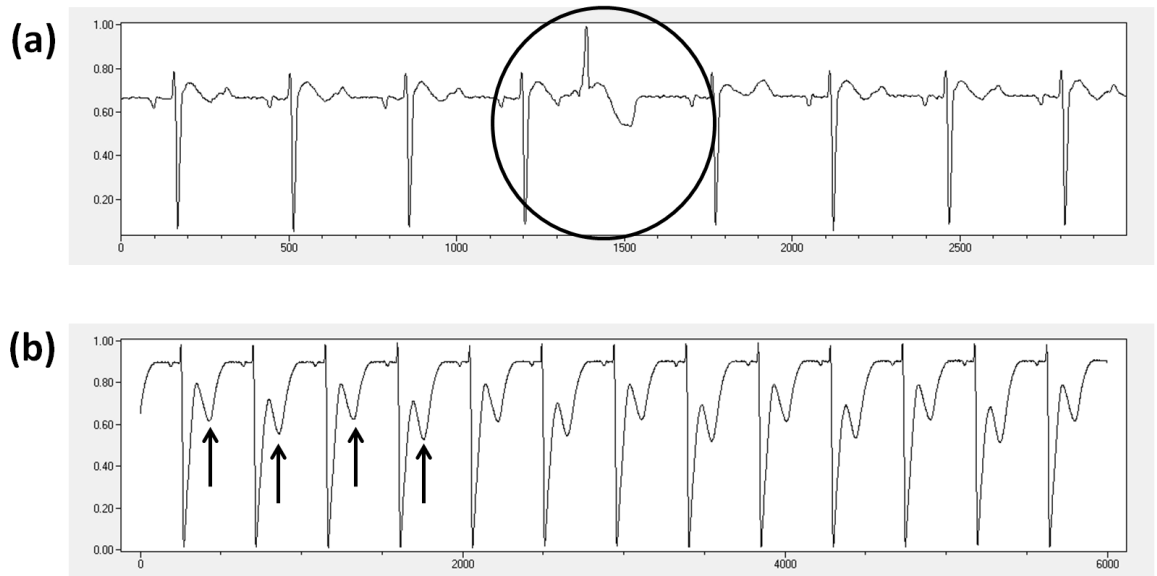


Figure 2.8 PVCs and TWA
Example of ECG demonstrating the instances of (a) PVCs and (b) TWA observed during the optical signal recording.

Statistical analysis

All data obtained in this study are expressed as mean \pm standard error of the mean (SEM). To perform significance testing, data were imported into GraphPad Prism software. Time courses of the APD changes from pre-occlusion period and occlusion period within the same heart were compared by repeated measures ANOVA. The parameters at specific time points in VF hearts were compared with the same parameters at corresponding time points in no-VF hearts using unpaired Student's t-test. A two-tailed p-value of less than 0.05 was considered significant. The data obtained in this study have been tested for normality using one-sample Kolmogorov-Smirnov test (one-sample K-S test) performed in SPSS software and based on this test, all data were normally distributed.

Chapter 3: Use of ratiometric approach to examine membrane potential signals with voltage-sensitive dye

Aim

This chapter will discuss the application of the voltage-sensitive fluorescence dye emission ratiometric technique as a means of studying the spatial distribution of voltage signals across the epicardial surface. This is desirable because successful application of this technique would allow *absolute* voltage signals to be compared, also in addition to reducing the effects of motion artefacts and baseline drift on the optical signal.

Introduction

Transmembrane potentiometric dyes have been widely used in electrophysiology study to monitor the electrical activity such as action potentials and membrane polarization in intact heart as well as in various cardiac cells or tissue preparations. However, voltage-sensitive fluorescence measurements are limited by baseline drift and motion artifacts which could obscure the changes in resting membrane potential and repolarisation, respectively. A study done by Knisley *et al.* (2000) found that the ratio calculated as the short wavelength divided by the long wavelength of the fluorescence emission reduces the effect of motion artifacts.

Work by Beach *et al.* (1996), Bullen *et al.* (1997), Knisley *et al.* (2000) and Montana *et al.* (1989) has employed the concept of dual wavelength ratiometric approach to measure membrane potential with voltage-sensitive dyes (VSDs). Dual wavelength ratiometric measurements with VSDs are based on the concept of spectral shift in which there are opposite changes in voltage-dependent optical signals at the low and high wavelength wings of the spectra as shown in Figure 3.1. Loew (2001) described that membrane depolarisation results in a shift of the emission spectrum of the dye to shorter wavelength upon excitation of the dye molecules from the ground state to the excited state. Thus, there will be an increase in the fluorescence intensity at short wavelengths and a decrease of the fluorescence intensity at long wavelengths.

This mechanism serves as a basis for the ratiometric approach, in which the fluorescence from bands either side of the peak of the emission spectrum are measured and their ratio calculated. This is based on the assumption that the

spectrum will only shift but not change shape or amplitude (Loew, 2001). The main advantage of this approach is that the ratio sensitivity is roughly equivalent to the absolute sensitivities at each wavelength. Another advantage is that the ratio value calculated from the dual wavelengths should relate to absolute voltage of the transmembrane potential independent of the absolute magnitude of the individual signals (Loew, 2001).

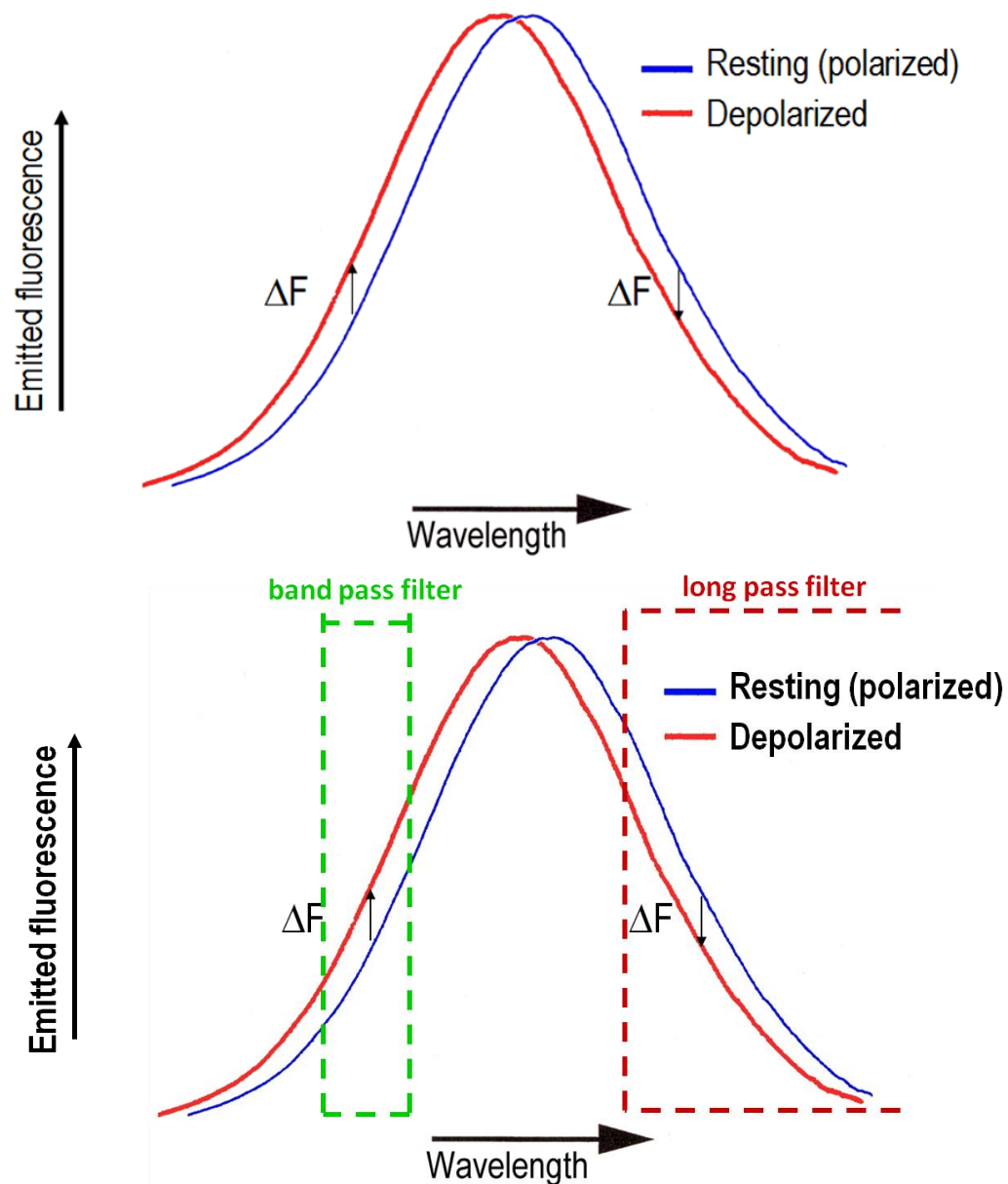


Figure 3.1 Voltage-dependent spectral shift.

Top: Voltage-dependent shift in spectrum for a voltage-sensitive dye. During depolarisation, there is a decrease in fluorescence at the red wing of the spectrum and an increase in fluorescence on the blue wing of the spectrum. **Bottom:** The spectral shift with band pass filter to monitor shorter wavelength and long pass filter to pick up the longer wavelength. Modified from Loew (2001).

Methods

Heart preparation

A total of 4 rabbits were used in this set of experiments. Hearts from male New Zealand White rabbits (2.5 - 3.5kg) were obtained as previously described, and Langendorff-perfused with the standard Tyrode's solution at 37°C.

Ratiometric fluorescence emission recording

Optical mapping set-up

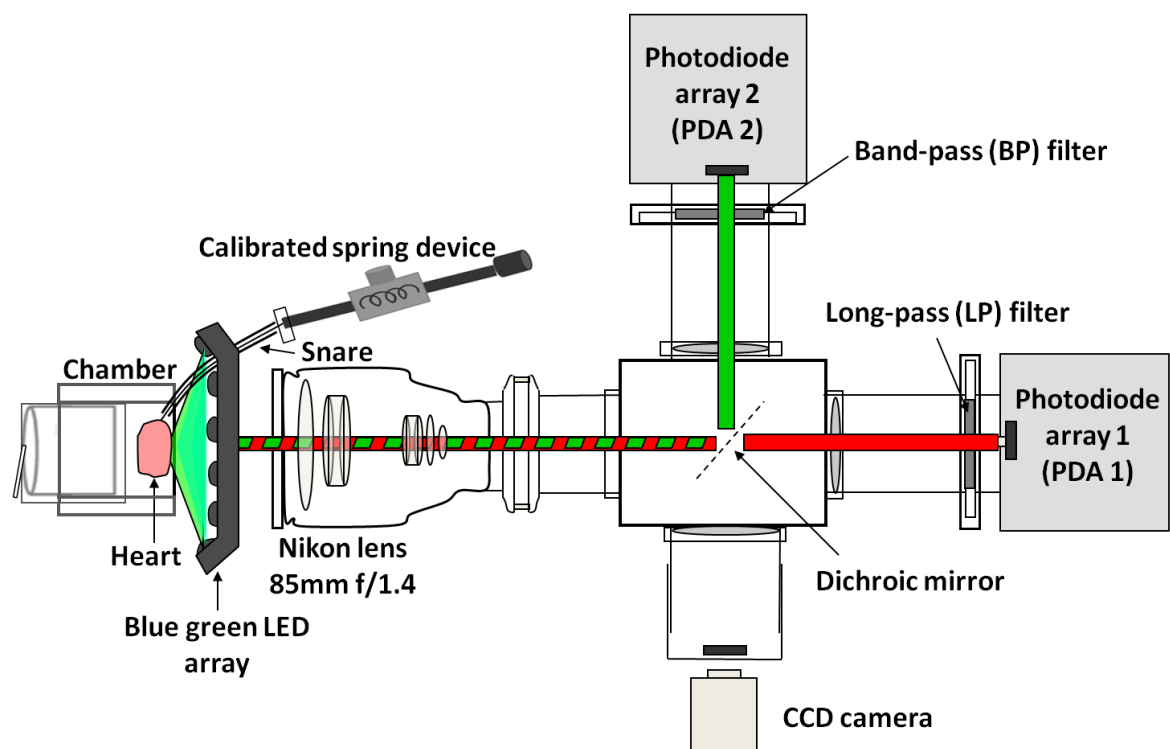


Figure 3.2 Schematic diagram of optical mapping set-up.
Optical mapping set-up for voltage-sensitive dye emission ratiometric experiments.

Figure 3.2 demonstrates the optical mapping arrangement for dye emission ratiometric experiments. Excitation light from an array of blue-green LEDs with a centre wavelength of 505nm (Cairn Research Ltd, Kent, UK) was used to excite dye molecules from the epicardial surface of the heart. The fluorescence emitted from the stained heart surface was collected with a camera lens (Nikon 85mm, f/1.4) and passed through a 45 degrees dichroic mirror (Comar Instruments). Fluorescence signals were then focused on two 16 × 16 element (256) photodiode arrays (PDA) (Hamamatsu Photonics). Depending on the filter

set being used, the image with longer wavelength than the cut-on wavelength of the dichroic mirror was focused on PDA1 after being passed through a long-pass filter whereas the image with shorter wavelength than the cut-on wavelength of the dichroic mirror was reflected and focused on PDA2 after passing through a band-pass filter.

In these experiments, different filter sets were used in two sets of experiment. The filter sets were as follows:

Filter set 1:

Dichroic mirror = 645nm

Band-pass filter = 605/55nm

Long-pass filter = 695nm

Filter set 2:

Dichroic mirror = 680nm

Band-pass filter = 645/75nm

Long-pass filter = 695nm

Three experimental protocols were done with filter set 1 and one experiment was done with filter set 2.

Experimental protocols

Background signals recording

After the heart was mounted in the chamber and retrogradely perfused in Langendorff mode with Tyrode's solution, background optical signals produced by the heart in the absence of voltage-sensitive dye were recorded.

Signals recording after dye loading

Then, a bolus of 100 μ L voltage-sensitive fluorescence dye RH237 (stock solution dissolved in DMSO, concentration 1mM) was injected into the heart, through an injection port proximal to the aortic cannula (Chapter 2). The optical signals were recorded after 5 minutes to give enough time for the dye to diffuse into the myocardium and stain it. Serial recordings were done at the intrinsic rate of

the heart and during ventricular pacing at 250ms cycle length. Action potentials (APs) were acquired for 6 seconds during each recording. Simultaneous ECG signals were obtained using two electrodes inserted into both sides of the chamber and amplified and displayed on an oscilloscope (Nicolet Instrument Corporation, Wisconsin, USA) to allow real-time viewing of the ECG.

Hyperkalaemic induction

Previous study done by Kishida *et al.* (1979) has shown that the resting membrane potential in cardiac tissue is depolarized by extracellular hyperkalaemic induction. Therefore, a bolus of potassium chloride (400mM) was injected into the heart to alter the resting membrane potential in order to study the efficacy of emission ratiometry. The KCl bolus was given through the same injection port used to inject the dye. Signals were recorded immediately after the KCl injection and acquired continuously over the following 2 minutes.

Coronary artery ligation

Coronary artery ligation to produce acute local ischaemia in isolated rabbit hearts was achieved by using snare technique as being described in Chapter 2. The left posterior division of the coronary artery was occluded with a suture using a short piece of polyethylene tubing to form a snare. The ligature was connected to a calibrated spring device. To produce a local ischaemia, the snare was tightened for 30 minutes. The electrical activity from this region was optically recorded at 1 minute intervals. At the end of this period, the snare was released to reperfuse the heart.

Spectrophotometry

Spectrophotometry was performed to characterize the excitation light produced by the different LEDs (green and blue-green) as well as the excitation and emission light produced by the voltage-sensitive dye, RH237. Based on this spectrophotometric analysis, the long-pass and band-pass filters that need to be used for the optical mapping set-up were revised.

Data analysis

Fluorescence emission signals obtained from the experiments were viewed and analysed using OPTIQ programme. Further ratiometric calculation of both long and short wavelength was done in MATLAB programme, Ratio Explorer written by Dr Francis Burton (University of Glasgow) (Figure 3.3).

Before calculating the ratiometric values, files containing long and short wavelength from the background (before the dye loading) need to be loaded into the programme. Subsequently, files of long and short wavelength from the recording after the dye loading were loaded into the programme. In any given pixel, changes in fluorescence and ratios were calculated by using this formula:

$$\text{Ratio} = (S - \text{Mean} (S_b)) / (L - \text{Mean} (L_b))$$

For a given pixel, S is the value of short wavelength, S_b is the value of short wavelength from the background, L is the long wavelength value, and L_b is the background value for the long wavelength. The Mean function takes the average signal value over the duration of the recording.

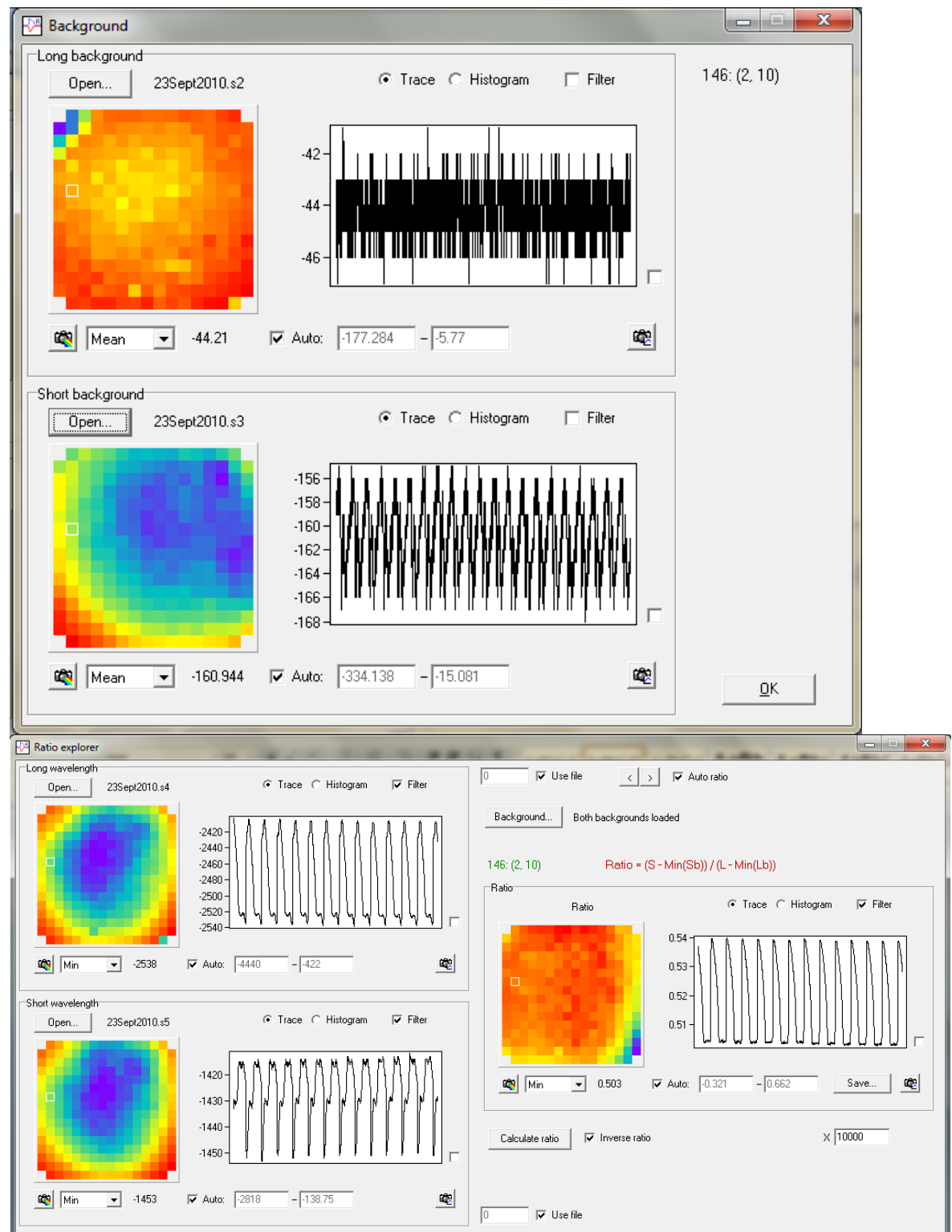


Figure 3.3 Example of display from Ratio Explorer programme.
Top: Signal recording from long and short wavelength acquired before the dye loading (background) displayed as mean fluorescence colour map and action potential traces.
Bottom: The left side shows colour map for minimum (min) fluorescence from long and short wavelengths (above and lower panels, respectively). The right side are the ratiometric values displayed as min fluorescence colour map and the action potential traces.

Experimental results

Spectrophotometric measurement

The measurement of the excitation spectra for two different LEDs (blue-green and green) together with the excitation and emission spectra of voltage-sensitive fluorescence dye RH237 were done using the spectrophotometer. This initial spectrophotometric measurement is important to serve as a basis for determining the LEDs and filter set to be used for the dual wavelength ratiometric experiments. From these results, the blue-green LEDs were chosen as the excitation light source and two different filter sets were used. The band marking for the filter relative to the emission spectra of RH237 are shown in Figure 3.4 (filter set 1) and Figure 3.5 (filter set 2).

Filter set 1

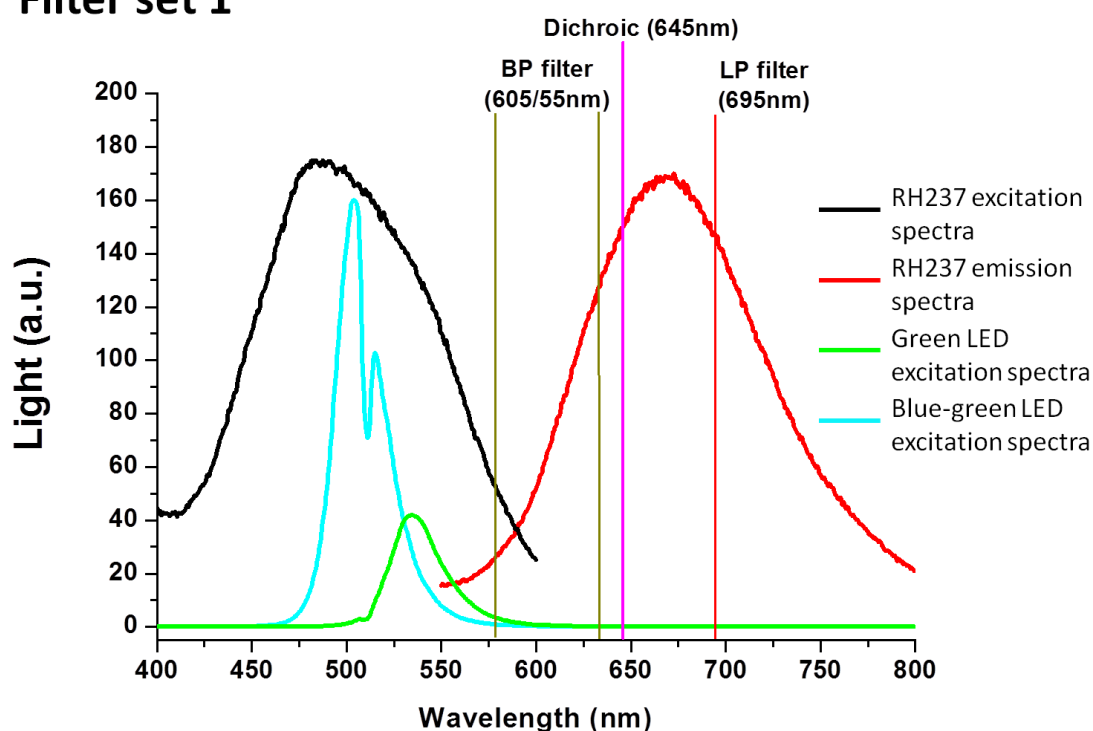


Figure 3.4 Excitation and emission spectra (filter set 1). Graph of excitation and emission spectra of RH237 and excitation spectra from 2 different LEDs with band marking for filter set 1 relative to the emission spectra of RH237.

Filter set 2

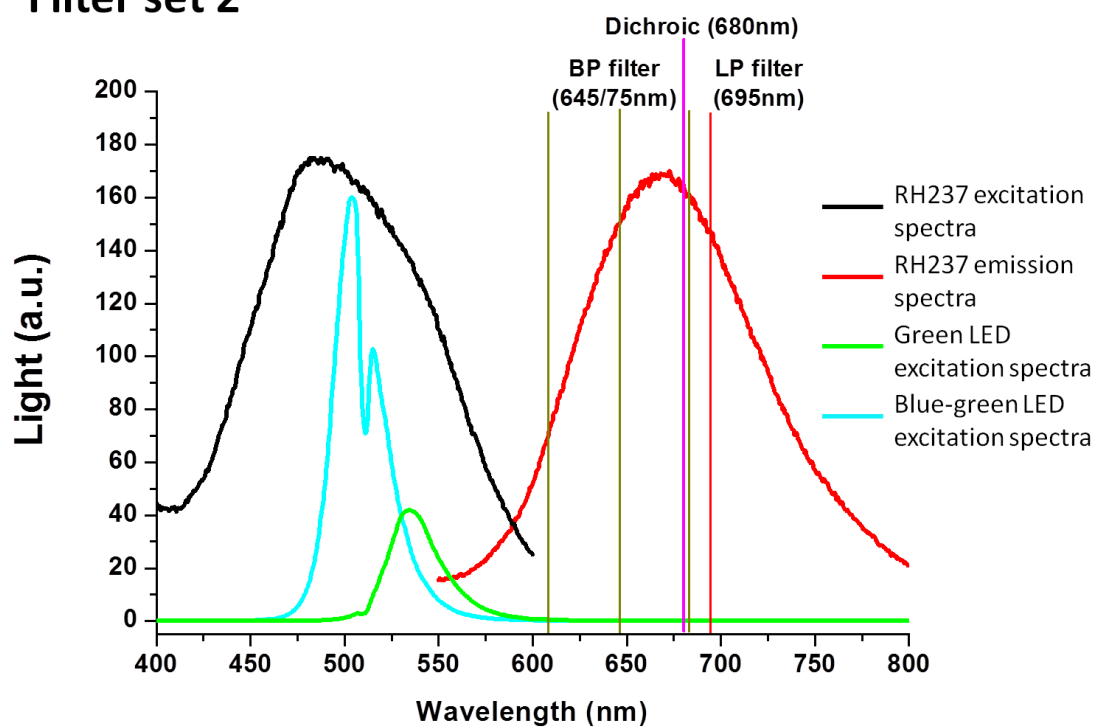


Figure 3.5 Excitation and emission spectra (filter set 2). Graph of excitation and emission spectra from RH237 and excitation spectra from 2 different LEDs with specific band marking for filter set 2 relative to the RH237 emission spectra.

Filter set 1 and Filter set 2

Initially, (n=3) experiments were done with filter set 1; these included acute coronary artery ligation. As Figure 3.6 shows, reasonably good AP traces were recorded at the long wavelength in terms of signal-to-noise, but the AP traces at the short wavelength had very small amplitude (<10 units on a 12-bit A/D). Hence the ratio also had poor signal-to-noise.

Filter set 1

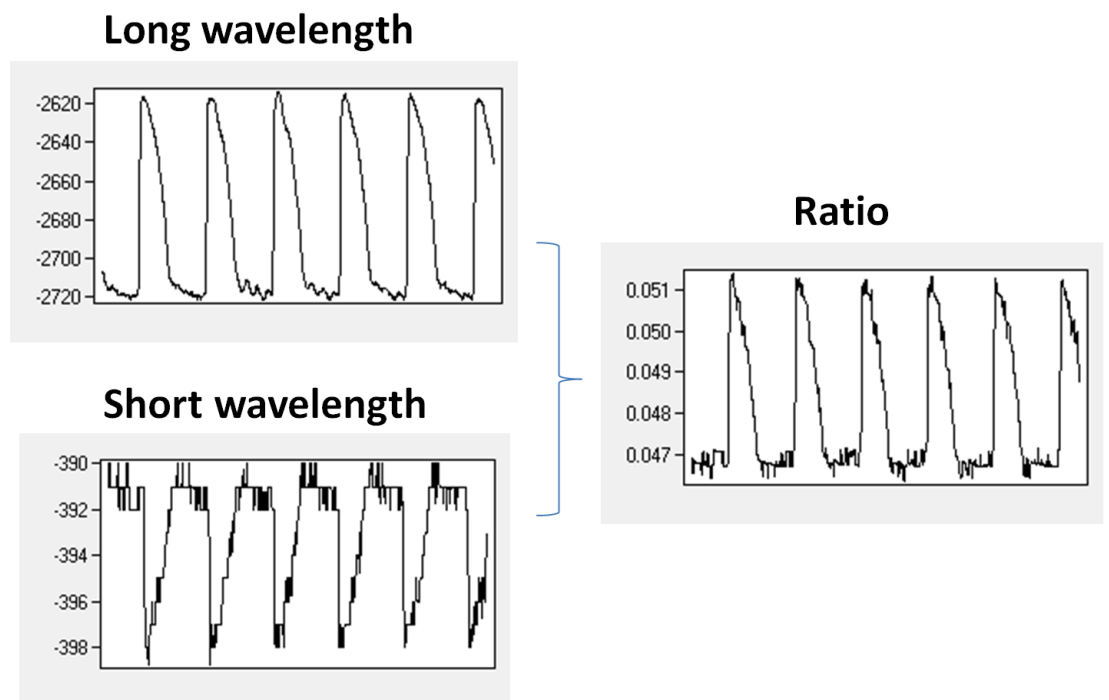


Figure 3.6 Example of signals recording with filter set 1.

After three experiments yielding similar results with filter set 1, the filter set was changed in an attempt to improve the amplitude of the short wavelength signal. Filter set 2 yielded much better signals (Figure 3.7): the amplitude of the signal obtained at the long wavelength was similar to that observed with filter set 1, but the short wavelength signals were significantly larger. Consequently, the ratio was less noisy.

Filter set 2

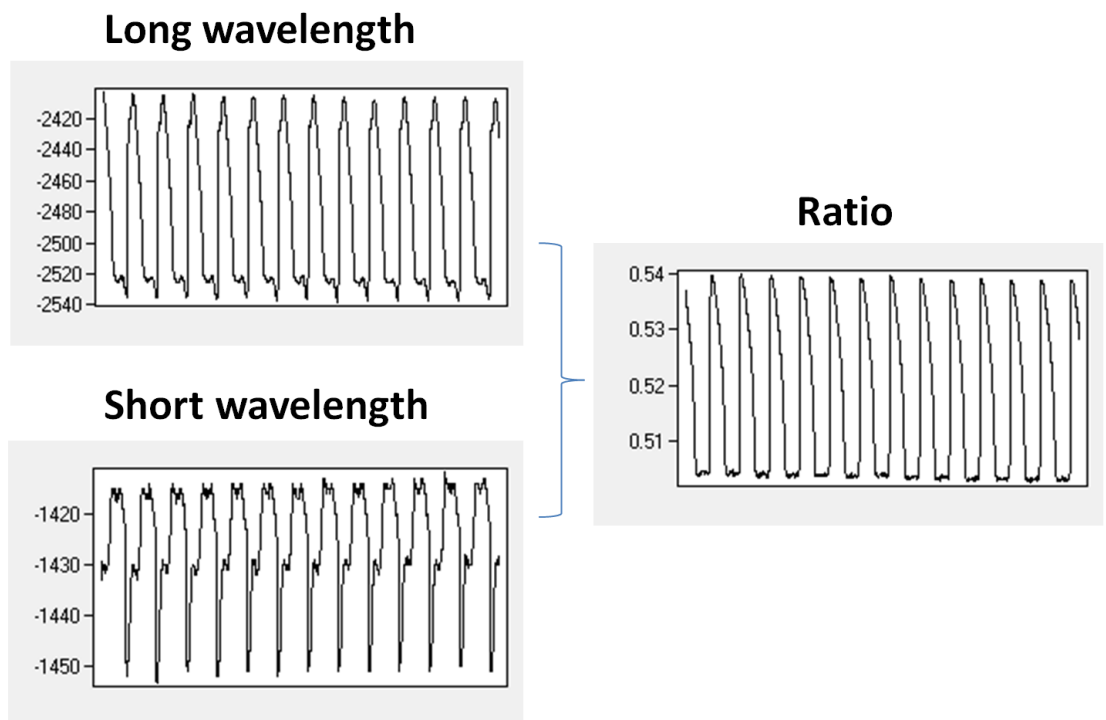


Figure 3.7 Example of signal recording with filter set 2.

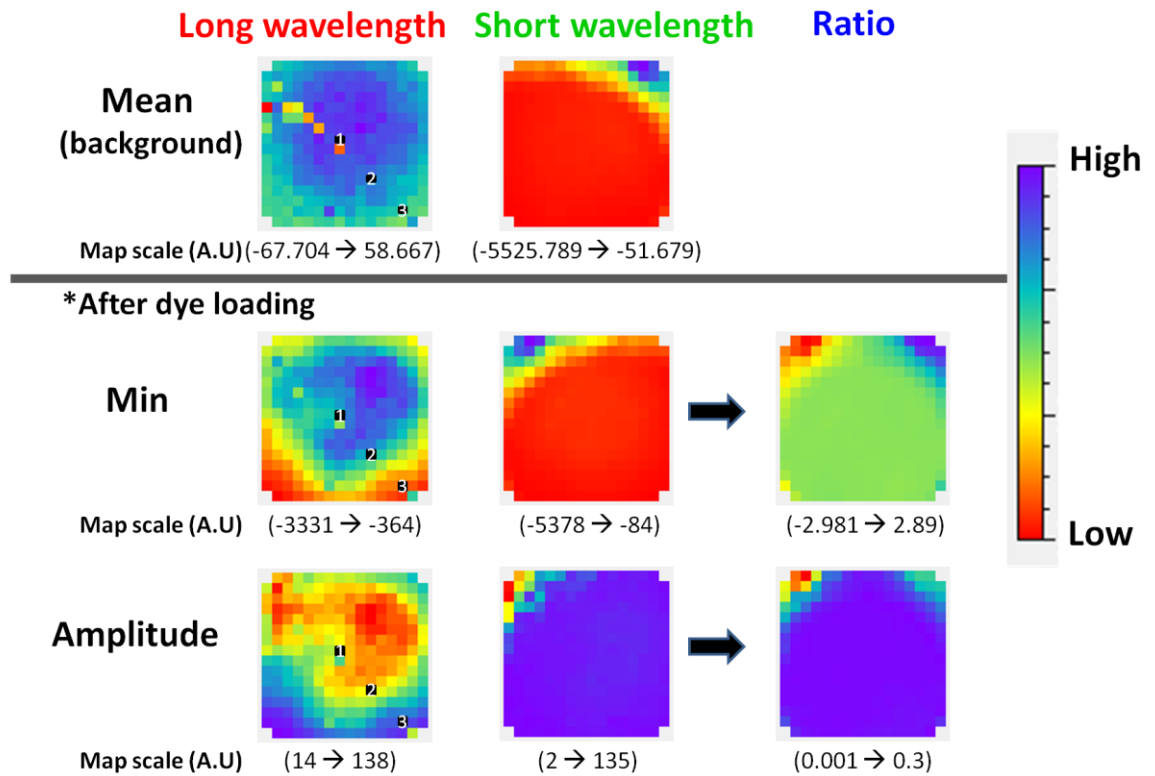
Dual-emission wavelength ratiometric measurement

Acute regional ischaemia (filter set 1)

Dual-emission wavelength measurements were performed for the acute coronary artery ligation experiments using filter set 1. Figure 3.8 shows an example of the colour map of the mean, min and amplitude fluorescence signals from one of these experiments before occlusion. The lower panels display the AP traces of the long and short wavelength as well as the ratio from three different sites marked on the colour map. These three different sites represent areas with different levels of illumination intensity as demonstrated by the colour map. Figure 3.9 shows the mean, min and amplitude colour map of the fluorescence signals obtained from the same experiment, this time recorded 10 minutes after coronary artery occlusion. The amplitude colour map for the long wavelength indicates that the level of fluorescence was uneven; in the middle of the field of view signals had high amplitude compared to the periphery. This was caused by the centre-bright distribution of illumination provided by the array of LEDs.

As shown in Figure 3.8 and Figure 3.9, the combination of filters used in this experiment (filter set 1) produced very small signals in the short wavelength compared to the long wavelength. Although the small amplitude of the short wavelength will reduce the ratio *amplitude* correspondingly, the resting potential from a whole heart should nevertheless be relatively constant. Therefore, we would expect to see a uniform ratio *baseline* throughout the whole field. However, in these experiments we found that the range of the ratios varied markedly between three sample sites of the mapping field in the same heart. The minimum ratio value was 0.054 for site 1 and 0.060 for site 2 and 3.

A) Pre-occlusion

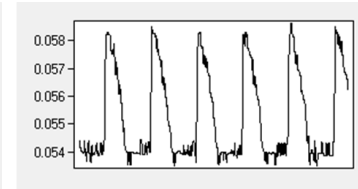
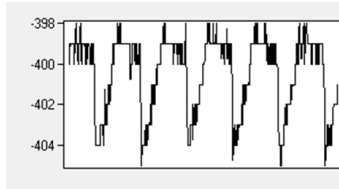
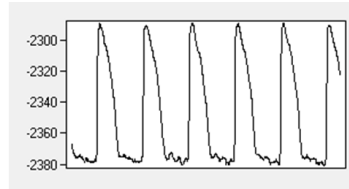


Long wavelength

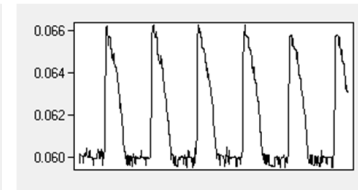
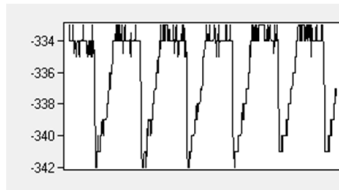
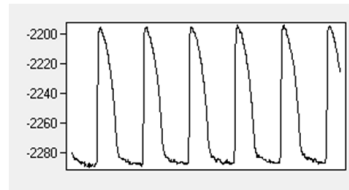
Short wavelength

Ratio

Site 1



Site 2



Site 3

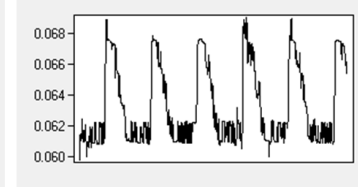
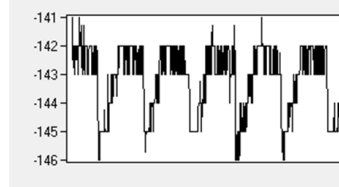
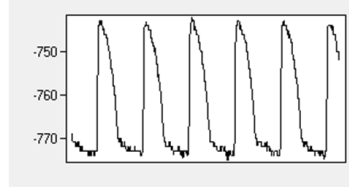


Figure 3.8 Fluorescence signal pre-occlusion.

Example of colour map showing min and amplitude fluorescence signals with the mean colour map from the background. The AP traces in the lower panel correspond to the 3 different sites marked on the colour map.

B) Occlusion 10 minutes

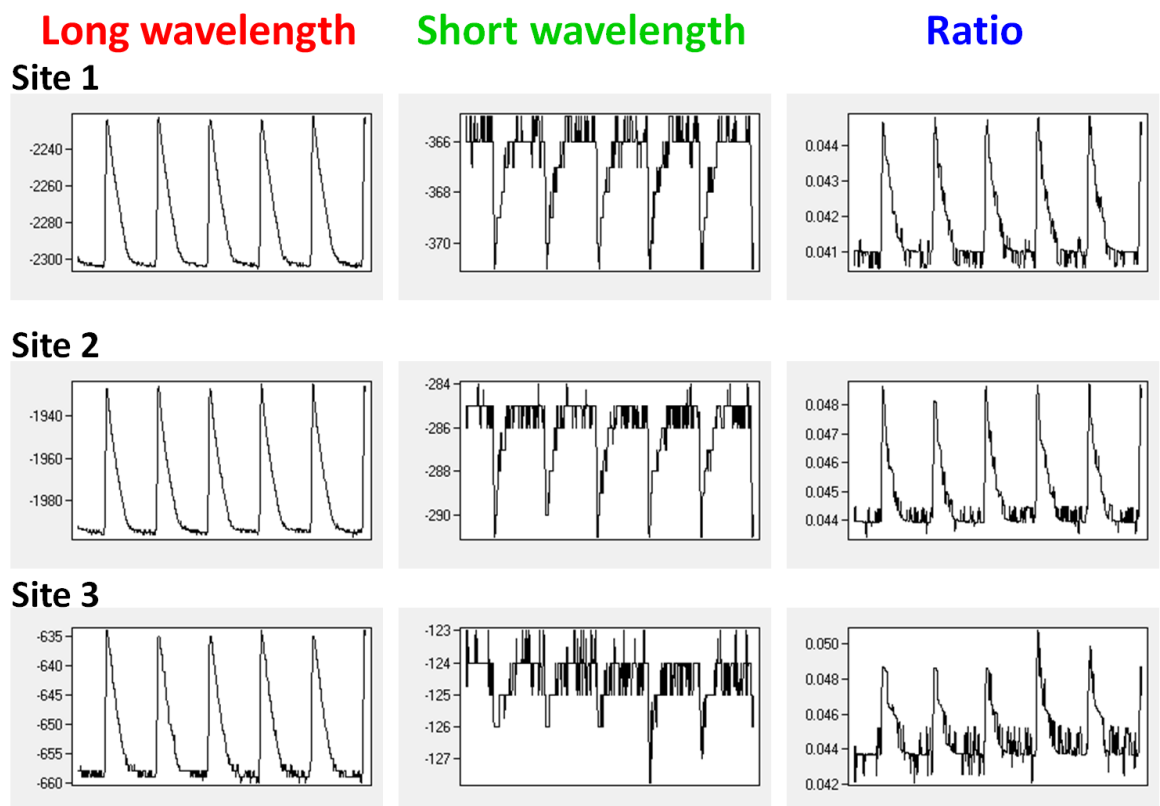
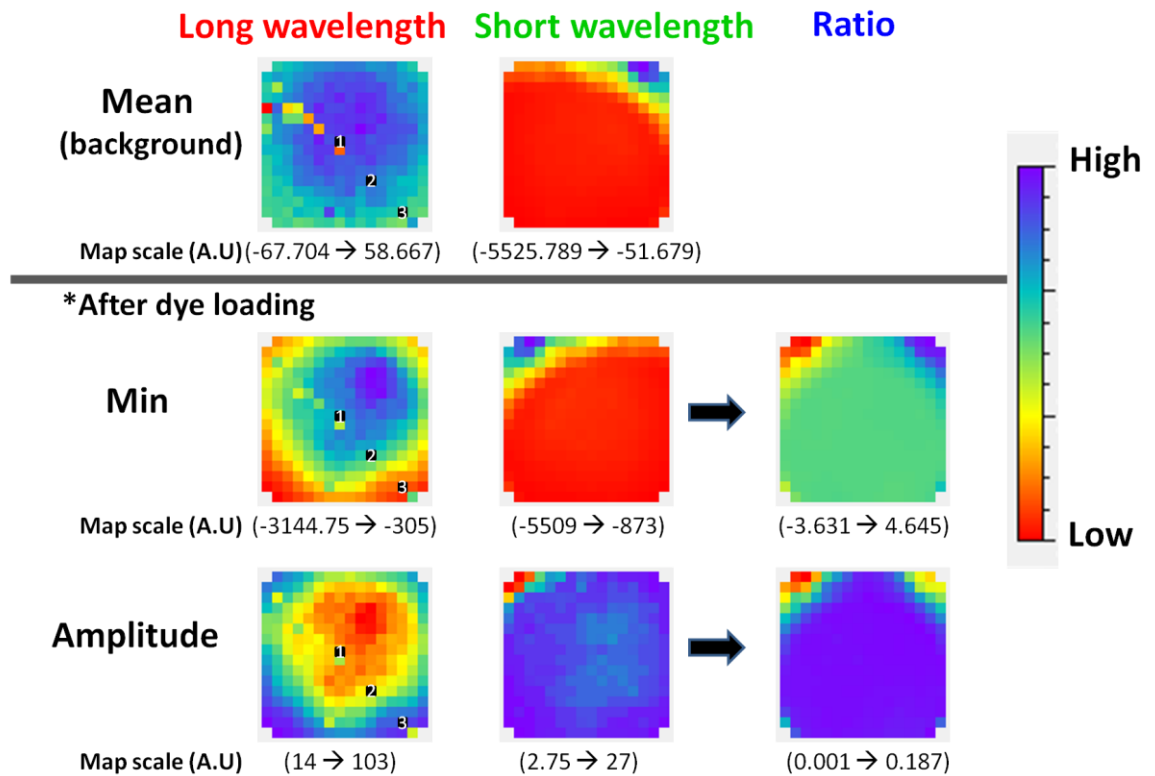


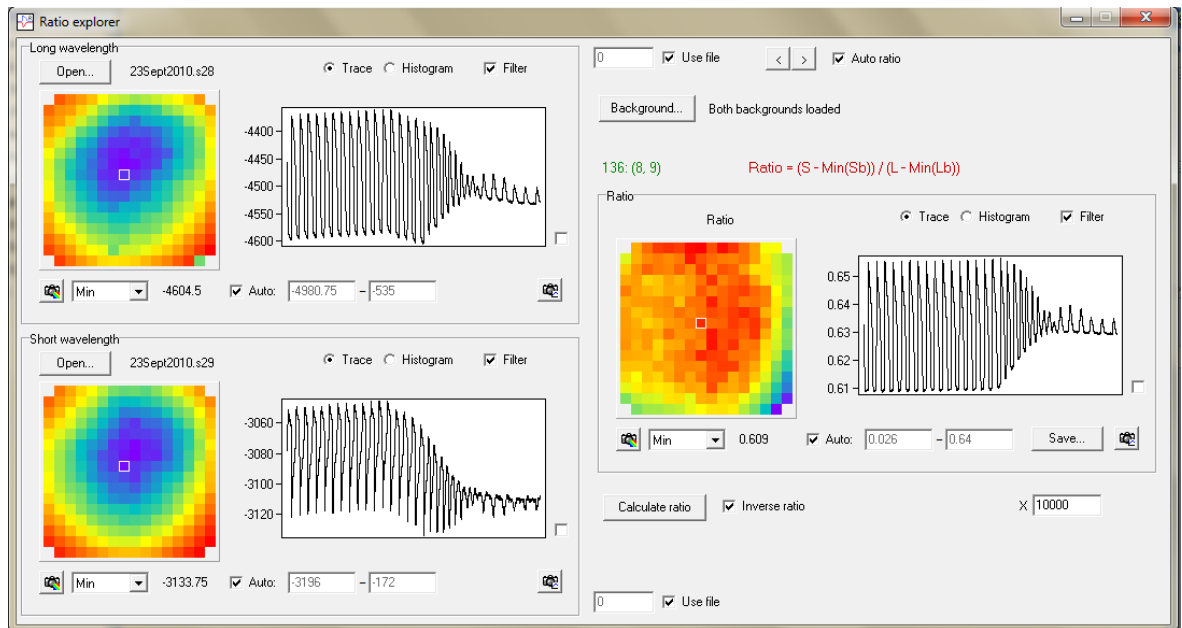
Figure 3.9 Fluorescence signal at 10 minutes occlusion.

Top panel: Example of colour map showing min and amplitude fluorescence signals with the mean colour map from the background. Lower panels show corresponding AP traces from 3 different sites marked on the colour map 10 minutes after ligation.

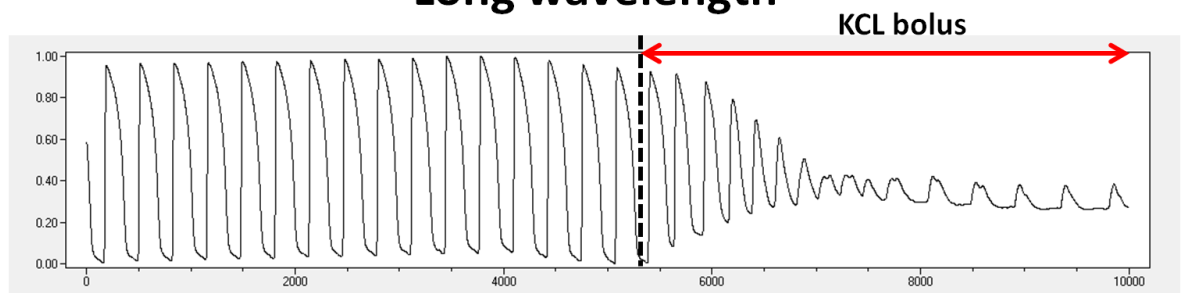
Hyperkalaemic challenge

This hyperkalaemic challenge study was done using filter set 2. A rapidly injected bolus of 1ml KCl (400mM) was used to cause transient changes in resting potential that were reversible and predictable and over a short time scale. The alternative way of producing hyperkalaemic induction by adding KCl to the perfusion solution would lead to much slower changes membrane potential, due to mixing in the perfusion system.

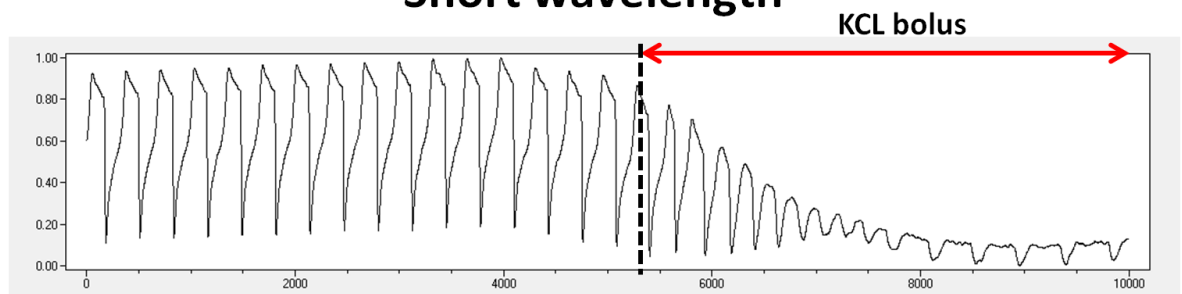
Figure 3.10 shows an example of changes that occur when bolus of KCl was injected into the heart. AP signal amplitude declined rapidly following KCl injection and more gradually returned to the original amplitude on washout (not shown). In this experiment, the amplitude of signals produced from the short wavelength were more similar to that of signals at the long wavelength (Figure 3.11). Even so, there were large variations in ratio values between the three sample sites within the same experiment (Table 3.1).



Long wavelength



Short wavelength



Ratio

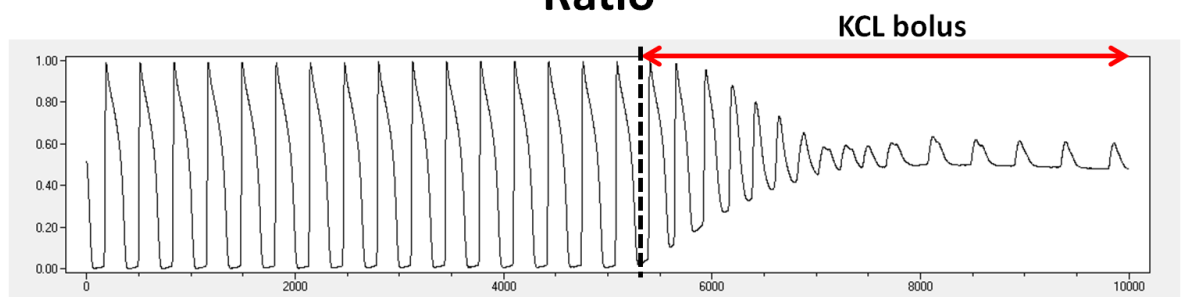


Figure 3.10 Hyperkalaemic induction.

Top panel: Example of display from Ratio Explorer during hyperkalaemic induction. **Bottom panel:** Expanded AP traces from long and short wavelength, and their corresponding ratio showing the AP before and during KCl bolus. The red arrows indicate the timing of KCl bolus.

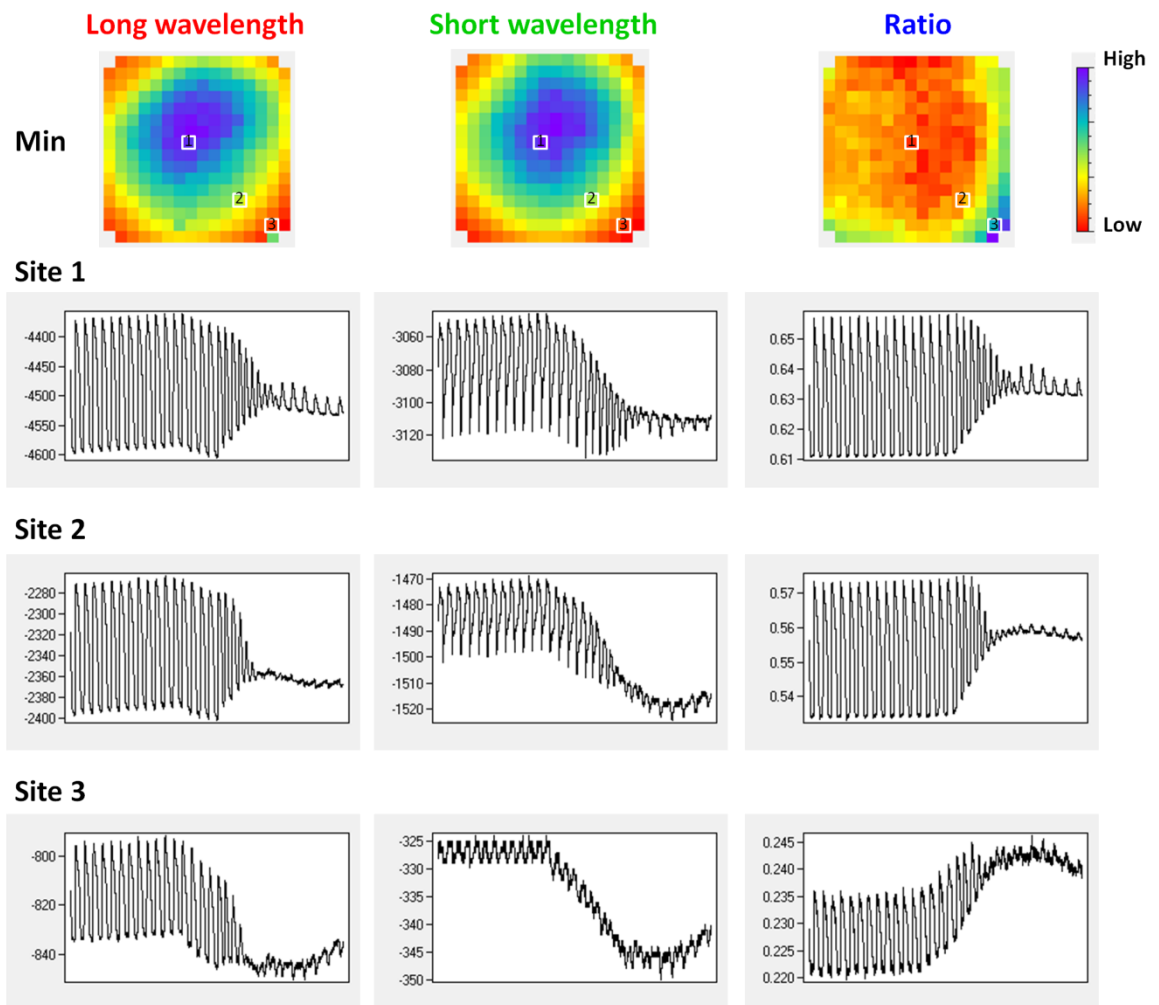


Figure 3.11 Fluorescence signal during hyperkalaemic induction.

Top panel: colour maps showing min fluorescence of long and short wavelength and ratio. Lower panels: APs from 3 different sites with varying level of fluorescence intensity marked on the colour map. The range of ratios produced from the ratiometric calculation for those three sites vary with varying intensity.

Table 3.1 Dual-wavelength ratiometric values with filter set 2.

Comparison between the range of ratio values (min and max) from three different sites as in Figure 3.11.

Figure 3.11	Site 1	Site 2	Site 3
Max	0.658	0.572	0.245
Min	0.610	0.540	0.220

Simulation of optical action potential

It is clear from these results that the ratiometric data obtained from these dual-emission wavelength experiments could not be used to calibrate the ratio into absolute voltage because the ratios were not uniform and the results showed a high variability in absolute value across the surface of the ventricle, even with the improved filter set 2.

Because ratiometric fluorescence techniques have been used extensively for intracellular Ca^{2+} measurements successfully in the past (Brack *et al.*, 2010), we proceeded to investigate possible sources of error by using a computational model to study the variables that might affect the reliability of the ratiometric measurement. The simulation programme, SimulateOAP (Figure 3.12) was written in MATLAB by Dr Francis Burton (University of Glasgow). It uses, as its starting point, an action potential template based on the optical action potentials recorded experimentally. The program simulates fluorescence signals for both short and long wavelength sections of the emission spectrum for a 16x16 array of values. The program then adds the effects of 3 major non-uniformities that could be present in the mapping system: (i) non-uniform illumination intensity across the surface of the myocardium, (ii) movement artefact, i.e. translations in X and Y of the individual fluorescence signals over time, and (iii) differences in the alignment of the two cameras used to record short and long wavelengths. Figure 3.12 shows a list of the adjustable parameters and their value displayed as a table on the left hand side.

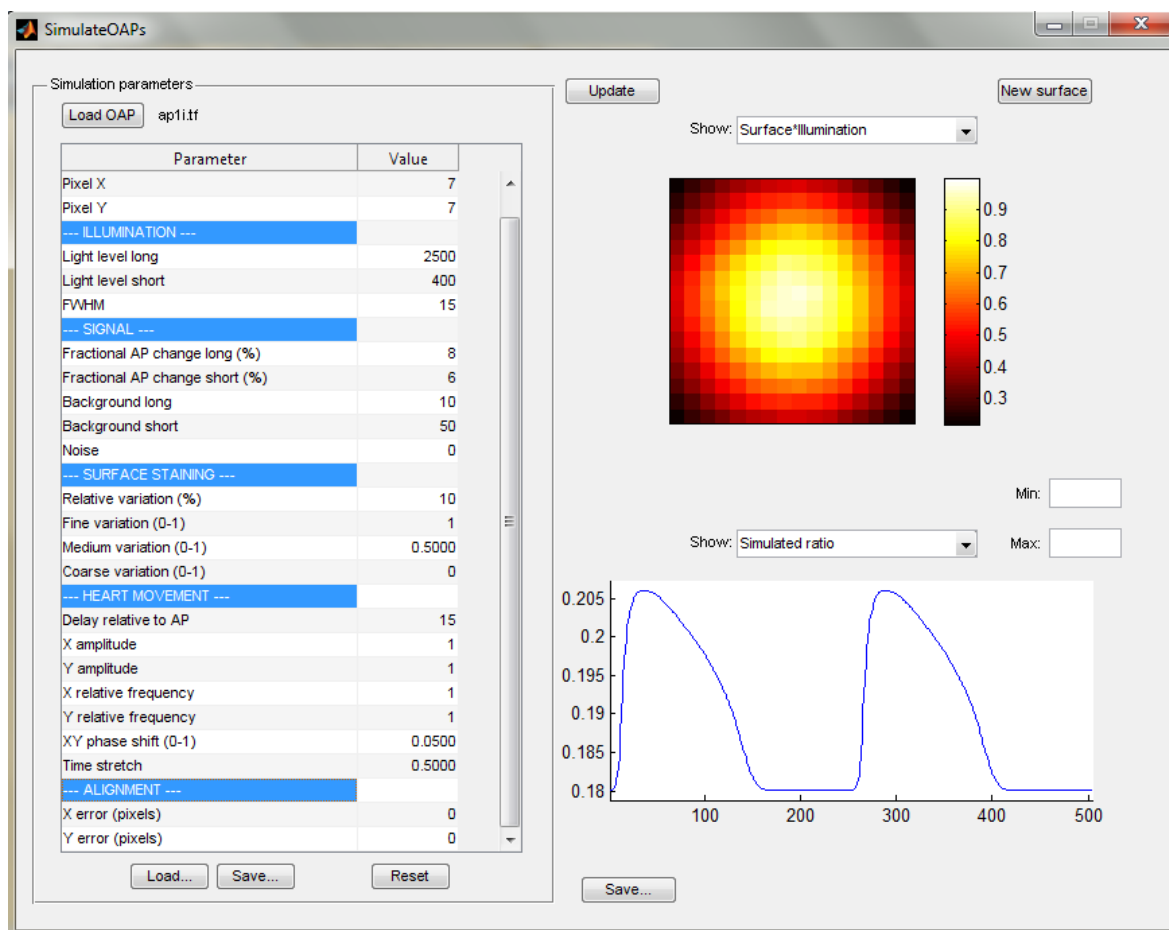


Figure 3.12 SimulateOAP.

Typical display from SimulateOAP. The left panel shows the parameters names and values. The main classes of variable involved in optical mapping experiments are shown in blue. The right panel (top) displays an example of colour map of surface fluorescence multiplied by illumination. The right panel (bottom) is an example of a simulated AP ratio trace from one site at coordinate (7,7).

1) *Ratio value is sensitive to illumination levels*

As is evident from the fluorescence colour maps from the experimental data (Figure 3.8, 3.9 and 3.10), there was variation in the illumination level at the long and short wavelength across the mapping field. The effect of unequal illumination level on ratiometric calculation was therefore simulated. Figure 3.13 shows an example of simulated AP ratio obtained by varying the illumination level at pixel coordinate (7, 7), near the middle of the mapped field, in the presence of constant background fluorescence at both long and short wavelengths. Relative magnitudes of background levels were similar to those seen experimentally. The baseline illumination level for the long wavelength was 2500 and the short wavelength was 400, again chosen to match approximately the relative magnitudes of the experimental signals. The simulated ratio for the baseline illumination level is shown in Figure 3.13a. Figure 3.13b shows the resulting AP ratio when the illumination level was reduced to half of the baseline value and increased to double the value (Figure 3.13c). In all three simulations, the ratio AP had a similar shape which was faithful to the underlying simulated voltage profile (template). However, there was variation in the minimum value for the ratio with varying light levels as depicted in Table 3.2. Clearly, the ratiometric measurement is sensitive to illumination level in the presence of uncorrected background fluorescence. When the simulation was repeated in the absence of background fluorescence, or subtracting background fluorescence, ratio values were within a constant range, as expected (results not shown).

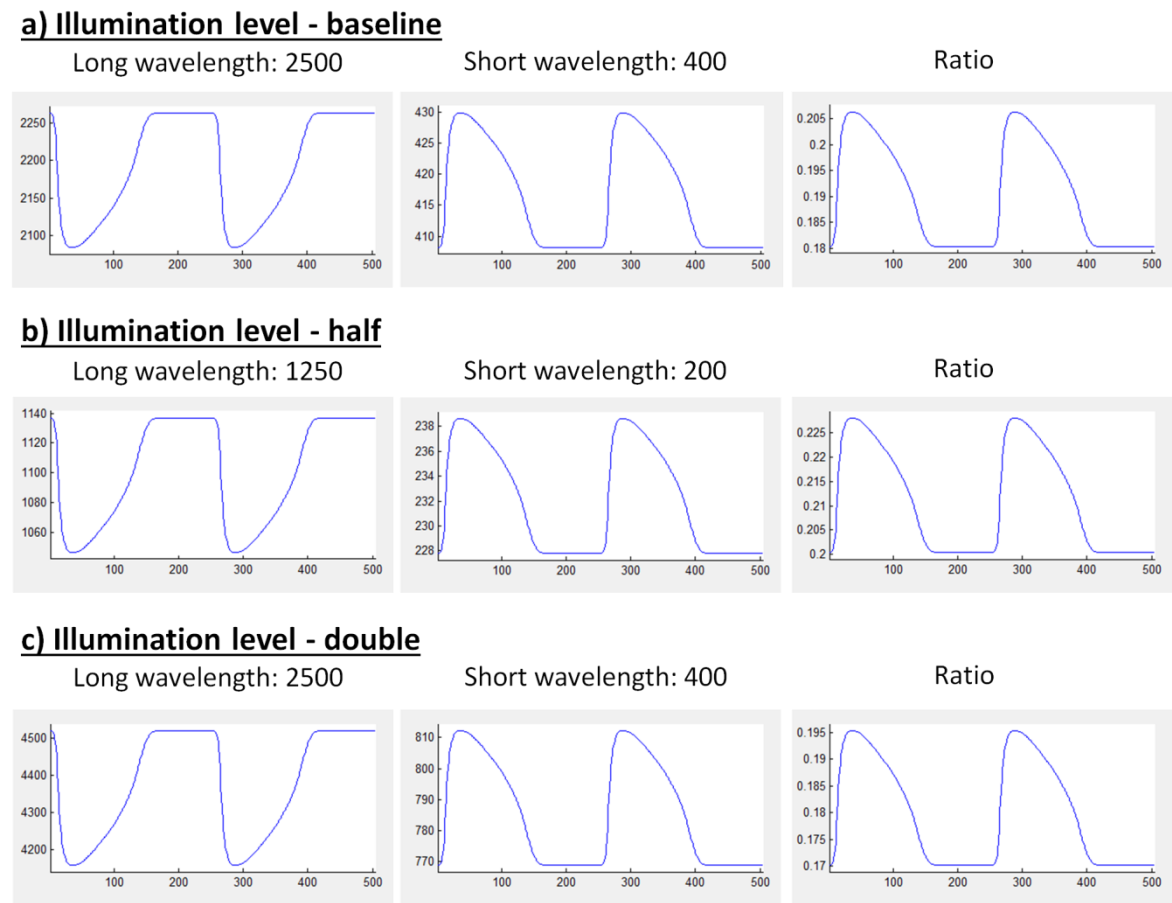


Figure 3.13 Effect of varying illumination level on ratio AP.
Simulated AP ratio produced with long and short wavelength at baseline illumination level (a), half illumination level from the baseline (b), and double illumination level from the baseline.

Table 3.2 Effect of varying illumination level on ratio AP.
Minimum and maximum values from the ratio AP simulated by varying the light level in Figure 3.12.

Figure 3.12	a	b	c
Max	0.206	0.228	0.195
Min	0.180	0.200	0.170

2) *Ratio AP produces reliable shape even at large movement*

It is clear from experiments that motion artifacts due to heart contraction can affect the shape of the AP. For this reason Blebbistatin was added to the solutions to eliminate motion artifacts and yield APs that could be analyzed. Given the presence of motion artifacts, we used simulation to investigate the effect of heart movement on ratio AP. To do this, the position of the heart in X and Y axes was changed over time following sinusoidal trajectories (Figure 3.14). Simulated ratios together with corresponding simulated long and short wavelength are shown in Figure 3.15. For reference, Figure 3.15a shows traces in the absence of movement in either X and Y axis. Figure 3.15b shows simulated AP ratio produced when there was a slight movement of 1 pixel in the direction of X and Y axis and the ratio looked almost the same as in Figure 3.15a. In Figure 3.15c and 3.15d, there was movement of 2 and 5 pixels respectively in X and Y axis direction. The simulated AP shapes mimic the distortions seen experimentally very well. At each level of simulated movement artefact, the AP ratio was remarkably true to the underlying voltage profile, although a small amount of distortion can be seen with larger movements, especially in the diastolic period of the traces. The range of ratio values was the same, namely 0.180 - 0.205, regardless of how much the heart moved in X and Y axis. In summary, ratiometric measurement produces reliable AP shape with consistent minimum value over a wide range of heart movement.

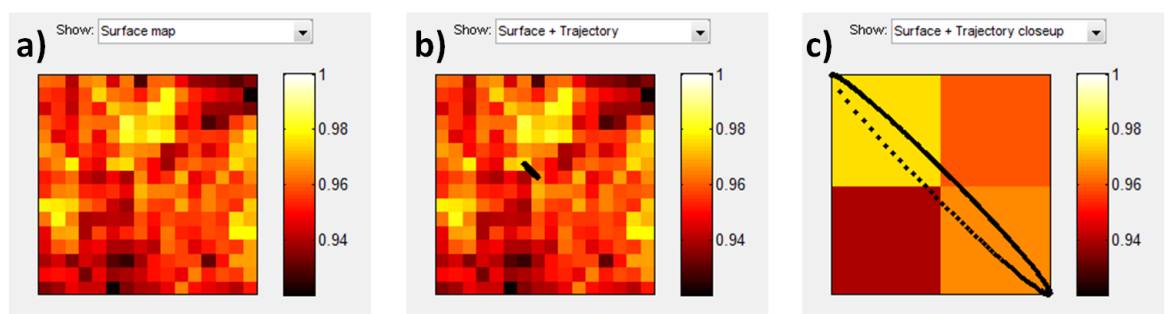


Figure 3.14 Sinusoidal movement trajectories on heart surface. Example of a) variation in surface fluorescence, b) movement trajectory in X and Y direction on the surface, and c) a close-up view of the movement trajectory illustrating the relation of heart movement with spatial variations in surface fluorescence.

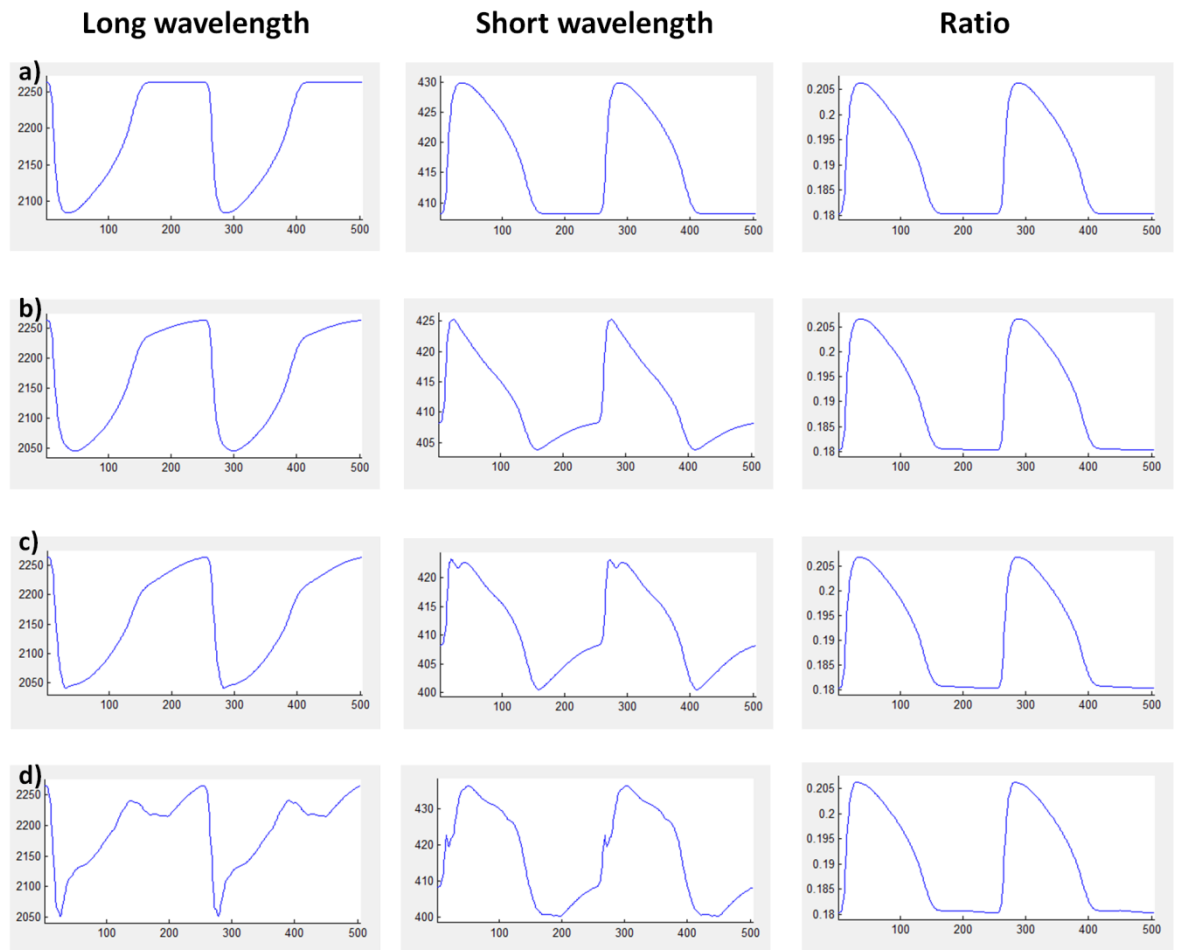


Figure 3.15 Effect of heart movement on ratio AP.

Effect of heart movement in X and Y axis direction on AP ratio with corresponding long and short wavelength. a) No movement X=0 Y=0, b) Slight movement X=1 pixel Y=1 pixel, c) X=2 pixels Y=2 pixels, d) Large movement X=5 pixels Y=5 pixels.

3) Camera alignment is important for accurate AP shape

Another potential artefact in the optical mapping method is due to camera misalignment. As described earlier, large heart movement with perfectly aligned cameras yielded ratio traces in which motion artefact was reliably eliminated. Therefore, the magnitude of the effect of camera misalignment in the presence of varying degrees of heart movement was studied. Camera misalignment of any number of pixels in X and Y directions could be incorporated into the simulation. For our purpose, to simulate severe but plausible misalignment between our cameras, displacements of 1 pixel in both X and Y direction was chosen. At the same time, the illumination profile was made to be uniform across the whole mapped field. Figure 3.16a demonstrates normal AP shape at both long and short wavelengths and the ratio when the simulated heart was completely still. However, when moderate heart movement of 3 pixels in X and Y directions was imposed (Figure 3.16b) AP ratio was no longer able to recover the underlying voltage profile accurately. As movement became even greater (Figure 3.16c) distortion of the ratio signal increase correspondingly. Even though the shape of the ratio AP changed with varying degrees of heart movement, all ratios had approximately the same minimum value (0.186-0.187).

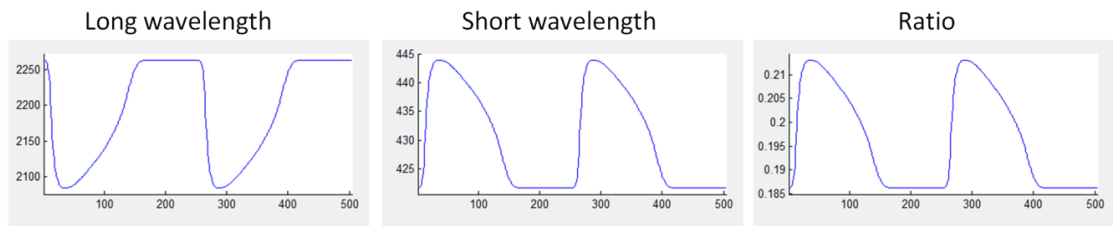
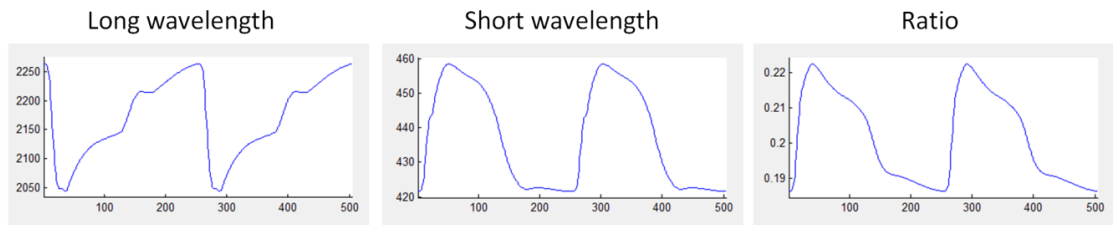
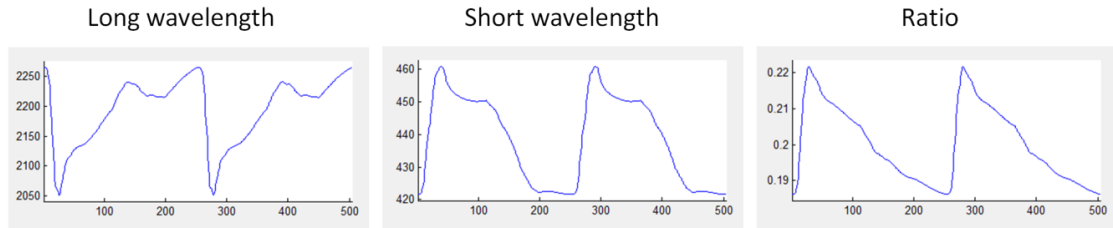
a) Camera misalignment, no heart movement**b) Camera misalignment, moderate heart movement****c) Camera misalignment, large heart movement**

Figure 3.16 Effect of camera misalignment and heart movement on ratio AP. Effect of camera misalignment (X error = 1 pixel; Y error = 1 pixel) on ratio AP with two degrees of heart movement. a) Perfect AP ratio produced when there was no movement. b) AP shape in the presence of movement by 3 pixels in X and Y directions. c) AP shape in the presence of movement by 5 pixels in X and Y directions.

Discussion

In the first part of this chapter, results from the dual-emission wavelength optical mapping experiments were described. The initial aim for this study was to use the ratiometric approach to examine the membrane potential and try to correlate the ratio with the absolute voltage. Even though I successfully obtained the ratiometric measurement and was able to demonstrate the change in membrane potential during hyperkalaemic induction, the ratio could not be calibrated to yield an absolute voltage across the image field. The explanation for the poor compensation of varying illumination and movement was not clear.

Therefore, a model was constructed to investigate all the variables that could affect the ratiometric measurement. In this model, the effects of three important variables, 1) illumination level, 2) heart movement, and 3) camera alignment on the ratiometric measurement, were simulated. From the model, it was shown that the fluorescence ratio was sensitive to illumination intensity if no (or incorrect) background fluorescence values were used. Even though the AP shapes produced in the ratio were similar at different levels of illumination, varying the light level changed the minimum values of the ratio. Despite measuring background fluorescence in these experiments prior to addition of dye, these values proved insufficiently accurate for the purpose of providing a uniform range of fluorescence ratio values across the image field. The reason for this is not clear. Two possibilities are: 1) minor movement of the heart between measurement of background and post-dye recording, and 2) time dependent changes in intrinsic fluorescence of the myocardium, e.g. due to oedema, means the initial measurement was not correct for the post-dye phase.

The simulations showed that with correct baseline illumination levels and aligned cameras, the ratiometric measurement successfully eliminated the motion artefacts caused by heart movement and produced a ratio signal that faithfully reproduced the AP. However, camera misalignment by just 1 pixel in X and Y direction produced distorted AP shapes in the ratio signal in the presence of heart movement, but the minimum values were unaffected.

In conclusion, dual-wavelength ratiometric measurement can be used to attenuate the problems of motion artefact, uneven staining and uneven illumination in optical mapping experiments when suitable filters are chosen to ensure comparable fluorescence signals on short and long wavelength signals. In this study, however, the technique could not be routinely used, signals still contained a persistent movement artefact and the ratio value varied dramatically over the field of view. Calculations suggest that in order for this technique to be routinely used experimentally both correct background fluorescence values and accurate camera alignment need to be obtained. The results of simulation suggest that the cameras need to be aligned within a tolerance of <1 pixel, and background measurements of both wavelength have to be correct within 10%. These two issues present particular technical problems that could not be resolved during the period of this PhD and are currently under consideration by others in the research group.

Chapter 4: Single view optical mapping – Effect of E-4031 on action potential duration

Aim

The aim of the study was to examine the effect of hERG channel block in the whole rabbit heart to assess the use of the drug as a means of manipulating rabbit ventricular action potential duration. This property of the drug E-4031 was investigated in this study because it was going to be used later in subsequent experiments as a way to manipulate the APD (see Chapter 6).

Introduction

Class III antiarrhythmic agents (Vaughan Williams classification) predominantly block potassium channels, thereby producing action potential duration lengthening by prolonging repolarisation (Lenz and Hilleman, 2000). Several studies have shown that most class III agents also produce other antiarrhythmic effects in addition to potassium channel-blocking action (Carmeliet, 1985; Singh and Vaughan Williams, 1970). Class III antiarrhythmic agents increase APD without affecting conduction by selectively blocking K^+ (and not Na^+) channels in non-pacemaker tissue (Follmer and Colatsky, 1990; Sanguinetti *et al.*, 1991; Wallace *et al.*, 1991). Moderate prolongation of the action potential duration and refractory period, together with the maintenance of normal conduction velocity, tend to prevent re-entrant arrhythmias via increase in AP wavelength.

E-4031 (1-[2-(6-methyl-2-pyridyl)ethyl]-4-(4-methylsulfonyl-aminobenzoyl)piperidine) is a potent methanesulfonanilide class III drug which selectively blocks the voltage-gated potassium channels encoded by human ether-a-go-go related gene (hERG) that mediate the repolarising delayed rectifier potassium (I_{Kr}) current. hERG is the main subunit of the potassium channel $K_{v11.1}$ coded by a gene KCNH2 (Gerlach *et al.*, 2010; Perrin *et al.*, 2008). Excessive prolongation of action potentials through inhibition of this channel by E-4031 can cause acquired long QT syndrome (LQTS). LQTS is associated with Torsade de Pointes (TdP) arrhythmia, a form of ventricular tachycardia that can rapidly degenerate into ventricular fibrillation (Ponte *et al.*, 2010). The effects of E-4031 on action potential duration have been investigated extensively in isolated tissue preparations in swine, guinea pigs, chicks (Agarwal *et al.*, 2012; Nouchi *et al.*, 2011; Oinuma *et al.*, 1990) and human stem cell-derived cardiomyocytes

(Jonsson *et al.*, 2010). However, only limited data exist about the effect of E-4031 on the APD of rabbits whole heart experiments.

Methods

Preparation of the rabbit hearts

A total of 16 animals were used in this set of experiments. Hearts from male New Zealand White rabbits (2.5 - 3.5kg) were Langendorff-perfused as described in Chapter 2. A constant perfusion rate of 30ml/min was used throughout the experiments. Perfusion pressure was continuously monitored with a transducer connected to the aortic cannula. In normal hearts, perfusion pressure ranged from 20-35mmHg.

Atrioventricular (AV) node ablation

To study the effect of E-4031 on rabbit ventricular APD, the hearts were paced over a range of pacing cycle lengths from 1000 to 200ms. After the heart was mounted onto the aortic cannula, the right atrium was cut to remove the SA node and to expose the AV node area. Anatomically, the AV node is located within the triangle of Koch, a region located at the base of the right atrium defined by the following landmarks: the coronary sinus ostium, tendon of Todaro, and the septal leaflet of the tricuspid valve. To assist in locating the AV node, the triangle of Koch region was delicately probed with the tips of a pair of forceps. The point at which there was a vigorous contraction of the heart when the forceps touched was taken as the AV node. To allow pacing slower than the heart's intrinsic cycle length, complete AV block was produced by injecting a small volume (<0.2ml) of 10% formalin solution into the AV node with a 23-gauge needle to uncouple atrial and ventricular activity (Guzman *et al.*, 1959).

Uncoupling was further confirmed by inspection of the pseudo ECG which demonstrated the presence of QRS complex in the absence of P wave. Maciver *et al.* (2010) states that the accomplishment of this AV block method depends on several factors: 1) the ability to obtain direct and accurate access to the AV node, 2) the reliability in delivering small volumes of the necrosis agent, and 3) the confirmation of the AV node tissue ablation. In our experiments, we were able to achieve all Maciver's three criteria for AV block in which 1) the direct and accurate access to the AV node was successfully achieved, 2) only small

volume of formalin solution (0.2 ml) was used to block the AV node, and 3) the AV node ablation was confirmed by absence of P wave on the ECG.

Electrophysiological recording and analysis

Epicardial membrane potentials from the anterior surface of the hearts were recorded using an optical mapping array (see Chapter 2). The isolated Langendorff-perfused heart was placed into the perspex chamber to reduce motion artefact and maintain the temperature of the hearts at 37°C by filling the chamber with thermostat-controlled heated solution. Further reduction of motion artefact was achieved by using Blebbistatin (10 μ M). The heart was loaded with 100 μ L (concentration 2mmol/L) bolus of the voltage-sensitive dye RH237 (Molecular Probes) by slow injection into the coronary circulation over duration of 30 seconds through an injection port in a bubble trap in line with the aortic cannula. Details of the optical mapping setup and recording may be found in Chapter 2.

E-4031 drug

E-4031 (Enzo Life Sciences, MWT:510.5) used in these experiments was made as stock solution dissolved in dimethylsulfoxide (DMSO) and stored at -20°C. There were 5 concentrations used for these experiments: 3nM, 10nM, 30nM, 0.3 μ M and 3 μ M. The chemical structure of E-4031 is demonstrated in Figure 4.1.

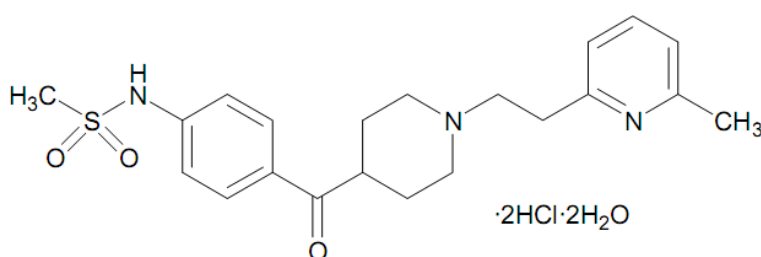


Figure 4.1 E-4031 structure.

Pacing protocol

After the AV node ablation procedure, the heart was put into the chamber and paced directly via electrodes placed over the base of the right ventricle. For each experiment, the heart was paced with the following protocols:

Continuous pacing at 500ms cycle length

At the beginning of the experiment, the heart was paced at 500ms cycle length for approximately 20-30 minutes to allow APD to reach a steady-state.

Abrupt rate changes 500ms→300ms→500ms cycle length

To study the time course of the change in APD after an abrupt step in cycle length, hearts were paced at basic cycle length of 500ms for 30 seconds duration. Then, the cycle length was shortened to 300ms (1 minute) and then returned to 500ms (1 minute). Optical recordings were obtained every 10s throughout this period. The 1 minute period was chosen on the basis of earlier studies showing that APD reached a steady-state in this time following abrupt rate changes.

Range of cycle lengths: 1000ms, 800ms, 700ms, 600ms, 500ms, 400ms, 300ms and 200ms

To examine the cycle length related changes in ventricular APD, the hearts were paced at a range of cycle lengths from long to short cycle length (1000-200ms). At each pacing cycle length, optical recordings were made after 16 beats to allow adaptation to the new rate.

Continuous pacing at 500ms cycle length

In the final part of the protocol, hearts were paced at 500ms cycle length and the optical signals recorded every 1 minute intervals for 10 minutes duration to track recovery.

All these protocols (4 sets) were performed before the drug was perfused into the heart. In the presence of E-4031, the same sets of protocol were repeated. The results obtained from these protocols before and after drug were compared.

Electrocardiogram (ECG)

During the experiments, ECG signals were obtained using two electrodes inserted into both sides of the chamber. Signals from these electrodes were amplified and displayed on an oscilloscope (Nicolet Instrument Corporation, Wisconsin, USA) to allow real-time viewing of the ECG.

Optical data analysis

The optical signals obtained from this study were analysed using an analysis programme OPTIQ (see Chapter 2). The key electrophysiological parameter examined in this study was APD_{90} because E-4031 selectively blocks the I_{Kr} channel, one of the primary channels involved during rapid repolarisation phase (phase 3) of action potential. Figure 4.2a illustrates a typical response to regular pacing at 1000ms. The action potential duration (APD_{90}) was calculated from the difference between activation time and the time at 90% repolarisation (Figure 4.2b). Figure 4.3a shows a typical activation map produced in the OPTIQ software from the experimental recording. Figure 4.3b shows average AP traces from 3x3 pixels (9 pixels) that were used for the analysis.

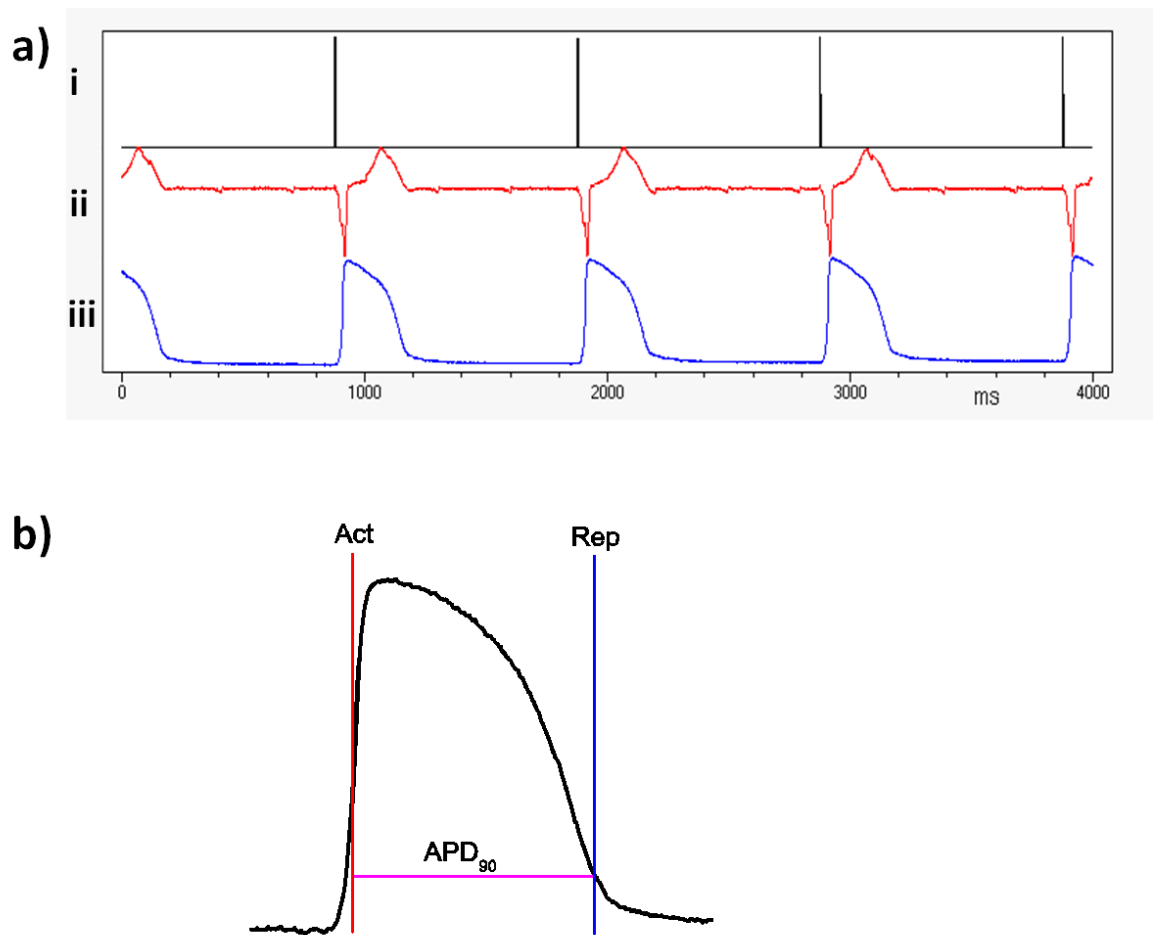


Figure 4.2 Optical data analysis.

a) Diagram showing AP train at 1000ms cycle length ventricular pacing i) Stimulus probe ii) ECG trace iii) Action potential recorded optically B: Method to determine APD_{90} . Act=Activation time, Rep=90% repolarisation time. The difference (Rep-Act)= APD_{90}

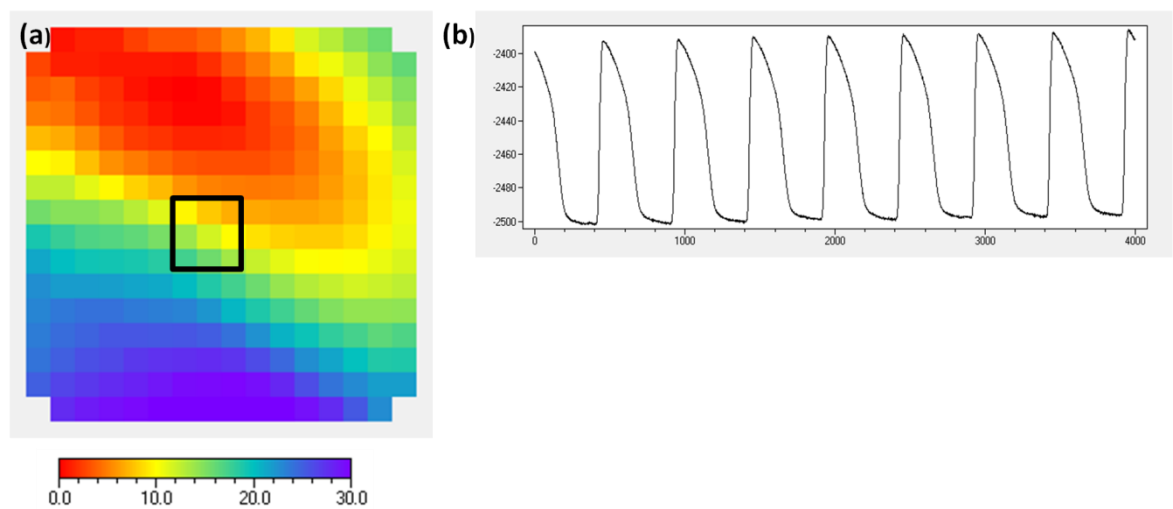


Figure 4.3 Optical data.

(a) Example of activation map showing 3x3 sites (9 pixels) chosen for APD analysis. (b) Mean optical action potential (OAP) from 9 sites paced at 500ms.

Results

Figure 4.4 illustrates a typical full protocol time course obtained from one experiment. Characteristic changes in APD_{90} at different times reflect the different parts of the protocol. Under control conditions, APD_{90} was stable; immediately after the drug was added, APD_{90} rose to a new steady state and the protocols were repeated. On washout of the drug, APD_{90} returned to baseline.

Effect of different concentrations of E-4031 on APD_{90}

The results summarized in Table 4.1 show that E-4031 ($0.01\mu\text{M}$) significantly prolonged APD_{90} ($P<0.01$) by $21.0 \pm 2.5\text{ms}$ ($n=4$); at $0.03\mu\text{M}$ ($n=6$), by $42.7 \pm 6.7\text{ms}$ ($P<0.01$); and at $0.3\mu\text{M}$ ($n=3$), by $48.6 \pm 5.8\text{ms}$ ($P<0.05$). Even though $3\mu\text{M}$ E-4031 prolonged the APD_{90} by $32.0 \pm 11.7\text{ms}$, the change in APD pre and post drug was not statistically significant. The effect of $0.003\mu\text{M}$ E-4031 was undetectable. Figure 4.5 shows the variation in action potential (AP) shape at different E-4031 concentrations. $0.03\mu\text{M}$ and $0.3\mu\text{M}$ E-4031 concentrations produced the largest effect on APD. The effect of E-4031 on APD_{90} was fully reversible, although the early phase of repolarisation did not return to control values (Figure 4.5). The mean APD_{90} prolongation for each drug concentration obtained in Table 4.1 was used to plot the dose-response (Figure 4.6). Based on this curve, the EC_{50} for E-4031 in this study was $0.01 \pm 0.003\mu\text{M}$.

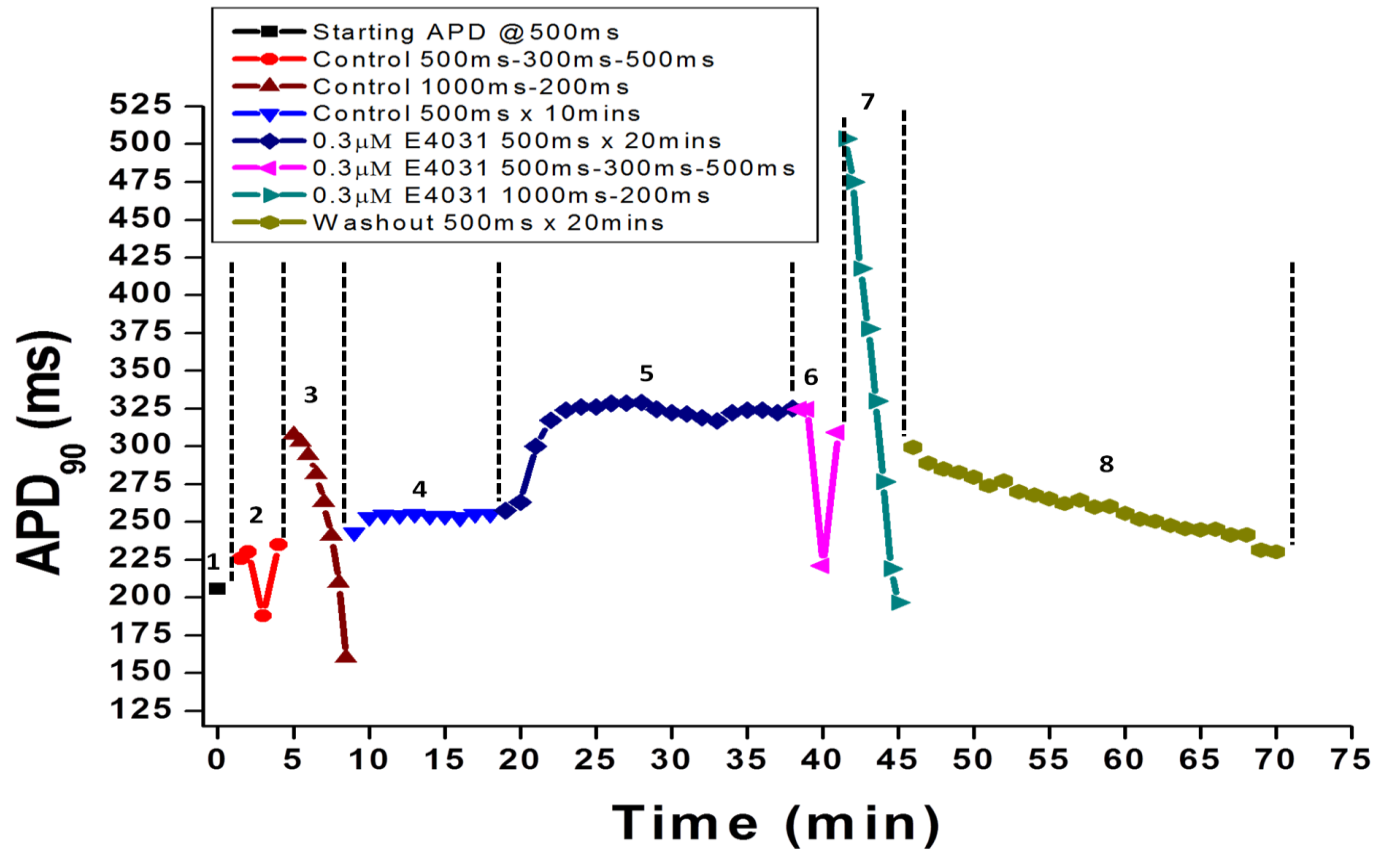
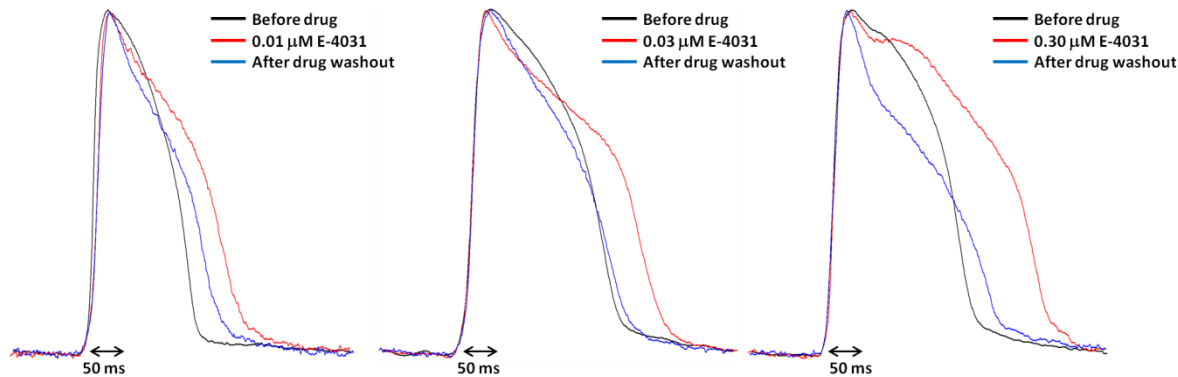


Figure 4.4 Full protocol time course at 0.3 μ M E-4031 concentration.

The dotted lines and the numbering in between the lines indicate different interventions. The experimental protocol began with abrupt rate changes, followed by different pacing cycle length and continuous pacing at 500ms. The whole sets of protocol were done for the control (protocols 1-4) and in the presence of the drug (protocols 5-7). Protocol 8 was the washout of the drug.

Table 4.1 Effect of different E-4031 concentrations on rabbit ventricular APD.

N	APD ₉₀ (ms)			APD ₉₀ (ms)			APD ₉₀ (ms)			APD ₉₀ (ms)		
	Pre-drug	0.01 μ M E-4031	Difference	Pre-drug	0.03 μ M E-4031	Difference	Pre-drug	0.3 μ M E-4031	Difference	Pre-drug	3 μ M E-4031	Difference
1	188.5	212.4	23.9	197.3	227.8	30.6	246.8	283.8	36.9	191.6	215.0	23.5
2	183.5	201.8	18.3	174.5	216.3	41.8	244.7	298.9	54.2	227.0	244.4	17.5
3	207.2	222.8	15.6	214.5	255.0	40.5	164.7	219.3	54.7	191.9	247.0	55.1
4	221.6	247.9	26.3	188.2	211.5	23.3						
5				225.1	274.1	49.0						
6				192.4	263.2	70.9						
Mean	200.2	221.2	21.0	198.7	241.3	42.7	218.7	267.3	48.6	203.5	235.5	32.0
SEM	8.8	9.9	2.5	7.5	10.7	6.7	27.0	24.4	5.8	11.7	10.3	11.7
** $P < 0.01$				** $P < 0.01$			* $P < 0.05$			ns		

**Figure 4.5 Effect of E-4031 on action potential.**

Variations in action potential shapes at maximum effect during control (black line), during the drug (red line) and after drug washout (blue line). Comparison of APs at three different E-4031 concentrations (0.01, 0.03 and 0.3 μ M).

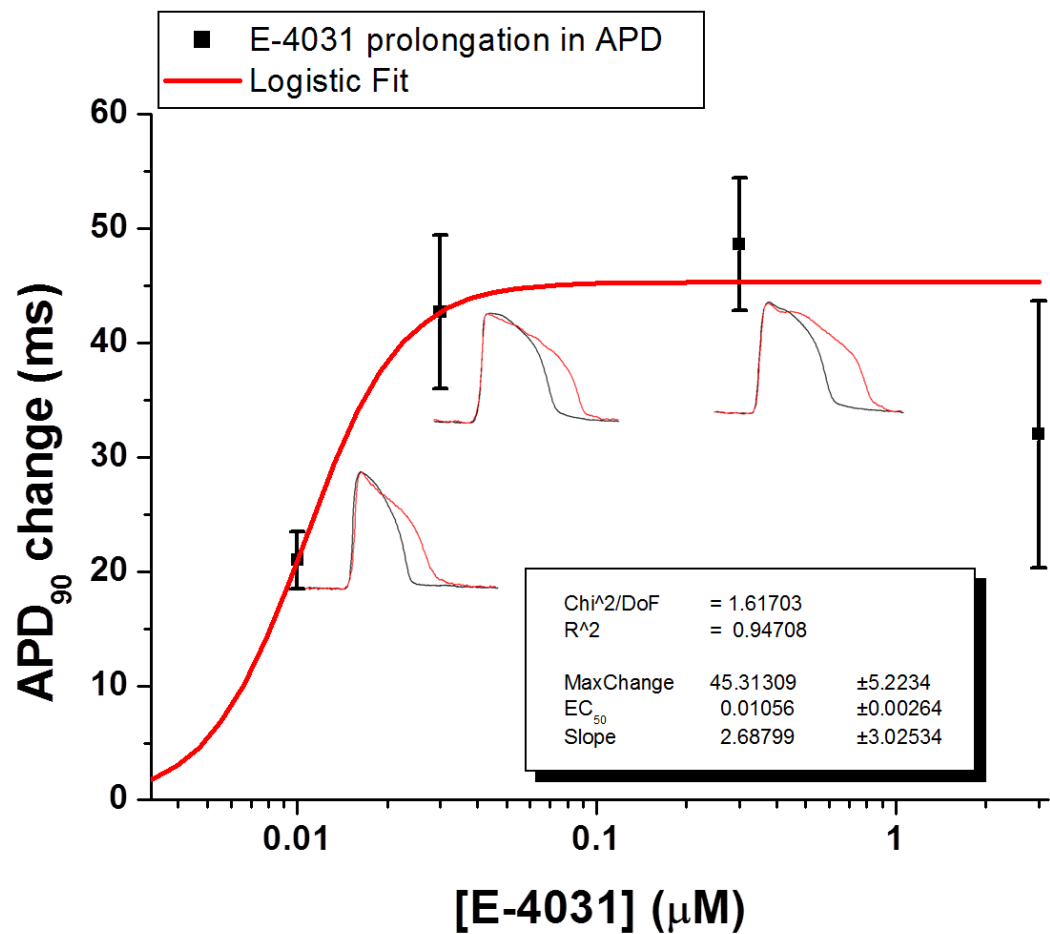


Figure 4.6 Dose-response curve for 4 different concentrations of E-4031. AP traces show example of control APD (black) and prolongation of APD (red) after the heart being perfused with corresponding drug concentration. Logistic curve of APD change = $\frac{\text{MaxChange}}{[1 + (X/\text{EC}_{50})^{\text{Slope}}]}$.

APD adaptation during rate changes

Abrupt sustained rate changes from long cycle length to shorter cycle length and back to long cycle length (500ms→300ms→500ms) showed clear memory effects in terms of APD. Figure 4.7 shows an example of the time course of APD shortening and lengthening after sequential changes in step decrease and step increase in cycle length. During rate changes, APD did not adjust immediately to the new cycle length but required some time to reach a new steady state. The first action potential after changing the cycle length from 500ms to 300ms showed abrupt shortening followed by a much slower time course until steady-state was reached. When the cycle length was changed back abruptly, APD was incompletely restored and gradually returned to the control value over a period of ~60s. Figure 4.7b shows an example of APD alternans that was sometimes observed at higher drug concentrations and at the faster pacing rate.

Figure 4.8b shows that abrupt rate changes exhibited a shorter mean time constant in the presence of 0.03 μ M E-4031. For example, rate changes from short cycle length to longer cycle length exhibit a significantly shorter time constant (30.1 ± 5.0 s during control, 11.9 ± 1.4 s during E-4031).

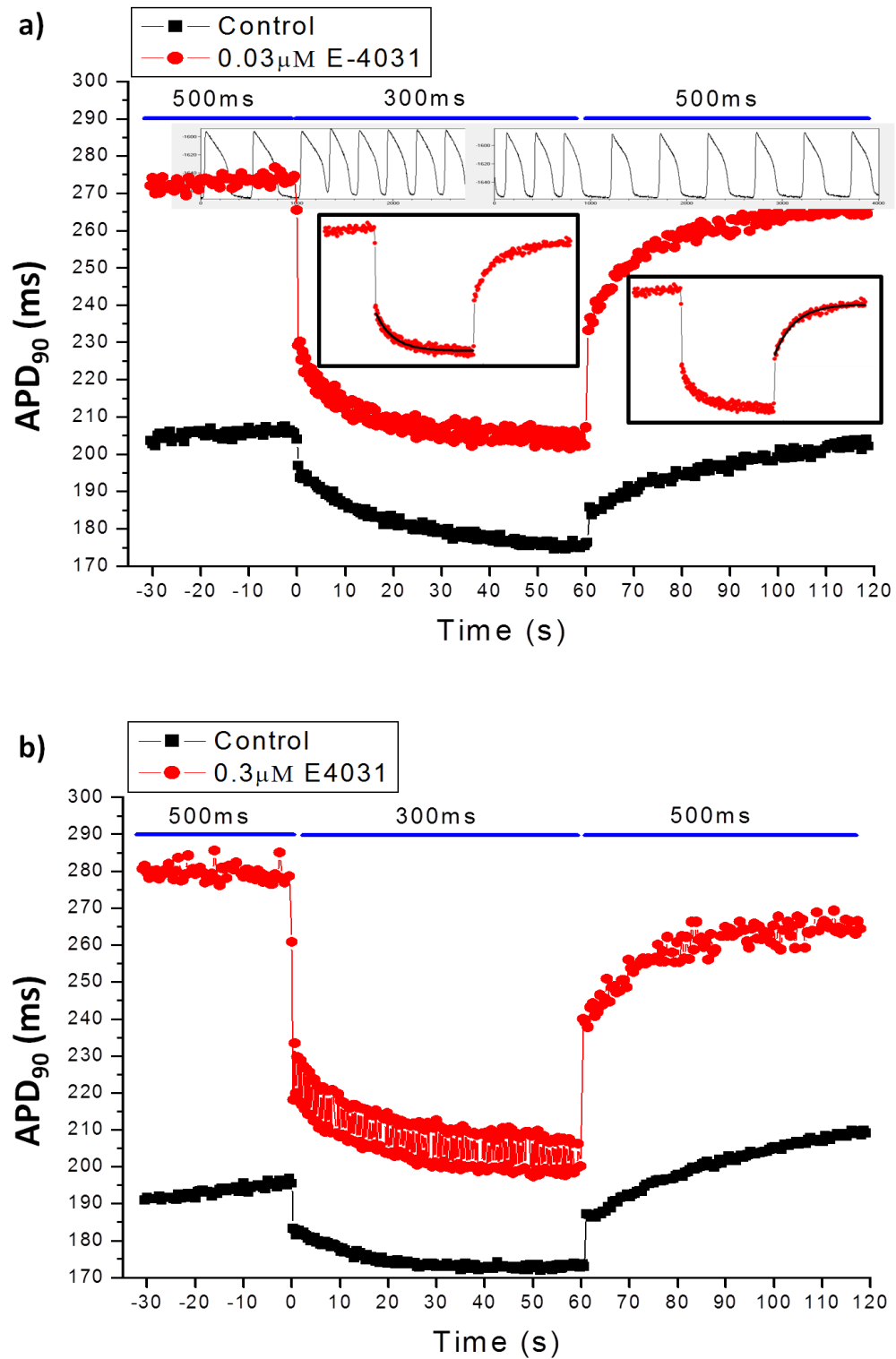


Figure 4.7 APD adaptation during rate changes.

Time course of APD adaptation after sequential increases and decreases in pacing cycle length. Both changes from long to shorter cycle length (500ms \rightarrow 300ms) and from shorter back to long cycle length (300ms \rightarrow 500ms) were followed by an initial rapid phase and a subsequent slow phase of action potential shortening and lengthening, respectively. (a) Comparison between control and 0.03 μM E-4031. The inserts in the black boxes show illustration of the exponential fits used for analysis. (b) Comparison between control and 0.3 μM E-4031. In presence of 0.3 μM E-4031, abrupt decrease in cycle length produced alternation between shorter and longer APD (alternans).

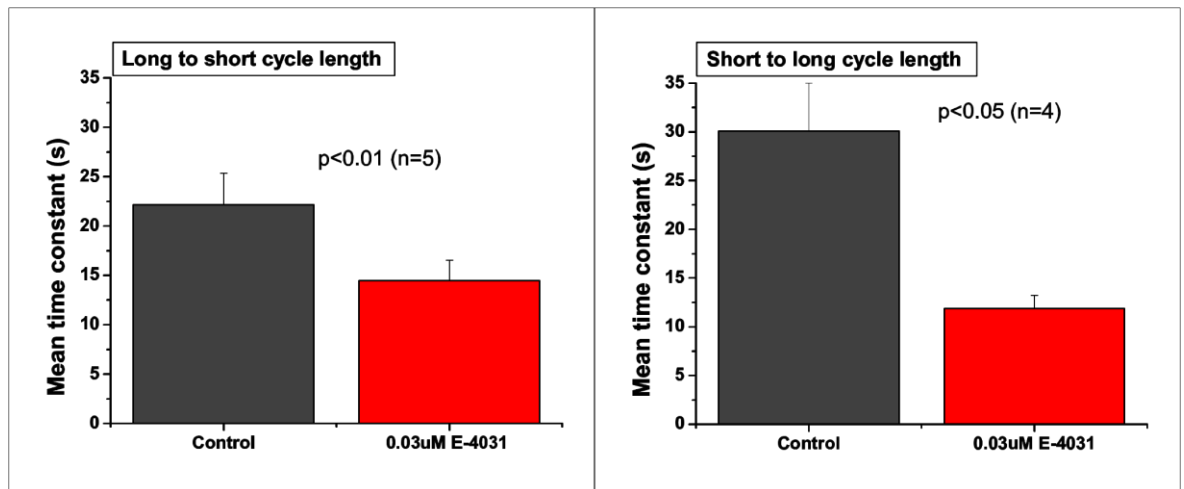


Figure 4.8 Mean time constant during abrupt rate changes at 0.03 μ M E-4031
 (a) From long to short cycle length (500ms \rightarrow 300ms) (b) From short to long cycle length (300ms \rightarrow 500ms).

Rate-dependent property of E-4031

The hearts were also subjected to a range of pacing cycle lengths from 1000ms down to 200ms to study the rate-dependent property of the drug. Figure 4.9 illustrates the frequency dependent effect of E4031. The drug exhibits greater effect at longer cycle length compared to shorter cycle length. At slower than physiological rates (approximately 300ms), the effect of the drug was larger than that seen at higher than physiological rates. For example, at 200ms cycle length there was no significant change in APD_{90} at 0.3 μ M E-4031 (7.8 ± 11.7 ms, n=3). At normal heart rate (300ms cycle length), 0.03 μ M E-4031 significantly prolonged the APD_{90} by 8.5 ± 1.7 ms ($P < 0.01$) whereas at lower stimulation frequency (1Hz) the effect was considerably larger with the APD prolongation of 73.7 ± 13.7 ms ($P < 0.05$).

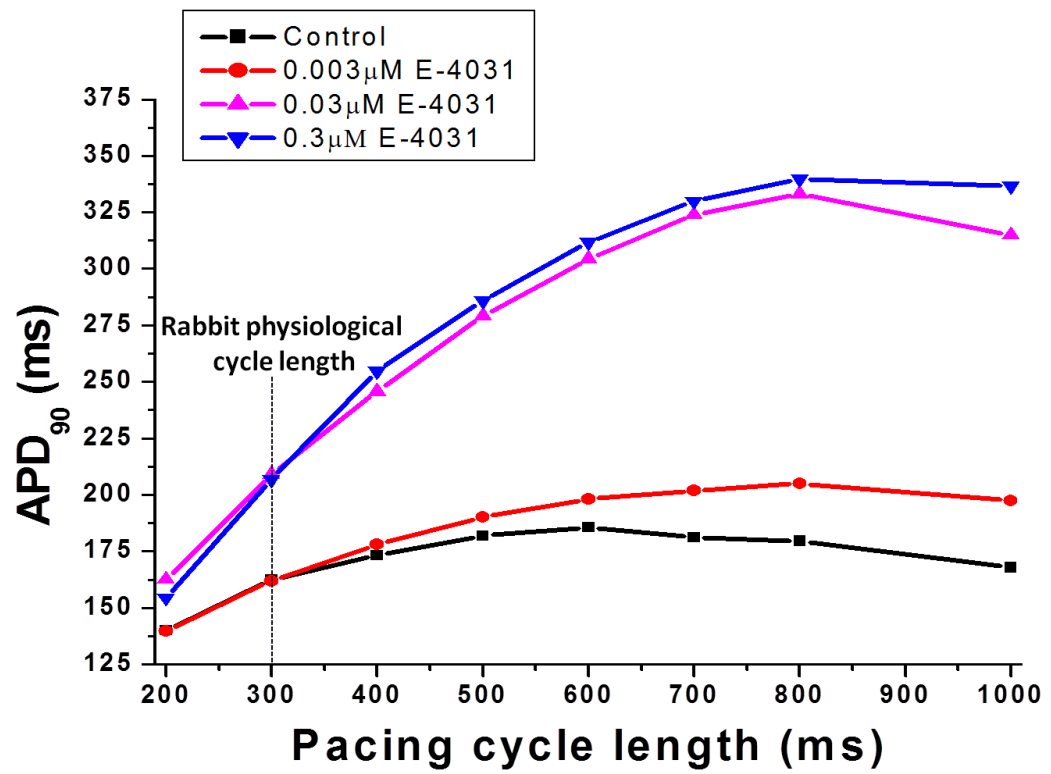


Figure 4.9 Reverse rate-dependent effect of E-4031.
Cycle-length related changes in rabbit ventricular action potential duration by different concentrations of E-4031.

T-wave alternans (TWA), early afterdepolarisations (EADs) and ventricular tachycardia (VT)

In these experiments, incidence of TWA, EADs and VT at different cycle lengths were recorded after exposure to the four different E-4031 concentrations. The observations are summarized in Table 4.2. During control (pre-drug phase), episodes of alternans were observed at 200ms cycle length in 6 out of 15 hearts; in contrast, no EADs or instances of VT were observed. Some (~50%) of the hearts which exhibit APD alternans at 200ms cycle length pre-drug also showed alternans after E-4031 perfusion. Incidences of EADs were observed at all drug concentrations at various cycle lengths ranging from 1000ms down to 500ms. Some hearts also developed VT at slower cycle lengths. In most but not all hearts, VT was preceded by EADs, but not all hearts with EADs developed VT. All episodes of VT were non-sustained and reverted back to sinus rhythm within seconds; none of them progressed into ventricular fibrillation. Examples of AP recordings with corresponding ECG signals showing the incidence of APD alternans, EADs, and VT after exposure to different drug concentrations are displayed in Figure 4.10 (0.01 μ M E-4031) and Figure 4.11 (0.3 μ M E-4031).

Table 4.2 T-wave alternans, EADs, and VT.

Incidence of alternans, early afterdepolarisations (EADs), and ventricular tachycardia (VT) at different cycle lengths in hearts perfused with 4 different E-4031 concentrations. “Control” was the initial pre-drug phase of each experiment before the hearts being perfused with the drug. Star with the same colour indicates the same heart.

CL (ms)	Alternans					EADs					VT				
	Control	0.01 μ M E-4031	0.03 μ M E-4031	0.3 μ M E-4031	3 μ M E-4031	Control	0.01 μ M E-4031	0.03 μ M E-4031	0.3 μ M E-4031	3 μ M E-4031	Control	0.01 μ M E-4031	0.03 μ M E-4031	0.3 μ M E-4031	3 μ M E-4031
1000							★ ★	★ ★ ★	★	★ ★				★	★
800							★ ★ ★	★	★	★ ★ ★		★		★	★
700							★ ★ ★	★		★ ★ ★		★			★
600								★		★ ★					★
500							★ ★		★	★					★
400															
300															
200	★ ★ ★ ★ ★ ★	★ ★	★ ★ ★	★ ★	★ ★ ★										
Total hearts (n)	15	4	5	3	3	15	4	5	3	3	15	4	5	3	3

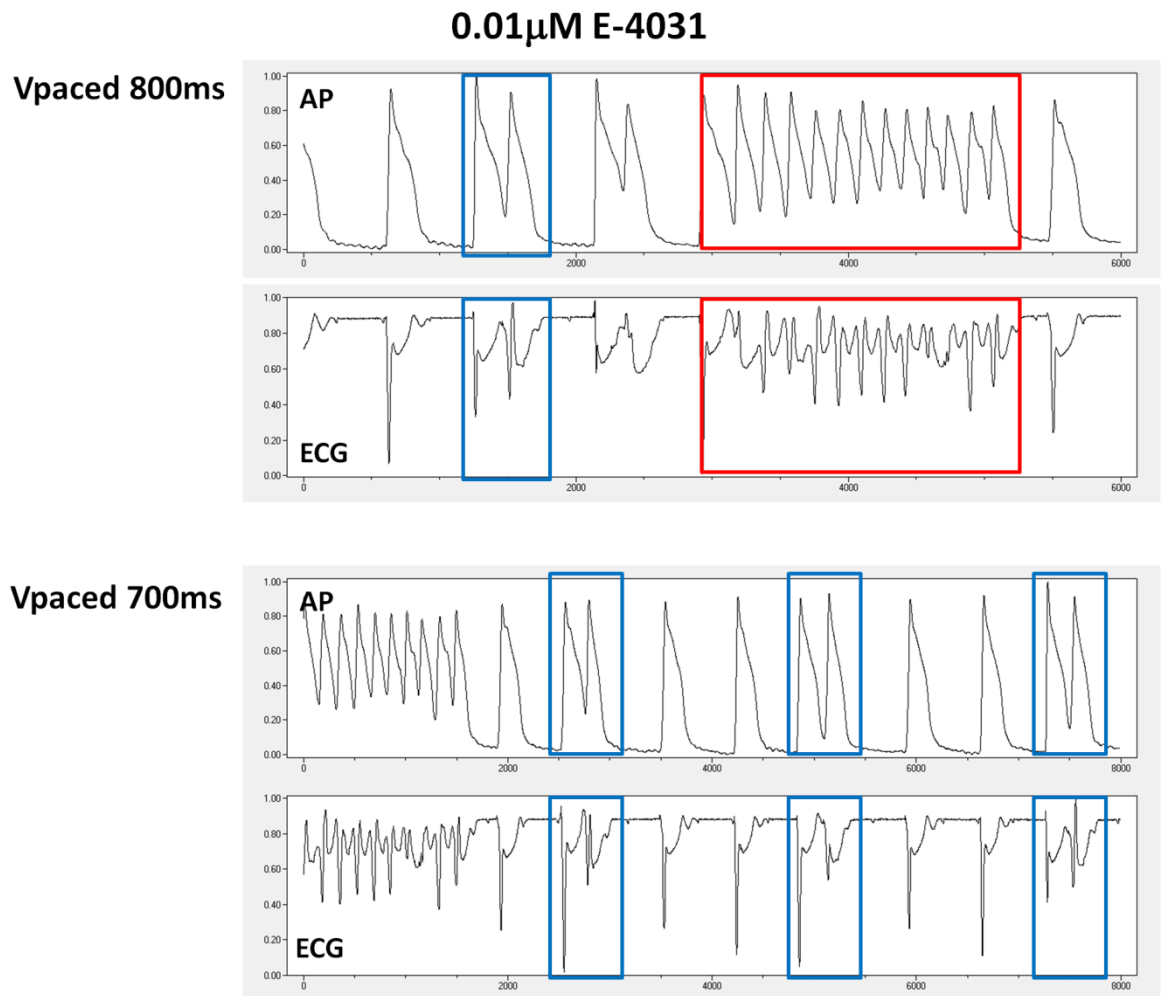


Figure 4.10 EADs and VT in the presence of 0.01 μ M E-4031.
Example of EADs (indicated by the blue box) and VT (indicated by the red box) occurred at Vpaced 800ms and 700ms cycle lengths in heart perfused with 0.01 μ M E-4031 concentration. Top panel shows the AP with corresponding ECG in the lower panel.

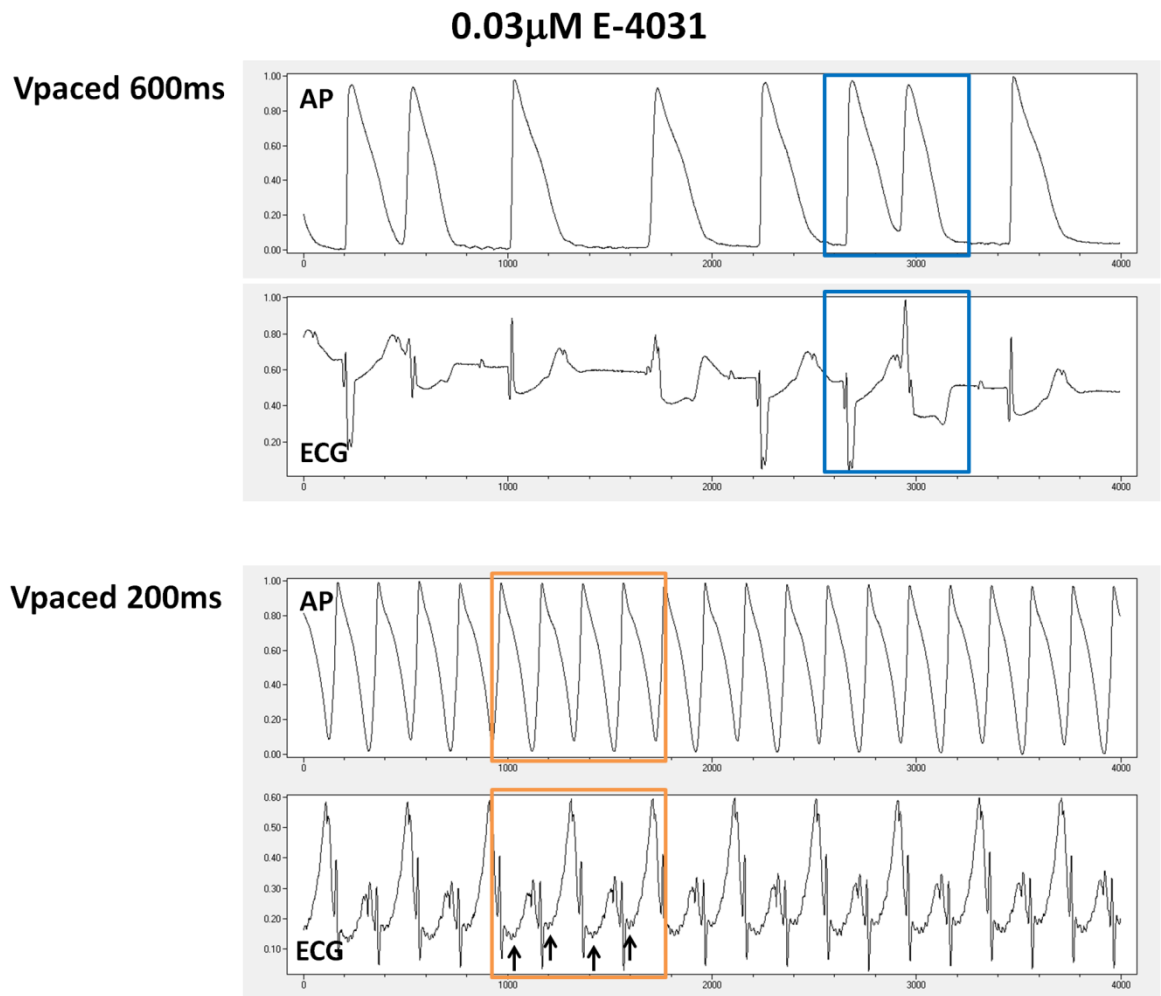


Figure 4.11 EADs and alternans in the presence of 0.03 μ M E-4031. Example of EADs (indicated by the blue box) occurred at Vpaced 600ms cycle length and T-wave alternans (indicated by the orange box) occurred at Vpaced 200ms cycle length in heart perfused with 0.03 μ M E-4031 concentration. The arrows are pointing the alternating pattern of the T-wave. Top panel shows the AP with corresponding ECG in the lower panel.

Discussion

Role of I_{Kr} in repolarisation, rate dependence of APD and adaptation

The repolarisation phase of the cardiac action potential involves many interacting ionic conductances, including the inactivation of the L-type Ca current and the activation of the delayed rectifier currents (I_K). In ventricular muscle, I_K has two components: the rapidly inactivating I_{Kr} and the slower component I_{Ks} . I_{Kr} is generated by the hERG channel (Kv11.1). The role of this channel in repolarisation is complex. The channel is rapidly activated in the plateau phase (Phase 2) and subsequently inactivates, but its influence on APD arises mainly from the recovery from inactivation (re-activation) that occurs during Phase 3 and results in a secondary rise in current which provides the steep return of the membrane voltage to the resting potential (Gintant, 2000). Hereditary defects in this channel typically give rise to abnormally long APs, predisposition to early afterdepolarisations, and to Torsade de Pointes.

Recovery from inactivation of I_{Kr} at negative membrane potentials occurs over hundreds of milliseconds, so at high heart rates, when the diastolic interval is reduced, I_{Kr} has insufficient time to recover fully and is therefore less available for repolarisation. Under these circumstances, other ionic currents become dominant: for example, I_{NCX} (sodium-calcium exchanger current) and, in some species, $I_{Cl(Ca)}$ (calcium-activated chloride current). In larger mammals, including rabbits, dogs and humans, APD decreases at higher stimulation rates during continuous pacing. At cycle lengths >1 second, rabbit ventricular APs have been reported to show a decrease in APD below the peak achieved at ~1s. This biphasic relationship is not present in human and guinea-pig. In the experiments described in this chapter, the range of cycle lengths used was restricted to <1 second and only monophasic restitution curves were seen.

In vivo and *in vitro* studies have shown that APD adaptation to abrupt changes in rate show two phases. A rapid phase, last only 1 or 2 beats, is followed by a slow, exponential phase with a time constant of tens of seconds. This behaviour, sometimes also known as ‘cardiac memory’, is not properly understood but is thought to have its basis in a number of time-dependent processes including: 1)

recovery from inactivation of I_{Kr} and I_{Ks} , 2) changes in SR Ca^{2+} content and subsequent changes in Ca^{2+} transient amplitude, and 3) the L-type Ca^{2+} current $I_{Ca,L}$. The consequences in terms of heart function are linked to the inotropic response to altered heart rate, in that rapid changes cause slower changes in inotropic state similar to that of AP adaptation. Altered cardiac memory is thought to occur during ischaemia and other pathological situations, and may have consequences for arrhythmogenic status (Patberg *et al.*, 2005).

E-4031 dose-dependence on isolated channel and whole heart

In this chapter, E-4031, a Class III anti-arrhythmic agent that selectively inhibits I_{Kr} , prolonged the APD in a dose dependent fashion. The concentration dependence of the action of E-4031 on I_{Kr} has been studied in a number of preparations. Commonly the behaviour of the isolated channel is studied in expression systems (oocytes or mammalian cell lines) and under these circumstances the EC_{50} for E-4031's blocking action ranges from ~10nM to 1 μ M (Anderson *et al.*, 2006; Herzberg *et al.*, 1998). More consistent results were obtained in intact myocardium where EC_{50} values in terms of ventricular APD prolongation were approximately 10nM in guinea-pig (Wettwer *et al.*, 1991) and dog (Holahan *et al.*, 1992; Wallace *et al.*, 1991). These values are close to the EC_{50} value observed in the current study (10.5nM) which appears to be the first report of the dose-dependence of E-4031 in rabbit ventricle. As seen in other studies at high concentrations of E-4031, APD values reach a peak value and then decline. The reason for this is unknown but could represent effects of the drug on other ion channels other than I_{Kr} .

As reported in other species, the effect of E-4031 is considerably smaller at shorter cycle length. At values approximating physiological heart rates of the rabbit (cycle length = 300ms) the maximal effect of E-4031 prolongs APD to ~115% of control level, while at a cycle length of 1s, APD is prolonged by 215%. This reverse rate dependence of the effect of hERG channel blockers has been reported in a number of studies and represents the reduced role of I_{Kr} in AP repolarisation at short diastolic intervals due to the incomplete recovery from inactivation.

E-4031 on adaptation

As shown in Figure 4.8, the time constant for the slow phase of recovery of APD following a step change in cycle length was 20-30s. Using a maximal dose of E-4031 to effectively block I_{Kr} , caused an approximate halving of the time constant for adaptation. These data suggest that recovery of I_{Kr} during the diastolic period is the major rate-determining process governing the APD following abrupt changes in cycle length. In the absence of I_{Kr} , the rate of recovery is determined by other processes such as the equilibration of SR Ca^{2+} content or the rate of recovery of $I_{Ca,L}$. The physiological significance of this result is that at normal heart rates for rabbits (cycle length <300ms), I_{Kr} is unlikely to play a major role in cardiac memory or adaptation. In this respect, rabbit may differ from mammals with lower heart rates, e.g. canine or human, where I_{Kr} may have a significant role in repolarisation.

E-4031 and alternans (role of I_{Kr})

In this study, alternans was routinely observed at short cycle lengths in the presence and absence of E-4031 (Table 4.2). The role of I_{Kr} in alternans has been previously studied (Hua and Gilmour, Jr., 2004). This study suggested that I_{Kr} stabilized APD and reduced the incidence and amplitude of alternans in canine myocardium. Partial inhibition of I_{Kr} increased the relative amplitude of alternans, such that short APDs were caused by a larger I_{Kr} component than the corresponding long APD. The current study appears to contradict this last point; alternans was only observed at short cycle lengths when the contribution of I_{Kr} to repolarisation was small. Furthermore, suppression of I_{Kr} reduced the incidence of alternans but did not abolish it. These results suggest that, in agreement with the published study, I_{Kr} may stabilize APD and may thus prevent alternans since alternating APDs were not observed at longer cycle lengths where I_{Kr} is active in the rabbit. In further agreement with Hua & Gilmour, Jr. (2004), the small amount of I_{Kr} present at short cycle lengths facilitated alternans, which was less likely after E-4031 treatment despite the minimal role of I_{Kr} in repolarisation at these rates and the small change in APD as a consequence of E-4031.

Early afterdepolarisations (EADs)

As reported in this chapter, I_{Kr} block is associated with prolongation of APD and development of EADs. A common consequence of higher doses of E-4031 is the development of tachycardia in the form of Torsade de Pointes (TdP) in larger mammals (Nalos *et al.*, 2012). In the present study, VT was observed, but TdP did not occur in any rabbits studied despite use of high concentrations of E-4031. However, EADs were common at the long cycle lengths (sub-physiological rates), while at physiological rates, EADs were never observed. The EADs reported in this study appeared in the later stages of repolarisation with a coupling interval >100ms. These late EADs are relatively rarely reported in the literature. In single cell preparations, EADs occur in the plateau phase of the AP in guinea pig, rabbit and dog (Nalos *et al.*, 2012). The late coupling of the EADs observed in the current study may be due to the propagation of arrhythmic events originating below the epicardial surface. Propagation of a non-sinus depolarisation may generate EAD-like deflections in the epicardial optical signal. For example, hERG channel block may lead to EADs in the Purkinje fibre system on the endocardial surface (Carlsson *et al.*, 1997) which provides triggered events which can propagate to the rest of the myocardium.

Conclusion

E-4031 significantly and reversibly prolonged APD_{90} at different drug concentrations with the largest effect observed at $0.03\mu\text{M}$. Abrupt rate changes from long to short cycle length and back ($500\text{ms} \rightarrow 300\text{ms} \rightarrow 500\text{ms}$) evinced clear memory effects in terms of APD. The time constant for recovery after a rate change was shorter after E-4031 block, suggesting that I_{Kr} recovery is the dominant factor at low heart rates in the rabbit ventricle. This study also demonstrated that the reverse rate-dependent effect of E-4031 in which the effect of the drug was diminished at shorter cycle lengths. Tachycardia-induced alternans behaviour was less common but not abolished in the presence of E-4031, suggesting that I_{Kr} was not a prerequisite for alternating APD. VT was present at high concentrations of E-4031, but TdP (a form of VF) did not occur in the rabbit ventricle on I_{Kr} block, unlike that seen in canine and human studies (Fujiki *et al.*, 1994; Nalos *et al.*, 2012).

Chapter 5: Single view optical mapping - Acute regional ischaemia in isolated rabbit hearts

Aim

The main aim of these experiments was to get a better understanding of the mechanistic link between acute regional ischaemia and the incidence of ventricular arrhythmia in rabbit.

Introduction

According to cardiovascular disease statistics from British Heart Foundation (2013a), coronary heart disease (CHD) is the UK's biggest killer, in which around one in six men and more than one in ten women die from the disease amounting to around 74,000 deaths in the UK each year with an average of 200 people each day. People with CHD are having a high risk of myocardial infarction as a result of atherosclerosis (2013b). Clinical evidence suggests that post-infarction patients are at risk of sudden cardiac death secondary to arrhythmia (De Groot and Coronel, 2004; Luqman *et al.*, 2007; Marcus *et al.*, 1988; Prystowsky, 2004). Approximately 50% of deaths from cardiac causes are arrhythmic and occur within 1 hour of the onset of symptoms. Pathological examination reveals that in the majority of cases show signs of acute myocardial infarction. However, the mechanistic link between ischaemia and lethal arrhythmia is poorly understood. Acute myocardial ischaemia results from interruption of blood supply to part of the heart (Figure 5.1) commonly due to occlusion of one or more coronary arteries. The research described in this chapter is designed to examine the electrophysiological events during acute regional ischaemia and subsequent ventricular arrhythmias by using a model of coronary artery occlusion in the isolated rabbit heart.

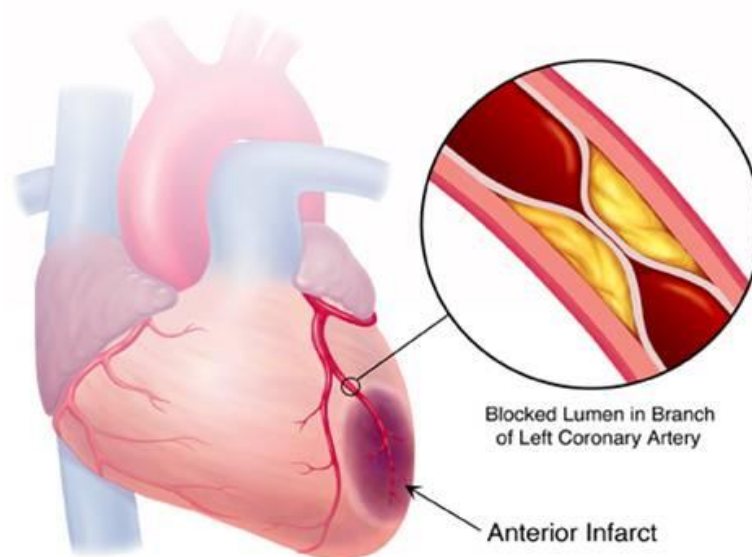


Figure 5.1 Acute regional ischaemia.
Diagram showing region of myocardial infarction secondary to acute coronary artery occlusion.

Methods

Preparation of the rabbit hearts for coronary artery occlusion

A total of 21 animals were used in this set of experiments. In this study, New Zealand White rabbits (2.5-3.5kg) were used. After the rabbit was sacrificed with overdose injection of anaesthesia, the heart was removed and perfused in Langendorff mode. The left posterior division of the coronary artery was occluded with a suture using a short piece of polyethylene tubing to form a snare. The ligature was then connected to a calibrated spring device to ensure standardised occlusion forces. Details on the method to produce acute coronary artery occlusion were explained in detail in Chapter 2. Two additional measures were taken to reduce motion artefact: (i) mechanically constraining the heart within a perspex chamber and (ii) pharmacologically reducing contraction by adding Blebbistatin ($10\mu\text{M}$) into the Tyrode's solution. The perfusing solution and the solution surrounding the hearts inside the chamber was maintained at 37°C . A constant perfusion rate of $30\text{ml}/\text{min}$ was used throughout the experiments. Perfusion pressure was continuously monitored via a transducer connected to the aortic cannula.

Experimental protocols

The experimental protocol is illustrated in Figure 5.2. All optical signal recordings in this study were recorded at the intrinsic heart rate, i.e. hearts were not paced externally.

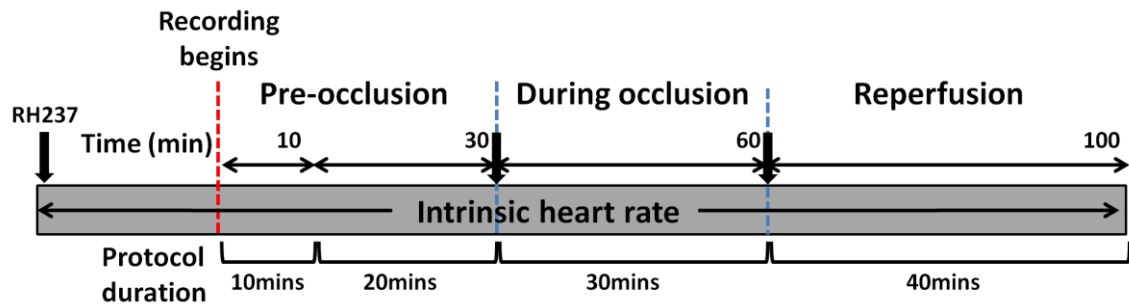


Figure 5.2 Experimental protocol for control experiments.

Dye loading

At the beginning of the experiment, the heart was loaded with 100 μ L bolus of RH237 administered by slow injection into the coronary circulation over 1 minute through an injection port in a bubble trap in line with the aortic cannula. During the experiment, bolus injections of RH237 were repeated twice; before the occlusion period and before the reperfusion period.

Pre-occlusion

Approximately 10-15 minutes after dye injection when the optical signals were stabilized, serial recordings of optical signals were performed at 1 minute intervals for 30 minutes. For the purpose of analyzing the data, the analysis was performed using the data recorded at *Pre-occlusion 10min* (time point at 10 minutes after beginning of the pre-occlusion period) and at *Pre-occlusion 30min* (time point at 30 minutes after beginning of the pre-occlusion period).

Coronary artery occlusion

After 30 minutes of pre-occlusion period, the coronary artery was occluded by tightening the snare to produce regional ischaemia (see Chapter 2). Serial recordings were made at 1 minute intervals for 30 minutes. During this protocol,

some hearts developed VF and some hearts did not. If the heart went into VF, the snare was released to reperfuse the heart and allow the rhythm to revert back to sinus rhythm. However, if the heart was still in VF after releasing the snare, a small bolus (0.2ml) of potassium chloride (KCl) (1M concentration) was injected into the heart through the injection port to provide a phase of uniform transient depolarisation, sinus rhythm returned after the potassium returned to normal levels.

Reperfusion

For the hearts that did not develop VF, the snare was released after 30 minutes of occlusion to reperfuse the heart. Serial recording at 1 minute intervals was done for 40 minutes.

Optical data analysis

The optical signals obtained from this study were analysed using the programme OPTIQ (see Chapter 2). The results presented in this chapter (except for Figure 5.6 and 5.7) were analysed from the whole mapping field of 252 sites (excluding the 4 corner sites) as displayed in Figure 5.3a. Figure 5.3b shows average AP traces from 252 pixels from Figure 5.3a. The parameters that were analysed include the action potential duration at 50% repolarisation (APD_{50}), the range of APD_{50} , the activation time (T_{ActM}) and the range of T_{ActM} . The value for each parameter was expressed as mean \pm SEM. As for Figure 5.6 and 5.7, the results were representing the data from 3 x 3 pixel selections (9 sites) from 3 different zones.

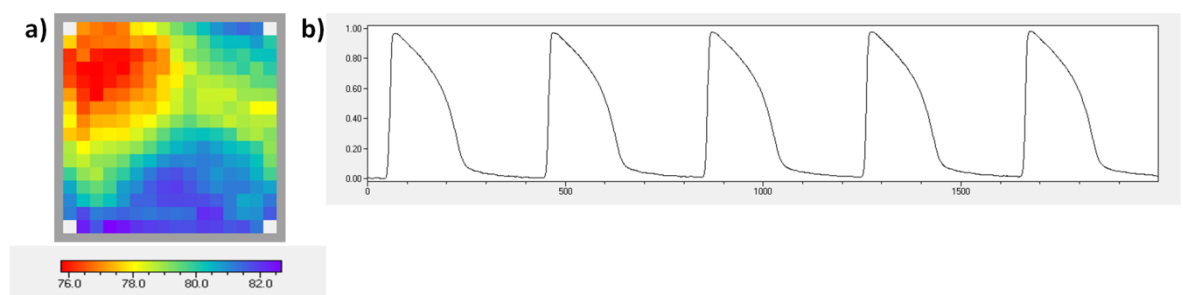


Figure 5.3 Optical data analysis in OPTIQ software.

a) Example of activation map from the apex of the left ventricle showing 252 pixels used for analyzing purposes. The pixels at each corner were excluded. b) Mean optical action potentials (OAPs) from 252 sites at intrinsic heart rate.

Results

Incidence

From the response to the protocol, the hearts could be placed into one of two groups, those that developed arrhythmia during acute regional ischaemia following the coronary artery occlusion and those that did not (up to the time limit of 30 minutes). The bar graph in Figure 5.4a displays the comparison between the incidence of hearts that went into VF and the hearts that did not develop VF. From 21 experiments performed with this protocol, almost 50% of the hearts developed VF during coronary artery occlusion within 30 minutes and the rest did not. Some of the hearts developed VF as early as within the first 5 minutes of occlusion and some hearts developed VF later during the occlusion. Most of the arrhythmic events (40%) occur between 15 to 20 minutes of occlusion (Figure 5.4b).

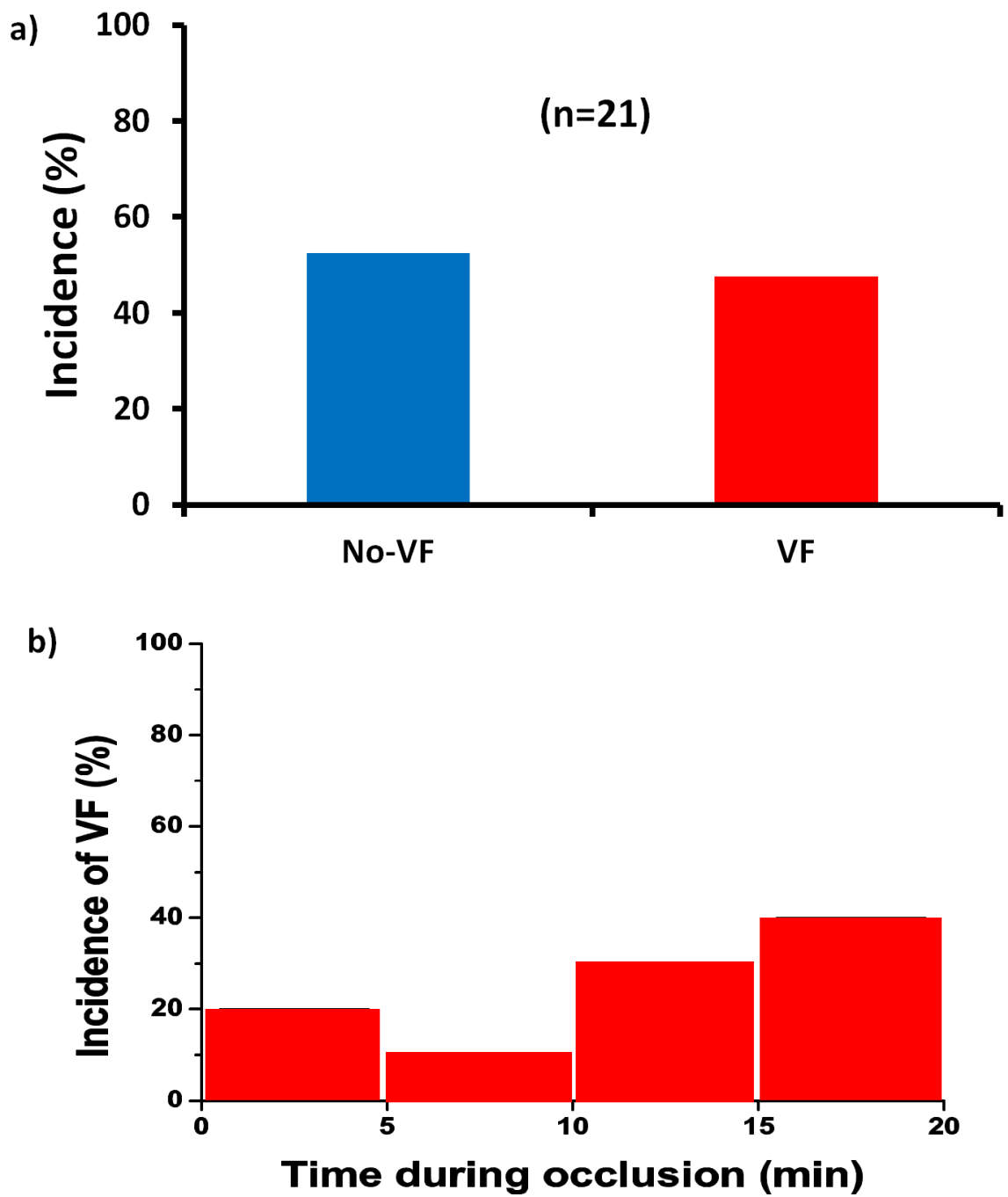


Figure 5.4 Incidence of VF during acute coronary artery occlusion.

a) Incidence of hearts that developed VF and did not develop VF during acute ischaemia (VF = 47.6% and no-VF = 52.4%). b) Incidence of VF relative to the time during occlusion. More hearts developed VF between 15 to 20 minutes of occlusion.

Premature ventricular contractions (PVCs) and T-wave alternans (TWA)

Two phenomena that have been clinically associated with arrhythmia are PVCs (Boineau and Cox, 1973) and TWA (Pastore *et al.*, 1999; Rosenbaum *et al.*, 1994). During the optical signal recordings in our experiments, the instances of PVCs and TWA were noted. The incidence of PVCs and TWA before and during occlusion was analysed to see whether there was any correlation between these phenomena and the incidence of arrhythmia as demonstrated in Figure 5.5. The occurrence of PVCs was noted before and during occlusion whereas TWA were only present during the occlusion. Both no-VF and VF groups had roughly the same incidence of PVCs and TWA.

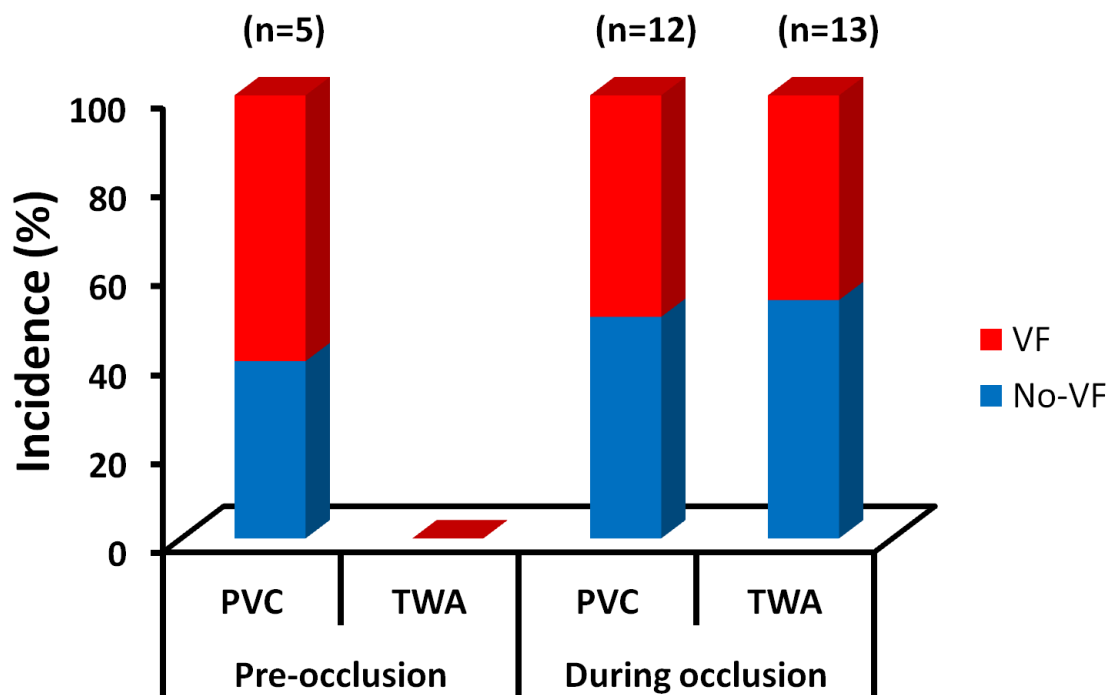


Figure 5.5 PVCs and TWA.

Incidence of PVCs and TWA before and during occlusion in no-VF and VF groups. There were no instances of TWA before occlusion in both groups.

Effect of coronary artery occlusion

Figure 5.6 shows an example of the optical mapping data obtained during the experiments showing the effect of coronary artery occlusion. In this example, the OAPs were sampled from 3 x 3 pixel selections from normal (A), border (B) and ischaemic (C) zones. The pixel selections were indicated by the small white boxes. These pixel selections were chosen based on the degree of shortening of the APD during coronary artery occlusion. The normal zone was chosen on the basis of the region that having the longest APD during occlusion. For the infarct zone, it was selected from the region where there were maximal shortening in APD and the border zone was the region where there was an intermediate change of the APD.

In Figure 5.6, the above panels show the ECG signals and the lower panels show the APD₅₀ colour maps together with the representative AP from different zones before, during and after occlusion. The blue colour indicates the APD₅₀ of about 140-160ms. During occlusion, the area in zone C became ischaemic and the APD₅₀ shortened which generated a gradient of APD which is shown in the colour map in the middle. The ECG recorded during occlusion demonstrates S-T segment depression which is a classic clinical signs of acute ischaemia. On reversal when the snare was released to reperfuse the heart, the APD returned to normal and the ECG returned towards normal even though there were some slight S-T changes.

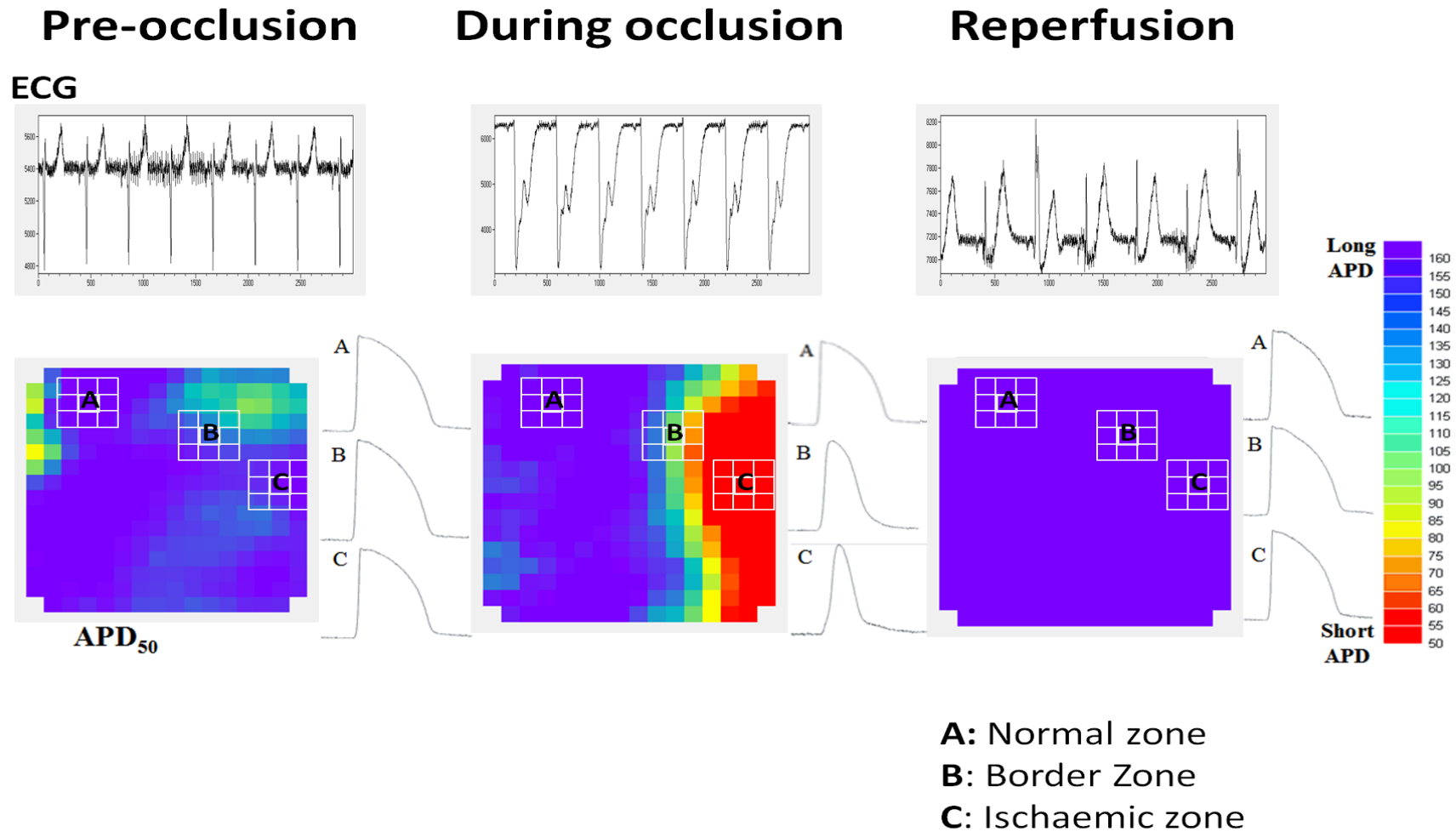


Figure 5.6 Effect of coronary artery occlusion.

Example of optical mapping data before, during and after occlusion. Above panels show ECG signals, lower panels show the APD₅₀ colour maps together with the representative AP from different zones. The OAPs from each zone were sampled from 3 x 3 pixel selections as indicated by the small white boxes.

Figure 5.7 demonstrates an example of full protocol time course in our experiments. During the pre-occlusion period, the APD_{50} stabilised to a steady-state value. During occlusion, the APD_{50} especially in Zone C showed dramatic shortening. Reperfusion restored the APD_{50} to normal, but the value appeared to continue to gradually increase for the duration of the reperfusion period. Some hearts developed VF during the occlusion, in this case ~20 minutes after occlusion. For the purpose of this study, only arrhythmic events - either sustained or non-sustained VF - that occurred within 30 minutes duration of occlusion were included in the VF group. Any episode of arrhythmia that took place pre-occlusion or during reperfusion was not included in the VF group.

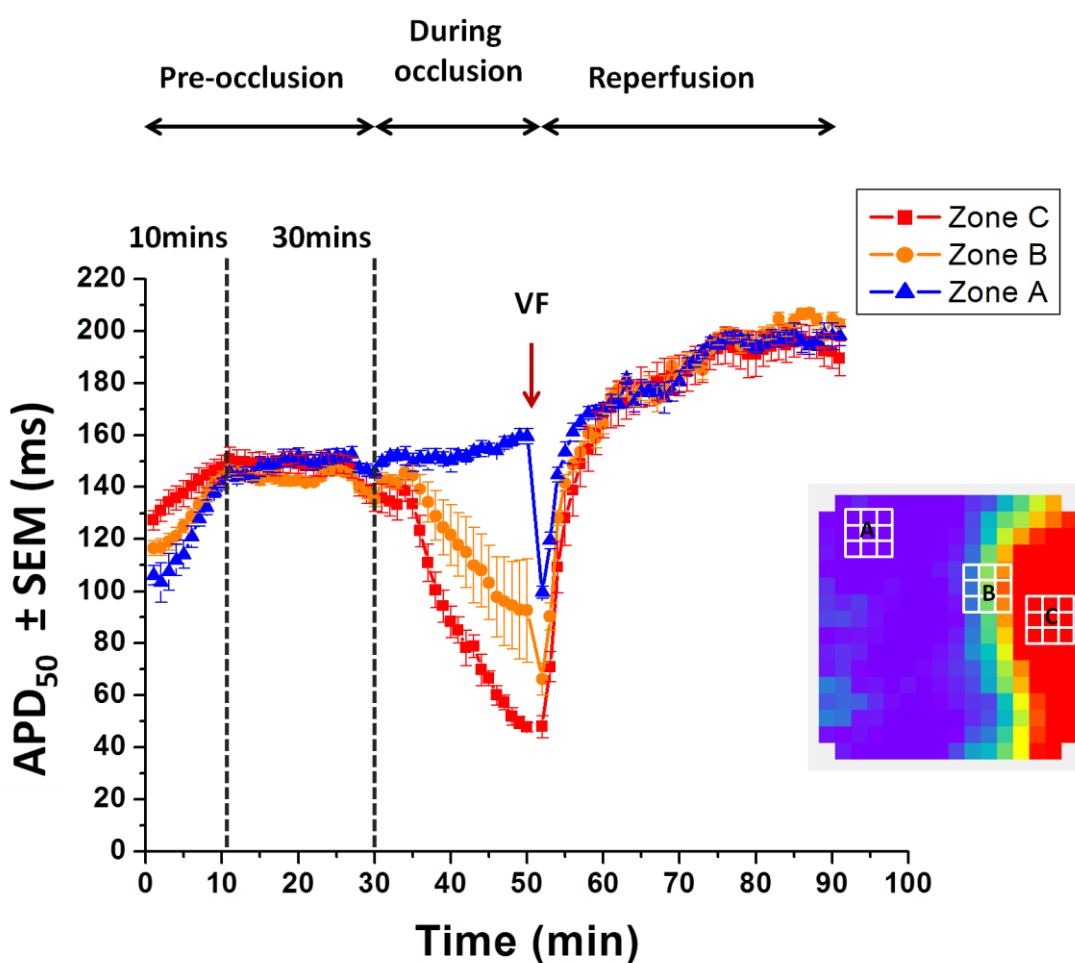


Figure 5.7 Full protocol time course.

Example of full protocol time course showing changes of APD_{50} obtained from three different zones during acute coronary artery occlusion experiment. The value is expressed as the mean APD_{50} and the error bars indicate the standard error of the mean (SEM) from 3 x 3 pixel selections from each zone as indicated by the white boxes on the colour map. Zone A= Normal zone, Zone B= Border zone, Zone C= Ischaemic zone.

For the purpose of comparing the results effectively, the electrophysiological parameters were analysed at the same time points throughout the experiments for both no-VF and VF groups. The standard time points used in this study were 10 minutes into the pre-occlusion phase (*Pre-occlusion 10min*), after 30 minutes of control period, i.e. immediately prior to occlusion (*Pre-occlusion 30min*), 5 and 10 minutes after occlusion (*Occlusion 5min* and *Occlusion 10min*).

APD₅₀ (no-VF vs. VF groups)

One of the electrophysiological parameters analysed in this study was the APD₅₀. The plotted graph of APD₅₀ at *Pre-occlusion 30min* for each individual experiments (n=21) interestingly revealed that the hearts which developed VF had significantly shorter APD with the mean APD₅₀ of $141.5 \pm 3.5\text{ms}$ whereas the hearts that did not develop VF have a longer APD₅₀ with the mean of $168.8 \pm 5.5\text{ms}$ as demonstrated in Figure 5.8. The APD₅₀ difference between the two groups was greatly significant ($P<0.001$).

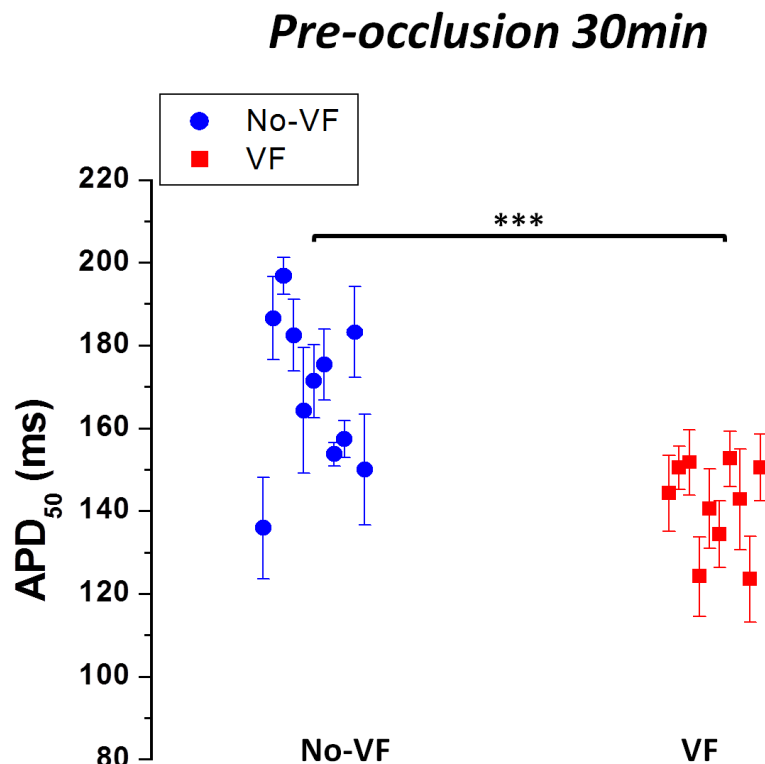


Figure 5.8 APD₅₀ (no-VF vs. VF groups)

APD₅₀ (mean \pm SEM) for each individual experiment at *Pre-occlusion 30min* (n=21). The hearts that developed VF had a significantly shorter APD₅₀ ($P<0.001$) as compared to the no-VF hearts.

Box plots diagram in Figure 5.9 further demonstrates the difference in the APD_{50} between both groups. The APD_{50} was significantly prolonged at *Pre-occlusion 30min* as compared to the APD_{50} at *Pre-occlusion 10min* in both groups. The result also shows that the APD_{50} at 10 and 30 minutes of the pre-occlusion period in VF group were significantly shorter as compared to the no-VF group at the corresponding time point. The mean values for the APD_{50} at *Pre-occlusion 10min* and *Pre-occlusion 30min* in both no-VF and VF groups were listed in Table 5.1.

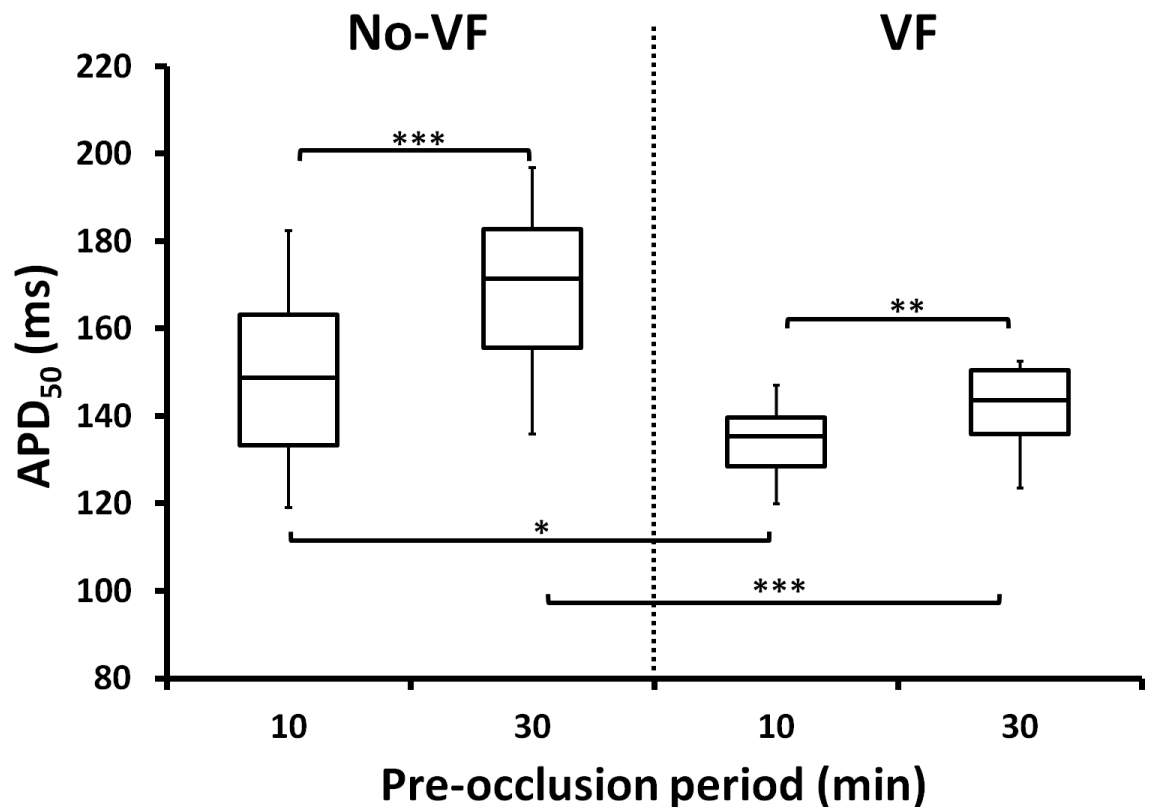


Figure 5.9 APD_{50} at pre-occlusion period.

Box plots of the mean APD_{50} between no-VF and VF groups at 10 and 30 minutes pre-occlusion. The upper and lower limits of the box represent the 75th and 25th percentile, respectively. The upper and lower limits of the error bars represent the maximum and minimum, respectively and the line in the middle represents the median. APD_{50} was significantly longer at *Pre-occlusion 30min* as compared to APD_{50} at *Pre-occlusion 10min* in both groups. Both APD_{50} at 10 and 30 minutes in the VF group were significantly shorter than the APD_{50} at corresponding time frame in the no-VF group. (* $P < 0.05$, ** $P < 0.01$, *** $P < 0.001$)

Table 5.1 APD₅₀ at *Pre-occlusion 10min* and *Pre-occlusion 30min*. Comparison between no-VF and VF groups.

	No-VF		VF	
	<i>Pre-occlusion 10min</i>	<i>Pre-occlusion 30min</i>	<i>Pre-occlusion 10min</i>	<i>Pre-occlusion 30min</i>
Mean APD ₅₀ (ms)	149.1	168.8	133.8	141.5
SEM	6.3	5.5	2.7	3.5

The APD₅₀ at *Pre-occlusion 30min*, *Occlusion 5min* and *Occlusion 10min* were analysed and plotted in box plots diagram as in Figure 5.10. Comparison of the APD₅₀ was made between the two groups. The result reveals that in both no-VF and VF groups, the APD₅₀ were significantly shorter during occlusion as compared to the pre-occlusion period. Further analyses show that the APD₅₀ at *Pre-occlusion 30min* and during *Occlusion 5min* in the VF group were significantly shorter than the APD₅₀ at corresponding time points in the no-VF group. The mean APD₅₀ values at each time point in both groups were listed in Table 5.2.

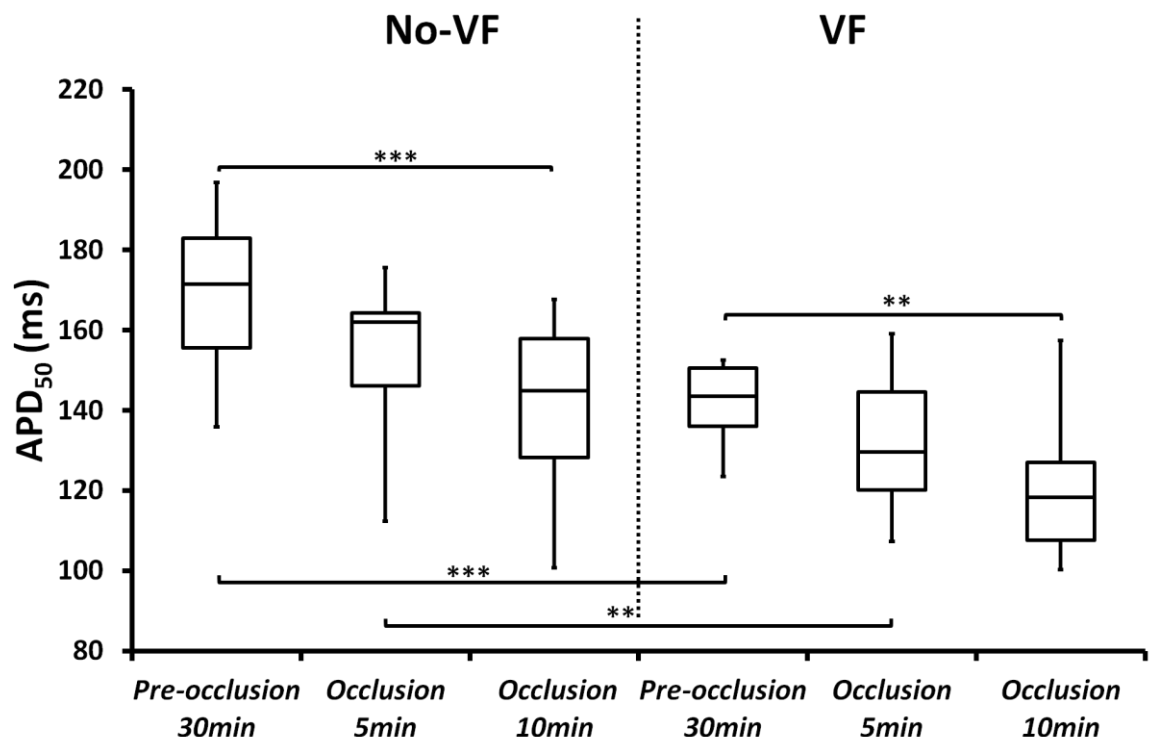


Figure 5.10 APD₅₀ before and during occlusion.

Box plots of the mean APD₅₀ at *Pre-occlusion 30min*, *Occlusion 5min* and *Occlusion 10min* for no-VF and VF groups. The hearts in VF group have significantly shorter APD₅₀ at pre-occlusion and during *Occlusion 5min* as compared to the no-VF group at the same time point. (* $P < 0.05$, ** $P < 0.01$, *** $P < 0.001$)

Table 5.2 APD₅₀ before and during occlusion.

APD₅₀ at *Pre-occlusion 30min*, *Occlusion 5min* and *Occlusion 10min* in no-VF (n=11) and VF (n=10) groups.

	No-VF			VF		
	<i>Pre-occlusion 30min</i>	<i>Occlusion 5min</i>	<i>Occlusion 10min</i>	<i>Pre-occlusion 30min</i>	<i>Occlusion 5min</i>	<i>Occlusion 10min</i>
Mean APD₅₀ (ms)	168.8	154.1	139.6	141.5	131.5	120.7
SEM	5.5	5.2	7	3.5	5.5	7.5

Apart from the APD₅₀, the range of APD₅₀ (difference between the longest APD and the shortest APD from 252 sites) was also analysed to look at the heterogeneity of the hearts. The results for the range of APD₅₀ in both groups were plotted in box plots diagram in Figure 5.11. The range of APD₅₀ was larger during occlusion as compared to the range of APD₅₀ at *Pre-occlusion 30min* in each no-VF and VF groups. At *Pre-occlusion 30min*, there was no significant difference between the two groups. However, during *Occlusion 5min*, the hearts that developed VF had a greater range of APD₅₀ as compared to the hearts that did not develop VF. This result indicates that in the hearts that went into VF, there was greater heterogeneity in terms of APD₅₀ which might predispose the hearts to VF.

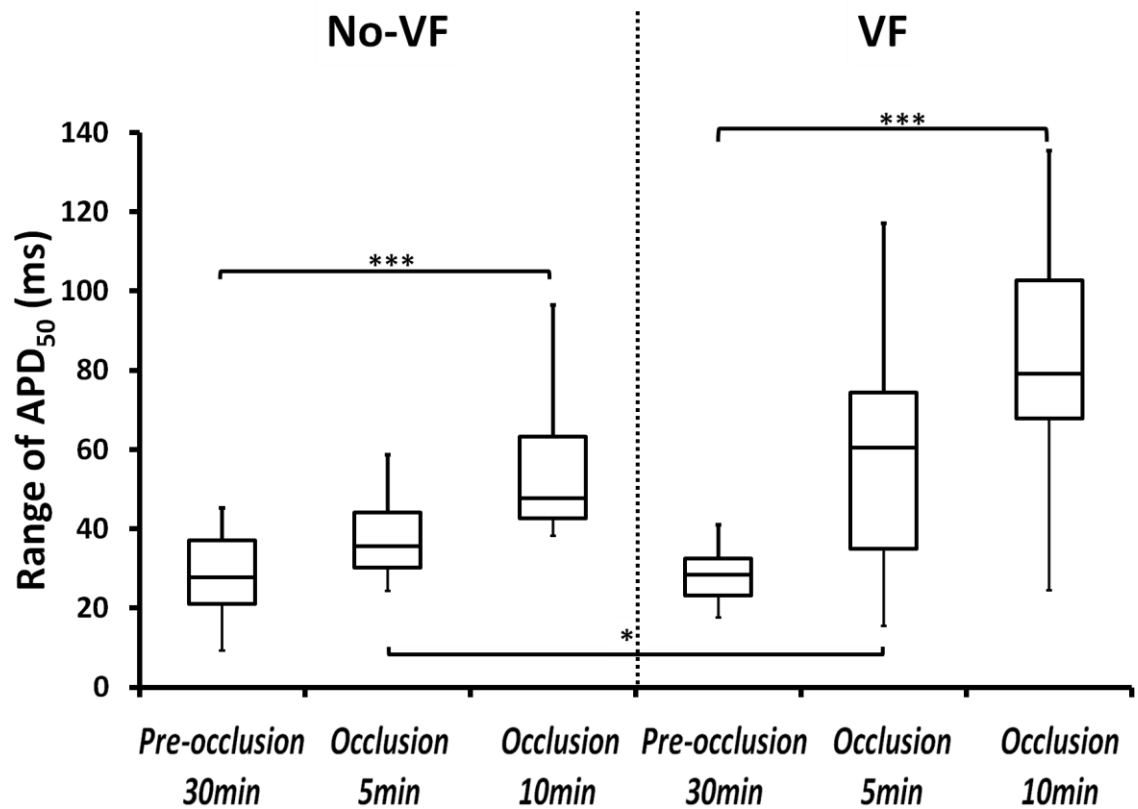


Figure 5.11 Range of APD₅₀ before and during occlusion.

Box plots of the range of APD₅₀ at *Pre-occlusion 30min* and during *Occlusion 5min* and *Occlusion 10min*. In each no-VF and VF groups, the range of APD₅₀ was significantly larger during occlusion as compared to the *Pre-occlusion 30min*. However, when the range of APD₅₀ was compared between the two groups, only the range of APD₅₀ during *Occlusion 5min* was significantly different (* $p < 0.05$) in which the VF group had a greater range of APD₅₀. (* $P < 0.05$, ** $P < 0.01$, *** $P < 0.001$)

Activation time (no-VF vs. VF groups)

Analysis of the activation time in both no-VF and VF groups revealed no significant difference between the two groups either pre-occlusion or during occlusion as shown in Figure 5.12a. As the range of activation time during occlusion became significantly longer compared to the *Pre-occlusion 30min* in the no-VF group, the box plots diagram in Figure 5.12b show no significant difference in the range of activation time between the two groups.

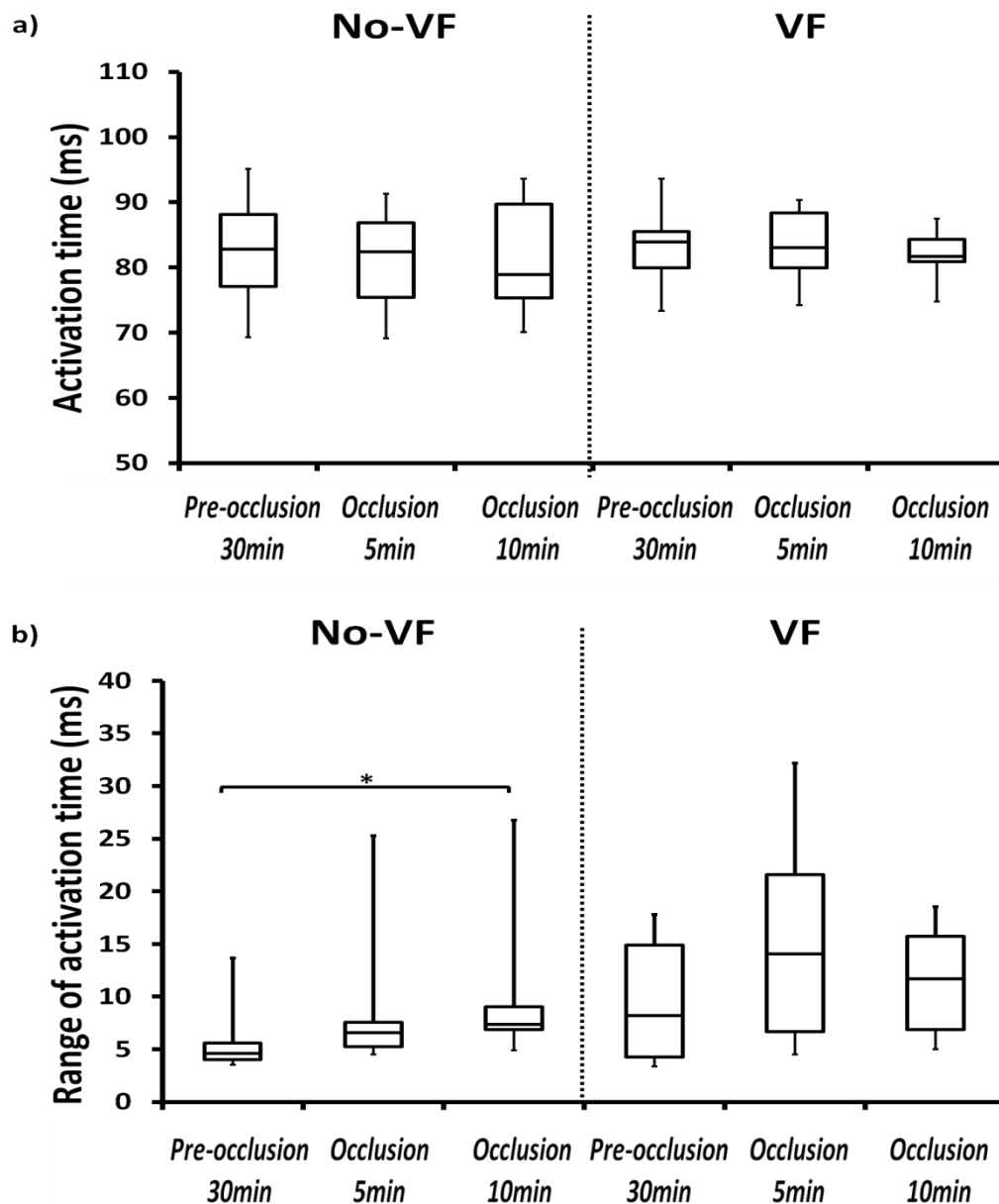


Figure 5.12 Activation time before and during occlusion.

a) Box plots of the activation time at *Pre-occlusion 30min* and during *Occlusion 5min* and *Occlusion 10min* in both groups. b) Box plots graph of the range of activation time at similar time points in no-VF and VF groups. There was no significant difference in the activation time as well as the range of activation time between both groups either pre-occlusion or during occlusion.

APD₅₀ vs. heart rate

From the results shown so far, the only significantly different parameter prior to occlusion that correlated with the presence of arrhythmias is the APD₅₀. Based on this finding, the relation between the APD₅₀ and the heart rate was studied. Figure 5.13 demonstrates the mean APD₅₀ at *Pre-occlusion 30min* from each experiment plotted against the sinus cycle length. The result reveals that the hearts in VF group had significantly shorter APD₅₀ ($P<0.001$) and shorter cycle length (mean cycle length $0.359 \pm 0.007\text{ms}$) whereas the hearts in no-VF group had longer APD₅₀ and longer cycle length (mean cycle length $0.391 \pm 0.012\text{ms}$). Therefore the sinus cycle length was significantly different between the two groups ($P<0.05$) even though there was also considerable overlap between the two groups.

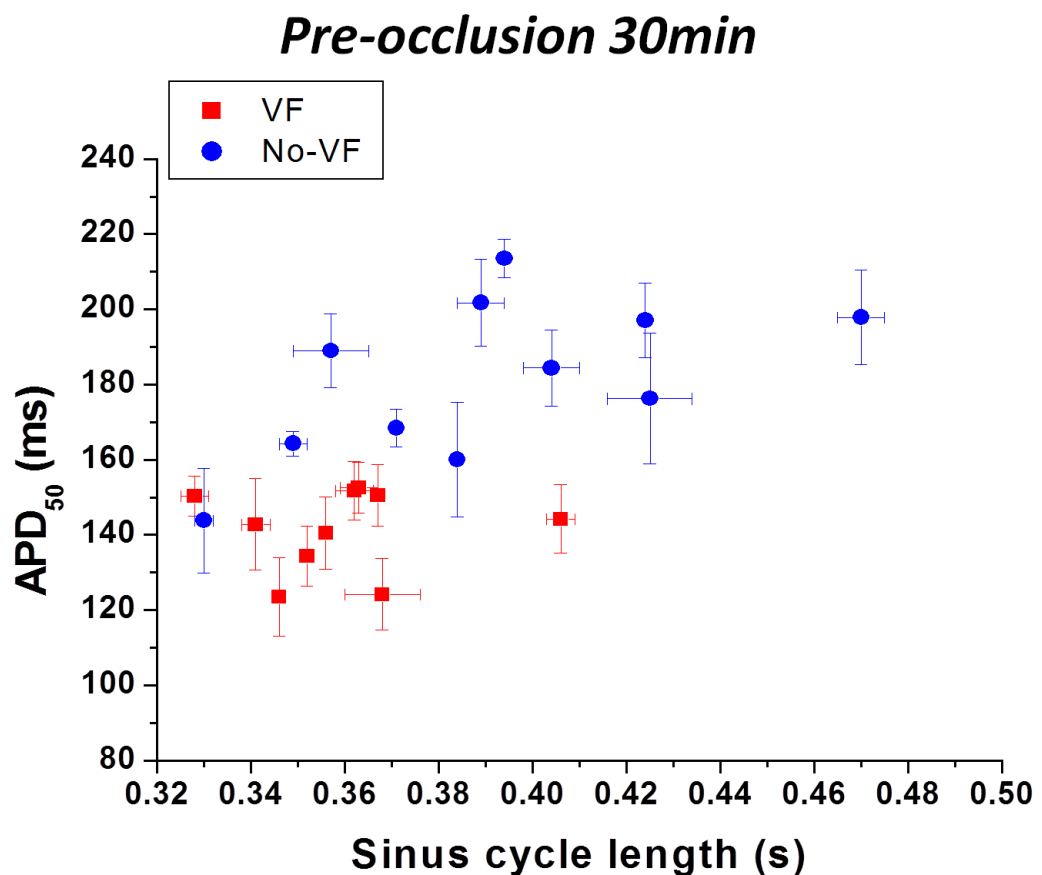


Figure 5.13 APD₅₀ vs. heart rate.

APD₅₀ (mean \pm SEM) plotted against the sinus cycle length (mean \pm SEM) for all hearts in both no-VF and VF groups. Hearts in VF group had significantly shorter APD₅₀ and shorter cycle length.

ECG parameters

In addition to the electrophysiological parameters, the ECG parameters were also analysed to see whether there was any correlation between the electrophysiological parameters and the ECG parameters in both groups of hearts. The values for the ECG parameters were taken from the average of 5 consecutive ECG complexes. Based on the relation between APD_{50} and the heart rate seen in Figure 5.13, the relationship between the QT and RR interval at *Pre-occlusion 30min* was studied. The graph of the QT interval against the RR interval was plotted in Figure 5.14 (top panel). The result reveals a similar pattern as seen in the previous figure in which the hearts that went into VF had shorter QT and shorter RR intervals compared to the hearts that did not develop VF. The mean QT interval for VF group was 0.204 ± 0.004 ms whereas the mean QT interval for no-VF group was 0.230 ± 0.006 ms. The means were significantly different ($P < 0.01$). The graph of corrected QT interval (QT_c) against the RR interval was plotted as well (Figure 5.14 bottom panel). In our experiments, the mean heart rate (HR) for the VF group was 168 ± 3 bpm and the mean HR for the no-VF group was 155 ± 5 bpm. The mean \pm SEM for the ECG parameters in both no-VF and VF group were listed in Table 5.3. It shows that the mean RR and QT interval was significantly shorter in VF hearts as compared to the hearts that did not develop VF. In addition, even after correcting the QT interval for the heart rate, the difference between the two groups still existed.

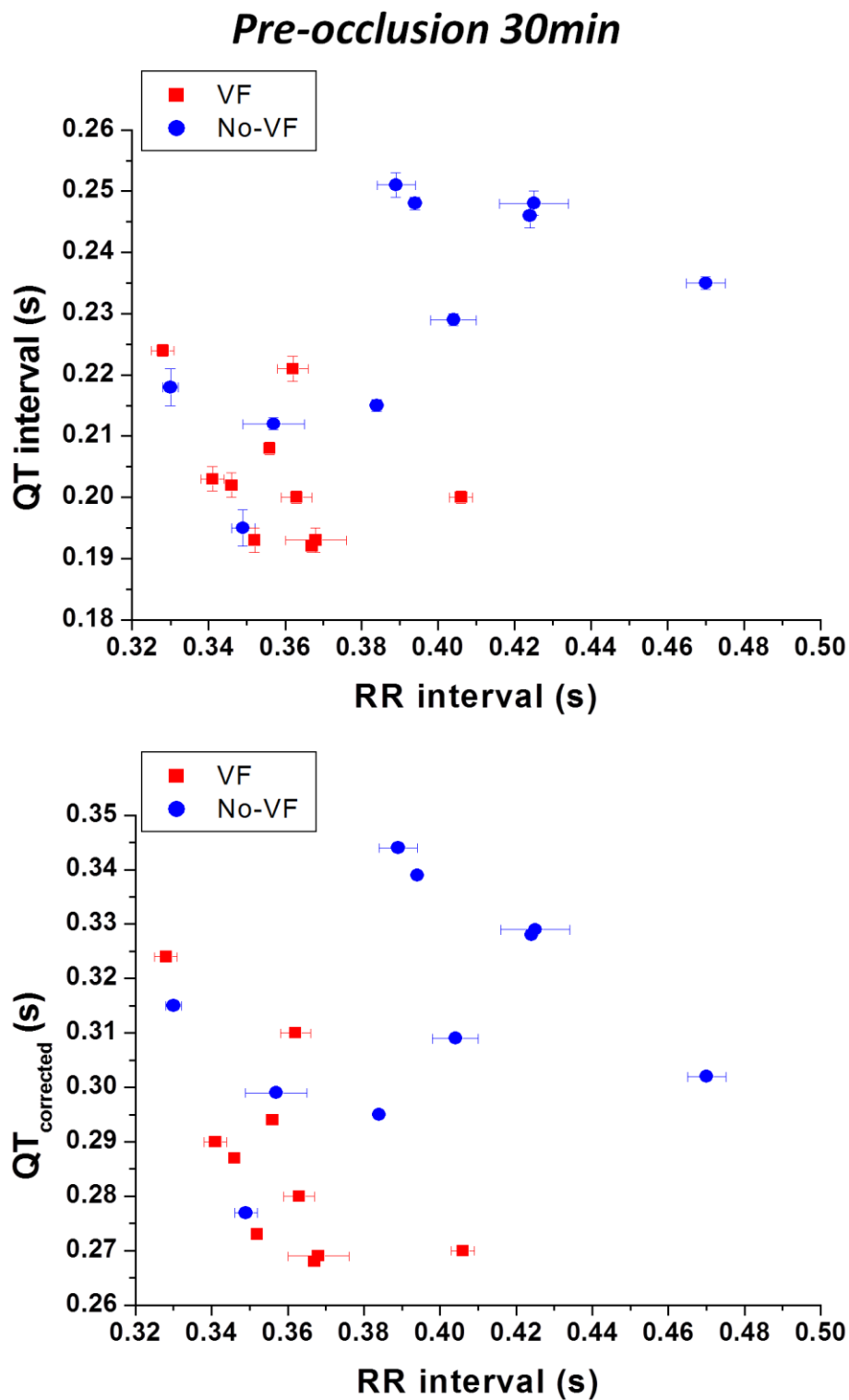


Figure 5.14 ECG parameters at *Pre-occlusion 30min*.

Top: Graph of QT interval against the RR interval in both no-VF and VF groups. Bottom: The graph of QT_c against RR interval was plotted as well. Error bar on both X and Y axis represents the SEM from 5 consecutive ECG complexes.

Table 5.3 ECG parameters at *Pre-occlusion 30min*.

Comparison of the ECG parameters (mean \pm SEM) at *Pre-occlusion 30min* between the no-VF and VF hearts. The hearts that developed VF during occlusion had intrinsically faster heart rate at *Pre-occlusion 30min* as compared to the hearts that did not develop VF. The RR, QT and QTc intervals in the VF group was significantly shorter than the no-VF group.

Pre-occlusion 30min

	RR Interval (s)	PR Interval (s)	QRS Interval (s)	QT Interval (s)	QT _{corrected} (s)	Heart rate (bpm)
No-VF	0.391 \pm 0.012	0.062 \pm 0.002	0.032 \pm 0.003	0.230 \pm 0.006	0.314 \pm 0.007	155 \pm 5
VF	0.359 \pm 0.007	0.060 \pm 0.002	0.035 \pm 0.002	0.203 \pm 0.004	0.286 \pm 0.006	168 \pm 3
P value	*P<0.05	NS	NS	**P<0.01	**P<0.01	*P<0.05

In this study, the Fredericia's formula was used to calculate the corrected QT interval.

$$\text{Fredericia's formula: } QT_c = QT / RR^{1/3}$$

An alternative formula for the calculation of the QT_c is Bazett's formula. In Bazett's formula, the QT interval is divided by the square root of RR interval instead of the cube root. Although Bazett's formula is the most commonly used formula for the corrected QT calculation, it has a tendency to over-correct at heart rates > 100bpm and under-correct at heart rates < 60bpm. In this study, the hearts that developed VF had intrinsically faster heart rates as compared to the hearts that did not develop VF and the mean heart rates for both groups were > 100bpm. Therefore, the Fredericia's formula is more appropriate and was chosen to calculate the QT_c values.

Is the behaviour of the epicardial sites homogeneous in terms of APD₅₀ (no-VF vs. VF groups)

The histogram in Figure 5.15 indicates the change in APD₅₀ in terms of the number of sites getting shorter or longer at certain periods of time during the protocol in both groups of hearts (no-VF and VF). Each colour represents a different heart; colour in the same group represents the same heart.

Behaviour pre-occlusion

Figure 5.15a shows the number of sites that got longer or shorter between the 10 and 30 minutes pre-occlusion phases. In the VF group, the average number of sites that showed an increase in APD₅₀ from the *Pre-occlusion 10min* phase to the *Pre-occlusion 30min* phase was 198 and on average 54 sites became shorter. On the other hand, at very few sites did the APD₅₀ decrease in the no-VF group, instead at most of the sites (247) the APD₅₀ became longer. The number of sites with longer and shorter APD₅₀ was significantly different between the two groups (Figure 5.15a).

Behaviour on occlusion

Figure 5.15b demonstrates the change in APD₅₀ between *Pre-occlusion 30min* and the *Occlusion 5min*. It reveals that the APD₅₀ at some sites got longer and some sites got shorter in both groups but most of the sites got shorter. In the VF group, on average there were 101 sites where the APD₅₀ got longer and 151 sites where APD₅₀ shortened. On the contrary, in the no-VF group, the APD₅₀ got longer only in 56 sites and the APD₅₀ shortened in 196 sites. However, the differences between the two groups were not significant. Between *Pre-occlusion 30min* and *Occlusion 10min*, more sites got shorter in both no-VF and VF groups as represented in Figure 5.15c but the difference between the two groups was not significant. This was probably because, as the duration of the coronary artery occlusion increased, more epicardial sites exhibited APD₅₀ shortening.

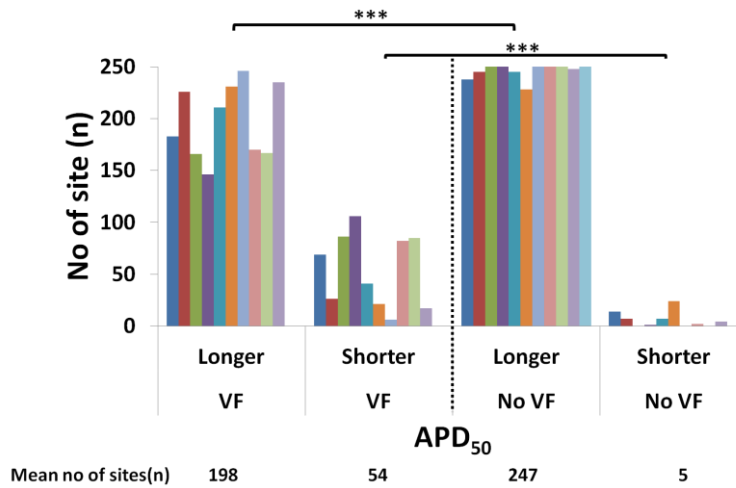
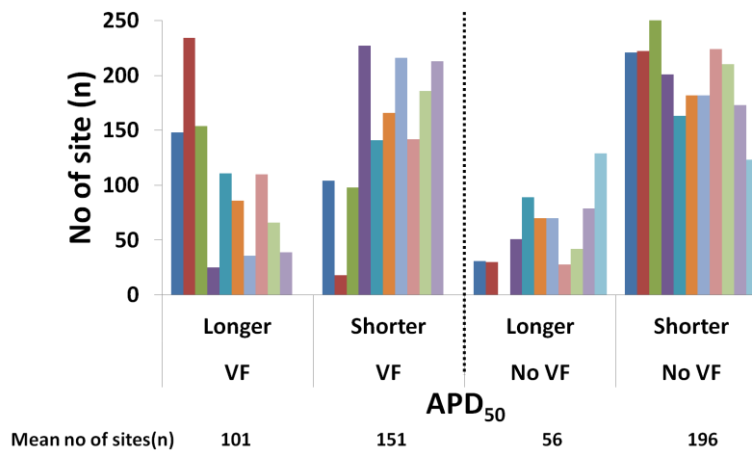
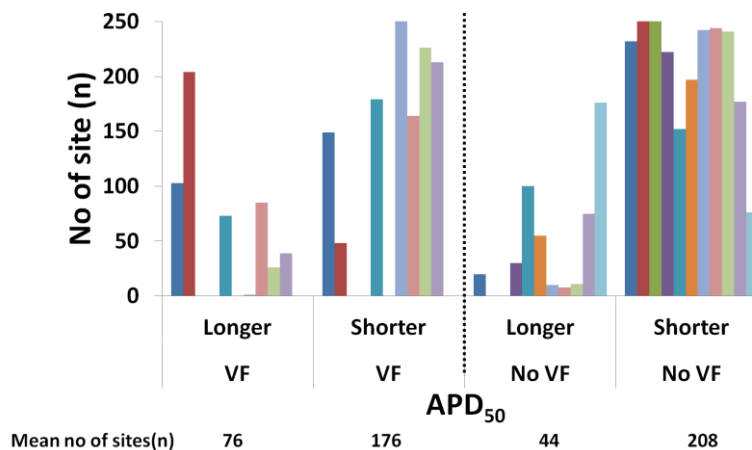
a) *Pre-occlusion 30min vs. Pre-occlusion 10min*b) *Occlusion 5min vs. Pre-occlusion 30min*c) *Occlusion 10min vs. Pre-occlusion 30min*

Figure 5.15 Behaviour of APD_{50} on epicardial surface pre-occlusion and during occlusion. Histograms showing the number of sites in which the APD_{50} got longer or shorter at certain period of time in both no-VF and VF groups. a) APD_{50} changes between *Pre-occlusion 10min* and *Pre-occlusion 30min*. b) APD_{50} changes between *Pre-occlusion 30min* and *Occlusion 5min*. c) APD_{50} changes between *Pre-occlusion 30min* and *Occlusion 10min*.

Further analysis on the absolute shortening of APD_{50} during occlusion relative to the pre-occlusion period (Figure 5.16) also did not reveal any significant finding. Although the mean APD_{50} was shorter in the VF group, the average absolute shortening of APD_{50} was not significantly different from the no-VF group with longer mean APD_{50} .

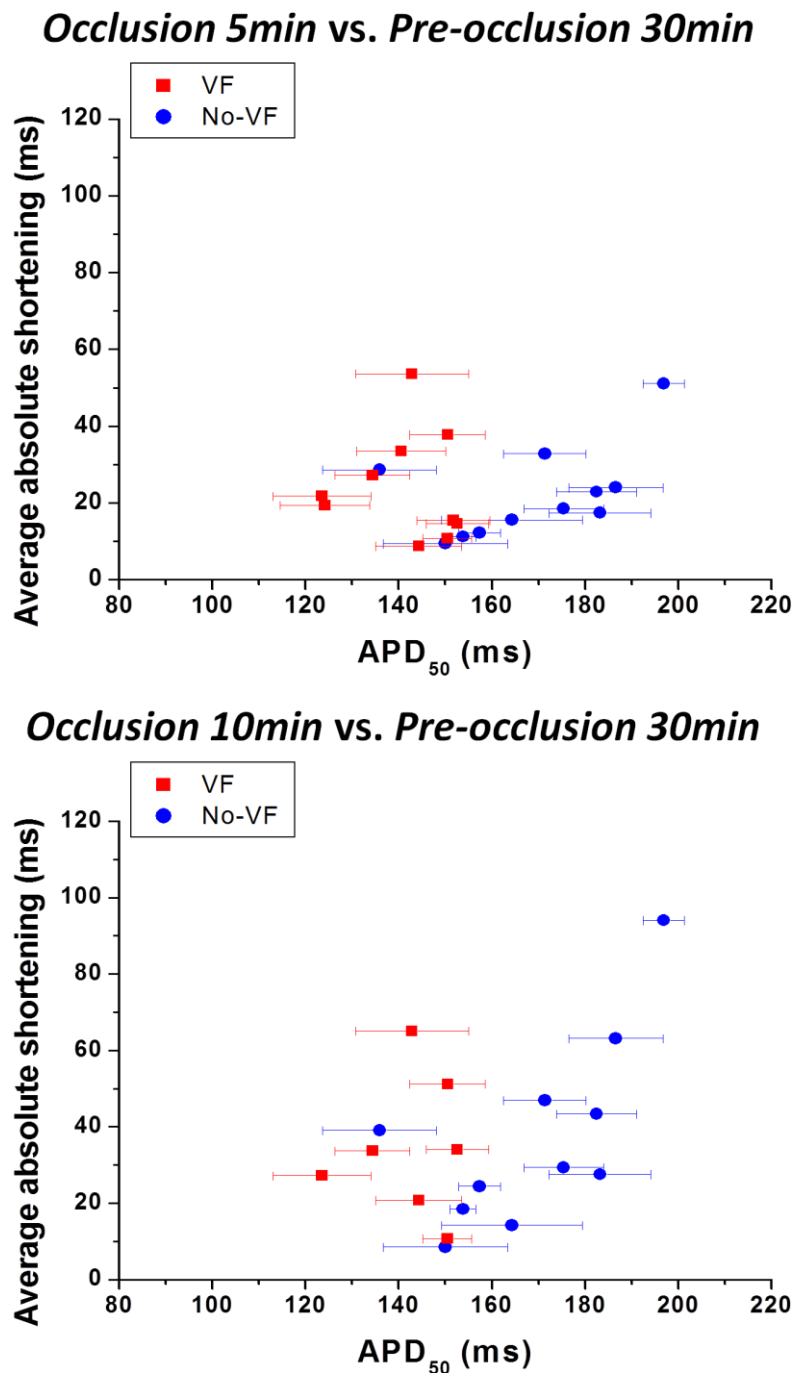


Figure 5.16 Absolute shortening of APD_{50} .
Average absolute shortening of APD_{50} at *Occlusion 5min* (top panel) and *Occlusion 10min* (bottom panel) relative to the APD_{50} at *Pre-occlusion 30min* for each individual experiment in both groups.

Discussion

The purpose of this chapter was to examine LV epicardial electrophysiology before and during local occlusion of the coronary artery in an effort to find the underlying causes of ischemia-induced arrhythmias. In approximately 50% of experimental preparations VF occurred within 30 minutes of occlusion of the coronary artery. The area of LV epicardium imaged in these experiments included regions served by the coronary artery and sub-regions within the imaged field showed changes in action potential characteristics that are consistent with underlying ischaemia. Correlating electrophysiological changes to the presence of VF suggested that electrophysiological characteristics prior to occlusion were a significant determinant of tendency to VF during ischaemia.

Shorter APD prior to occlusion predicts tendency to VF

The mean APD₅₀ prior to occlusion both at the *Pre-occlusion 30min* and *Pre-occlusion 10min* time points were good predictors of VF: on average the hearts that developed VF had an APD₅₀ value approximately 15-20ms less than those that remained in sinus rhythm during coronary artery occlusion. The difference in APD could be due to differences in sinus rates of individual hearts, i.e. shorter APD could be a consequence of a higher intrinsic rate, but this is not the explanation for this data because choosing a subgroup with comparable range of heart rates still exhibited shorter APDs in the VF group.

An alternative explanation is that within the population of animals used in this study, there was a range of variation in the ventricular action potential duration from one individual heart to the next. This spread in electrophysiological characteristic is due to a range of ion channel expression levels across a population. This type of variation has been studied in computational models and the extent of changes in ion channel activity that would cause a range of AP repolarisation characteristics was quantified (Romero *et al.*, 2009).

In both groups, there was a trend to shortening of APD₅₀ between 30 minutes and 10 minutes prior to occlusion, and in the VF group a greater number of sites significantly shortened during this period. This could be explained by supposing the existence of a slowly developing ischaemic region before the occlusion of

the coronary artery. However, this is unlikely because: (i) APD shortening due to slowly developing ischaemic changes during the experiment may be expected to be paralleled by slowly increasing perfusion pressure. The perfusion pressure at the pre occlusion 30 minutes phase was not significantly different in the two groups (for the VF hearts 46.8 ± 3.1 mmHg and the no-VF hearts 52.8 ± 2.7 mmHg). (ii) There were no obvious ST segment changes observed on the ECG during the pre-occlusion phase which would be indicative of the development of an ischaemic region.

Extrinsic pacing was not used in these experiments in order to replicate as closely as possible the *in vivo* circumstances, and it could be argued that a regular pacing stimulus would mask any changes in heart rate and rhythm during ischaemia and arrhythmia. On the other hand, one disadvantage of not pacing the heart is that there are two sources of variation in APD, one due to intrinsic rate and the other arising from other processes. However, based on previous works done in the lab, the variation in intrinsic rate within any one heart was minimal. In this chapter, it emerged that the intrinsic rate of the heart appeared to be different in the two groups. Further experiments revealed that the intrinsic rate was not a critical variable: experiments in Chapter 6 (isoprenaline experiments) and Chapter 8 (panoramic view optical mapping experiments) in which the heart was controlled at certain rate demonstrated that there were the same splits between no-VF and VF incidence.

Decreased APD equates to shorter QT interval

Parallel ECG measurements showed a decreased QT interval in the VF group which remained after QT correction. The vulnerability of arrhythmias associated with a decreased QT interval is a known syndrome in humans as short QT syndrome (SQTS). Studies have described that abnormal QT intervals are associated with increased risk of ventricular arrhythmia (Modell and Lehmann, 2006; Sanguinetti and Mitcheson, 2005). Over the last 15 years, distinct genetic syndromes involving abnormally abbreviated QT interval (and hence accelerated ventricular repolarisation) have been identified (Bjerregaard *et al.*, 2006; Gussak *et al.*, 2000; McPate *et al.*, 2006). Patients with the genetic short QT syndrome (SQTS) typically exhibit: abbreviated QT intervals (<320ms) (Bjerregaard *et al.*, 2006); poor rate-adaptation of the QT interval; tall, upright T waves; shortened

atrial and ventricular effective refractory periods; and an increased risk of ventricular and atrial arrhythmias and of sudden death in the absence of structural heart disease (Giustetto *et al.*, 2006; Gollob *et al.*, 2011; Gussak *et al.*, 2000; Gussak *et al.*, 2002; Schimpf *et al.*, 2005). Recent analysis of 61 SQTs cases reported arrhythmia-linked index events in ~57% of the cases (Gollob *et al.*, 2011); an analysis of a long-term follow-up of a paediatric cohort with the SQTs reported ventricular fibrillation in ~28% of patients (Villafane *et al.*, 2013).

The SQTs is genetically heterogeneous. Since 2004, defects in three cardiac potassium (K^+) channel genes have been found in SQTs patients (Giustetto *et al.*, 2011; Maury *et al.*, 2008; Schimpf *et al.*, 2005): (i) *KCNH2* ('*HERG*', responsible for the α -subunit of the I_{Kr} channel) for SQT1 (Brugada *et al.*, 2004; Hong *et al.*, 2005a; Sun *et al.*, 2011); (ii) *KCNQ1* (*KvLQT1*, responsible for the α -subunit of the I_{Ks} channel) for SQT2 (Bellocq *et al.*, 2004; Hong *et al.*, 2005b); and (iii) *KCNJ2*, responsible for the Kir2.1 inwardly rectifier K^+ channel) for SQT3 (Hattori *et al.*, 2012; Priori *et al.*, 2005). In addition, loss-of-function cardiac calcium channel mutations (*CACNA1C* (SQT4), *CACNB2* (SQT5) and *CACNA2D1* (SQT6)) have also been identified in association with QT shortening, S-T segment elevation and arrhythmia risk (Antzelevitch *et al.*, 2007; Templin *et al.*, 2011). However, no one has found a SQTs variant linked to altered mutation of the K_{ATP} channel.

A clinical study in patients with a first ST-elevation myocardial infarction (STEMI) revealed that family history of sudden death and higher cumulative ST deviation from ECG analysis are strong predictors for primary VF (Dekker *et al.*, 2006). Based on this finding, the existence of familial sudden death might suggest that there is a possibility of genetic abnormality related to K_{ATP} channel mutation and short QT syndrome. Although these phenomena are rare, this suggests that, within the population of people with myocardial infarction, there could be an inherited predisposition to precipitating or maintaining VF following myocardial infarction.

VF is associated with decreased APD and increased variability of APD.

The data from this study also showed that hearts that exhibited VF shortly after occlusion had a significantly decreased APD_{50} at the *Occlusion 5min* time point along with a higher variability of APD_{50} values. These changes are consistent with previous literature suggesting that: (i) decreased APD will predispose the myocardium to re-entrant arrhythmias, (ii) increased variability of APD is a pro-arrhythmic change (Extramiana and Antzelevitch, 2004). The combined effect of these changes would make the myocardium more capable of initiating and maintaining re-entrant arrhythmias. These changes may be the result of a more severe ischaemic challenge since there is considerable variability in the size and extent of the ischaemic region caused by the occlusion of the coronary artery. However, the group of hearts prone to VF also displayed shorter APD_{50} in the pre-occlusion phase. This suggests that these hearts may have exhibited a shorter APD_{50} during occlusion because of pre-existing tendency to shorter APD values.

Is there a correlation with area of myocardium that undergoes ischaemic changes in APD?

To see if the size of the infarct during occlusion was correlated with the incidence of arrhythmia, the changes of APD_{50} during occlusion were compared with those during the pre-occlusion period. Quantifying the number of sites where the APD_{50} decreased during occlusion revealed that there was no significant difference in the number of sites i.e. the area affected by occlusion between no-VF and VF groups. This can only be an estimate since only part of the myocardium affected by occlusion was imaged in these experiments and areas outside the field of view may represent the majority of the myocardium involved.

Conclusion

The electrophysiology of hearts before the occlusion appears to predispose the heart to VF during the occlusion. The APD_{50} prior to the occlusion was significantly shorter in the hearts that developed VF. This difference in APD_{50} was also reflected in the ECG parameters in which the QT interval is also shorter in the hearts that developed VF. The VF group also had a significantly faster HR, but the data does not support this as the primary cause. The group of hearts that developed VF also displayed shorter and more variable APD_{50} values during occlusion, changes that are known to predispose to arrhythmias, but the mechanistic link to the electrophysiology prior to occlusion is unclear. One explanation is the inherently shorter QT interval in the VF group of hearts which may predispose this group to arrhythmias, to test this hypothesis the APD_{50} was manipulated experimentally in an effort to change the relative population of hearts prone to VF (see Chapter 6).

Chapter 6: Single view optical mapping during acute regional ischaemia after pharmacological manipulation of action potential duration

This chapter continues the studies from the previous chapter (Chapter 5) in an effort to understand the mechanistic link between acute regional ischaemia and ventricular arrhythmia. Results from the previous chapter have shown that pre-occlusion APD seems to be a key variable that might predispose the hearts to VF during occlusion. In this chapter, we varied the APD by the chronic application of E-4031 and transient application of isoprenaline to test whether modifying the APD either by prolonging or simulation of sympathetic activity would alter the tendency of the hearts towards showing VF. E-4031 was chosen because the drug is selective for the hERG channel and previous work (Chapter 4) quantified the extent of the effect and allowed selection of a drug concentration to be used in these experiments. Prolongation of APD by E-4031 should shift the gross electrophysiology of the hearts to the “no-VF” population and reduce the incidence of VF if APD alone is the main determinant.

A transient exposure to isoprenaline was used to address one main hypothesis, i.e. that sympathetic activity of the animal prior to sacrifice may be a factor in determining predisposition to VF. If sympathetic activation was high prior to sacrifice and removal of the heart, this may have a long term effect on the heart that persists into the experimental phase. For this reason, a group of hearts were exposed to isoprenaline for a period of 15 minutes then perfusion was returned to the normal solution. This was done to simulate sympathetic activation prior to sacrifice. If this was a significant factor, then this manoeuvre should shift the predisposition to VF. Ng *et al.* (2007) have reported that sympathetic stimulation in the isolated rabbit heart decreased ERP and VF threshold. Another study by Brunner *et al.* (2008) has reported that exposure to isoproterenol triggered EADs that degenerates into polymorphic ventricular tachycardia (pVT) and VF in long QT syndrome (LQTS) rabbits.

Part 1: E-4031 experiments

Experimental protocol

The experimental protocol is illustrated in Figure 6.1. All optical signal recordings in this study were obtained at the intrinsic heart rate. The protocol was identical to the experimental protocol used in previous chapter, except that the pre-occlusion period was divided into two phases: during the first 10 minutes of the pre-occlusion period, the heart was perfused with Tyrode's solution without the drug, and during the subsequent 20 minutes, the heart was perfused with 0.03 μ M E-4031 added into the Tyrode's solution. A total of 14 animals were used in this set of experiments.

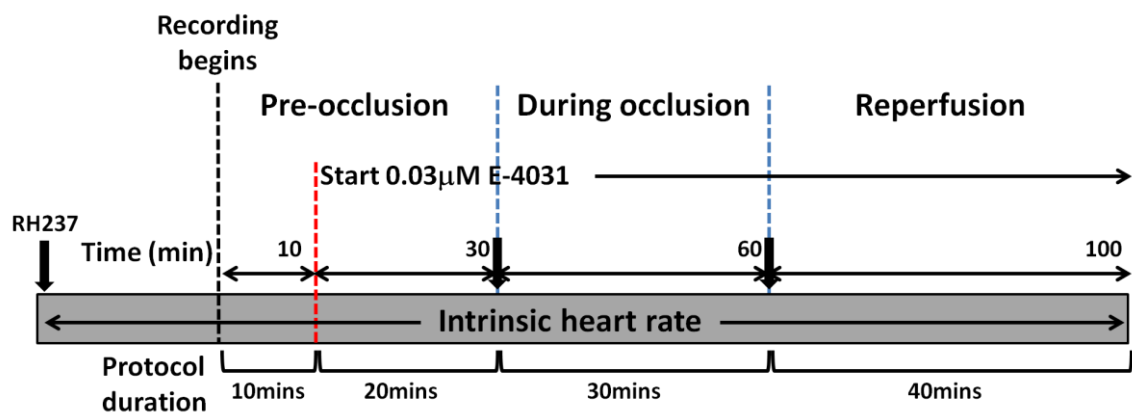


Figure 6.1 Experimental protocol for E-4031 experiments.

Dye loading

Initially, the heart was loaded with 100 μ L bolus of RH237 administered by slow injection into the coronary circulation over duration of 1 minute through an injection port in a bubble trap in line with the aortic cannula. During the experiment, bolus injection of RH237 was repeated twice; before the occlusion period and before the reperfusion period.

Pre-occlusion

Approximately 10-15 minutes after dye injection when the optical signals were already stabilized, serial recordings of optical signals were performed at 1 minute intervals for 30 minutes. The data obtained during the pre-occlusion

period were analysed at two different time points and presented in the result section as *Pre-occlusion 10min* (without the drug) and *Pre-occlusion 30min* (after 20 minutes perfused with E-4031).

Coronary artery occlusion

After 30 minutes of pre-occlusion period, the coronary artery was occluded by tightening the snare to produce regional ischaemia (see Chapter 2). Serial recordings were made at 1 minute intervals for 30 minutes. During this protocol, some hearts developed VF and some hearts did not. If the heart went into VF, the snare was released to reperfuse the heart and the rhythm would revert back to sinus rhythm. However, if the heart was still in VF after releasing the snare, a small bolus (<0.2ml) of KCL (1M concentration) was injected into the heart through the injection port.

Reperfusion

For the hearts that did not develop VF, the snare was released after 30 minutes of occlusion to reperfuse the heart. Serial recording at 1 minute intervals was done for 40 minutes.

E-4031 drug

As described in Chapter 4, E-4031 is a selective inhibitor of delayed rectifier K⁺ current (I_{Kr}). In this study, only one concentration of E-4031 (0.03 μ M) was used to study the electrophysiological property of heart during acute regional ischaemia in the presence of E-4031. This drug concentration was chosen because it was the lowest concentration of the drug that produced a prolongation of APD comparable to the difference observed between the no-VF and VF group (prior to occlusion). The drug was dissolved in DMSO into a stock solution (2mM) and stored at -20°C.

Results

Incidence

From total number of 14 hearts that were exposed to E-4031, 8 hearts developed VF during coronary artery occlusion and the rest did not develop VF (Figure 6.2).

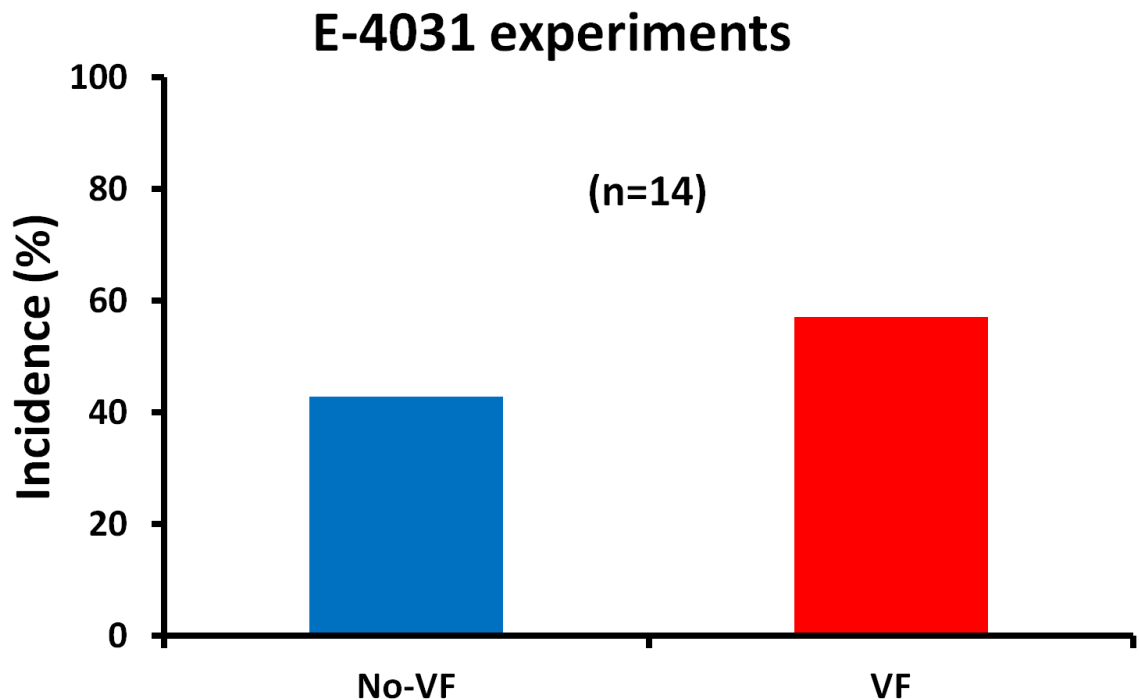


Figure 6.2 Incidence of VF during coronary artery occlusion. Incidence of hearts that developed VF and did not develop VF during acute regional ischaemia in experiments with 0.03 μ M E-4031 (no-VF = 42.9% and VF = 57.1%)

Effect of coronary artery occlusion

Figure 6.3 demonstrates an example of full protocol time course during experiments with E-4031. During the pre-occlusion period, the APD₅₀ from all three zones gradually prolonged as the heart went from phase 1 (without drug) to phase 2 (with 0.03 μ M E-4031). During occlusion, the APD₅₀ especially in Zone C which was the ischaemic zone showed dramatic shortening. The reperfusion brought back the APD₅₀ to the pre-occlusion level. Some hearts developed VF during the occlusion as shown in the Figure 6.3. As mentioned in the previous chapter, only arrhythmic events either sustained or non-sustained VF that occurred within 30 minutes duration of occlusion were included in the VF group. Any episode of arrhythmia that took place pre-occlusion or during reperfusion was not included in the VF group.

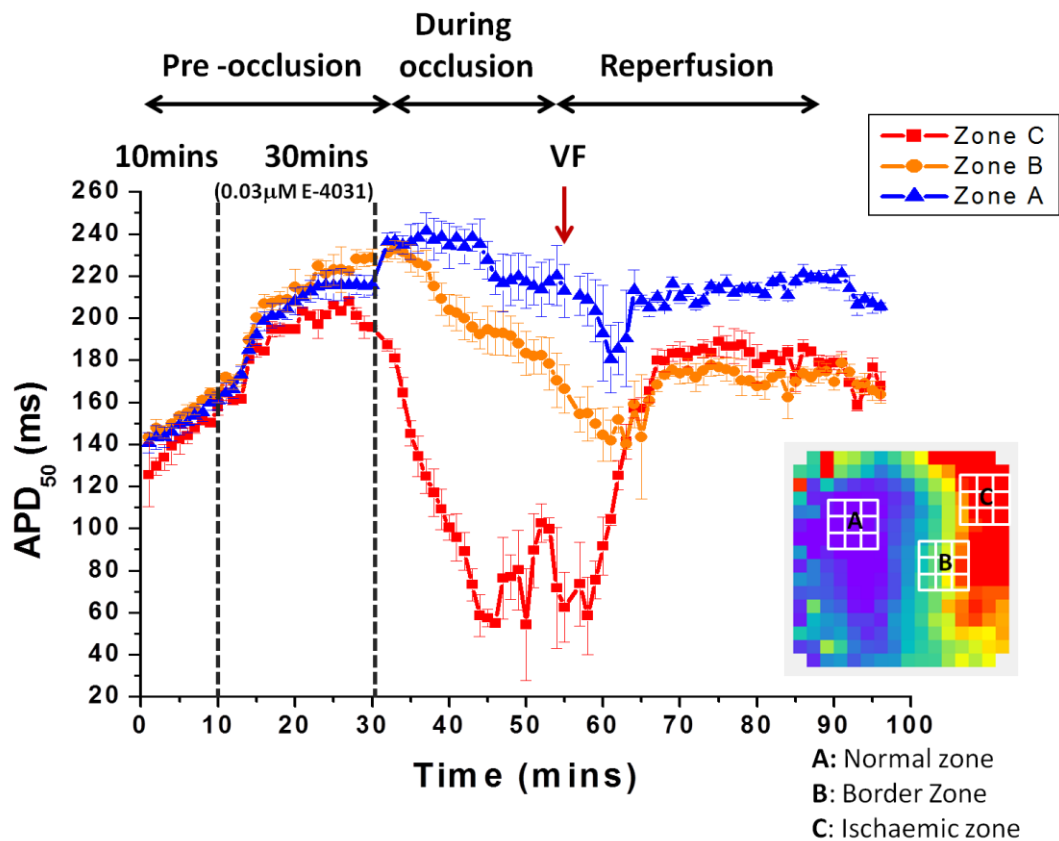


Figure 6.3 Example of full protocol time course during E-4031 experiment.

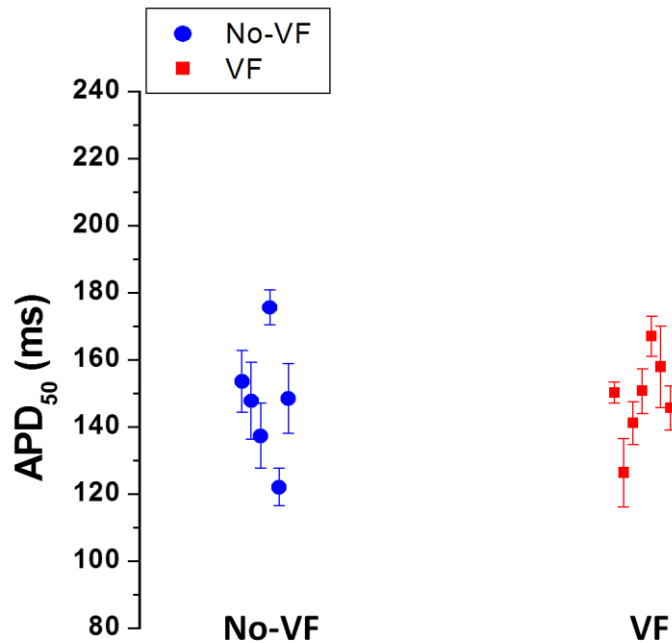
APD₅₀ plotted in the graph were the mean APD \pm SEM from 3 x 3 pixel selections (indicated by the white boxes) from 3 different zones. Zone A = Normal zone, Zone B = Border zone, Zone C = Ischaemic zone

APD₅₀ (no-VF vs. VF groups)

In the study described in the previous chapter (control experiments), it was shown that those hearts with intrinsically longer APD prior to the occlusion did not develop VF. In order to study the basis of that and to correlate with the incidence of arrhythmia, the APD was artificially prolonged with the drug E-4031 (concentration 0.03 μM) before the period of ischaemic induction by coronary artery occlusion. The graphs shown in Figure 6.4 demonstrate the APD₅₀ from both no-VF and VF groups at *Pre-occlusion 10min* (Figure 6.4a) and at *Pre-occlusion 30min* (Figure 6.4b). The APD₅₀ was significantly prolonged at *Pre-occlusion 30min* as compared to the *Pre-occlusion 10min* (Figure 6.5) in both groups. The mean APD₅₀ at *Pre-occlusion 10min* in VF hearts was 144.7 ± 5.5 ms and in no-VF hearts was 147.4 ± 7.3 ms. After exposure to the drug, the mean APD₅₀ at *Pre-occlusion 30min* was 168.0 ± 9.5 ms and 176.4 ± 7.4 ms in VF and no-VF hearts, respectively (Table 6.1). These changes in APD were accompanied by a significant decrease in spontaneous heart rate: in VF group; mean RR pre drug

0.362 ± 0.011 s, mean RR post drug 0.391 ± 0.011 s and in no-VF group; mean RR pre drug 0.367 ± 0.018 s, mean RR post drug 0.396 ± 0.018 s. However, there was no significant difference in the APD_{50} between the two groups at both pre-occlusions 10 and 30 minutes.

a) *Pre-occlusion 10min (no drug)*



b) *Pre-occlusion 30min (0.03 μ M E-4031)*

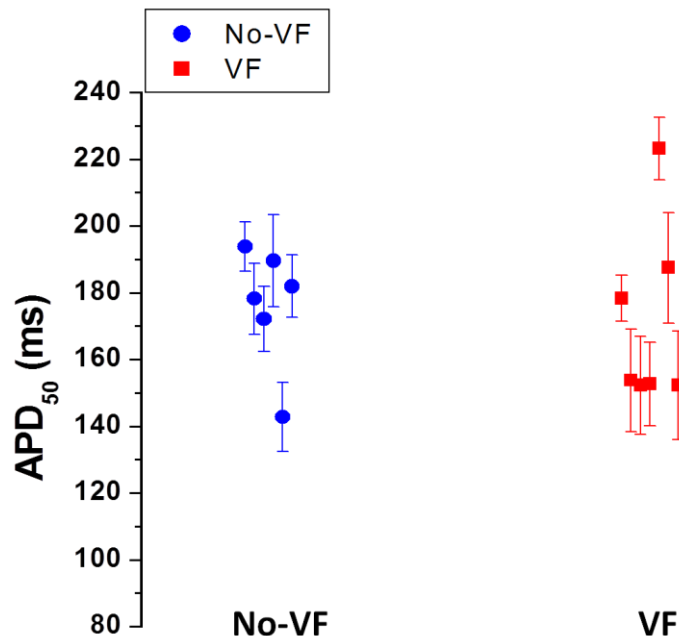


Figure 6.4 APD_{50} prior to coronary artery occlusion.

Graph showing the APD_{50} (mean \pm SEM) at a) *Pre-occlusion 10min* (without drug), and b) *Pre-occlusion 30min* (after exposure to 0.03 μ M E-4031) prior to ischaemia between the hearts that developed VF and the hearts that did not develop VF.

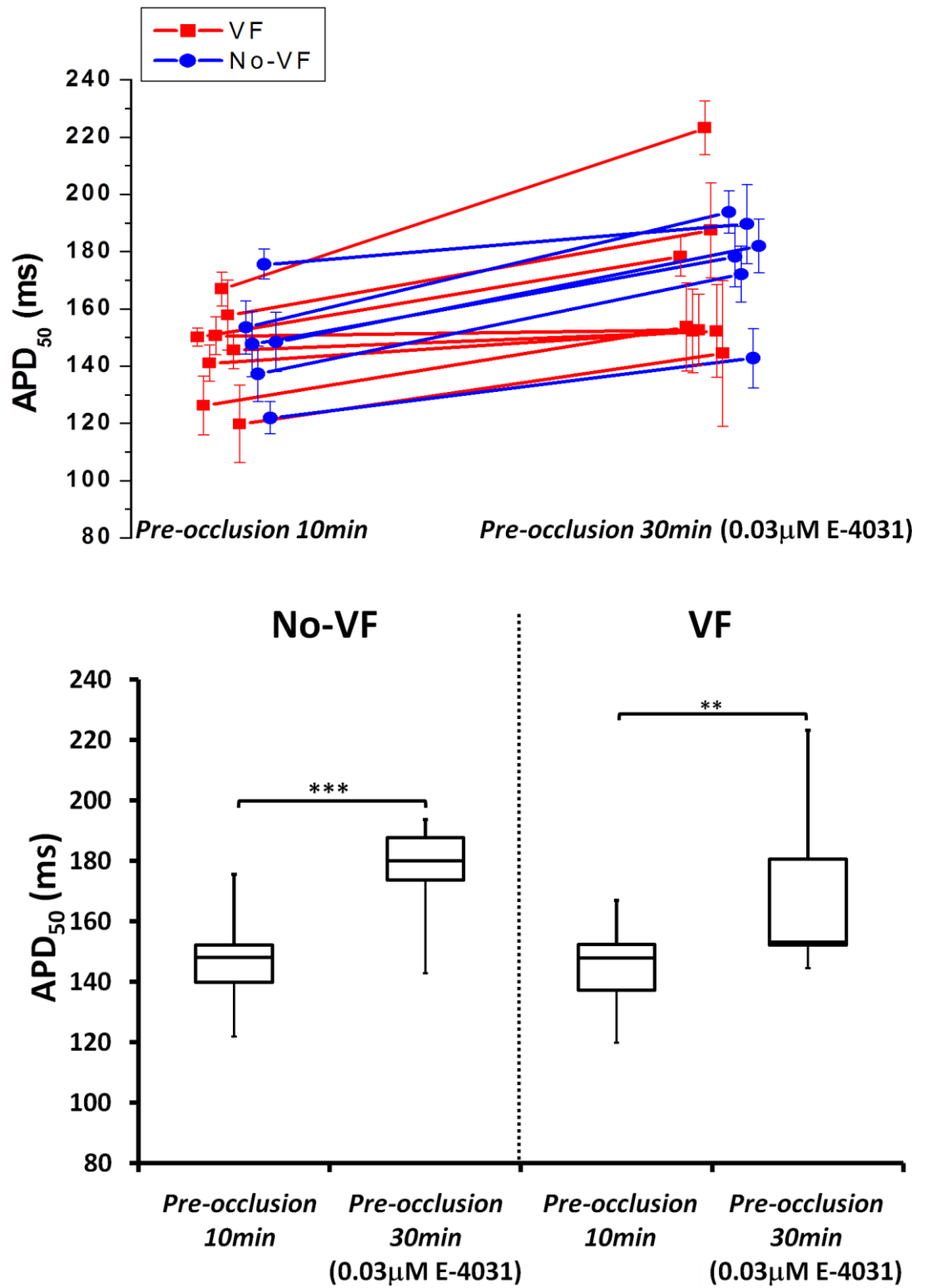


Figure 6.5 Effect of E-4031 on APD₅₀.

Exposure to 0.03μM E-4031 significantly prolonged the APD₅₀ in both no-VF and VF groups.

Table 6.1 APD₅₀ (no-VF vs. VF groups).

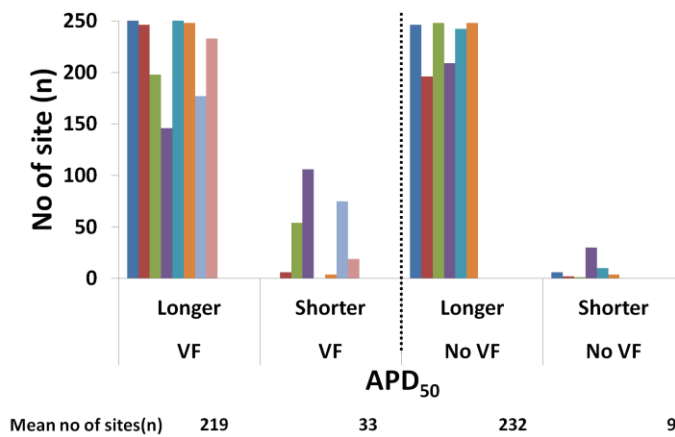
Mean APD₅₀ at *Pre-occlusion 10min* and *Pre-occlusion 30min* (after 20 minutes perfusion with 0.03 μ M E-4031) in both no-VF and VF groups.

	No-VF		VF	
	<i>Pre-occlusion 10min</i>	<i>Pre-occlusion 30min (0.03μM E-4031)</i>	<i>Pre-occlusion 10min</i>	<i>Pre-occlusion 30min (0.03μM E-4031)</i>
Mean APD₅₀ (ms)	147.4	176.4	144.7	168.0
SEM	7.3	7.4	5.5	9.5

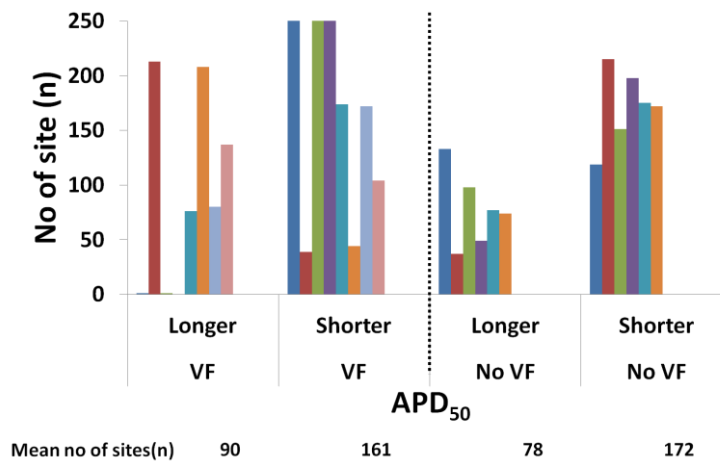
APD₅₀ changes (no-VF vs. VF groups)

Further analysis to look at the change in APD₅₀ before and during occlusion was performed. The histogram in Figure 6.6 indicates the change in APD₅₀ in terms of the number of sites getting shorter or longer APD₅₀ at certain periods of time during the experiments in both groups of animal. The colours represent different hearts. Figure 6.6a shows the APD₅₀ changes between 10 and 30 minutes of the pre-occlusion phase. As the hearts was perfused with E-4031, more sites got longer APD₅₀ in both groups of hearts. However, at *Pre-occlusion 30min* the VF group had more sites with shorter APD₅₀ (33 sites) whereas only at 9 sites did the APD shorten in the no-VF group but the different between the two groups was not significant. During *Occlusion 5min*, some sites showed APD₅₀ increases and some decreases relative to the APD₅₀ at *Pre-occlusion 30min* in both groups of animal as shown in Figure 6.6b, but there was no significant difference between groups. Between *Pre-occlusion 30min* and *Occlusion 10min* as the heart became more ischaemic, the APD₅₀ for most of the sites got shorter. Only small number of sites got longer in both groups as shown in Figure 6.6c.

a) *Pre-occlusion 30min (E-4031) vs. Pre-occlusion 10min (no drug)*



b) *Occlusion 5min vs. Pre-occlusion 30min (E-4031)*



c) *Occlusion 10min vs. Pre-occlusion 30min (E-4031)*

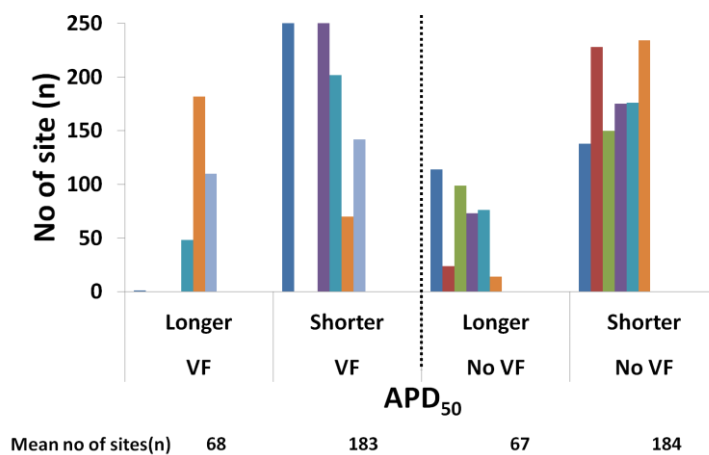


Figure 6.6 Changes in APD_{50} before and during occlusion.

Histograms showing the number of sites in which the APD_{50} got longer or shorter at certain period of time in both no-VF and VF groups. a) APD_{50} changes between *Pre-occlusion 10min* and *Pre-occlusion 30min* (with E-4031) b) APD_{50} changes between *Pre-occlusion 30min* (with E-4031) and *Occlusion 5min* c) APD_{50} changes between *Pre-occlusion 30min* (with E-4031) and *Occlusion 10min*.

T-wave alternans and EADs

In control experiments (Chapter 5), instances of PVCs and T-wave alternans were observed during the pre-occlusion period as well as during the occlusion. In this study with E-4031, abnormality in the heart rhythm in the form of T-wave alternans and EADs were observed as well. Examples of EADs and T-wave alternans in heart are shown in Figure 6.7 (VF heart) and Figure 6.8 (no-VF heart). The observations are summarized in Table 6.2; in the presence of E-4031, T-wave alternans and EADs were more common in the hearts that developed VF.

VF

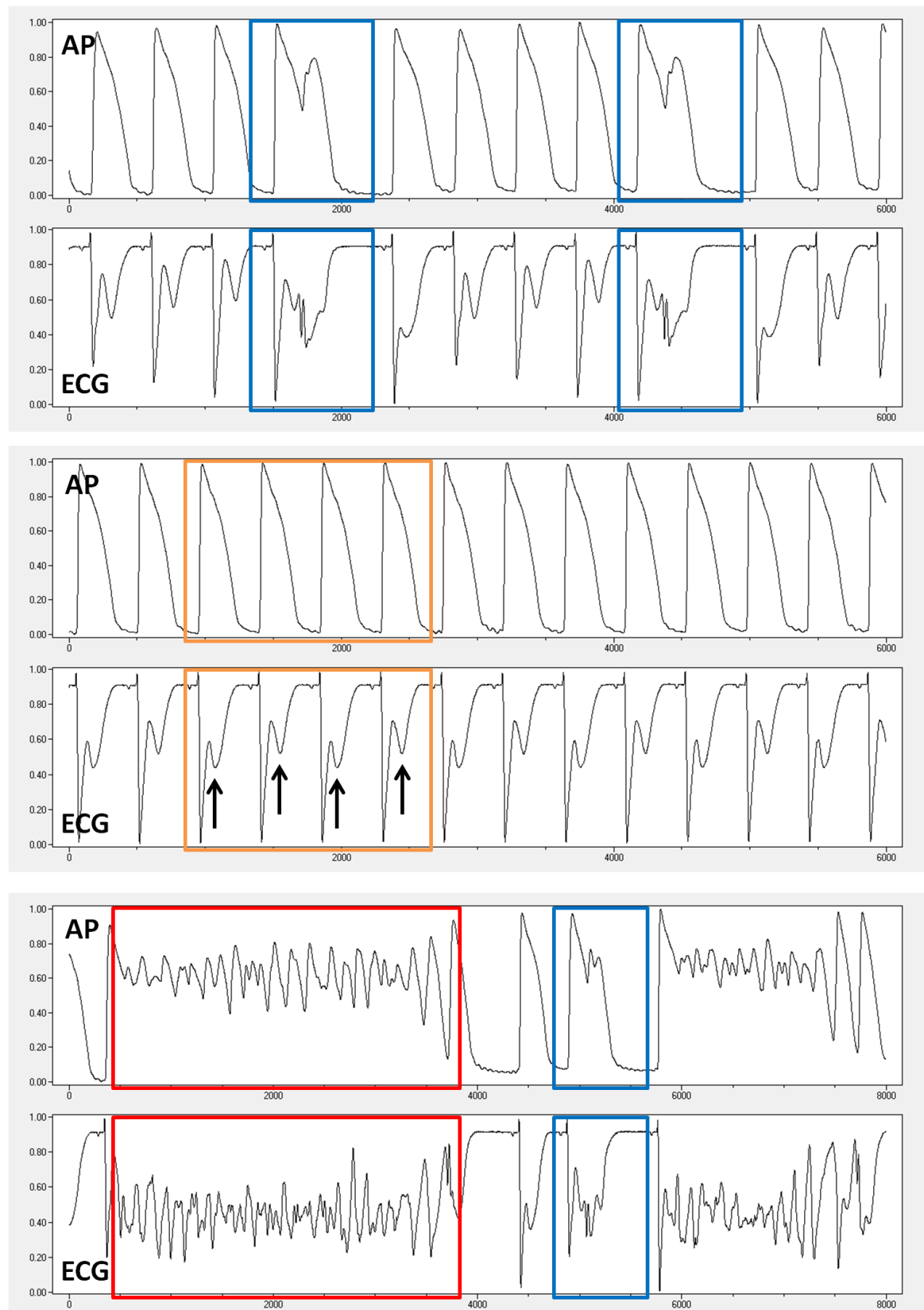


Figure 6.7 EADs and TWA in heart that developed VF.
 AP signals with parallel ECG recordings in E-4031 experiments (VF heart). Example of EADs (indicated by the blue boxes) and T-wave alternans (indicated by the arrow in the orange box) observed during acute coronary artery occlusion before the heart went into VF (shows in the red box).

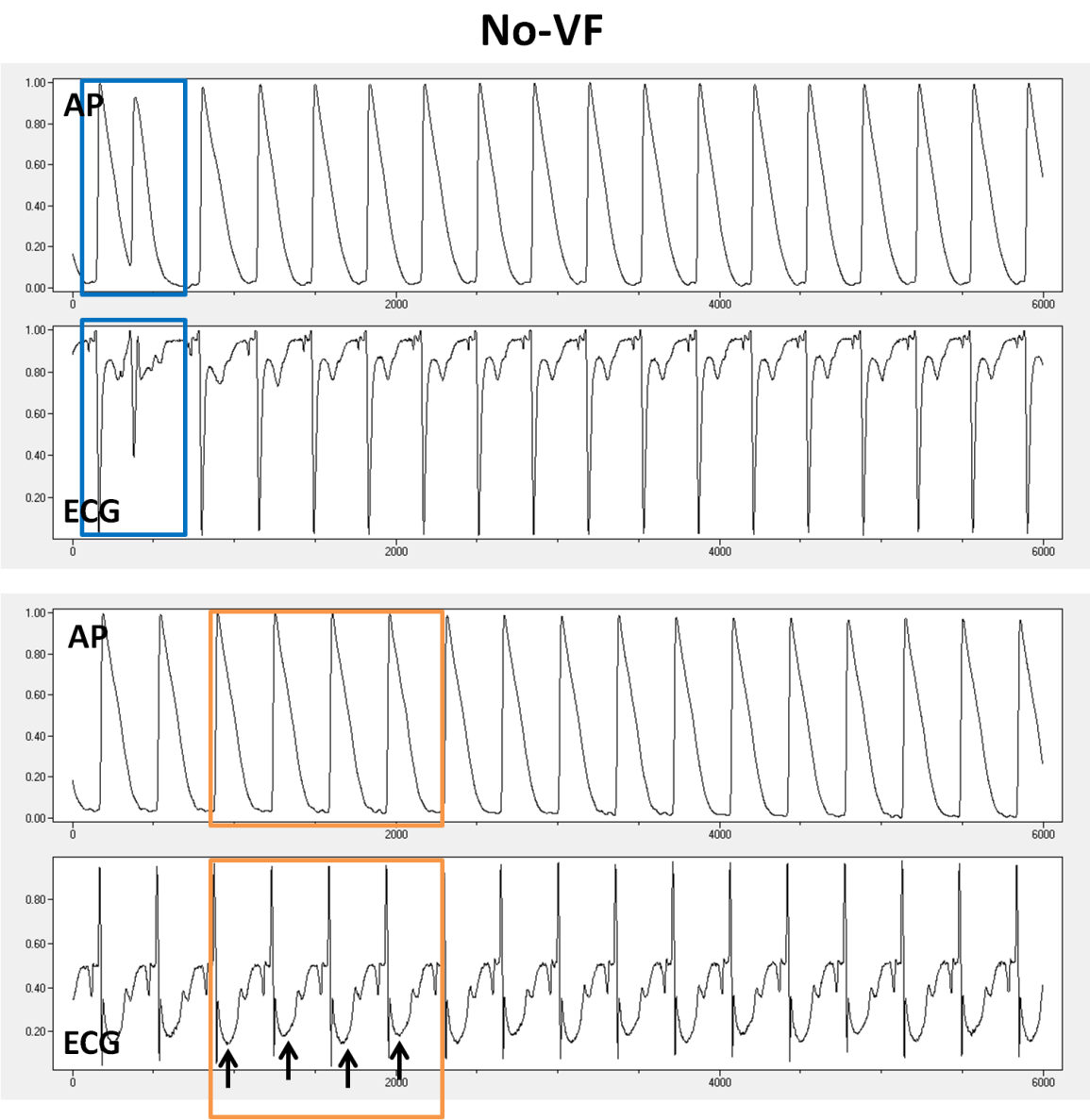


Figure 6.8 EADs and TWA in heart that did not go into VF.
AP signals with parallel ECG recordings in E-4031 experiments (no-VF heart). Example of heart that had episodes of EADs (indicated by the blue boxes) and T-wave alternans (indicated by the arrow in the orange box) during acute coronary artery occlusion but this heart did not go into VF.

Table 6.2 Incidence of EADs and TWA.
No of hearts having T-wave alternans and EADs during 30 minutes of acute regional ischaemia in no-VF and VF groups.

	No-VF	VF
	0.03μM E-4031	0.03μM E-4031
TWA (incidence)	1 out of 6 hearts	3 out of 8 hearts
EADs (incidence)	1 out of 6 hearts	5 out of 8 hearts

Part 2: Isoprenaline experiments

We considered that some hearts tend to be more prone to develop arrhythmia due to some status of the hearts before we isolated the hearts from the rabbits. In order to simulate the sympathetic drive due to stress in the rabbits, we exposed the hearts to a high level of isoprenaline for 15 minutes before starting the standard coronary artery occlusion protocol. A total of 7 animals were used in this set of experiments.

Experimental protocol

The experimental protocol for the isoprenaline experiments is illustrated in Figure 6.9.

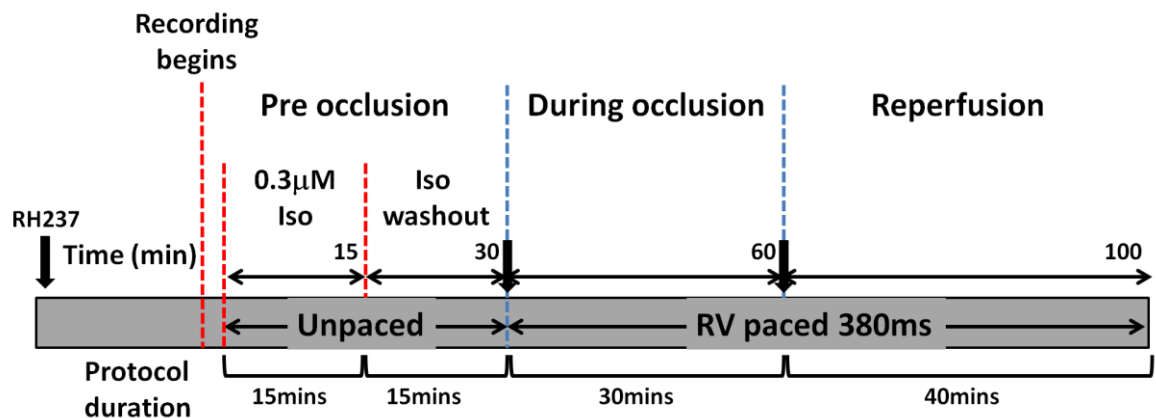


Figure 6.9 Experimental protocol for experiments with 0.3μM isoprenaline.

AV node ablation

In this study, the AV node ablation was performed to ensure that the heart could be paced slower than the intrinsic cycle length. Details on the procedure to perform AV node ablation was explained in Chapter 4.

Pacing protocol

The control experiments described in previous chapter and the E-4031 experiments explained in Part 1 of this chapter were performed at intrinsic heart rates. However, in the series of experiments involving isoprenaline the heart was subjected to right ventricular pacing at a pacing rate of 380ms cycle

length during occlusion and reperfusion. During the pre-occlusion period as the isoprenaline was washed in and washed off, the heart was unpaced to see the effect of isoprenaline on APD and heart rate.

Dye loading

The protocol for dye loading was similar as previous experiments with E-4031. The bolus of RH237 was repeated two times throughout the experiment. Approximately 10 - 15 minutes after the dye loading, the heart was temporarily paced at 380ms cycle length in order to obtain a baseline recording.

Pre-occlusion

In this study, the pre-occlusion period was divided into two phases. The first phase was when the 0.3 μ M isoprenaline was perfused for 15 minutes. Serial optical signal recordings were performed at 1 minute intervals. In the second phase, the isoprenaline was washed off from the hearts. The duration for the second phase varied between the hearts. Some hearts took longer to wash off the drug but the majority of the hearts took approximately 15 minutes to remove the effect of isoprenaline. During the second phase, serial optical signal recordings were also performed at 1 minute intervals. The heart was unpaced in both phases. Just prior to the coronary artery occlusion, the heart was paced at 380ms cycle length and another signal recording at RV paced was obtained prior to occlusion.

Coronary artery occlusion

The coronary artery was occluded to produce acute regional ischaemia. Serial recordings were made at 1 minute intervals for 30 minutes. The optical signal recordings were obtained at RV paced 380ms cycle length.

Reperfusion

For the hearts that did not develop VF, the snare was released after 30 minutes of occlusion to reperfuse the heart. Serial recording at 1 minute intervals was done for 40 minutes. This protocol was conducted at pacing rate as well.

Isoprenaline drug

Isoprenaline [1-(3',4'-Dihydroxyphenyl)-2-isopropylaminoethanol] (Figure 6.10) is a catecholamine compound and non-selective β -adrenoceptor agonist that is commonly used in cardiovascular research. The drug was dissolved in water (H_2O) into a stock solution (0.1M), freshly prepared before each experiment. A high dose of isoprenaline ($0.3\mu M$ concentration) was used to study the predisposition of heart towards VF during acute regional ischaemia in the presence of sympathetic stimulation before the episode of ischaemia.

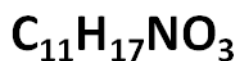
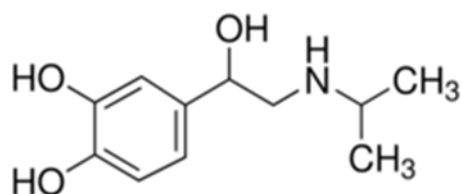


Figure 6.10 Chemical structure of isoprenaline

Results

Incidence

In this study, 2 hearts went into VF during occlusion after brief exposure to $0.3\mu\text{M}$ isoprenaline and 5 hearts did not (Figure 6.11). From the 5 hearts in the no-VF group, 3 hearts developed VF during reperfusion. However, according to our criteria, only hearts that developed VF during coronary artery occlusion will be included in the VF group. Any heart which developed arrhythmic event during reperfusion will be included in the no-VF group.

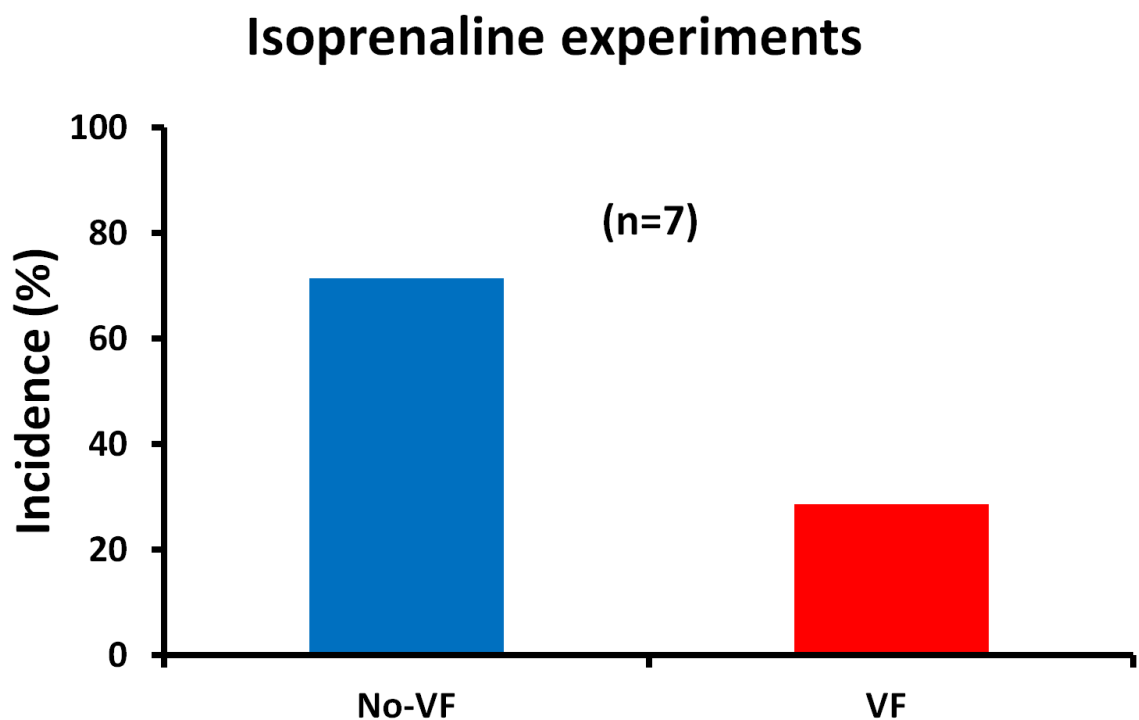


Figure 6.11 Incidence of no-VF and VF during isoprenaline experiments.

APD₅₀

Figure 6.12 displays an example of full protocol time course during the isoprenaline experiment. The mapping field was divided into 3 zones, the normal zone, border zone and ischaemic zone. During the first 15 minutes of pre-occlusion period, the heart was perfused with $0.3\mu\text{M}$ isoprenaline. During this period of time, the APD₅₀ gradually shortened in all 3 zones. After 15 minutes, the isoprenaline was washed off and the APD₅₀ in the 3 regions steadily prolonged. Occlusion of the coronary artery to produce regional ischaemia

dramatically shortened the APD_{50} . The greatest shortening of the APD_{50} was mainly seen in zone C. During the reperfusion period, the APD_{50} from the 3 zones returned back to almost similar levels.

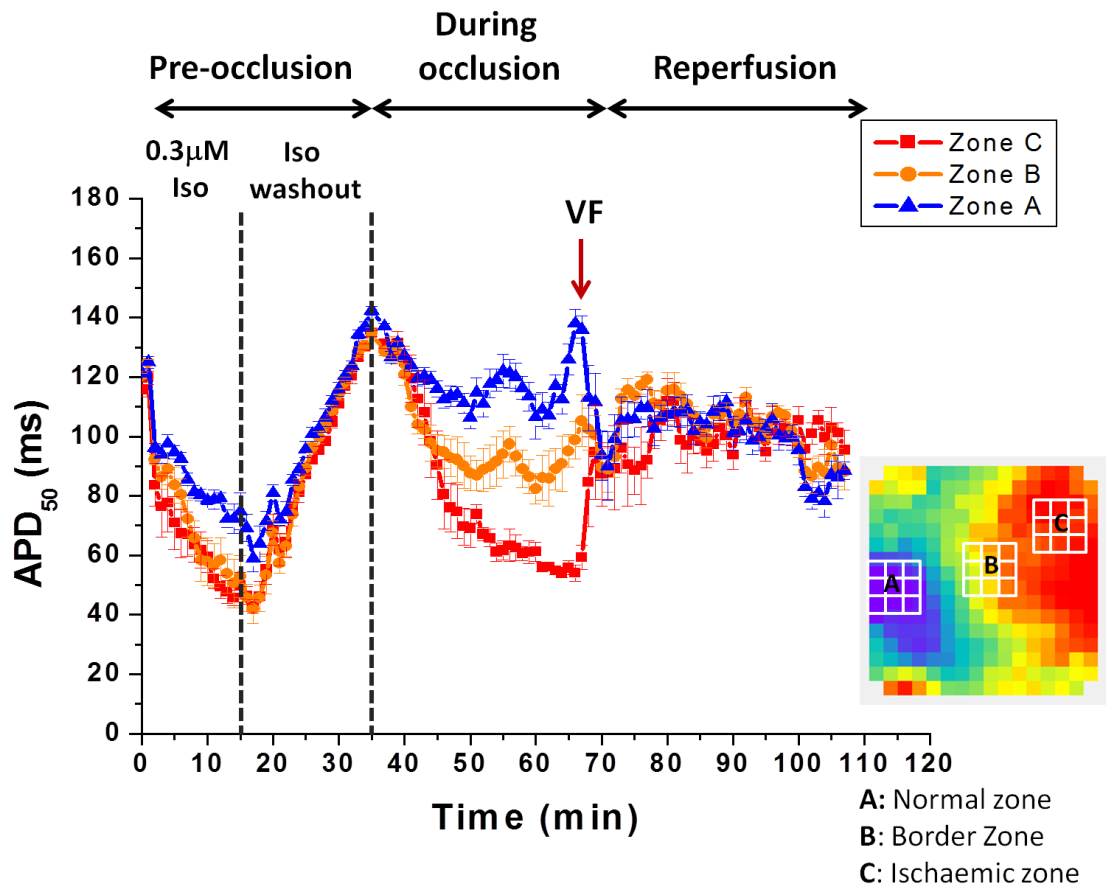


Figure 6.12 Full protocol time course for isoprenaline experiment. Example of full protocol time course for the isoprenaline experiment showing the APD_{50} changes throughout the experiment. The data were presented as mean \pm SEM from 3 x 3 pixel selections (indicated by the white boxes on the colour map) from three different zones.

The mean APD_{50} (at RV paced 380ms cycle length) before and after the heart was perfused with isoprenaline were plotted in Figure 6.13. The APD_{50} in some hearts were prolonged and some hearts were shortened but the mean APD_{50} was somewhat shortened after isoprenaline in hearts that developed VF and did not develop VF but the difference was not significantly different. Comparison between the mean APD_{50} before and after isoprenaline in both groups is displayed in Table 6.3.

Pre-occlusion (RV-paced 380ms cycle length)

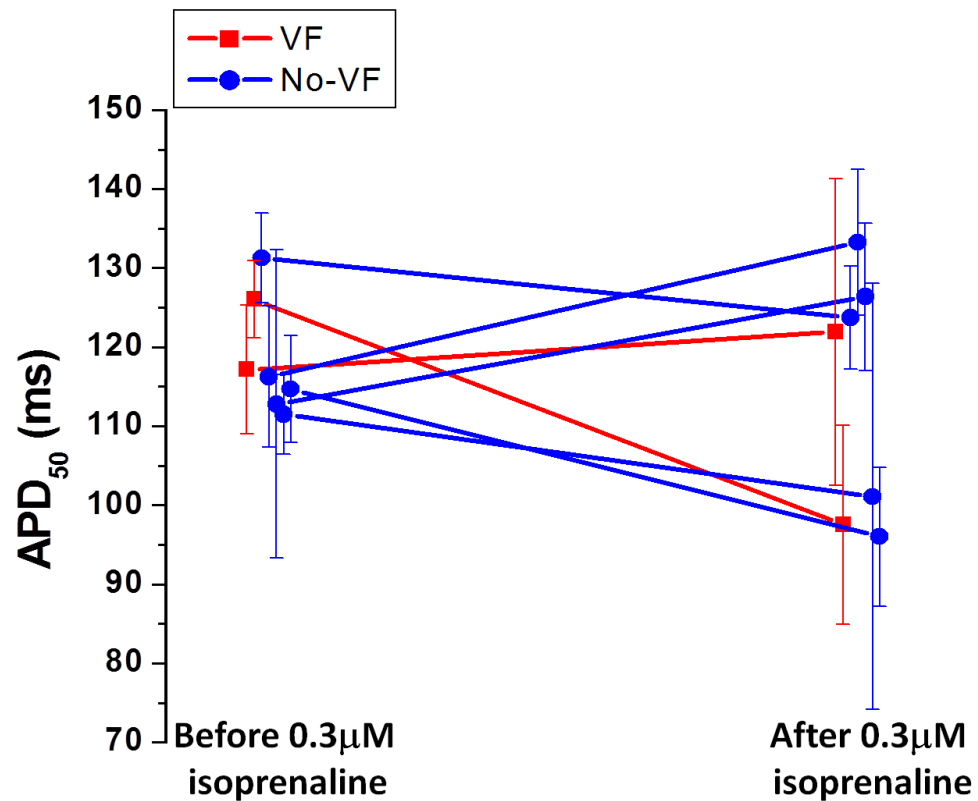


Figure 6.13 APD₅₀ before and after exposure to isoprenaline.

APD₅₀ (mean ± SEM) before isoprenaline and after isoprenaline washout in no-VF and VF hearts during pre-occlusion. The recording was obtained when the hearts were paced at 380ms cycle length. There was no significant difference between the two groups.

Table 6.3 APD₅₀ before and after exposure to isoprenaline.

APD₅₀ before and after isoprenaline recorded at RV-paced 380ms cycle length in both no-VF and VF groups. Exposure to isoprenaline had shortened the APD₅₀ in both groups but the difference was not significant.

	No-VF		VF	
	Before Iso	After Iso	Before Iso	After Iso
Mean APD ₅₀ (ms)	117.3	116.1	121.6	109.7
SEM	3.6	7.4	4.5	12.2

Discussion

The experiments described in the previous chapter (5), suggest that the electrophysiological status of the myocardium was significantly different in a group of hearts that rendered them more prone to VF after occlusion of the coronary artery. In the experiments described in this chapter we attempted to alter the status of the myocardium to either suppress or accentuate the tendency to VF using E-4031 and transient exposure to isoprenaline.

Effects of E-4031

In the control situation, the APD of epicardial surface prior to the ligation were significantly smaller in the hearts that developed VF. Using E-4031 to prolong the APD (and reduce the heart rate) to the extent that the epicardial APD values are now as long as those in the no-VF group, there was no change in the tendency of hearts to develop VF. The incidence of hearts that developed VF in control experiments and in E-4031 experiments was comparable to that after treatment with E-4031 (Figure 6.14).

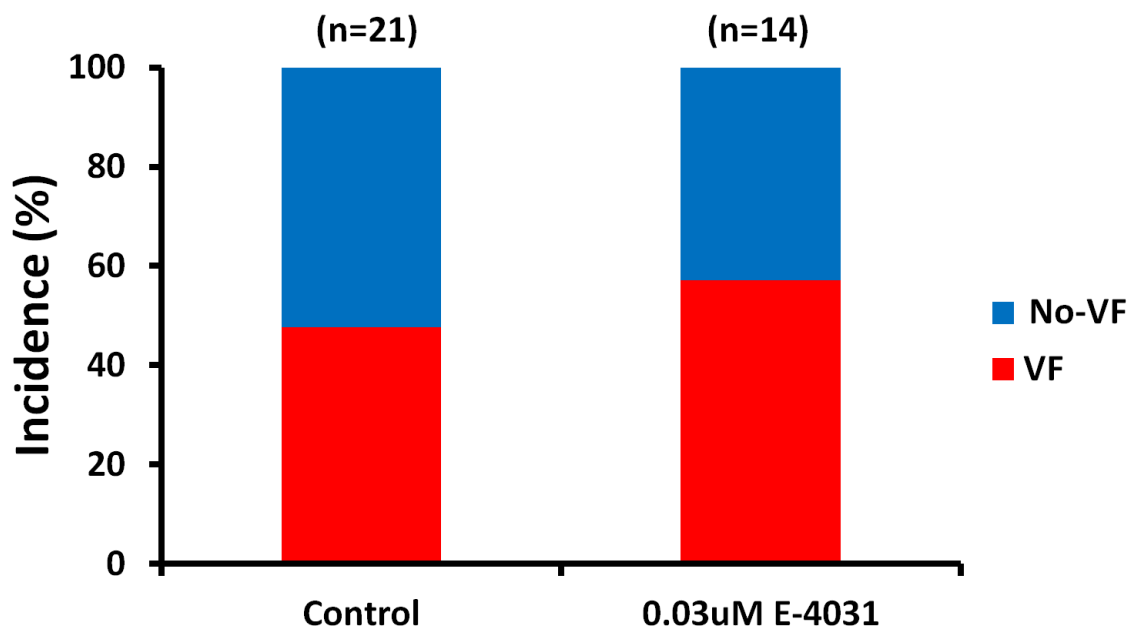


Figure 6.14 Incidence of no-VF and VF in control and E-4031 experiments.

Comparison of the mean APD_{50} between control and E-4031 experiments revealed that the mean APD_{50} at *Pre-occlusion 30min* in no-VF and VF groups from the set of E-4031 experiments were significantly longer as compared to the APD_{50} from the VF group in control experiments (Figure 6.15). Statistical analysis using a Split-Plot ANOVA test revealed that the APD_{50} were significantly different within the groups and between the groups in both sets of experiments.

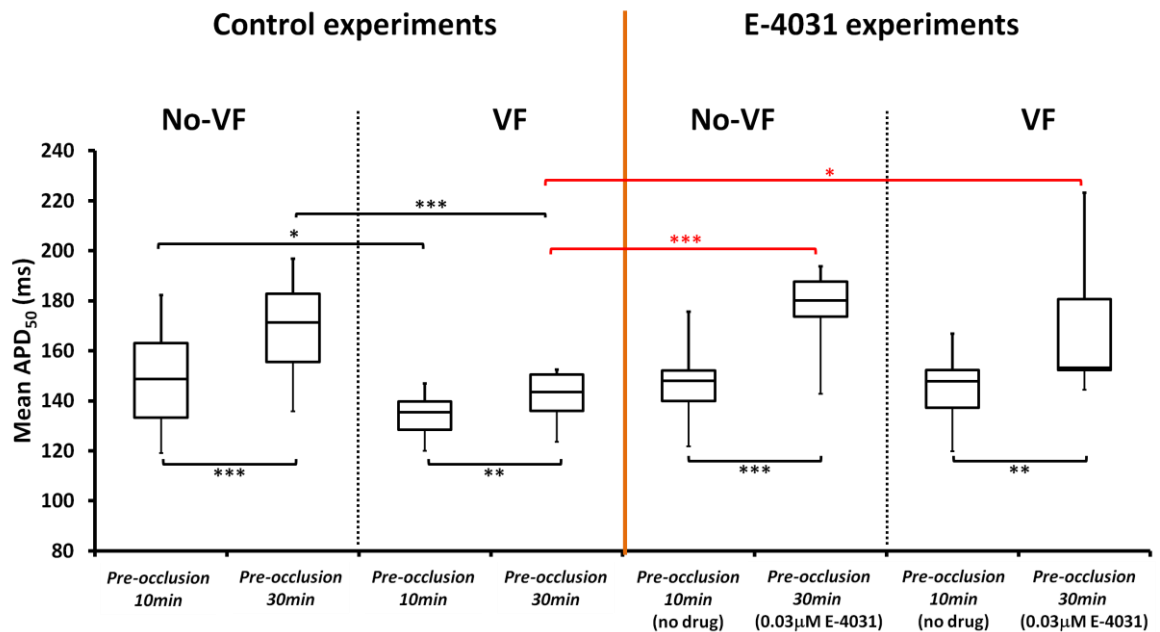


Figure 6.15 APD_{50} in control experiments and E-4031 experiments.

Box plots of mean APD_{50} at *Pre-occlusion 10min* and *Pre-occlusion 30min*. It displays the comparison between the mean APD_{50} from no-VF and VF groups in control and E-4031 experiments.

In addition to the APD_{50} , we also looked at the change of APD_{50} at certain period of time during the protocol. Table 6.4 lists the average number of sites where the APD_{50} got shorter or longer during the pre-occlusion period. It shows that in both control and E-4031 experiments, more sites got shorter in the VF group even before the occlusion as compared to the no-VF group.

Table 6.4 Behaviour of APD₅₀ prior to coronary artery occlusion.
Average number of sites that got longer or shorter APD₅₀ between 10 and 30 minutes pre-occlusion. Comparison between no-VF and VF hearts in control and E-4031 experiments.

<i>Pre-occlusion 30min vs. Pre-occlusion 10min</i>				
	No-VF		VF	
	Average no of site (n)		Average no of site (n)	
	Long	Short	Long	Short
Control experiments	247	5	198	54
E-4031 experiments	232	9	219	33

Effects of transient isoprenaline treatment

The second set of experiments described in this chapter was designed to address the concern that the sympathetic activity of the animal prior to sacrifice may have a bearing on the incidence of VF after occlusion of a coronary artery. As described earlier, there is considerable evidence that increased sympathetic activity increases predisposition to VF in humans. The reasons for this are unclear and therefore the extent to which sympathetic effects may still remain after sacrifice of the animal is uncertain. In an effort to test this hypothesis, all hearts within one experimental group were exposed to isoprenaline to mimic sympathetic activation. An unanticipated effect of this procedure is that APD₅₀ values after washout of isoprenaline (prior to occlusion) were significantly shorter ($P < 0.001$) than the no-VF hearts at *Pre-occlusion 30min* in control experiments (mean APD₅₀ of 131.5 ± 3.3 ms in the hearts from isoprenaline experiments and 168.8 ± 5.5 ms in the no-VF group from control experiments). However, despite the shorter APD, there was a significant group of hearts that did not develop VF (Figure 6.16). Ventricular APD shortening during β -adrenergic stimulation has been previously reported (Ng *et al.*, 2007) and is thought to be the result of changes in several ionic conductances including I_{Cl} , I_{Ks} and I_{Kr} (Harvey *et al.*, 1990; Thomas *et al.*, 2006; Volders *et al.*, 2003). The reason for the sustained shortening after wash-off of the agonist as observed in the current study is not clear and suggests that some of the electrophysiological changes may require a considerable time to recover.

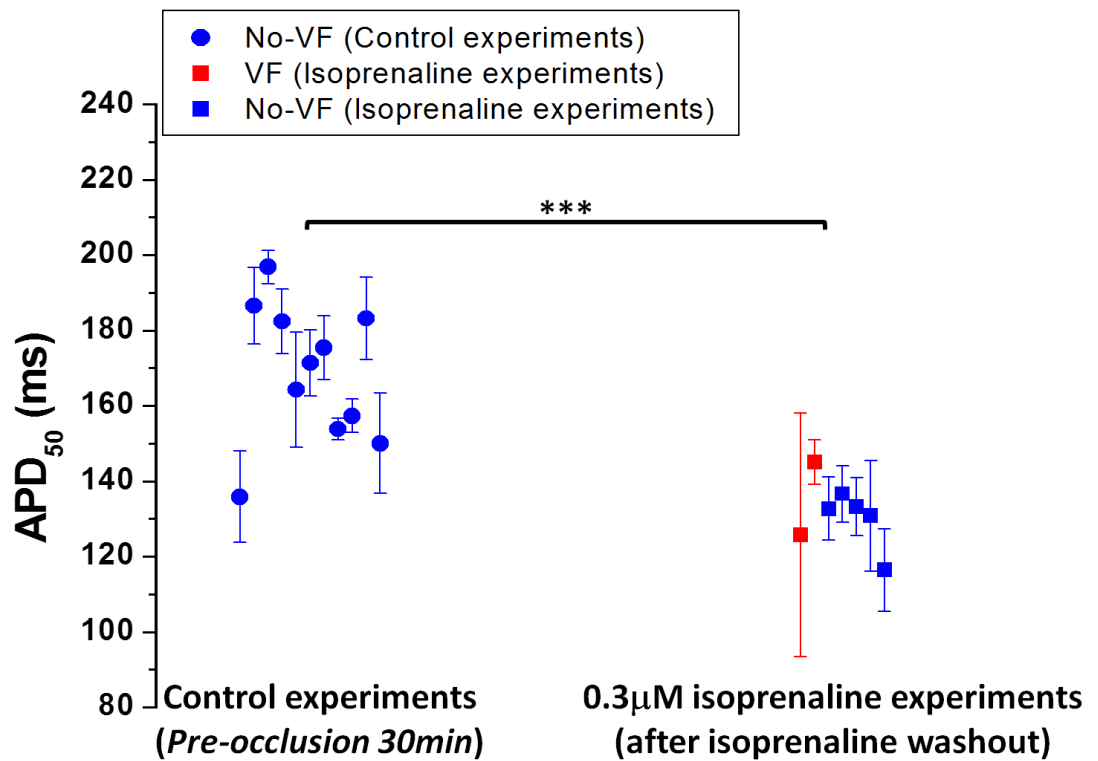


Figure 6.16 APD₅₀ in control experiments vs. isoprenaline experiments. Hearts exposed to 0.3µM isoprenaline prior to occlusion (both no-VF and VF groups) revealed a significantly shorter APD₅₀ than the no-VF hearts from control experiments at *Pre-occlusion 30min*.

Based on the findings of this section of experiments, several conclusions can be drawn:

- (1) Prior sympathetic activity in the intact animal prior to sacrifice is unlikely to be the cause of the predisposition to VF in a subgroup of hearts.
- (2) Shortened APD (cause uncertain) did not predispose the hearts to VF.
- (3) Standardisation of the pacing cycle length to a set value does not alter significantly the fraction of hearts that develop VF after occlusion of the coronary artery.

Conclusion

Artificially prolonging the APD (and reducing HR) by inhibited hERG (with $0.03\mu\text{M}$ E-4031) prior to ischaemia did not significantly change the incidence of arrhythmia post occlusion. Brief and transient exposure to a high dose of isoprenaline (concentration $0.3\mu\text{M}$) before the coronary artery occlusion shortened the average APD prior to occlusion but did not increase the likelihood of VF. Therefore, intrinsically shorter epicardial APD is associated with, but is not the cause of, the predisposition to arrhythmias post-occlusion. Alternative cellular mechanisms that link APD to predisposition to arrhythmias should be considered as an explanation.

Chapter 7: ECG simulation

Aim

The aim of this study is to look at the relationship between the site and size of the ischaemic region that might contribute to the variation seen in the ECG patterns during acute coronary artery occlusion experiments by simulating the ECG using a simulation programme.

Introduction

ECG during coronary artery occlusion

ECG changes during acute myocardial ischaemia following coronary artery occlusion have been discussed in Chapter 1. Severe myocardial ischaemia results in several ECG changes within minutes. These ECG changes disappear when the myocardium is reperfused.

Modelling of ECG

In this study, ECG recordings made in parallel with the optical measurement suggest distinct pattern of changes of ECG in hearts that went into VF and those that did not and these suggest that there may be distinct changes that precipitate VF. In order to understand this better, an attempt was made to simulate the ECG findings. There are marked changes in the ECG profiles during occlusion of the coronary artery clinically and they are characterized by ST segment changes (see Chapter 1). In parallel with the optical measurement, ECGs were recorded and appeared to have distinct changes depending on whether the heart went into VF or non VF. These are presented in this chapter along with computational model to try and help understand the causes of these changes.

Methods

Experimental ECG measurement

Method of ECG signal recordings during coronary artery occlusion experiments was described in Chapter 2.

ECGSim software

ECGSim, the software used in this study is free software and can be downloaded at www.ecgsim.org. It is an interactive simulation programme developed by two researchers at the Radboud University Medical Center, Netherland (Oostendorp and van, 2004). This software allows the user to study the relationship between the electrical activity of the heart and the resulting 12-lead ECG signals. There are two basic heart models with different orientation, normal male and normal young male. In this simulation study, the normal male heart model was chosen because the orientation of this model seemed to produce an ECG pattern that was closer to that generated experimentally. By using the software, the AP in certain regions of the heart can be shortened to mimic the ischaemic AP. The position of the shortened AP can be changed to different areas of the heart to study the effect of such changes on the ECG.

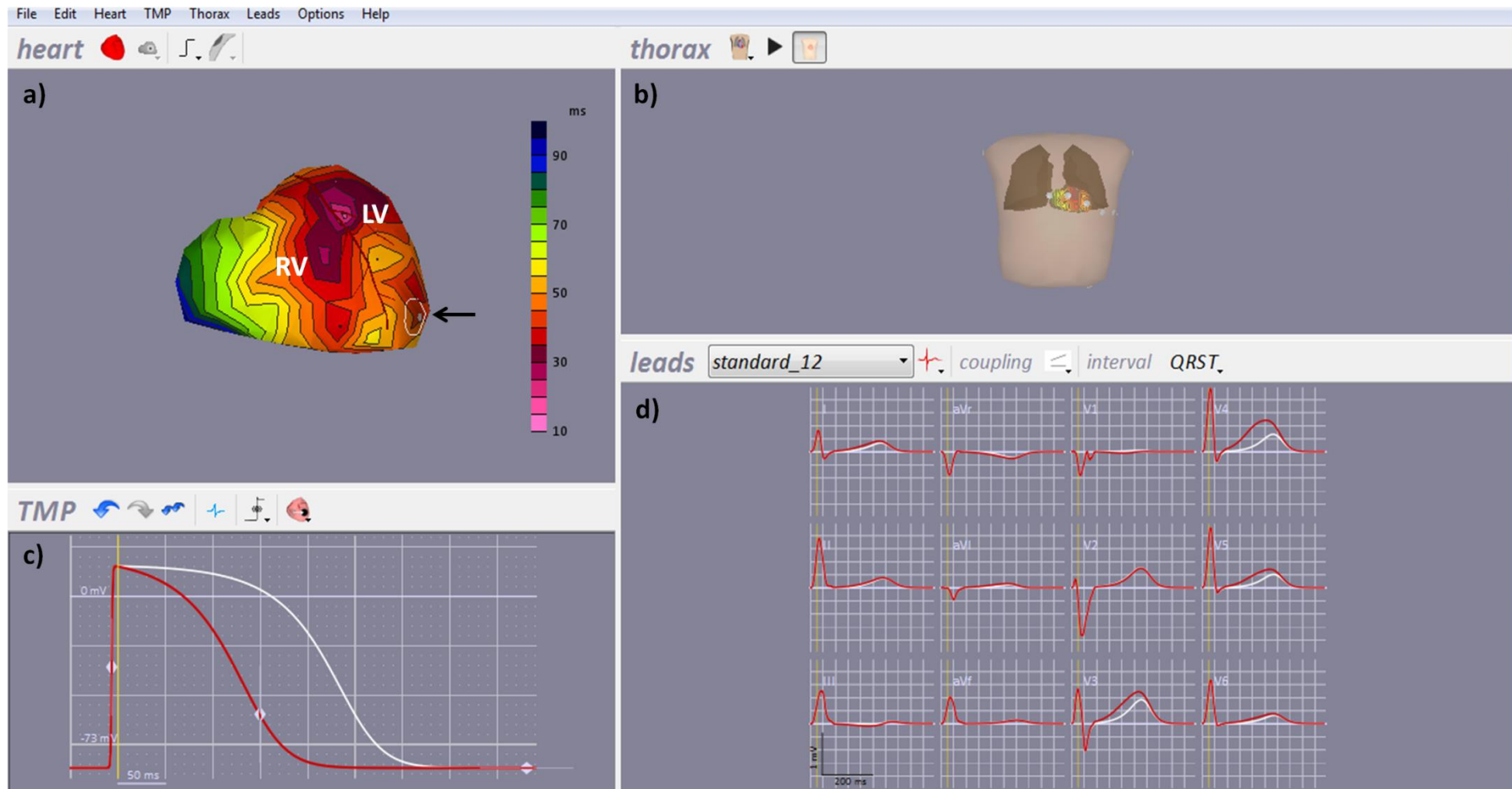


Figure 7.1 Example of ECGSim display.

a) the heart pane with the normal male heart model. The colour represents the depolarisation pattern on the heart surface, b) the thorax pane showing the thorax geometry and position of the ECG leads (grey patches), c) the transmembrane potential (TMP) pane displaying the transmembrane potential at the selected node indicated by the arrow in panel a), and d) the leads pane displaying the standard 12-lead ECG.

Figure 7.1 demonstrates the display of the ECGSim software. It consists of:

- a) the heart pane which is used to display the geometry of the heart (left and right ventricles) as well as a wide range of functions on its surface such as changing the parameters of the local transmembrane potential (TMP) in the area of the node indicated by the white circles in the figure as well as changing the location and radius of the node,
- b) the thorax pane which is used to display the geometry of the thorax and the position of the nine electrodes (shown as grey patches) of the standard 12-lead system,
- c) the TMP pane which displays the transmembrane potential at the selected node on the heart surface (shown by the black arrow in panel a). The white trace indicates the initial parameter values, whereas the red trace relates to the user adapted parameters. The shape of the TMP can be adjusted to either shorten or lengthen the action potential.
- d) the leads pane which allows the display of the signals from the standard 12-lead system. The white trace indicates the initial signals while the red trace display the resulting signals after changing the parameters on the TMP pane.

Results

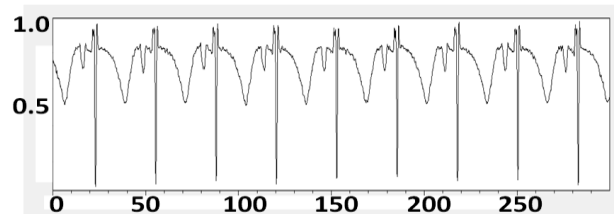
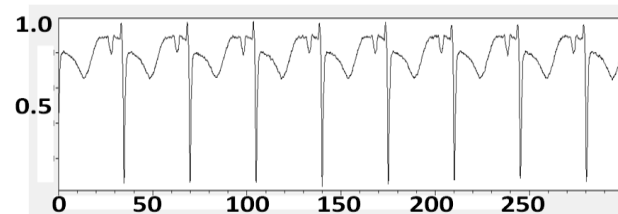
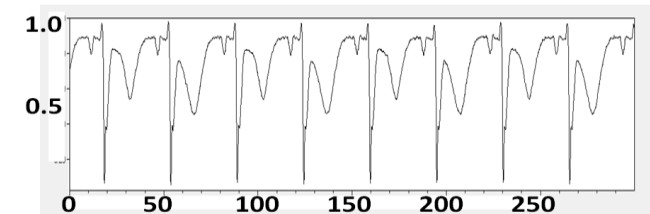
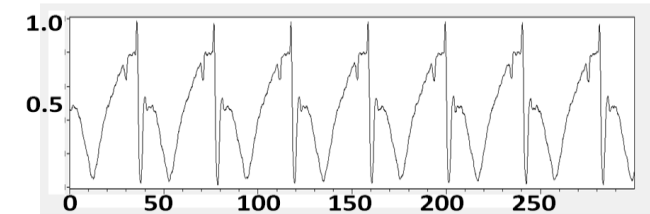
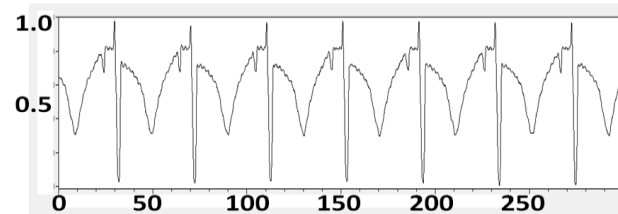
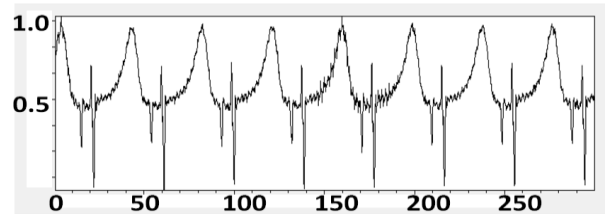
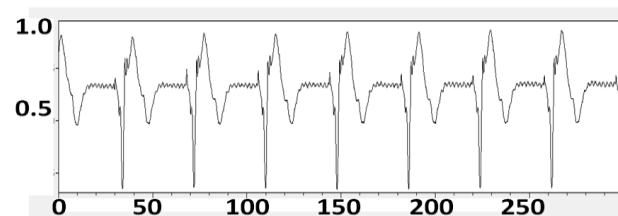
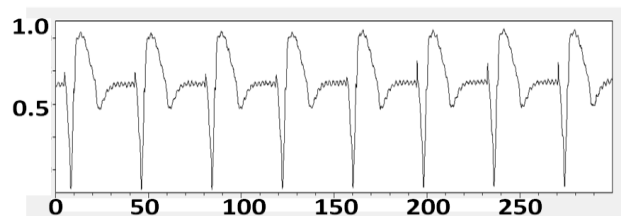
Experimental ECG

During the coronary artery occlusion experiments, simultaneous ECG signal recordings were obtained together with the optical signal recordings. From the ECG signals, some variations in the ECG before and during occlusion were observed.

Figure 7.2 shows examples of ECG signals from three different sets of coronary artery occlusion experiments at *Pre-occlusion 30min* and during *Occlusion 5min* and *Occlusion 10min* in hearts that developed VF during occlusion. In example 1 from a control experiment, the T wave had a negative polarity. At *Occlusion 5min*, there was ST segment depression and at *Occlusion 10min*, there were instances of TWA observed. During occlusion, the T wave retained a negative polarity. Example 2 shows ECG signals from a coronary artery occlusion experiment with E-4031. Under these conditions, the T wave had a positive polarity. During *Occlusion 5min* and *Occlusion 10min*, there was ST depression but this time the T wave changed its polarity. ECG signals obtained during an experiment using the isoprenaline intervention described in chapter 6 is shown in example 3. The ST segment was higher than the isoelectric point at *Pre-occlusion 30min* with an inverted T wave. At *Occlusion 5min*, the ST depression became prominent, this heart developed VF at 6 minutes occlusion.

Examples of ECG signals obtained from the hearts that did *not* develop VF from three sets of experiments are demonstrated in Figure 7.3. From the examples given, all hearts show positive polarity of the T wave at *Pre-occlusion 30min*. Later during the occlusion, the T wave changed its polarity in all three examples along with ST segment depression.

VF

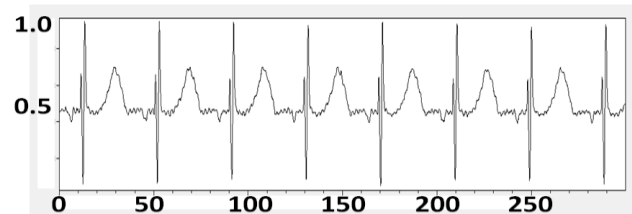
Pre-occlusion 30min**Example 1 – control experiment:*****Occlusion 5min******Occlusion 10min*****Example 2 – E-4031 experiment:****Example 3 – Isoprenaline experiment:****Figure 7.2 ECG from VF heart.**

Examples of ECG from the hearts that developed VF in three different sets of experiment showing variation in the repolarisation pattern as indicated by the ST changes at *Pre-occlusion 30min*, *Occlusion 5min* and *Occlusion 10min*.

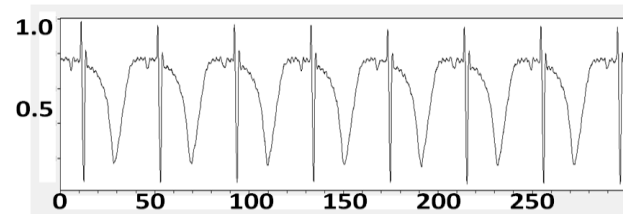
No-VF

Pre-occlusion 30min

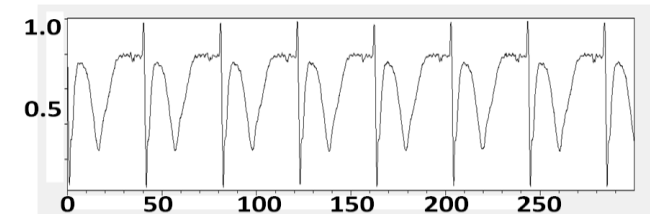
Example 1 – control experiment:



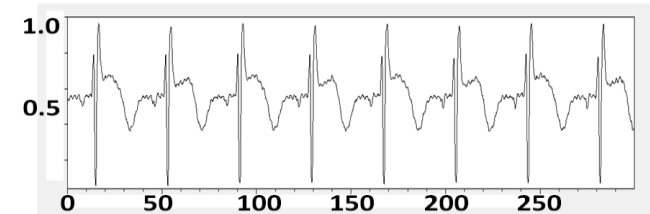
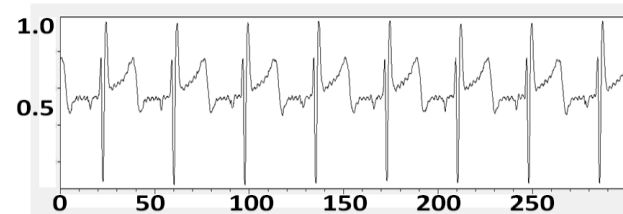
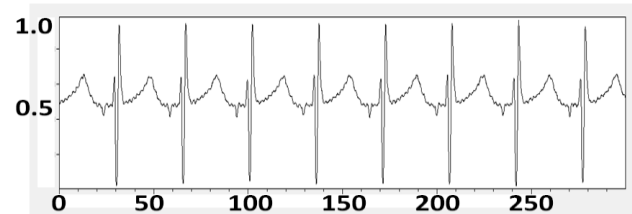
Occlusion 5min



Occlusion 10min



Example 2 – E-4031 experiment:



Example 3 – Isoprenaline experiment:

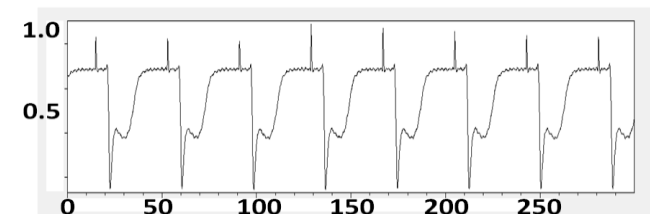
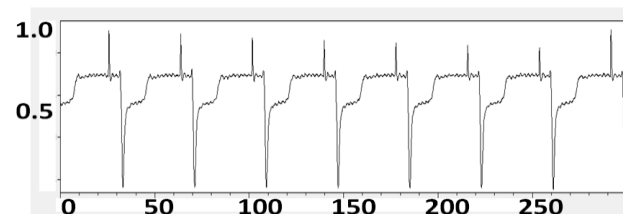
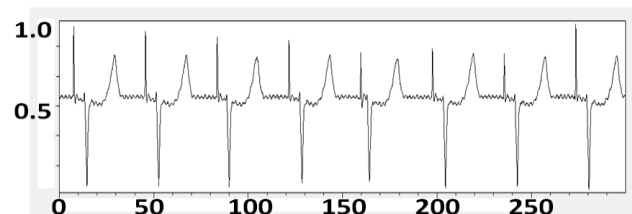


Figure 7.3 ECG from no-VF heart.

Examples of ECG from the hearts that did not develop VF in three different sets of experiment showing variation in the repolarisation pattern as indicated by the ST changes at *Pre-occlusion 30min*, *Occlusion 5min* and *Occlusion 10min*.

Simulation of ECG

When implementing the model, two different sites were chosen to mimic an ischaemic event via local shortening the AP. The sites were the anterior region of the heart (site 1) and the postero-lateral side of the LV (site 2). Site 1 was representative of the mapping region from the experimental work whereas site 2 was the site which was not mapped during the optical mapping experiments but the region was supplied by the coronary artery occluded during the experiments. The degree or size of the infarct was varied from mild which only localised to the centre to moderate which involved slightly bigger area and severe infarct which involved most LV regions.

Anterior infarction (Site 1)

Figure 7.4 shows a simulation of normal AP at the anterior inferior region of the LV. The corresponding ECG signal in lead II shows normal QRS and T wave with positive polarity of the T wave. There was no ST elevation or ST depression observed.

In Figure 7.5, the heart was simulated to have mild, moderate and severe infarction with the centre area marked with the black arrow. During mild infarction, there was slight ST segment depression but the T wave was still in the same polarity. As the size of the infarct was increased to simulate moderate infarction, ST depression and the T wave changes were observed. With a severe infarction that involved almost all regions of the LV, the ST depression became more prominent and this time the T wave also changed its polarity.

Normal heart – Site 1

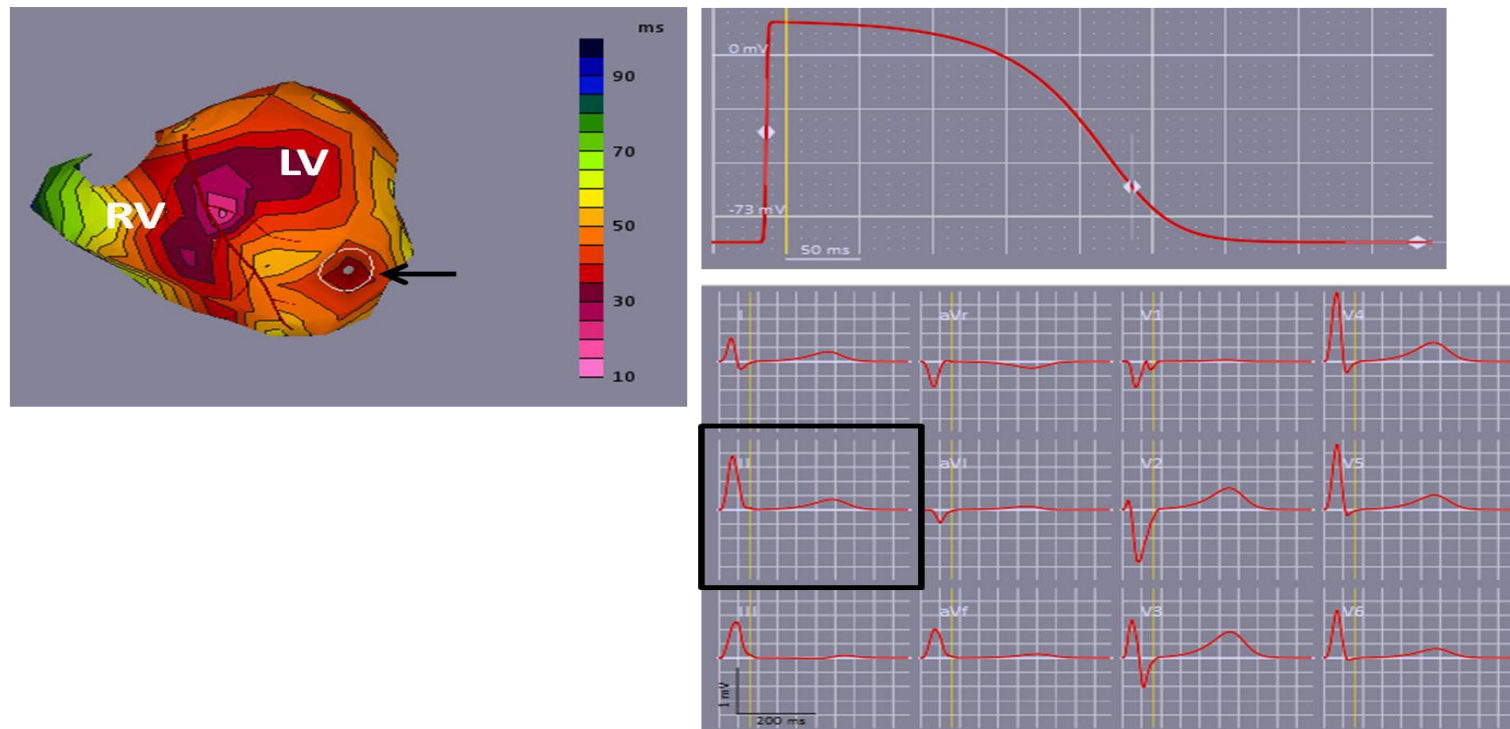
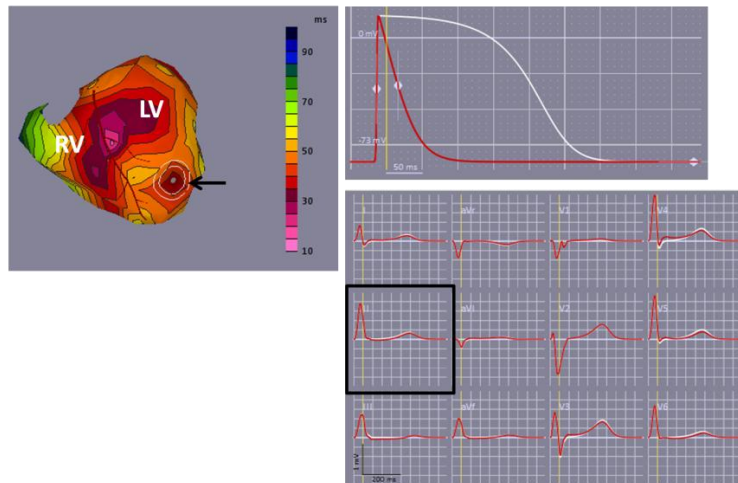


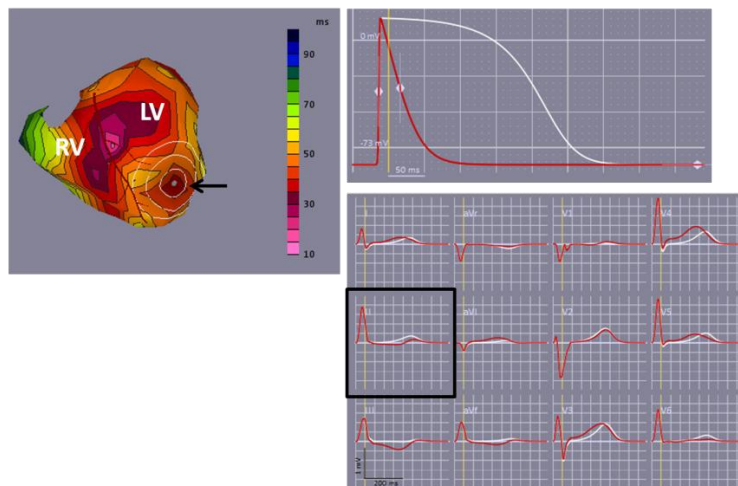
Figure 7.4 Simulation of normal AP at site 1 (indicated by black arrow).

The heart pane on the left figure illustrates the heart model with the black arrow pointing towards the centre of site 1. ECG signal at lead II (in the black square) shows flat ST segment with positive polarity of the T wave.

Mild infarct – Site 1



Moderate infarct – Site 1



Severe infarct – Site 1

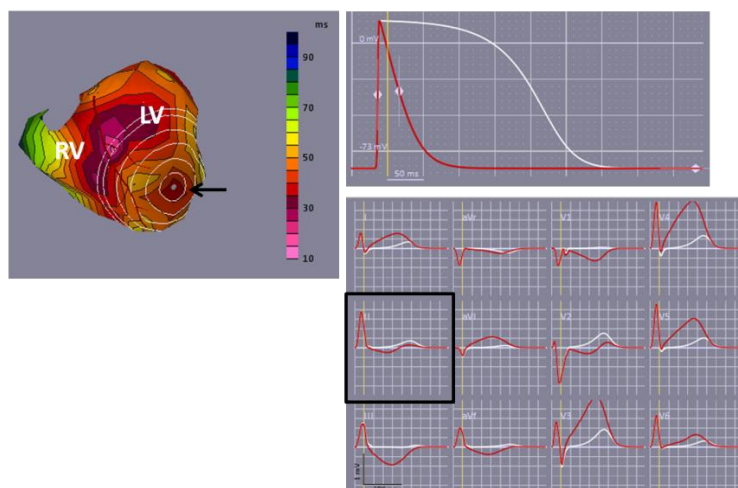


Figure 7.5 Simulation of varying severity of infarction.

Simulation of mild, moderate and severe infarction at site 1 produced by shortening the AP in this region. ECG signals in lead II shows slight depression of the ST segment in mild infarct but there is no change in the T wave polarity. As the size of the infarct became larger, the ST depression became more prominent and T wave also change its polarity.

Postero-lateral infarction (Site 2)

In this model, the heart was simulated to have an ischaemic condition at the postero-lateral aspect of the LV (site 2). The AP and ECG signals before the episode of infarction are displayed in Figure 7.6. Under normal conditions, the T wave observed in lead II had a positive polarity with no ST segment changes.

The model was then adjusted to produce varying degree of infarction; mild, moderate and severe infarction by increasing the size of the infarct as shown in Figure 7.7. During mild infarction, there was no obvious change on the T wave and the ST segment. In moderate infarction, there was slight ST segment elevation. Severe infarction involving most regions of the LV resulted in a very prominent ST segment elevation in lead II. In all three varying degrees of infarction at site 2, the T wave maintained its positive polarity.

Normal heart – Site 2

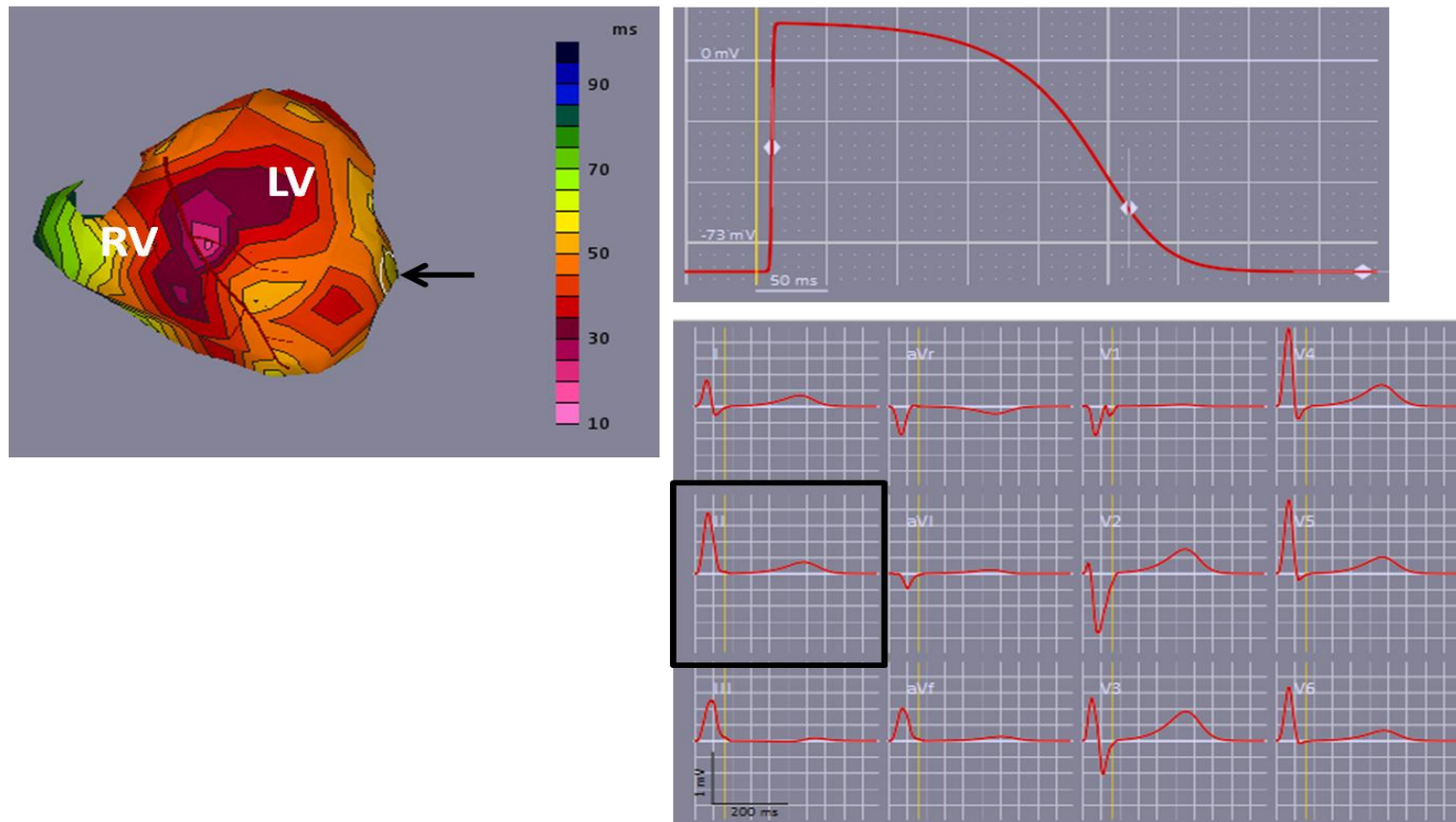
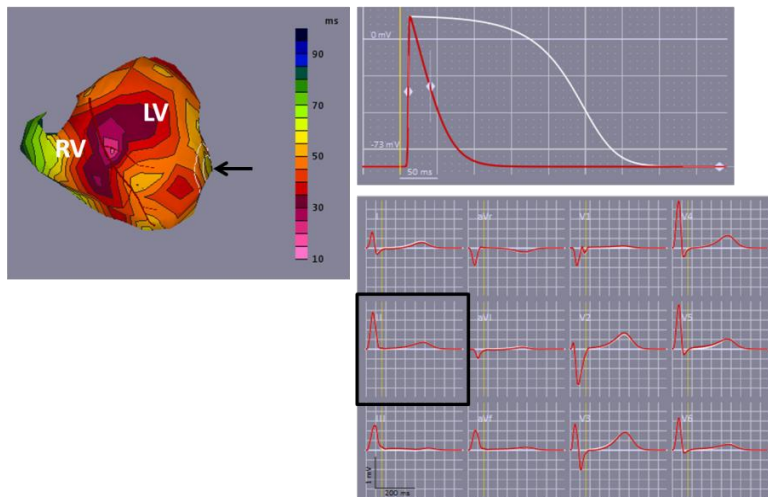


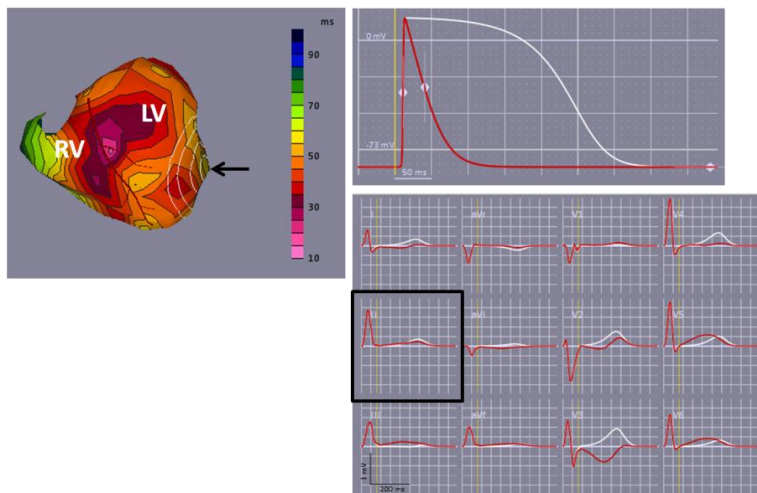
Figure 7.6 Simulation at site 2.

The heart pane on the left figure illustrates the heart model with the black arrow pointing towards the centre of site 2 at the postero-lateral region of the LV. The ECG signals (left lower figure) in lead II (in the black square) shows normal QRS and T wave with positive polarity. The ST segment is flat.

Mild infarct – Site 2



Moderate infarct – Site 2



Severe infarct – Site 2

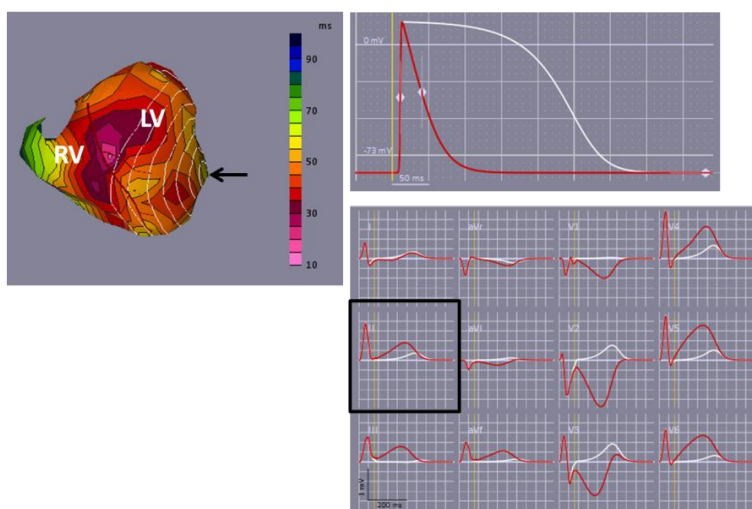


Figure 7.7 Simulation of varying severity of infarction. Simulation of mild, moderate and severe infarct at site 2 showing variation in ECG signals in lead II. As the size of the infarct became larger, the ST segment elevation became more prominent but the T wave was maintained in the positive polarity.

Discussion

The three sets of coronary artery occlusion experiments (control, E-4031 and isoprenaline experiments) revealed an incidental observation in terms of the variation in the repolarisation pattern on the ECG pattern and its relation to the incidence of VF. During the experiments, ST segment depression or elevation as well as changes of T wave polarity were observed. Invariably when the T wave changed polarity from positive polarity at pre occlusion to negative polarity during occlusion, the hearts did not develop VF and when the T wave did not change the polarity, the hearts went into VF. Therefore, the experimental situation was simulated with a computer programme to study factors that might contribute to the variation in the repolarisation pattern of the ECG. Two main factors studied in this simulation were the site and the size of the ischaemic regions. In this study, the normal male heart model was chosen because the orientation of heart appeared to generate an ECG pattern similar to that obtained experimentally. Lead II in the simulation programme was examined because this was representative of the lead used during the experimental works.

In the heart model ischaemia was simulated by shortening the AP shape at two different sites of the LV. The first site was at the anterior region of the LV with the centre at the apex (site 1). During mild ischaemia at site 1, there were few changes in the ST segment or T wave on lead II. As the area of the infarct increased representing the transition from moderate to severe infarction, there was ST depression which depressed the T wave and produced a T wave signal of negative polarity. Next, the heart was simulated to have an ischaemic condition at site 2 which was the postero-lateral site of the LV. Mild ischaemia did not show much change in lead II. Moderate to severe infarction caused ST segment elevation. As the size of the infarct got bigger, the ST elevation became more prominent.

Relating this information back to the experimental measurements is difficult because the size and position of the ischaemic area was not assessed. However, inversion of T-wave, a phenomenon which correlated to the absence of VF, was modelled by larger, more extensive ischaemia areas. This suggests that smaller infarct areas may be associated with a higher incidence of VF, a conclusion that will have to be tested experimentally.

From a clinical perspective, one of the big thrombolysis trials (Newby *et al.*, 1998) reported that patients with anterior STEMI rather than lateral STEMI or inferior STEMI were more likely to have VF.

Conclusion

The site and size of the infarct appear to be able to explain the ECG variation observed in isolated heart experiments. As the size of the infarct at the anterior region became larger, there was ST depression as well as changes in the T wave polarity observed in lead II. On the other hand, the infarct occurring at the postero-lateral region of the LV will cause ST segment elevation and no change in the T wave polarity monitored in lead II.

Chapter 8: Acute coronary artery occlusion – panoramic view optical mapping study

Aim:

This chapter reports a study of the repolarisation pattern on the majority of the epicardial surface of the heart and attempts to correlate these findings with the incidence of VF post coronary artery occlusion.

Introduction

Cardiac optical mapping is a powerful tool to study the initiation, maintenance and termination of arrhythmias (Efimov *et al.*, 2004). Typical 2D cardiac optical mapping has been limited to recording from only a single field of view of the optical sensor but in cardiac arrhythmias, especially of the re-entrant type, the pattern of arrhythmia can be unstable with rotors/wavelets moving around the heart. Thus conventional single-camera mapping is limited in terms of obtaining comprehensive information during the event of arrhythmia (Qu *et al.*, 2007). In recent years, there have been developments in panoramic 3D imaging of the heart allowing multiple field of views to be mapped and imaged from the entire epicardial heart surface using more than one camera (Lou *et al.*, 2008; Qu *et al.*, 2007; Ripplinger *et al.*, 2009).

Previous optical measurements in this laboratory were limited to recording from the anterior aspect of the left ventricle (LV) (see Chapter 5). These showed that during the pre-occlusion phase the epicardial APs were shorter in the subgroup that developed VF post-occlusion. However, the extent to which this observation applied to sites in regions outside the field of view was unknown. Also, the region directly affected by ischaemia on occlusion clearly involved sites outside the mapped area. To extend the coverage to include these regions, a panoramic optical mapping technique was developed to look at the electrophysiological properties across the majority of the ventricular surface.

Previously reported panoramic systems (Bourgeois *et al.*, 2012; Qu *et al.*, 2007) have used three cameras to provide 360 degree coverage to track complex patterns of activation and repolarisation. The essential point to realize here is that, to study steady-state phenomena that are not changing on a beat-to-beat basis, the requirement for multiple cameras is removed. Therefore, we devised a methodology that facilitated multiple *sequential* recordings from three

equivalent aspects of the heart surface. This necessitated constructing a perfusion apparatus that could be easily and rapidly rotated to each of three angles. Details of this apparatus are given below.

Methods

Preparation of the rabbit hearts

A total of 17 animals were used in this panoramic-view optical mapping experiments. Hearts from adult New Zealand White rabbits (2.5-3.5kg) used in this study were prepared as previously described. As before, the electromechanical uncoupler Blebbistatin (10 μ M) was used to reduce motion artefact. Once the heart was stabilised and aligned within the chamber, a bolus of voltage-sensitive dye di-4-ANEPPS (100 μ l of 1 mg/ml) was loaded into the heart.

Panoramic view optical mapping

A panoramic optical mapping system was recently developed in our lab by Francis Burton and Godfrey Smith (University of Glasgow). In this system, the heart inside a specialised rotating chamber was rotated through fixed angles and data acquired sequentially from each viewpoint using a single CCD camera. A schematic diagram of the panoramic view optical mapping setup is illustrated in Figure 8.1. The heart inside the chamber was illuminated by an annular array of cyan LEDs (OptoLED, Cairn Research Ltd.) at 480nm wavelength. The excitation light from each LED was passed through interference filters. The emitted fluorescence light was then collected through a photographic lens and passed through a LP filter (665nm wavelength) and focused onto a CCD camera (80x80 pixels, 1000 fps) which is part of a RedShirt Cardioplex system (RedShirt Imaging, Decatur, GA). Another higher resolution Dalsa camera (Coreco Imaging, Canada) with 256 x 256 spatial resolutions was used to acquire white light images of the preparation. During the experiment, the heart was rotated to record the epicardial membrane potentials from the whole ventricular surface of the heart. The mapping field was divided into 3 different views, namely the RV/LV view which comprised mainly the LV and part of the RV, the LV view which consisted of the postero-lateral part of the LV and the RV view which had only RV.

Example of images of the heart surface captured by the Dalsa camera from the three different views is displayed in Figure 8.2.

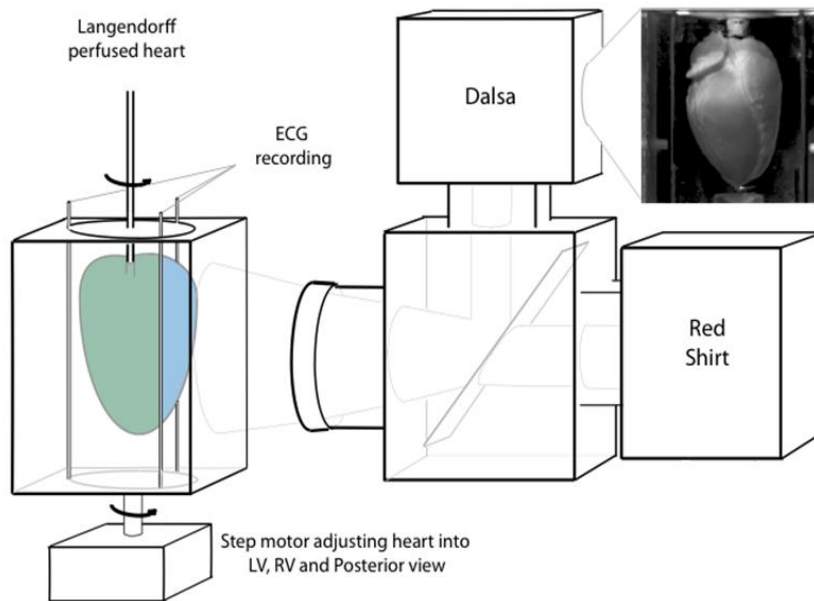


Figure 8.1 Schematic diagram of panoramic optical mapping setup.

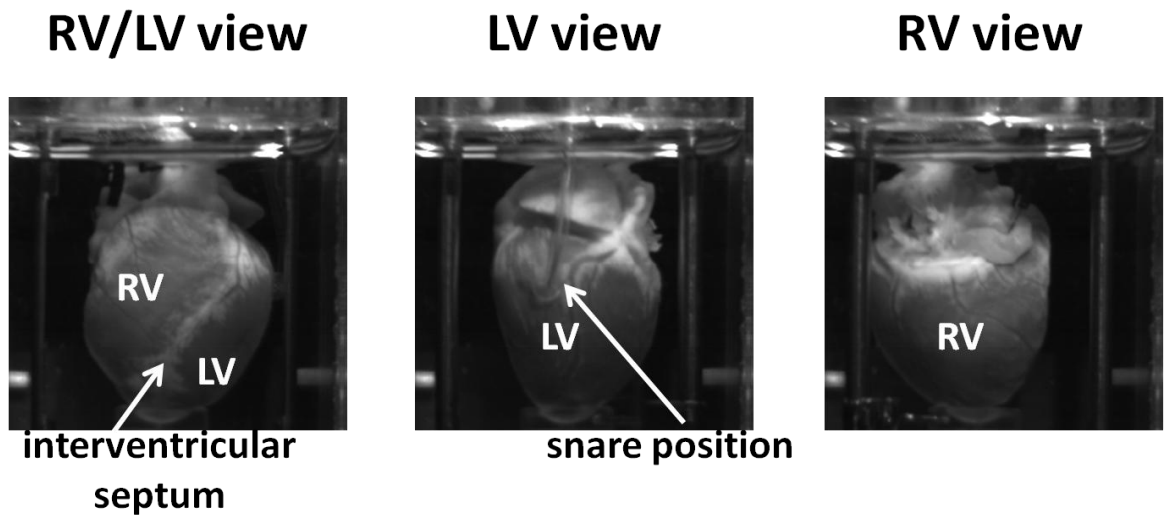


Figure 8.2 Images from three different heart surfaces.
Example of images obtained by the Dalsa camera from three different mapping views.

Rotating chamber

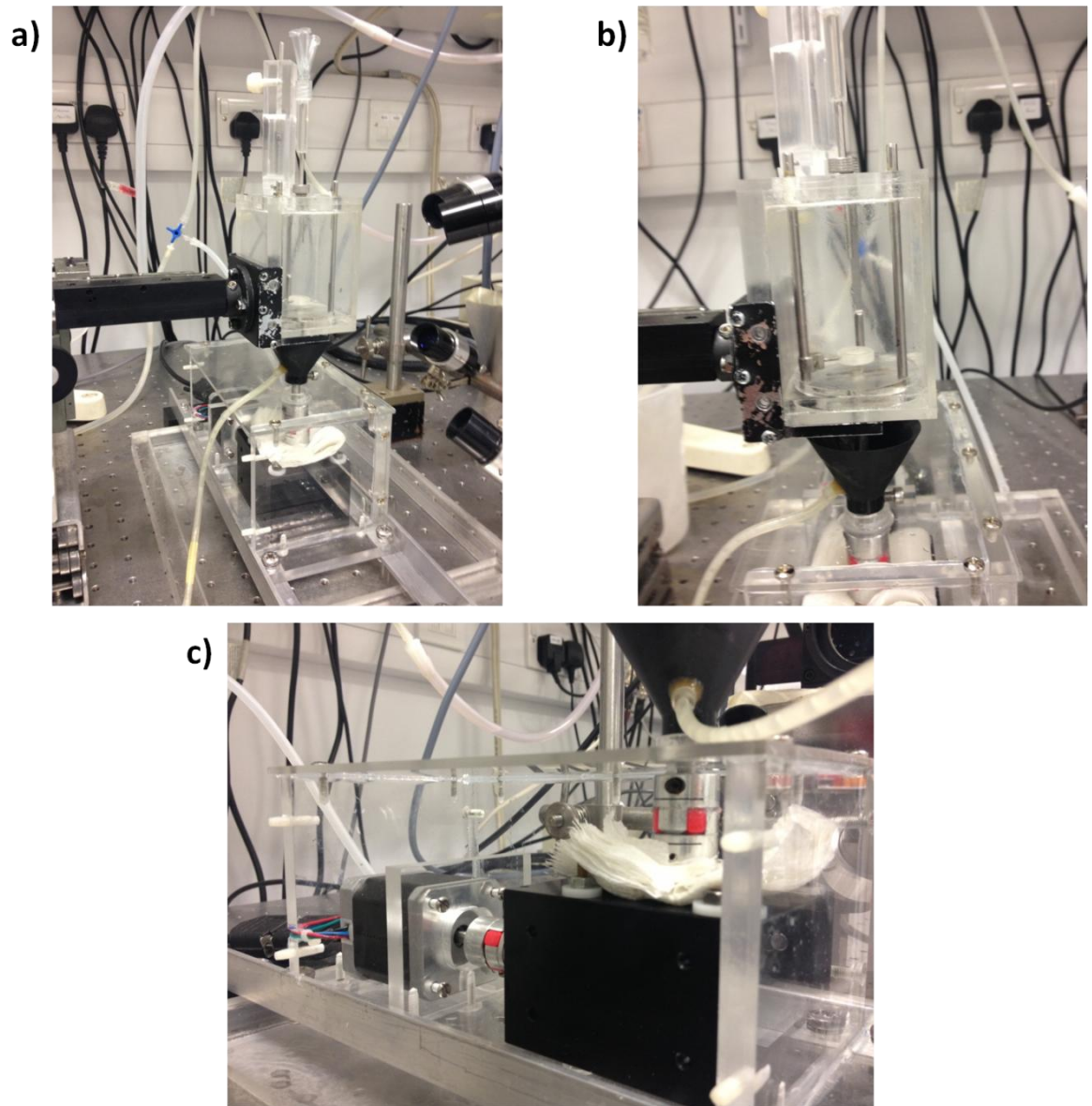


Figure 8.3 Rotating chamber.

Images of the components of specialised rotating chamber used together with the panoramic optical mapping system, showing a) the whole set-up, b) the main rotating chamber, and c) the gearbox container.

Figure 8.3a shows the different components of the rotating chamber used in the panoramic optical mapping system. It comprises the basic chamber (Figure 8.3b) with a screw and spindle that is attached to a hypoid gearbox (Reliance Precision Ltd.) via a coupling. The gearbox is attached to a stepping motor which is run by a driver circuit that can be run either manually or can be run from a computer. In this study, the speed and direction of rotation were controlled via a custom-made programme written by Francis Burton (University of Glasgow). Initially, after the heart was mounted on the aortic cannula and placed inside the

chamber, it was manually positioned so that the RV/LV view was facing the camera. The centre midline point was then determined and the heart was rotated ± 120 degrees from that centre point to move the heart to another view. Rotation to a new position takes less than 1s.

Coronary artery occlusion using vertical ligation system

In this study, a vertical ligation system was used to produce acute coronary artery occlusion instead of the horizontal ligation system used for the single view optical mapping experiments (see Chapter 2). This vertical ligation system was specifically designed to be used with this panoramic view optical mapping set-up. The ligature from the snare was passed through a small hole on top of the chamber and tied to a vertical spring device attached to the chamber (Figure 8.4). During the experiments, the spring was tightened for 30 minutes to occlude the vessel and produce a local ischaemia. Because the ligation site, suture thread and cannula tubing was identical to that used previously, it was assumed that the effect of ligation in this system would be comparable. After 30 minutes of occlusion, the snare was released to reperfuse the hearts.

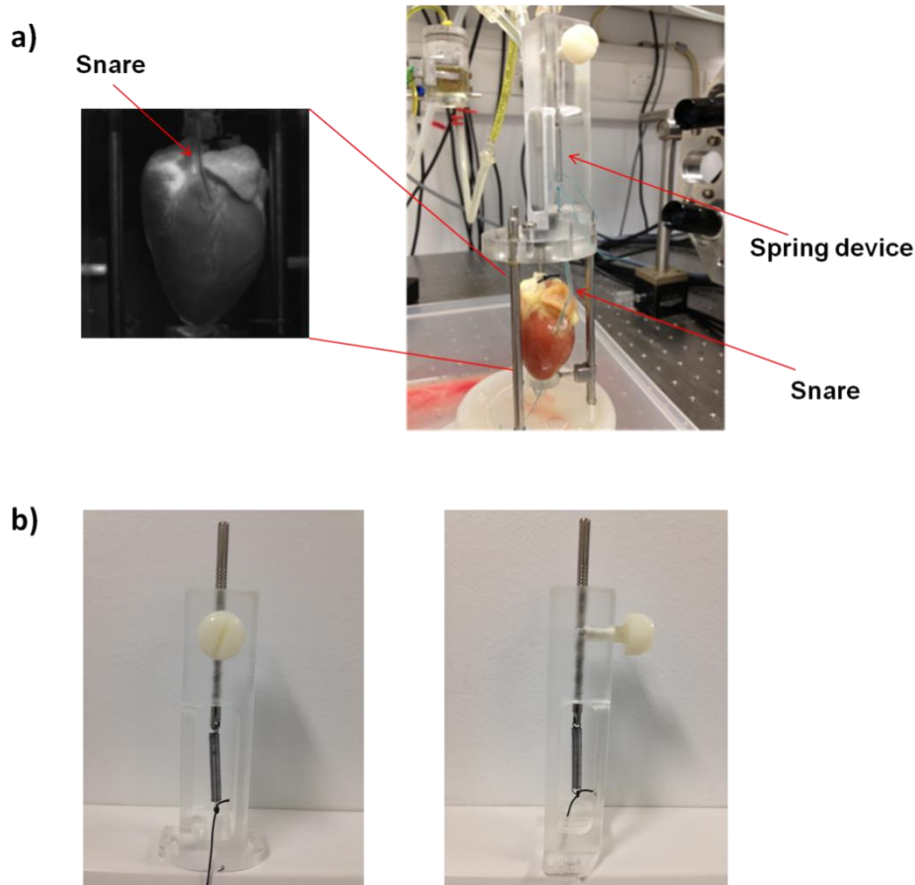
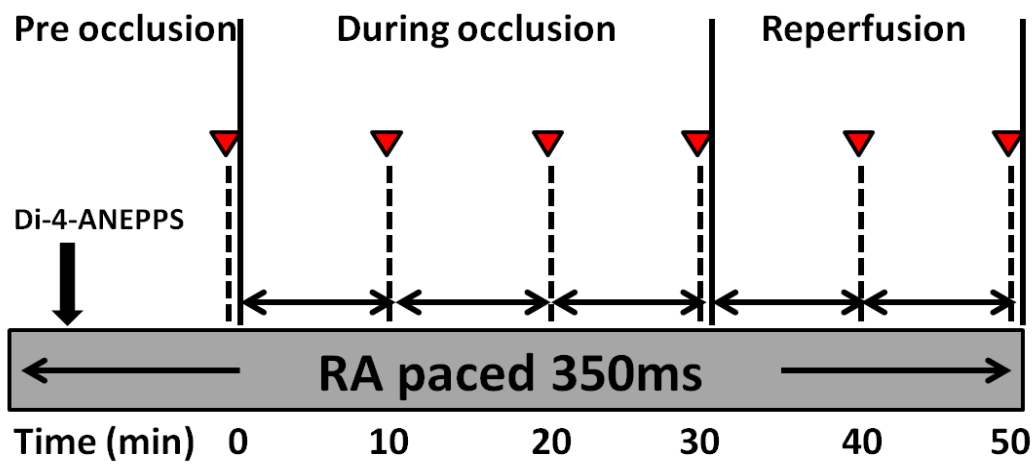


Figure 8.4 Vertical ligation set-up.

a) Arrangement of vertical ligation set-up used in panoramic view optical mapping experiments to produce acute local ischaemia. b) Close-up view of the ligation system from front (left) and side (right) view.

Experimental protocol

The experimental protocol for this study is illustrated in Figure 8.5. The experiment was divided into three periods; pre-occlusion, during occlusion and reperfusion similar to the time periods in previous single view studies. However, instead of using the intrinsic heart rate, the heart was paced at the right atrium at 350ms cycle length. Each recorded time point consisted of three consecutive recordings, one at each view (RV/LV, LV and RV). During the occlusion, if the heart went into VF, the snare was released to reperfuse the heart. If this failed to revert the heart back to sinus rhythm, a bolus of 1M KCl (0.2ml) was injected into the heart through the injection port (see Chapter 2).



▼ Signal recording

Figure 8.5 Experimental protocol.

Electrocardiogram (ECG)

During the experiments, simultaneous ECG recordings (see Chapter 2) with a configuration approximating to lead I in a 12-lead ECG were made (Figure 8.6) and could be viewed in real time during the course of the experiment.

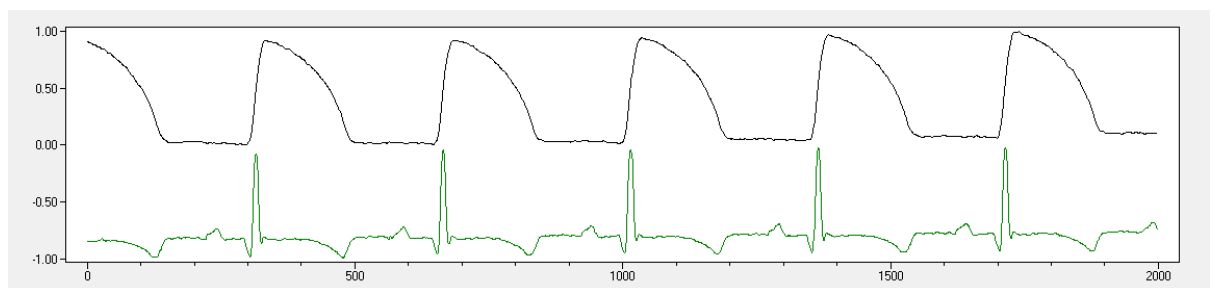


Figure 8.6 Example of ECG recording with corresponding APs.

Optical data analysis

Optiq

The optical signals obtained from this study were visualized and analysed using Optiq. Different settings were appropriate for these data sets because the signal-to-noise characteristic of the RedShirt camera and optics differs from the single-view system based on the Hamamatsu camera. Prior to analysis of the optical signals, spatial (Gaussian) and temporal (Medians + Boxcar) filtering was applied. Unlike the single-view system, all the camera views included pixels outside the profile of the heart. These background pixels were excluded on the assumption that no signal would be present. In practice, however, many pixels showed a very weak (noisy) signal presumed to be due to reflections from the sides of the chamber. Therefore, a signal-to-noise ratio (SNR) threshold criterion was used to exclude any pixels which did not correspond to the epicardial surface of the heart. Based on preliminary measurements, a threshold $\text{SNR} < 20$ was found to provide a faithful representation of the heart profile. This pixel selection was then trimmed further to exclude signals from myocardium lying at a steep angle with respect to the camera plane such that overlapping marginal regions were divided between the three views. A boundary angle of $\pm 60^\circ$ from the central line of the heart was imposed on the initial pixels selection, excluding any pixels which lay beyond this boundary (Figure 8.7). A typical experimental example of the exclusion criteria is demonstrated in Figure 8.8, showing the original pixel selection in Figure 8.8a and the applied exclusion criteria in Figure 8.8b.

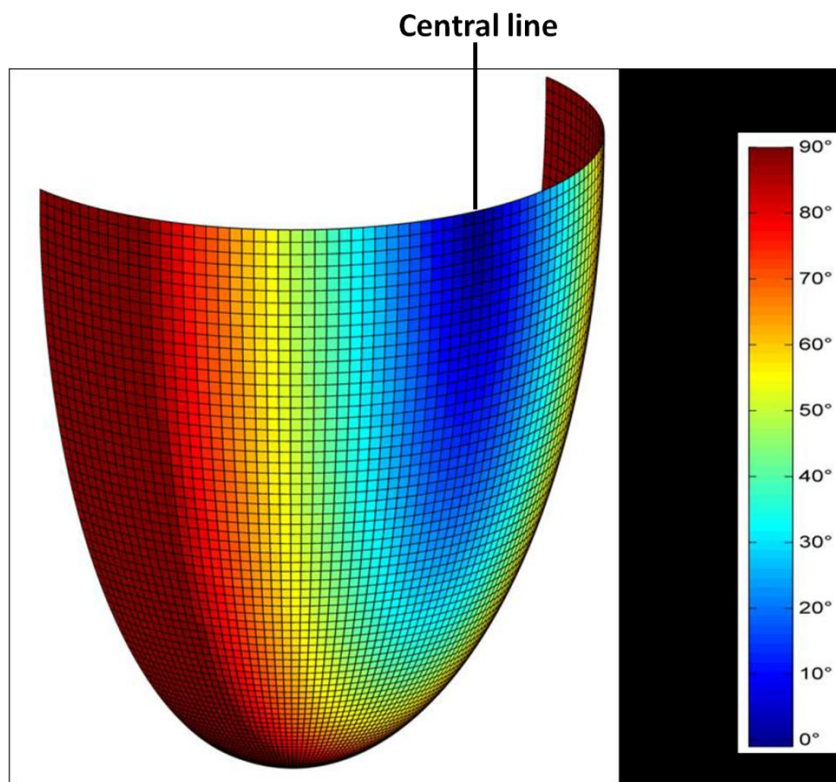


Figure 8.7 Idealised model of the surface of the heart based on a semi-prolate ellipsoid. The angles indicated by the colour bars on the right represent the angle at each point with respect to the difference between the surface normal and perpendicular to the central line. (Produced by Mr Andrew Allen, University of Glasgow)

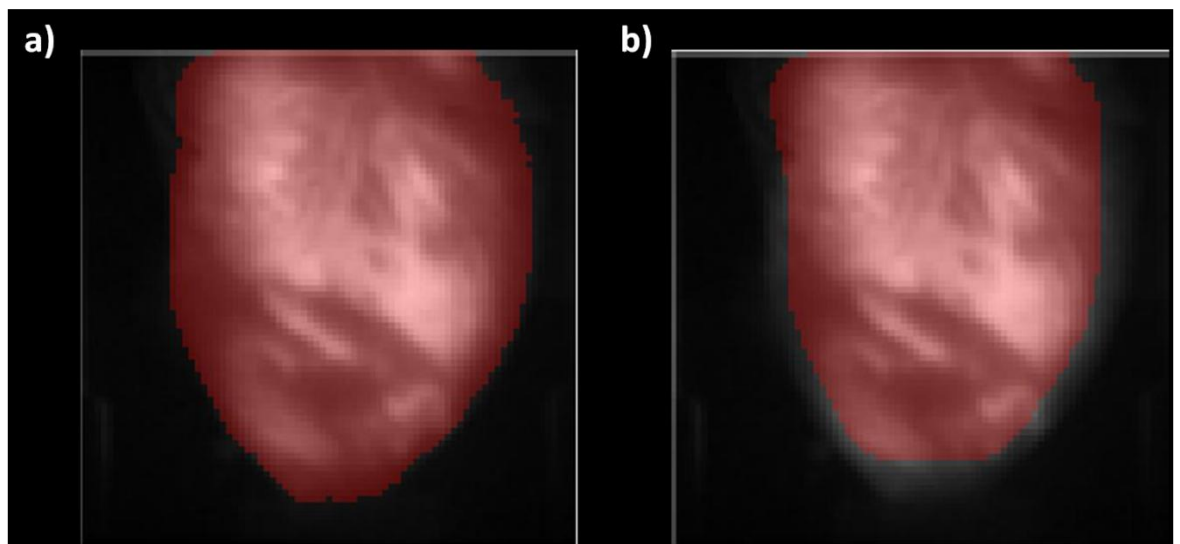


Figure 8.8 Application of exclusion criteria. Illustration of a typical selection of the heart, showing the a) original pixel selection, and b) selection after applying the exclusion criteria.

GGobi

Some of the optical data obtained in this study was analysed with GGobi, an interactive and dynamic graphic package that can be used for automatic brushing to change the colour, glyph type and size of points. Here GGobi was used to correlate the APD and the activation time on the heart surface. Optical data recorded from the experiments was imported into the software. Automatic brushing was applied to the data and the results are presented in the Result section. Example of automatic brushing by GGobi is displayed in Figure 8.9.

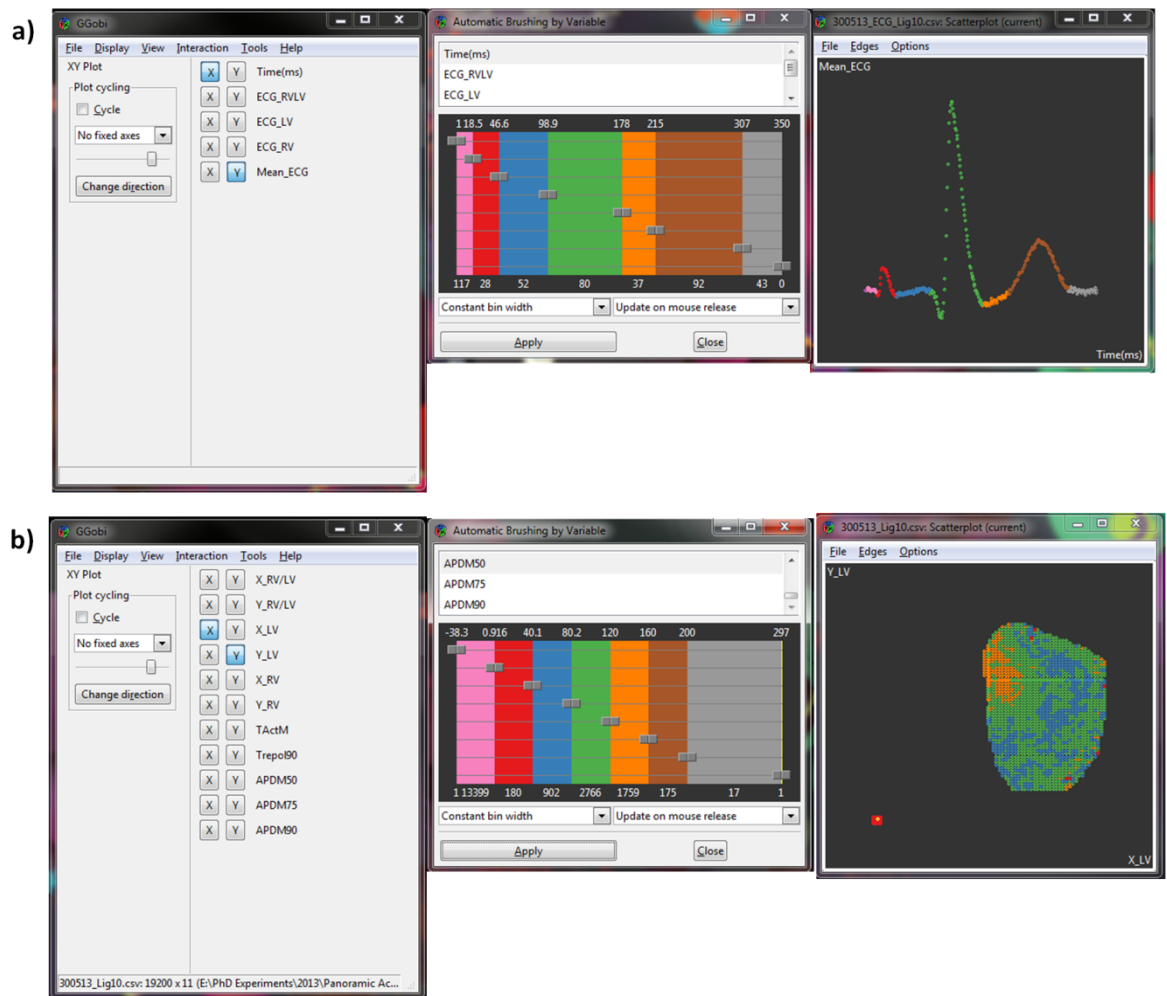


Figure 8.9 GGobi software display.

Example of automatic brushing for a) ECG showing each component of the ECG is marked with different colour, and b) APD₅₀ showing the distribution of AP duration across the heart surface.

Results

Incidence

Overall, 5 out of 17 hearts developed VF during acute ischaemia in this study (Figure 8.10). For the purpose of this analysis, only hearts that developed VF within 30 minutes of the start of occlusion were included in the VF group. Any episode of arrhythmia that occurred during the reperfusion period was included in the no-VF group.

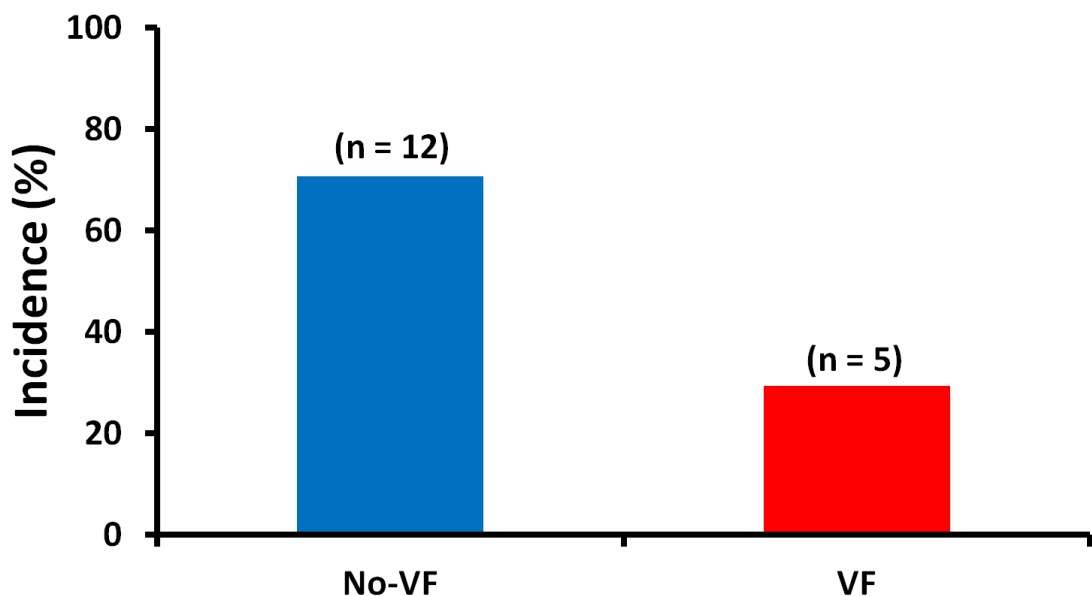


Figure 8.10 Incidence of VF in panoramic view experiments. Incidence of hearts that developed VF (29.4%) and did not develop VF (70.6%) in panoramic view optical mapping experiments.

Electrophysiological parameters

The electrophysiological parameters analysed were APD at 50% repolarisation (APD₅₀) and activation time (TActM). Figure 8.11 shows examples of contour maps of APD₅₀ and TActM prior to occlusion, 10 minutes after occlusion (*Occlusion 10min*) and during reperfusion. Prior to occlusion, APD₅₀ ranged from 100 - 140ms. During occlusion, there was shortening of APD₅₀, particularly in a region of the LV. During reperfusion, APD₅₀ returned to the pre-occlusion level over most of the heart surface but APD₅₀ at some sites on the LV still remained shorter than control values. Activation time was measured relative to the RA pacing stimulus. From the example shown in the bottom panel of Figure 8.11, the activation time at pre-occlusion ranged from 90 - 110ms. At *Occlusion 10*

min, there was delayed activation time in the region of shortened APD. However, the activation time was restored during reperfusion.

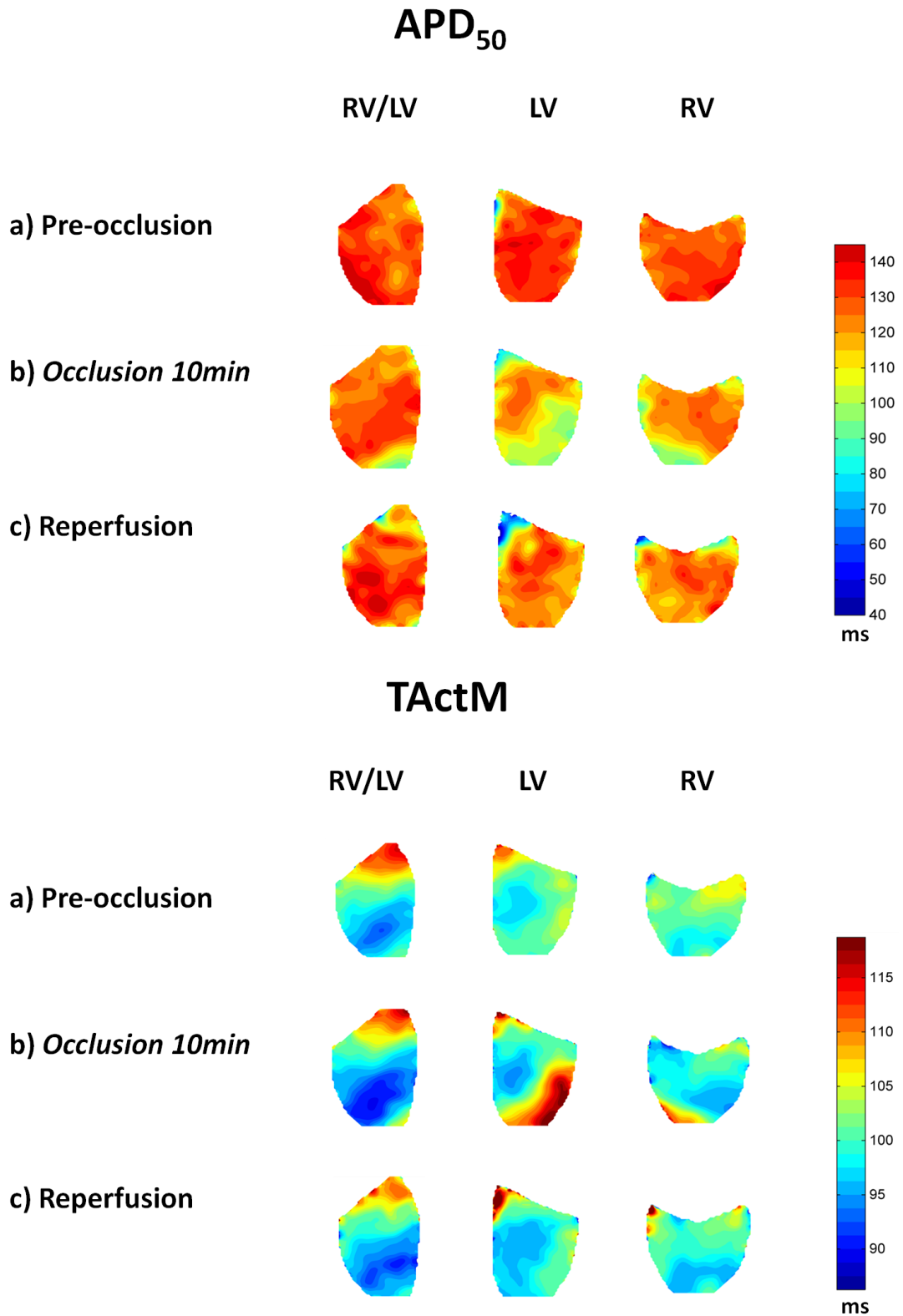


Figure 8.11 APD₅₀ and TActM.

Contour maps showing changes in APD₅₀ and TActM before, during and after occlusion from 3 different views of the heart; RV/LV, LV and RV.

APD₅₀

In the single-view optical mapping experiments, hearts with intrinsically longer APD prior to ischaemia tended not to develop VF and *vice versa*. In this experiment, there was no significant difference in combined (LV+RV) epicardial APD₅₀ prior to occlusion between the hearts that went into VF and those that did not (Figure 8.12). However, APD₅₀ in the LV was significantly shorter than the RV in hearts that developed VF. In the LV alone, APD₅₀ was not significantly shorter in the group that developed VF, with the current sample size. Therefore, the LV was further analysed to look for any difference of APD₅₀ between the apical and basal regions (Figure 8.13). Interestingly, the APD₅₀ in the apex of VF hearts was significantly shorter as compared to the apex of no-VF hearts. This region corresponds approximately to the single-camera view recorded in previous experiments.

The range (max-min) of APD₅₀ at the same time point was also analysed and the result shown in Figure 8.14. It shows that the range of APD₅₀ in the LV of hearts that developed VF was significantly greater compared to the no-VF hearts consistent with the expectation that greater heterogeneity in the hearts that developed VF would predispose the heart to develop VF during ischaemic insults. Most of the heterogeneity is due to the presence of shorter APD₅₀ in the apical region relative to the basal region in VF hearts.

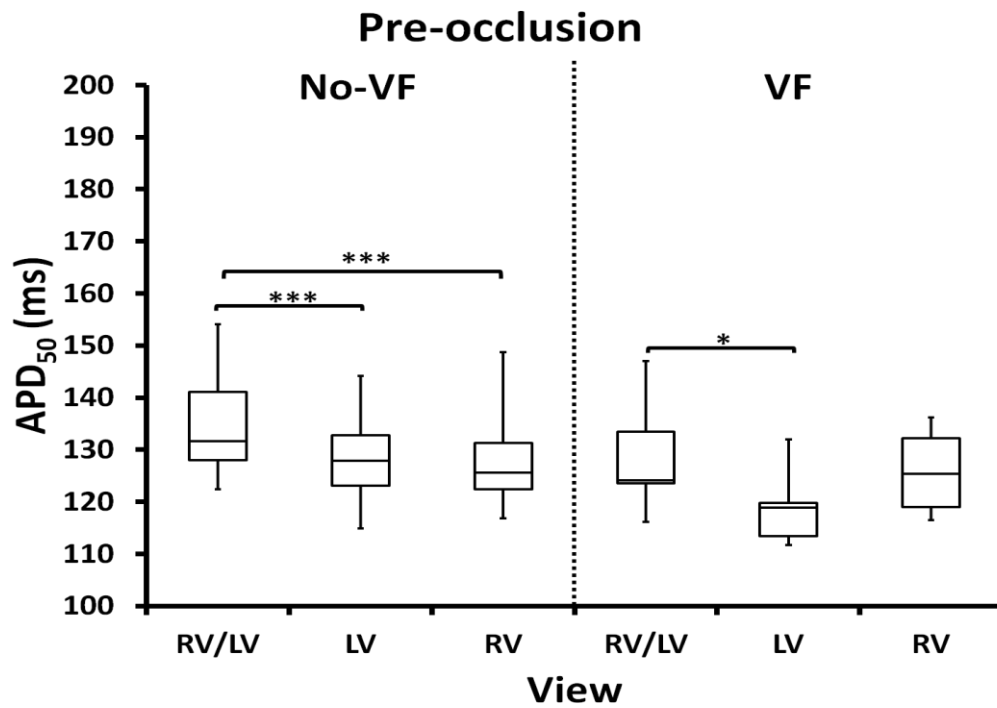


Figure 8.12 APD₅₀ from three different surfaces of the heart.

Box plots diagram comparing the APD₅₀ at pre-occlusion in three different views of the heart. It demonstrates significant APD differences between RV/LV and LV in both no-VF and VF groups, as well as between RV/LV and RV views in no-VF hearts which do not exist in VF hearts. (* $P<0.05$, *** $P<0.001$)

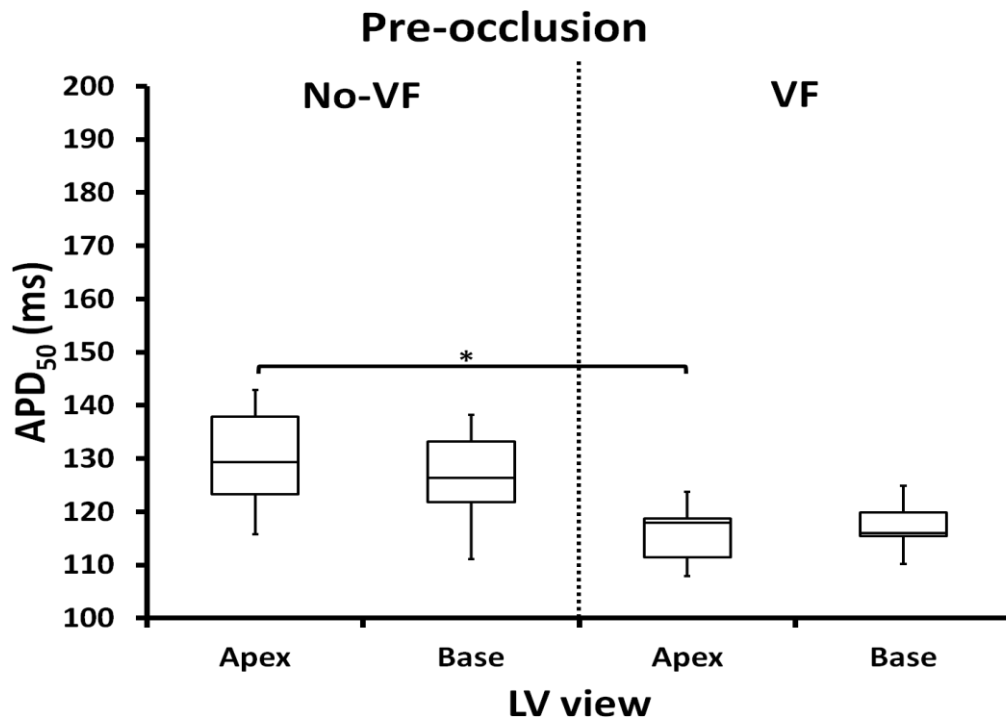


Figure 8.13 Apex-base difference in APD.

Apical to basal APD₅₀ differences during pre-occlusion period in hearts that developed VF and did not develop VF showing the APD₅₀ in apical region of LV was significantly shorter in hearts that went into VF. (* $P<0.05$)

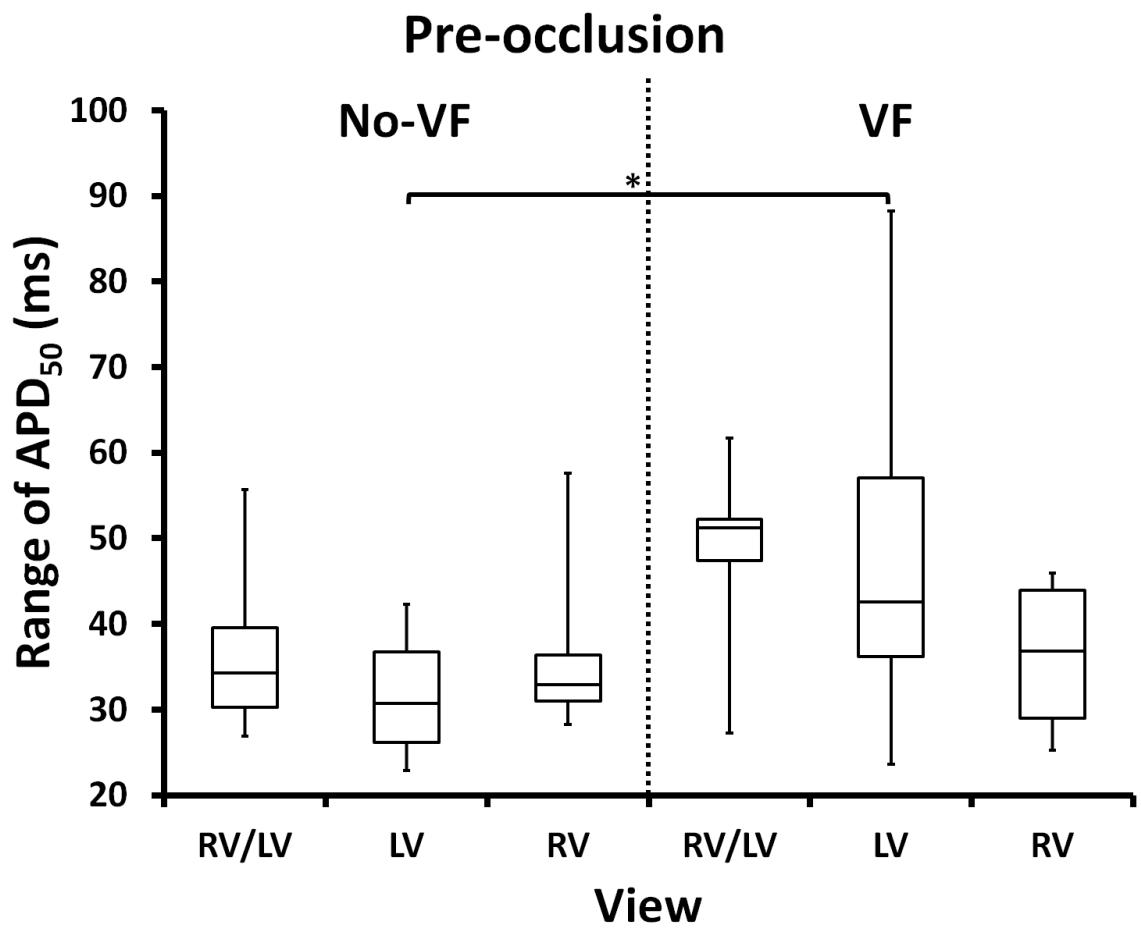


Figure 8.14 Range of APD₅₀ from three different heart surfaces.

Box plots diagram comparing the range of APD₅₀ at pre-occlusion period in hearts that did and did not develop VF. Hearts that developed VF had a significantly greater range of APD₅₀ in the LV. (* $P < 0.05$)

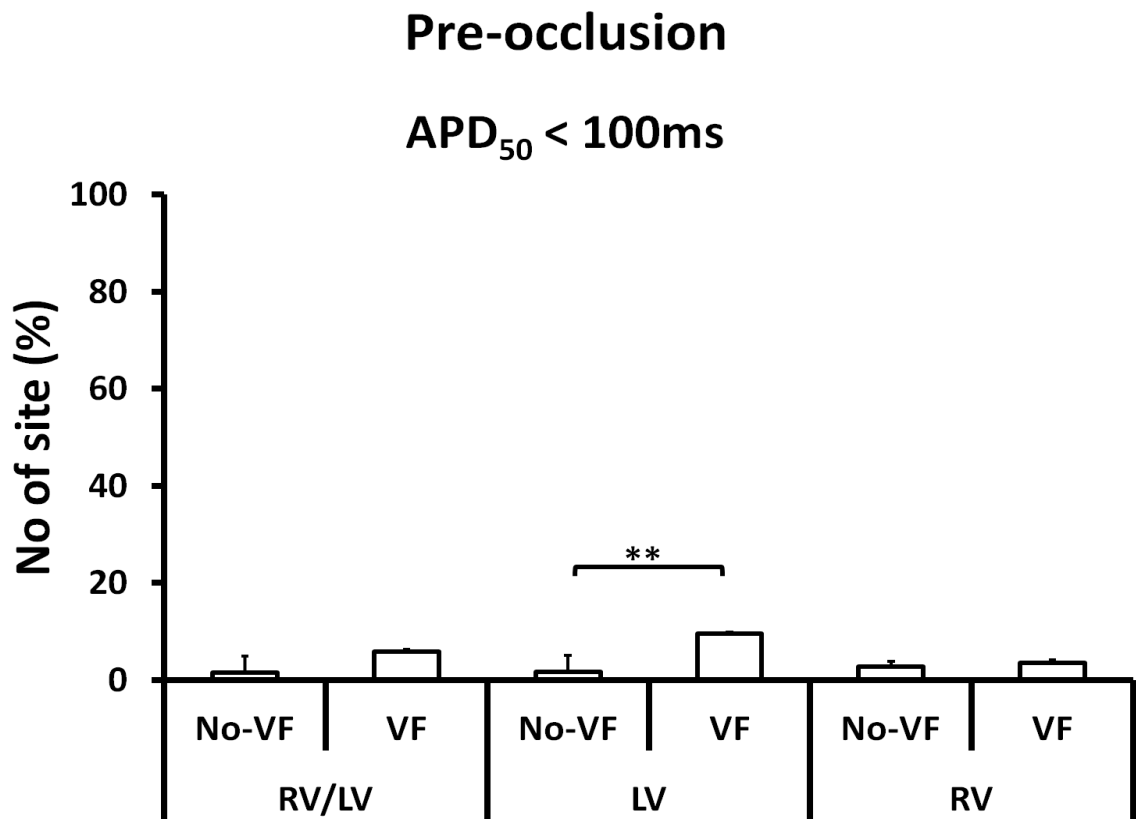


Figure 8.15 APD_{50} prior to coronary artery occlusion.

Bar graph of percentage of sites prior to ischaemia with $APD_{50} < 100ms$ in all three views: RV/LV, LV and RV. The LV in hearts that developed VF has significantly more sites of shorter APD. (** $P < 0.01$)

The number of sites with $APD_{50} < 100ms$ at the pre-occlusion time point was also analysed (Figure 8.15). VF hearts tended to have more sites with shorter APD ($APD_{50} < 100ms$) but only in the LV region was this difference significant.

In order to visualize the APD pattern across the whole epicardial surface of both groups of hearts, the APD distribution before and during occlusion was binned into 20ms ranges using GGobi and plotted (Figure 8.16). At the pre-occlusion time point, APD_{50} in VF hearts appeared to have greater heterogeneity (range of colours) compared to the no-VF heart, particularly on the LV. In general, both groups had APD_{50} ranged between 100 - 160ms in all three views. However, the VF heart had more sites with shorter APD_{50} less than 100ms as compared to the no-VF heart, and most of the shorter sites were located in the LV region. An unexpected observation in terms of the APD distribution in VF hearts was that, after 10 minutes of coronary artery occlusion, most of the APD_{50} in the LV region shortened with the APD_{50} ranged between 40 - 100ms, but at the same time there was *prolongation* of the APD ($APD_{50} > 160ms$) on most sites in the RV/LV

view. Interestingly, this phenomenon was not seen in the no-VF hearts even though the APD_{50} in the LV region also shortened in this group.

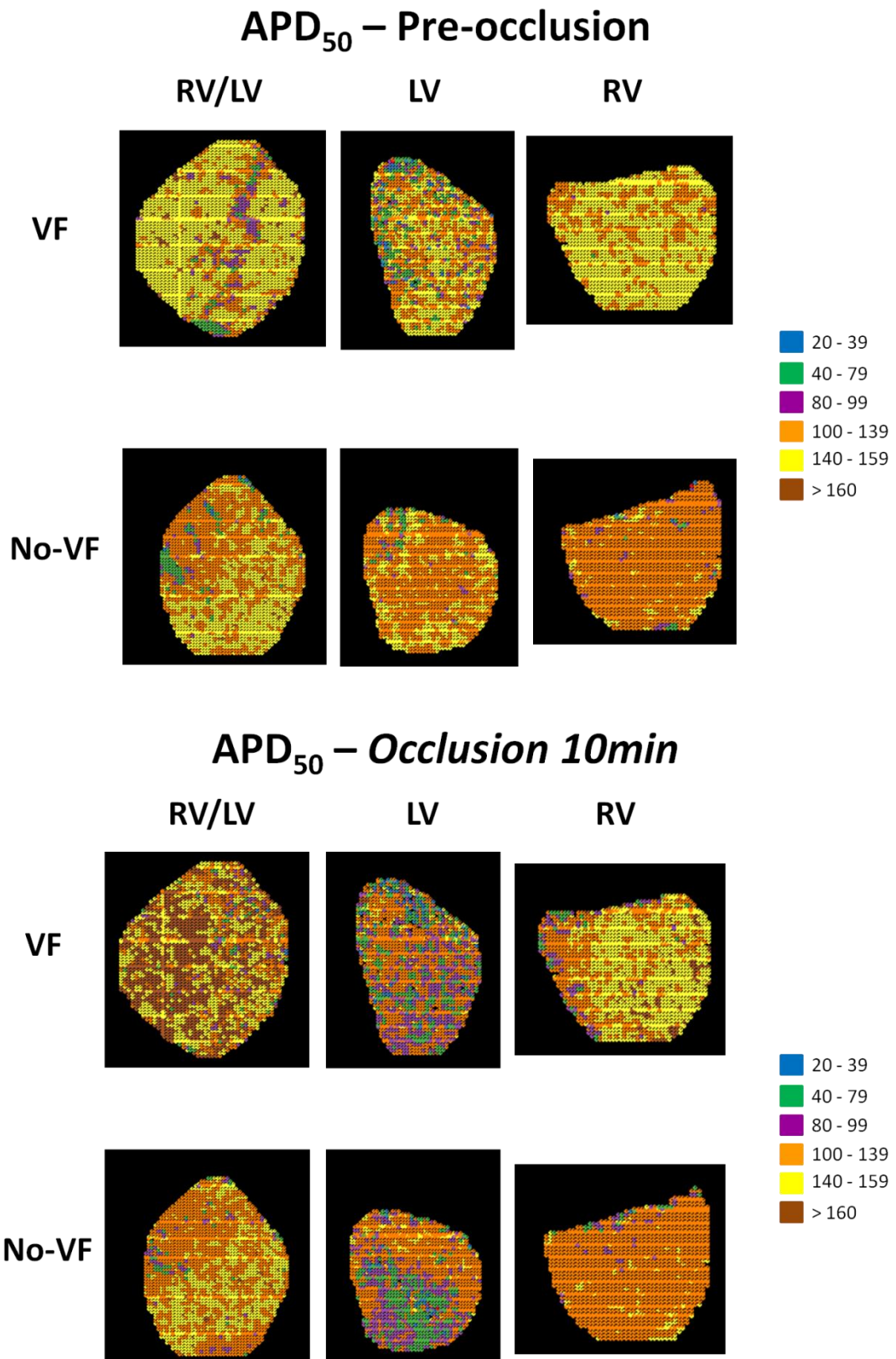


Figure 8.16 Distribution of APD_{50} across the heart surface.
 Example of APD_{50} distribution in no-VF and VF hearts at pre-occlusion and during *Occlusion 10min*.

Figure 8.16 tends to give the impression that in VF hearts there is a global APD shortening in response to regional ischaemia, in contrast to regional shortening seen in the no-VF hearts. However, scatter plot analysis of the APD_{50} during *Occlusion 10min* from 3 random samples of hearts in each no-VF (Figure 8.17a) and VF groups (Figure 8.17b) failed to show any difference in APD_{50} distribution pattern during acute regional ischaemia between the two groups.

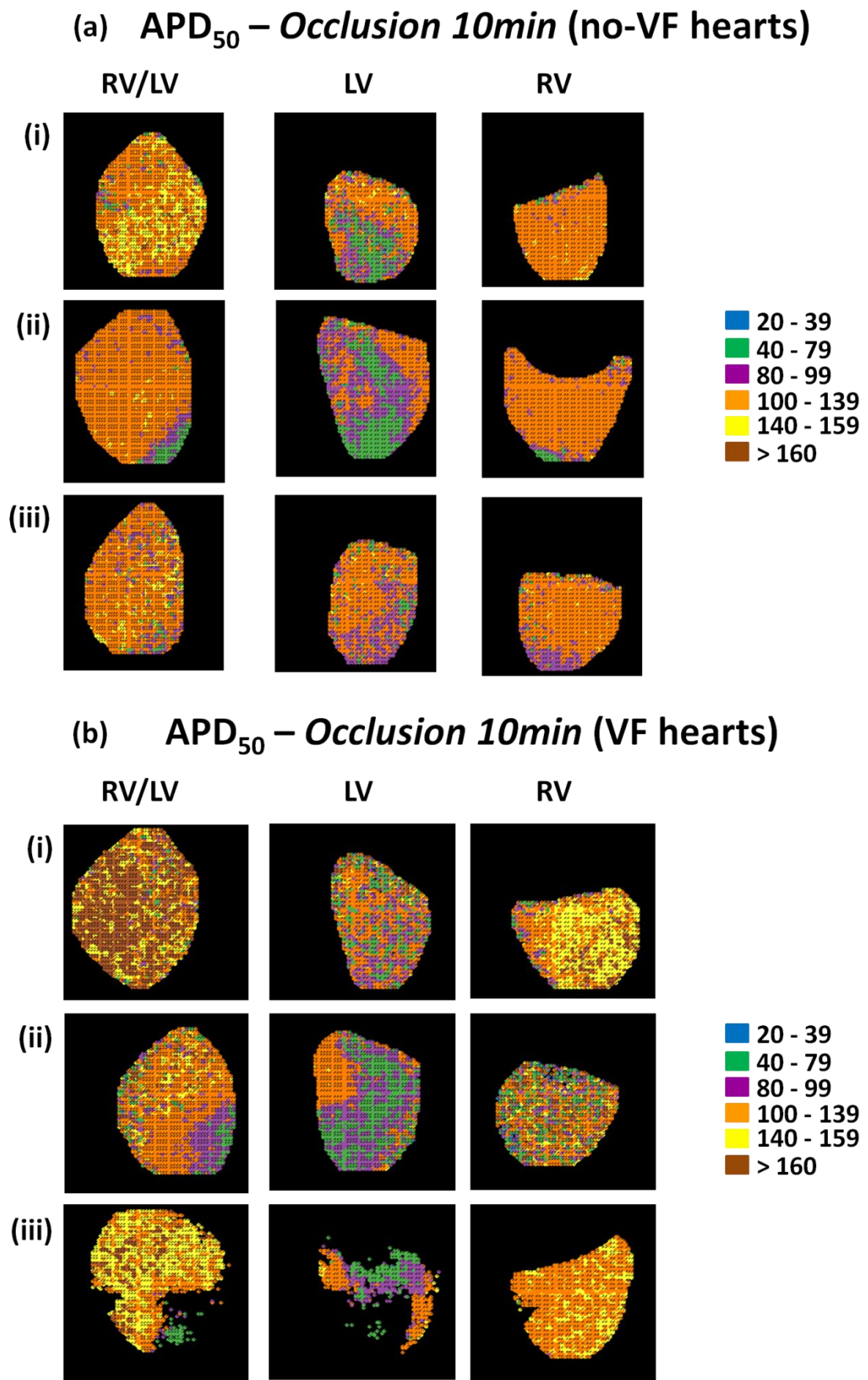


Figure 8.17 APD_{50} distribution during Occlusion 10min (no-VF vs. VF hearts). Scatter plot analysis showing the distribution of APD_{50} during acute regional ischaemia from 3 different hearts in each a) no-VF group, and b) VF group. In Figure b (iii) some of the pixels were excluded due to SNR < 20 (threshold for the exclusion criteria).

TActM

Another significant finding was that the hearts that developed VF had significantly delayed activation times compared to the no-VF hearts, predominantly in the LV view (Figure 8.18). Both apical and basal regions of the VF hearts had significantly longer activation times compared to the corresponding regions of the no-VF hearts (Figure 8.19).

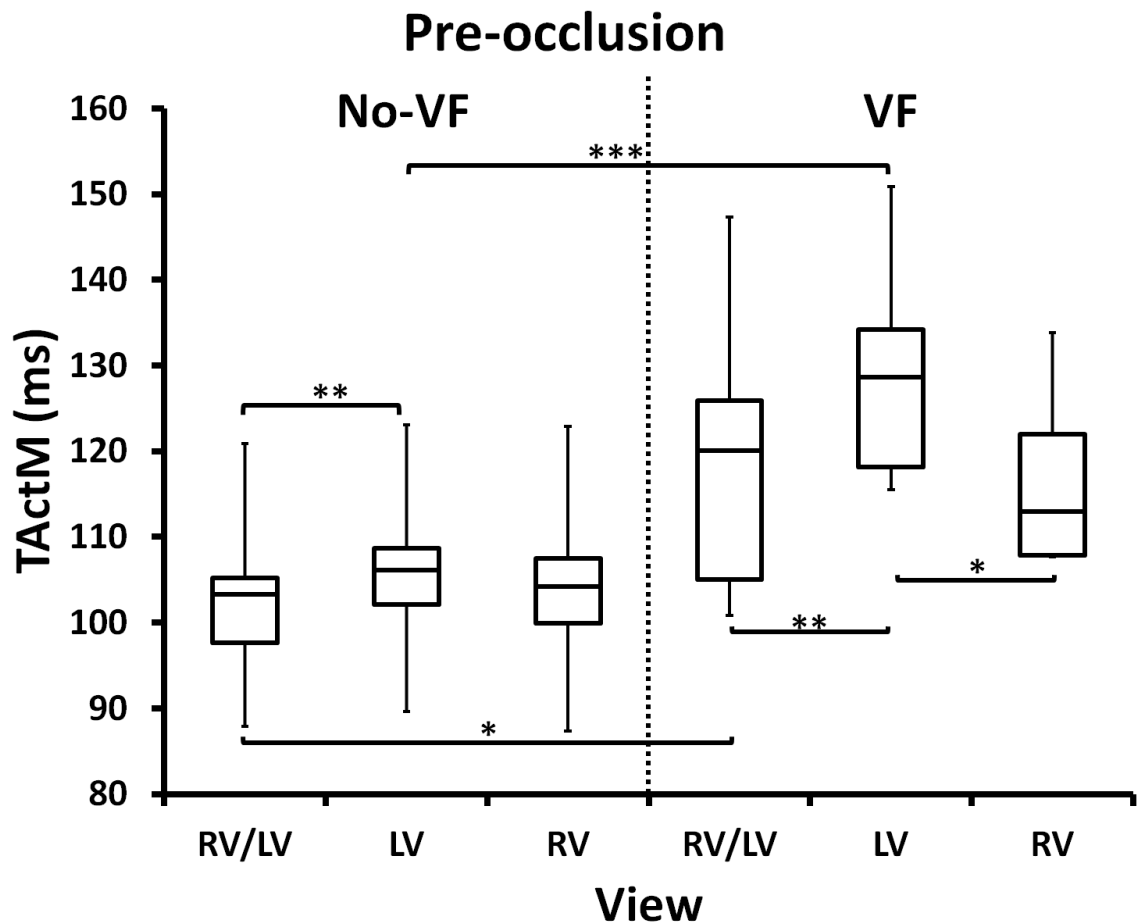


Figure 8.18 Activation time pre-occlusion.

Box plots diagram showing significantly longer activation times in hearts that developed VF, mainly in the LV. (* $P < 0.05$, *** $P < 0.001$)

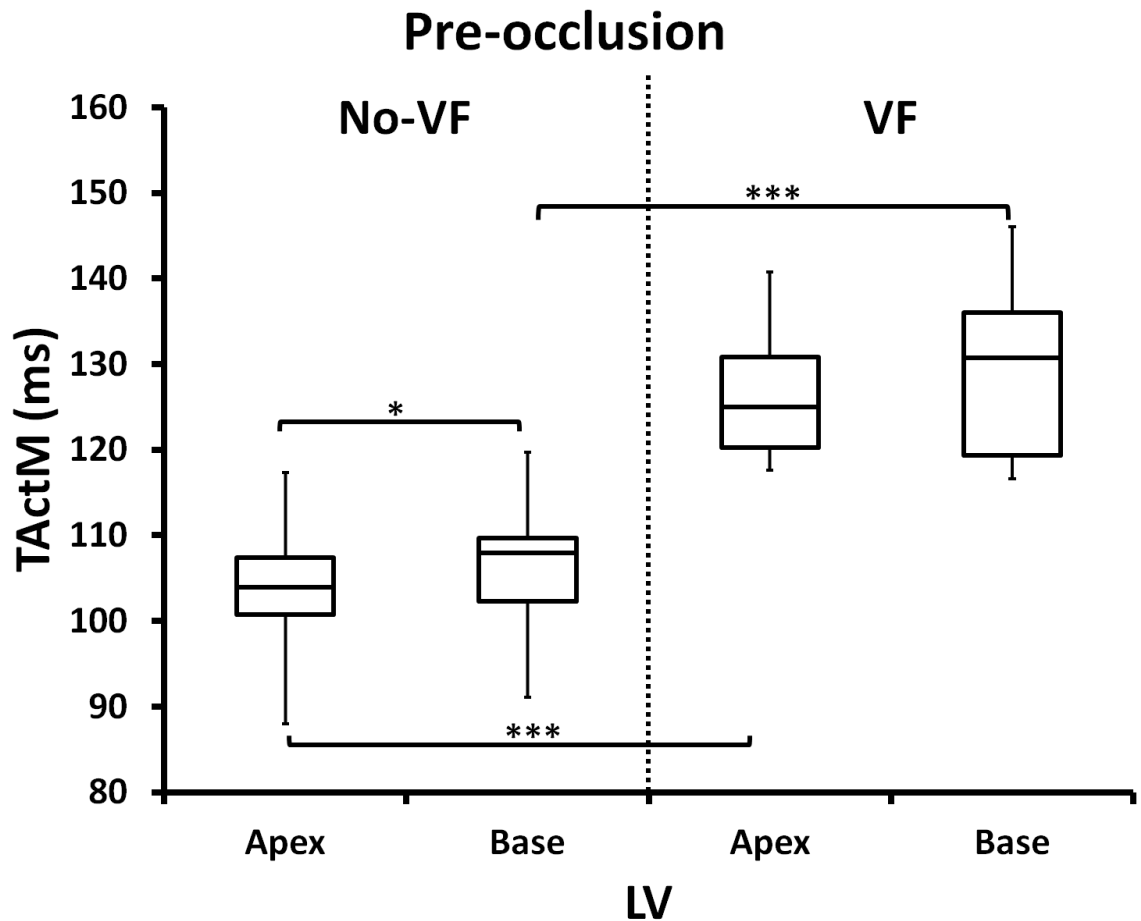


Figure 8.19 Apex-base difference in activation time.

Apex to base comparison of TActM in LV. Both apical and basal regions in VF hearts have significantly longer activation as compared to no-VF hearts. (* $P < 0.05$, *** $P < 0.001$)

QRS timing in relation to epicardial activation

One advantage of panoramic optical mapping is that it allows us to correlate total epicardial ventricular activation sequence with the recorded ECG. An example of the correlation between the activation time and the QRS complex is given in Figure 8.20. In this example, we compared the activation sequence in no-VF and VF hearts at both *Pre-occlusion 10min* and at *Occlusion 10min*. The QRS complex was arbitrarily split into 5 phases as follows: 1) phase 1 was from the beginning of the Q to the midpoint between Q and R waves, 2) phase 2 was from the end of phase 1 to the peak of R wave, 3) phase 3 began from the peak of R wave until midpoint between R and S waves, 4) phase 4 was from the end of phase 3 to the beginning of S wave, and 5) phase 5 was from the beginning of the S wave to the end of the S wave. In general, the activation time in VF heart prior to ischaemia ranged from 109 - 153ms whereas the activation time in no-VF

heart ranged from 67 - 125ms at *Pre-occlusion 10min*. At *Occlusion 10min*, the RV/LV regions tended to have earlier activation as compared to the ischaemic LV region in both groups of heart. The ischaemic sites on the LV region were activated the latest compared to other non ischaemic sites.

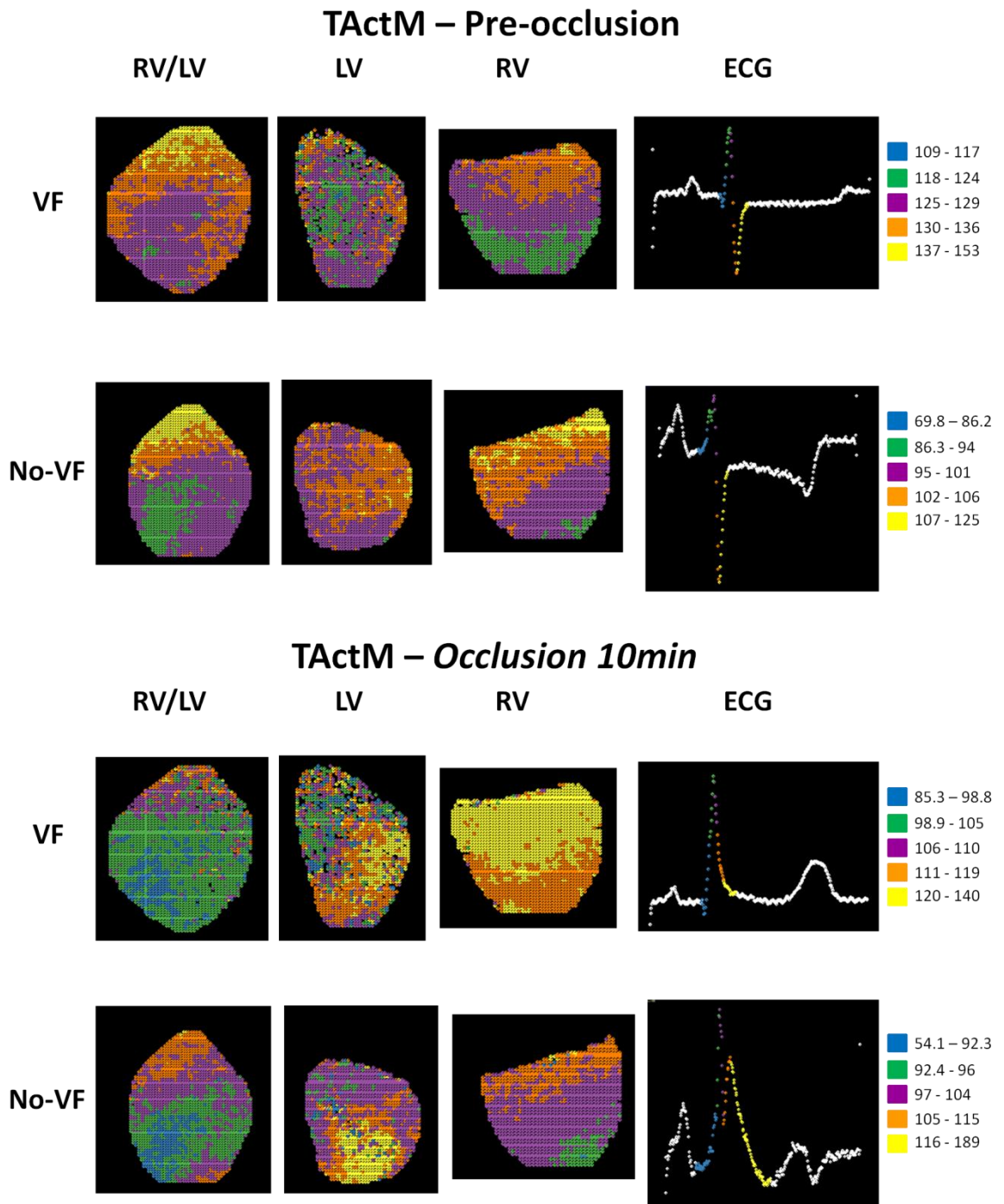


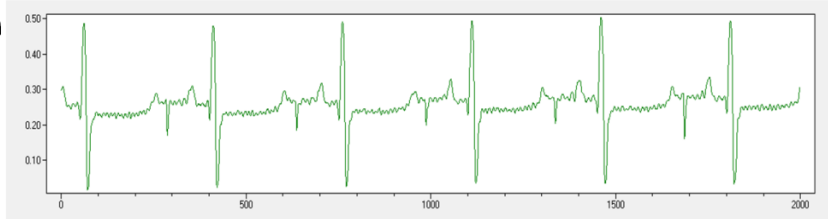
Figure 8.20 QRS timing in relation to epicardial activation.
 Example of correlation between the timing of activation matched with the QRS complex on the ECG in both no-VF and VF hearts during *Occlusion 10min*. The timing was split into 5 phases with blue indicating phase 1, green indicating phase 2, purple indicating phase 3, orange indicating phase 4 and yellow indicating the latest activation time, phase 5.

ECG

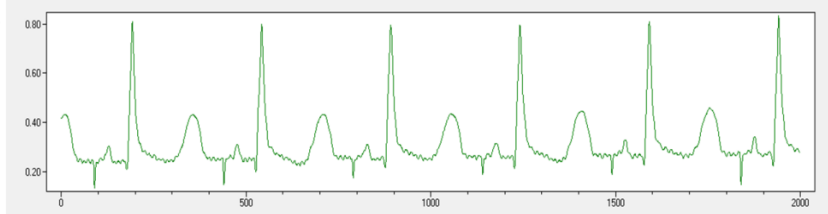
A notable observation from the previous single-view study was the alteration of the ECG shape before and during occlusion, in particular T wave polarity. In these experiments, variation in ECG in both groups of hearts was also observed. Figure 8.21 shows examples of ECG at three different time points before and during occlusion in both groups. At *Pre-occlusion 10min*, the T waves in all VF hearts had a positive polarity whereas the T waves in no-VF hearts had a negative polarity. At *Occlusion 10min*, there was broadening of the QRS complex and elevation of the ST segment observed in both groups of heart. However, I was unable to quantitatively analyze these ECG changes because it was difficult to determine the cursor placement for the ECG analysis. This limitation in analyzing the ECG has been discussed in previous chapter on ECG (see Chapter 7). As the duration of the ischaemic episodes prolonged further, the ST segment elevation became more prominent in both groups. It was difficult to distinguish changes in T wave polarity in both groups since the change in ST segment level affected the negative- and positive-going T waves differently. Therefore, it was not possible to determine whether the underlying electrical events responsible for the measured ECGs were the same in the two experiments.

VF

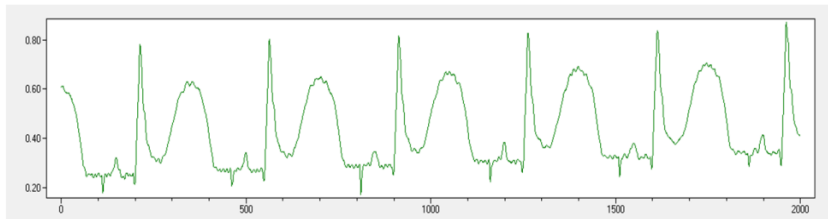
Pre-occlusion



Occlusion 10min

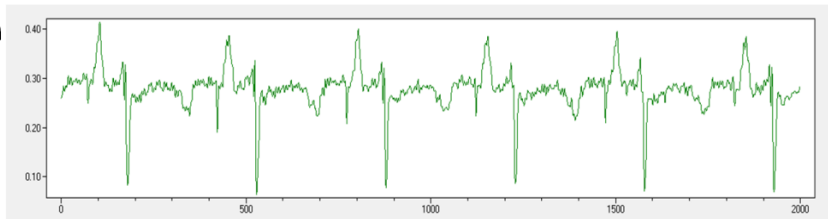


Occlusion 20min

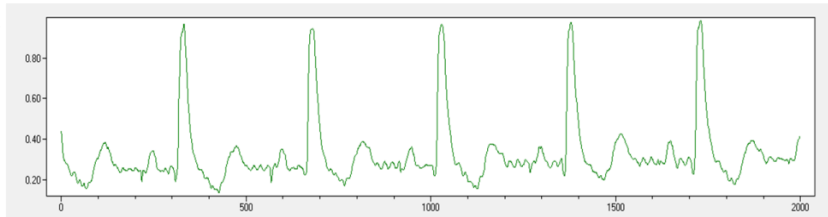


No-VF

Pre-occlusion



Occlusion 10min



Occlusion 20min

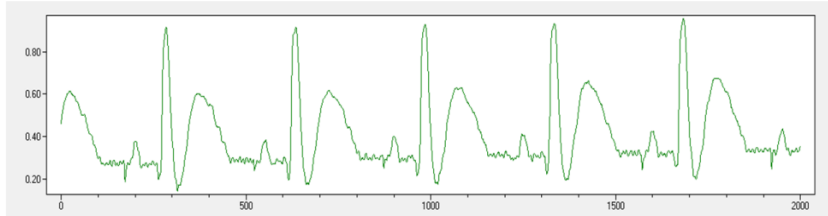


Figure 8.21 ECG from panoramic view optical mapping experiments.

Example of ECG from VF and no-VF hearts at pre-occlusion, *Occlusion 10min* and *Occlusion 20min*. In the VF heart, the T wave at pre-occlusion period had positive polarity. During *Occlusion 10min*, there was widening of the QRS complexes and slight elevation of the T wave. As the heart became more ischaemic, the ST elevation became more prominent at *Occlusion 20min*. On the other hand, the T wave in no-VF heart had negative polarity during pre-occlusion period. During occlusion, there was elevation of the ST segment together with broadening of the QRS complex. At *Occlusion 20min*, the ST elevation became more pronounced and it also dragged the T wave to a positive polarity.

Discussion

In summary, initial studies with single view optical mapping approach suggested that a shorter LV APD prior to local ischaemia predisposed the heart to VF. Current studies with the panoramic 3D view optical mapping technique confirmed this correlation and indicate that the shorter APD was confined to the apical half of the LV, and did not include basal LV or RV electrophysiology. Panoramic imaging also revealed a delayed activation time predominantly in the basal aspects of the LV. Both of these events, shorter APD in the apex and longer activation time in the base were features of hearts that developed VF on coronary artery ligation.

A number of previous papers have described differences in AP duration from different areas on the myocardium; in particular, cells from the apex of hearts are known to have shorter AP than cells isolated from the base (Bryant *et al.*, 1997; de Bakker and Opthof, 2002). This difference has been attributed to differences in expression of I_{to} or to I_K (Brahmajothi *et al.*, 1997; Bryant *et al.*, 1999; Cheng *et al.*, 1999; Szentadrassy *et al.*, 2005). Across both groups, this apex-base difference was observed. However, it is not clear why the apical region of hearts prone to VF possessed an APD that was shorter than the no-VF hearts, and therefore had an apical-basal APD gradient that was significant greater. These heart-to-heart differences in ventricular electrophysiology may arise from the natural variation in ion channel expression in these animals. In the single view experiments described previously, the area of myocardium imaged overlapped considerably with the LV apical region which demonstrated the AP shortening described here.

Although the ECG morphology changes observed using the two systems were similar in some respects, there were also clear differences that cannot be attributed to experimental conditions or optical configuration. Electrode positioning relative to the heart was similar in terms of distance and angle around the long axis, but the shape and “field of view” of the electrodes differed between the two setups. In the single camera system, the ECG electrodes were effectively two discs (diameter ~5mm); in the panoramic system, they were two metal pillars (~4mm diameter, 50mm long) which also served as structural elements for the chamber. This discrepancy limited

comparison between the two sets of ECG recordings, and in future experiments it would be beneficial to attempt to insulate the pillars in such a way as to approximate the “standard” electrode configuration of the single camera system.

Even though the incidence of VF in panoramic view optical mapping experiments is less than in earlier experiments with single view optical mapping, a Fisher’s exact probability test performed on the data revealed that they were not statistically significant. Results were expressed as the mean \pm SEM, with $P < 0.05$ considered significant.

Correlation of optical signals with phases of the ECG

Systematic analysis of the phase of the ECG relative to the optical mapping data was not performed. But what was clear from the initial measurements was that activation time followed the expected epicardial pattern, and earlier events were detected in the RV because of the thinner free wall compared to the LV. This difference in dimension means that activation will start at a similar time on the endocardium of both ventricles, and activation will appear on the epicardial surface of the thinner ventricle sooner.

Regarding the repolarisation event, there were no prominent differences in APD₅₀ under normal circumstances (Figure 8.16) across both ventricles. The unphysiologically short APD₅₀ (<50ms) values obtained may be due to analysis of inappropriate signals from tissue either damaged if at an acute angle to the illumination and camera.

Is the shorter APD in the LV apex an artefact of the experimental procedure?

One possibility is that the shorter APDs in the LV are due to the snare application at the beginning of the experiment procedure. During the snare application, damage to the coronary vessel may compromise some of the blood flow and cause the partial ischaemia before the actual occlusion procedure. However, similar analysis done using the data obtained from different study performed by another PhD student in the lab using a procedure that did not involve snare application revealed that there was still significant number of shorter sites on

the epicardial surface of the heart prior to occlusion. Furthermore, TActM times longer than 100ms were common. On the basis that the electrical activation and repolarisation times across the LV were no different from a “normal” heart, the concept that these differences were attributable to damage associated with the ligation procedure was not thought to be valid.

Physiological basis for shorter APD in LV apex

As mentioned earlier in this chapter and in Chapter 6, the electrophysiological bases for differences in APD between apical and basal regions have been studied previously. One possibility is the differential expression of ion channels (particularly I_{Ks} and I_{Kr}) across apical and basal regions (Brahmajothi *et al.*, 1997; Bryant *et al.*, 1999; Cheng *et al.*, 1999; Szentadrassy *et al.*, 2005). Further work is required to determine the underlying cause of the electrophysiological differences and why a shorter APD value in the apical region predisposes the heart to VF as discussed in Chapter 6.

Chapter 9: *In vivo* coronary artery ligation in rabbit – ECG measurements

Aim

The purpose of these experiments was to attempt a limited study to look at the tendency of the heart to develop ventricular fibrillation (VF) during *in vivo* procedure of acute coronary artery ligation and to analyse the ECG data recorded during ligation of left anterior descending artery in the rabbit.

Introduction

Acute MI is frequently used in animal models of myocardial ischaemia for both physiological and pharmacological studies (De Groot & Coronel, 2004; Man and Bril, 1991). In the rabbit, Bril *et al.* (1991) reported a cumulative incidence of VF after 20 minutes of coronary artery ligation in 27% of normal rabbit heart. Previous experiments on Langendorff-perfused rabbit hearts have indicated that, on ligation of the left anterior descending artery, approximately 50% of the preparations developed VF within 30 minutes. The data also showed that predisposition to VF in this phase was related to shortened QT interval and corresponding APD in the pre-occlusion phase. One concern about the *in vitro* data is that the artificial circumstances of the preparation may affect the physiology of the heart to the extent that the incidence of VF does not represent the situation *in vivo*. The *in vitro* preparation has several factors that could affect the physiological response to ischaemia: (1) Langendorff perfusion (retrograde) of the aorta using a crystalloid medium may not be an adequate model for a blood-perfused working heart, (2) the absence of autonomic innervations may alter the predisposition to arrhythmia, (3) the use of mechanical uncouplers may alter the arrhythmia substrate via removal of mechano-electrical feedback (Coronel, 2002) and/or side-effects on ion channels and calcium handling. Given these concerns, it seemed appropriate to attempt to reproduce the coronary artery occlusion procedure *in vivo*.

Methods

Left coronary artery ligation

In vivo surgical procedures were performed in collaboration with Mr Michael Dunne in accordance with the UK Animals (Scientific Procedures) Act 1986 and complying with the Guide for the Care and Use of Laboratory Animals published by the US National Institutes of Health (NIH Publication No. 85-23, revised 1996). A total of 12 animals were used in this *in vivo* study. Adult male New Zealand White rabbits were given premedication with 0.3ml/kg Hypnorm (fentanyl citrate 0.315mg/ml + fluanisone 10mg/ml) administered intramuscularly. Anaesthesia was induced with intravenous injection of 0.15 - 0.3 mg/kg midazolam (Hypnovel, Roche) given via a cannula in the marginal ear vein. The rabbit was then intubated and ventilated with a small animal positive pressure ventilator set to a frequency of 38 per minute and at 50ml stroke volume. The rabbit anaesthesia was maintained on 1% halothane with a 1:1 mixture of oxygen and nitrous oxide. A left thoracotomy through the 4th intercostal space was performed. The proximal branch of the left coronary artery was identified and ligated using a 4/0 Ethibond® suture. The heart was left for 20 minutes. If the heart went into VF, a gentle prod was given together with a cardiac massage to restore sinus rhythm. If this did not work, defibrillation was attempted with a 5-10J epicardial DC shock. Normally, an intravenous injection of quinidine hydrochloride solution 10mg/ml was administered before the coronary artery ligation as a measure to reduce the incidence of VF. However, all the ligation procedures for this study were done without the administration of quinidine because we wanted to mimic the *in vitro* conditions used previously. Once the animal was stable, the thoracotomy was closed. The rabbit was then intravenously infused with 20ml of isotonic saline to replace the perioperative fluid losses. Intramuscular injection of 0.05mg/kg Vetergesic (buprenorphine) was given immediately post surgery for post-operative analgesia. The animal was then extubated and placed in a heated recovery box. Rimadyl (4mg/kg) was administered subcutaneous for 2 days post-op to provide pain relief. These animals were used 8 weeks later in a separate study.

ECG monitoring and recording

Figure 9.1 shows a sample of an ECG signal recorded throughout the ligation surgery to monitor for incidence of VF. The ECG data obtained in this study were compared with the ECG from the *in vitro* acute coronary artery ligation experiments. Needle electrodes (Grass) were placed just under the skin in a lead II configuration. A clearly recognizable ECG was occasionally not evident, in which case a lead I or III was used instead. The area used for the placement of ECG electrodes was shaved and cleaned using 70% ethanol with chlorhexidine and the electrodes were taped in place. The ECG was recorded by a Biopac system (Biopac Systems Inc., CA) using their Acq software. The recordings were started after the animal had been anaesthetised and positioned for surgery so that the movement of the animal was kept to a minimum.

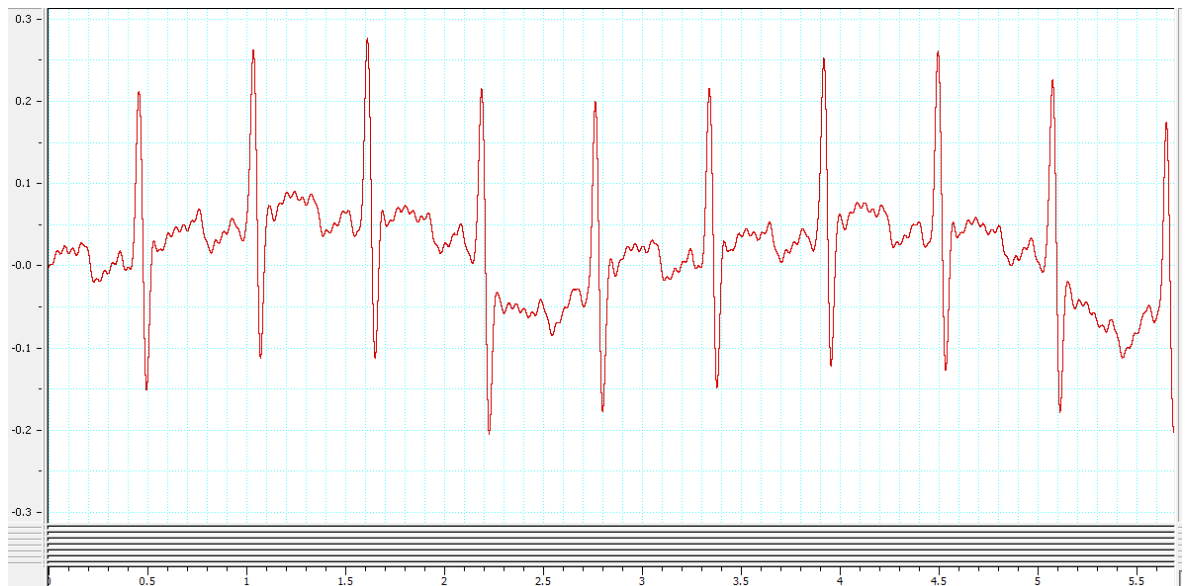


Figure 9.1 *In vivo* ECG data.

Example of ECG tracings from one of the *in vivo* coronary artery ligation experiments. This ECG was taken before ligation.

ECG analysis

The ECG recorded during the *in vivo* ligation procedure was analysed using semi-automated software, ChartTM 5 Pro (ADInstruments Ltd, UK) (see Chapter 2). The software assigns the cursor to certain points on each of the ECG beat prior to calculating the value for the ECG parameters mentioned above. The landmarks for the cursors are P start, P peak, QRS start, QRS end, T peak and T end (Figure 9.2a). However, when the quality of the ECG recordings (Figure 9.2b) was poor, the software was unable reliably to identify these features. As evident in Figure 9.1, the ECG signals were noisy and the P and T waves could not be differentiated from the baseline. The cursors could then be manually adjusted to appropriate landmarks (obviously a subjective procedure). An example of manual analysis is given (Figure 9.3). For every recording, 5 beats were analysed and the mean was taken as the value for each parameters.

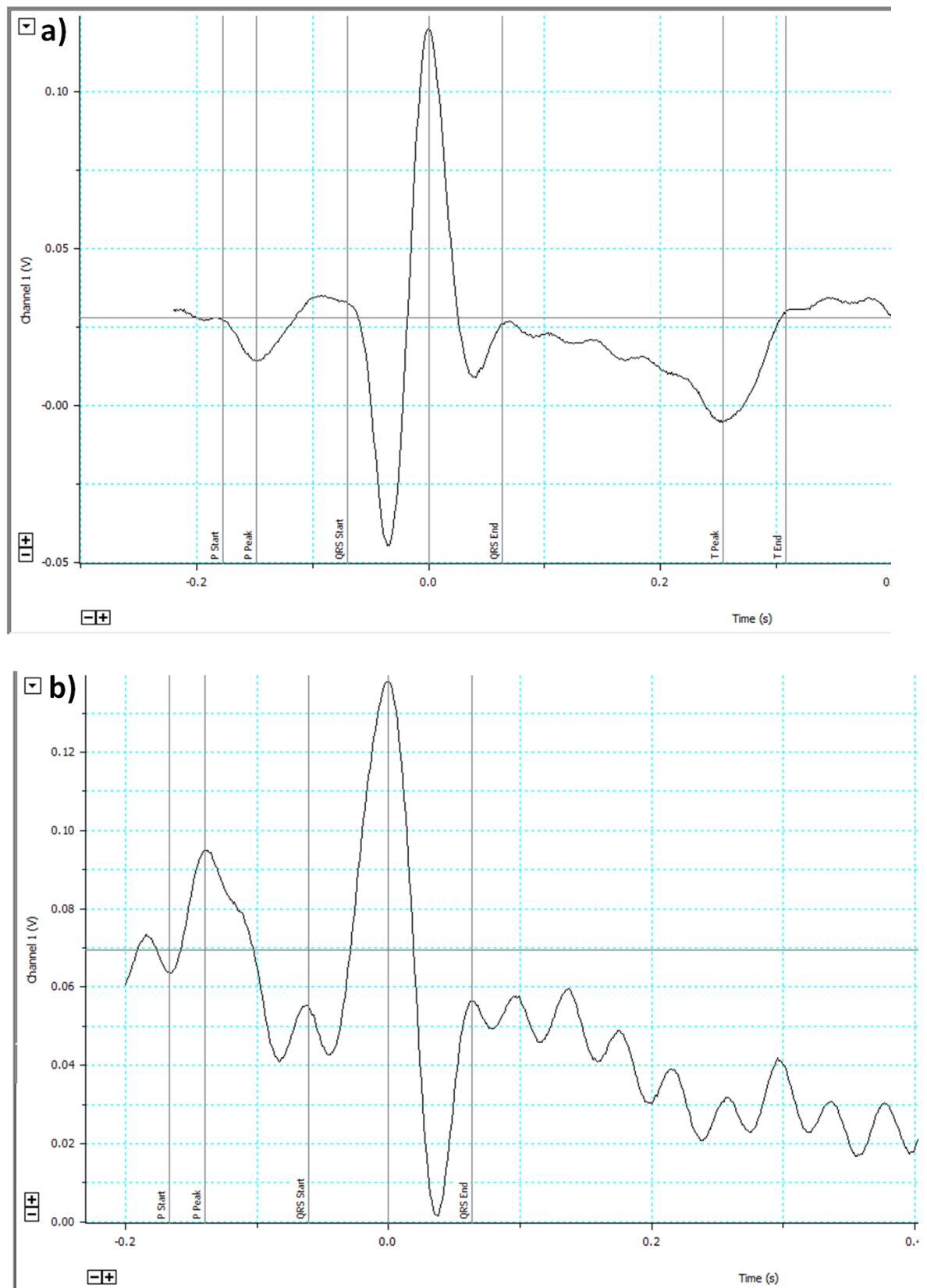
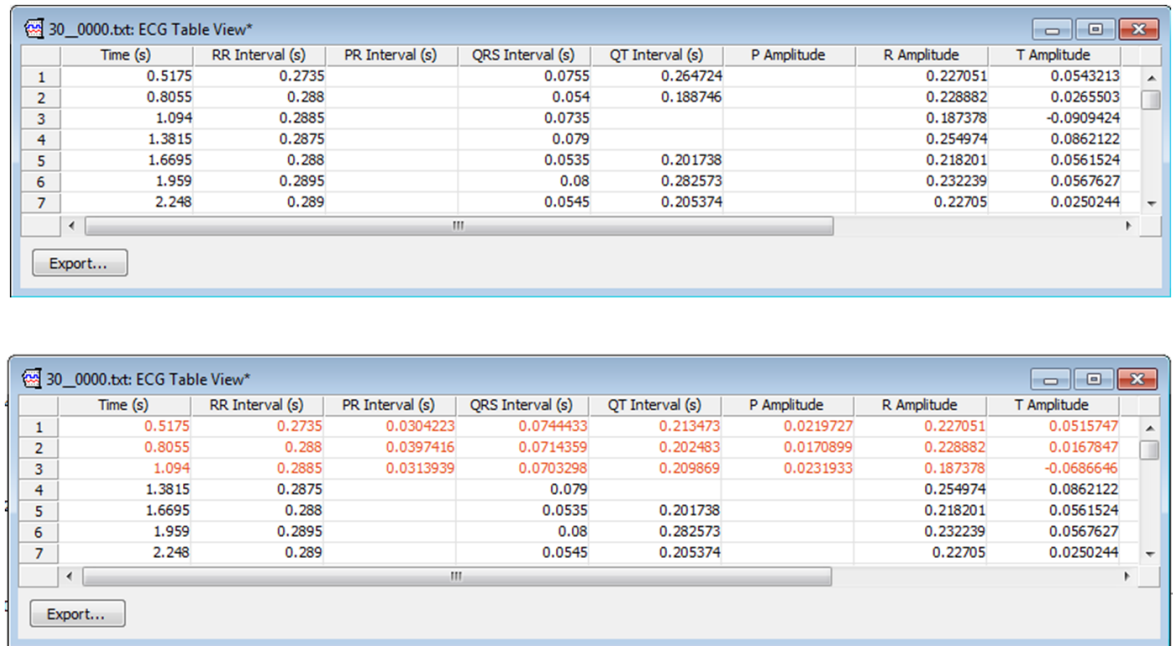


Figure 9.2 ECG analysis using ChartTM 5 Pro software.

Example of one beat from ECG tracing recorded during the ligation procedure. a) Completed set of cursor placements for calculation of ECG parameters. b) Some cursors are missing due to failure of the software to recognise ECG features.



Top Panel: Initial Analysis

	Time (s)	RR Interval (s)	PR Interval (s)	QRS Interval (s)	QT Interval (s)	P Amplitude	R Amplitude	T Amplitude
1	0.5175	0.2735		0.0755	0.264724		0.227051	0.0543213
2	0.8055	0.288		0.054	0.188746		0.228882	0.0265503
3	1.094	0.2885		0.0735			0.187378	-0.0909424
4	1.3815	0.2875		0.079			0.254974	0.0862122
5	1.6695	0.288		0.0535	0.201738		0.218201	0.0561524
6	1.959	0.2895		0.08	0.282573		0.232239	0.0567627
7	2.248	0.289		0.0545	0.205374		0.22705	0.0250244

Bottom Panel: After Manual Adjustments

	Time (s)	RR Interval (s)	PR Interval (s)	QRS Interval (s)	QT Interval (s)	P Amplitude	R Amplitude	T Amplitude
1	0.5175	0.2735	0.0304223	0.0744433	0.213473	0.0219727	0.227051	0.0515747
2	0.8055	0.288	0.0397416	0.0714359	0.202483	0.0170899	0.228882	0.0167847
3	1.094	0.2885	0.0313939	0.0703298	0.209869	0.0231933	0.187378	-0.0686646
4	1.3815	0.2875		0.079			0.254974	0.0862122
5	1.6695	0.288		0.0535	0.201738		0.218201	0.0561524
6	1.959	0.2895		0.08	0.282573		0.232239	0.0567627
7	2.248	0.289		0.0545	0.205374		0.22705	0.0250244

Figure 9.3 ECG parameters.

Top panel: Some parameter values such as PR and QT intervals were missing from initial analysis because the software failed to find sensible landmarks for correct placement of the cursors. **Bottom panel:** After manually adjusting the cursors, the values were recalculated and indicated in red font.

Statistical analysis

All data obtained in this study are expressed as mean \pm standard error of the mean (SEM). Significance testing was done using GraphPad Prism software. Comparison between groups of data was made with Student's t-test (paired when appropriate). A two-tailed p-value of less than 0.05 was considered significant. Multiple comparisons were performed using one-way ANOVA followed by Tukey-Kramer post test to allow multiple comparisons where appropriate.

Results

In this study, 12 healthy adult male New Zealand White rabbits weighing between 2.5 - 3.5kg were used. During the ligation surgery, 7 rabbits developed VF within 20 minutes of the LAD artery ligation and 5 did not. Table 9.1 displays an example of beat to beat variation in the ECG parameters in one experiment. The mean value for each parameter was calculated from 5 consecutive beats.

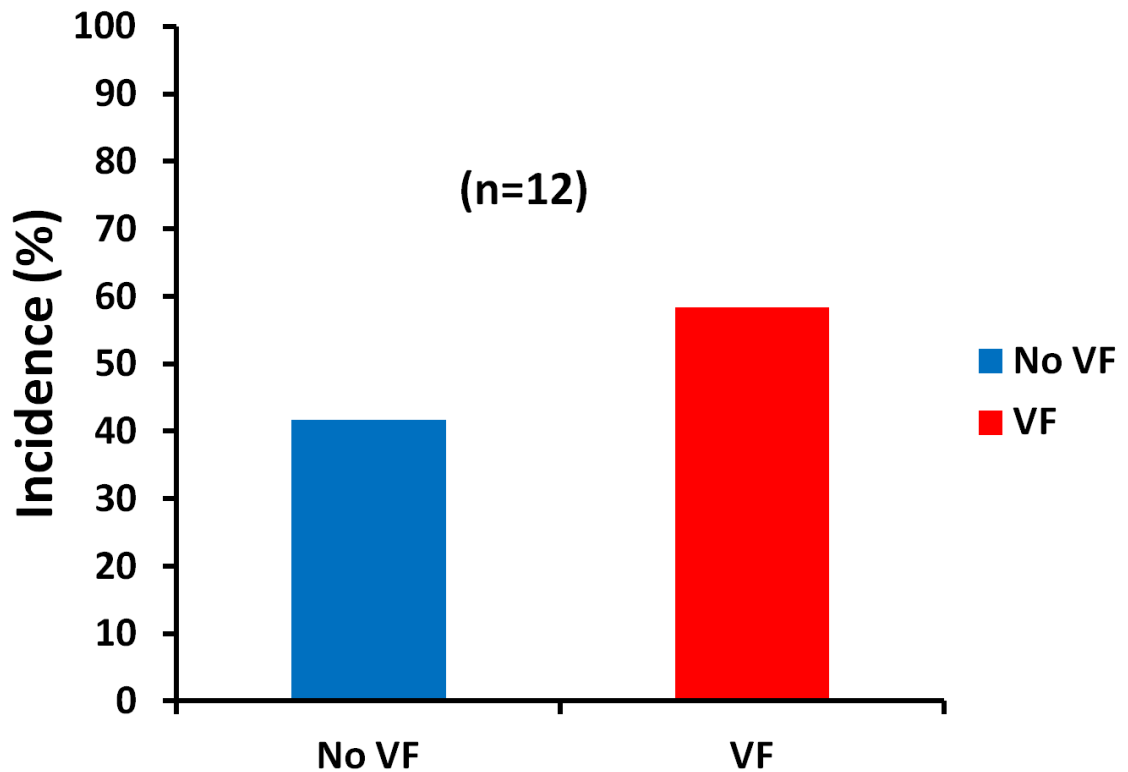


Figure 9.4 Incidence of no-VF and VF in *in vivo* study.

Bar graph displaying the percentage of hearts that developed and not developed VF during the *in vivo* procedure of coronary artery ligation. No-VF (n=5) and VF (n=7).

The heart rate in rabbits in the VF group before the coronary artery ligation varied from 142 to 257bpm with a mean of 203 ± 14 bpm. In no-VF group, the heart rate ranged from 194 to 252bpm with a mean of 215 ± 10 bpm. This difference in heart rates was not significant. The mean durations of RR, PR, QRS and QT intervals before the LAD artery ligation are presented in Table 9.2. It compares the results from the hearts that went into VF within 30 minutes of the coronary artery ligation and the hearts that did not develop VF. As shown in the table, although there appeared to be a trend towards the VF group having a shorter QT there was no statistically or physiologically significant difference between the two groups ($P=0.643$).

Table 9.1 Beat to beat variation in ECG parameters.

Example of individual value for different ECG parameters from 5 consecutive beats in one experiment.

Beat	RR Interval (s)	PR Interval (s)	QRS Interval (s)	QT Interval (s)
1	0.260	0.036	0.077	0.170
2	0.258	0.036	0.076	0.167
3	0.262	0.037	0.077	0.170
4	0.261	0.035	0.078	0.169
5	0.264	0.034	0.078	0.167
Mean	0.261	0.036	0.077	0.168
SEM	0.001	0.001	0.000	0.001

Table 9.2 ECG parameters (no-VF vs. VF groups).

Comparison of duration of different pre-ligation ECG parameters in rabbits between the hearts that developed VF and the hearts that did not develop VF (Mean \pm SEM).

	RR interval (s)	PR interval (s)	QRS interval (s)	QT interval (s)
No-VF	0.281 \pm 0.013	0.054 \pm 0.003	0.065 \pm 0.001	0.173 \pm 0.012
VF	0.306 \pm 0.024	0.049 \pm 0.006	0.070 \pm 0.002	0.167 \pm 0.005
P value	0.439	0.523	0.110	0.643

The relation between the rate and repolarisation, represented by RR and QT interval respectively, was examined. Figure 9.5 shows values of uncorrected QT plotted against the RR interval for both groups. Because there was no obvious relationship, the use of a correction factor was considered unnecessary.

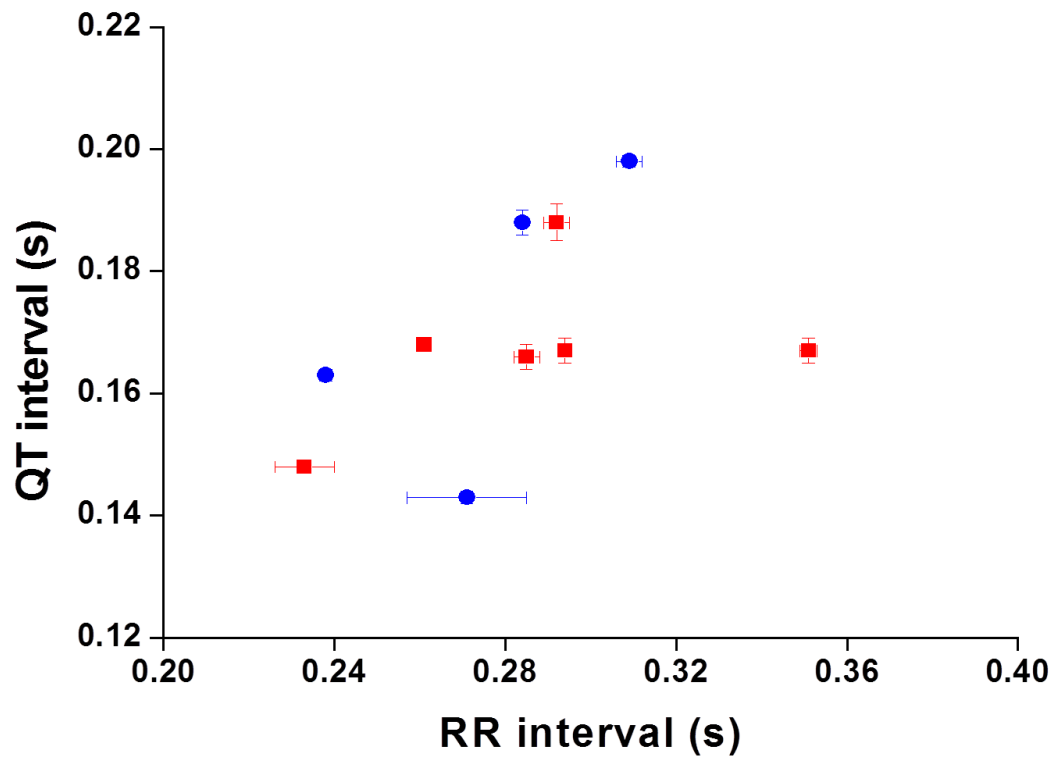


Figure 9.5 Graph showing the relation between RR interval and QT interval.

Discussion

Experimentally *in vivo* or *in vitro*, the coronary artery can be ligated to simulate an occlusion creating an ischaemic field. In this *in vivo* experiment, the incidence of VF was 58%. This was a higher proportion than a previous report (Bril *et al.*, 1991) using a similar procedure *in vivo*. One obvious factor that can account for this difference is the position of the ligature on the left descending artery and hence the size of the consequent ischaemic area. Of relevance here is that approximate 50% incidence *in vivo* is similar to that seen in the *in vitro* experiments, suggesting that the data gained *in vitro* does not misrepresent the vulnerability of the myocardium to arrhythmias *in vivo*. However, analysis of the ECG data did not reveal a correlation between incidence of VF and QT interval as was observed *in vitro*. The reasons for this are unclear, but one significant factor was the inter-subject variability of heart rate and ECG parameters. The variability of the latter is likely to be at least partly due to the lower signal-to-noise of the ECG recordings. Future studies should involve improvement of this aspect of the measurements. Another reason is likely due to the small number of sample size for this study. To determine the sample size required to get a significant difference in the QT interval between the two groups, it can be calculated based on the formula:

$$n = \left(\frac{(Z_{\alpha/2}) * \sigma}{E} \right)^2$$

$$n = \left(\frac{1.96 * 30}{12} \right)^2$$

$$n = 24$$

In this formula, the sample size (n) is calculated based on $Z_{\alpha/2}$, the 95% confidence coefficient which is equal to 1.96, sigma (σ) which is the standard deviation, and E which is the margin of error. The values for σ and E for this calculation were obtained from the QT interval data in the *in vitro* experiments

(see Chapter 5). From the calculation, it shows that the sample size need to be increased to at least $n = 24$ in order to detect a significant difference between the two groups when the underlying population difference approximates to the difference observed *in vitro* (12ms). This would suggest that a considerably higher number of procedures would be required. The group is currently acquiring this extra data to ensure sufficient resolution.

Chapter 10: Discussion

General discussion

Optical mapping studies have previously used single wavelength measurements to monitor cardiac electrophysiology. In the initial part of these studies, I attempted to upgrade this approach by investigating the use of dual-wavelength ratiometric measurement techniques applied to electrical mapping of isolated rabbit hearts. In theory, this approach offers important advantages over the single wavelength technique: (i) measurement of action potential amplitude in absolute units of mV and (ii) elimination (or at least reduction) of artefacts that arise from movement of the myocardium. However, despite optimising the wavelengths for ratiometric measurements and demonstrating the potential for measuring AP amplitude, several sources of artefact remained that could not be easily addressed without improvements in illumination techniques and camera alignment. Therefore the experimental sections of the thesis used conventional single wavelength approach.

The main finding in this study is that predisposition to VF during acute regional ischaemia following coronary artery occlusion was a function of the electrophysiology of the ventricle prior to occlusion. Approximately 50% of hearts with shorter than average QT intervals arising from shorter LV action potential duration values, particularly in the apical region of the LV free wall, were more prone to VF. Artificially prolonging ventricular action potential duration with a hERG channel blocker (E-4031) did not protect these hearts from VF post-occlusion. Potential confounding factors such as prior increased sympathetic activity did not alter the relative tendency to VF post occlusion. The conclusion from these studies was that the predisposition to VF post-occlusion was not a direct consequence of shorter than averaged QT interval but the strong association suggests that other underlying differences in electrophysiology are important determinants of predisposition to VF. Attempts to verify these observations *in vivo* failed because of the high variability of QT interval but a similar (approximately 50:50) ratio of VF/no-VF population was present.

As part of the preliminary studies, I investigated the effect of hERG channel inhibition on rabbit ventricular myocardium. Despite the well known role of this channel (I_{Kr}) in the repolarisation phase of the action potential, few studies on

rabbit myocardium exist. The drug produced a clear dose-dependent increase in action potential duration similar to a number of other species, at slower than physiological rates. Early after-depolarisations were present, again as seen in other species including man. There were also examples of spontaneous ventricular tachycardia at the higher E4031 concentrations, but no examples of spontaneous VF (in the form of Torsade de Pointes) which is a common occurrence in man and some larger experimental animals. This work suggested that, in rabbit, I_{Kr} is present in myocardium, but contributes only to a small extent to the action potential duration at normal physiological heart rates in rabbit. This difference and the monomorphic tachycardia observed after profound I_{Kr} block suggests that rabbit ventricular myocardium may not be ideal for screening for potentially lethal drugs that act via I_{Kr} block since these responses differ significantly from human myocardium.

Clinical studies on victims of sudden cardiac death following acute coronary events and survivors of such events have shown that patients with a higher prevalence of electrocardiographic early repolarisation are more susceptible to sudden cardiac death during acute myocardial ischaemia (Tikkanen *et al.*, 2012). In another study (Haissaguerre *et al.*, 2009), early repolarisation has been associated with a variant of the mutation of the K_{ATP} channel subunit. One of the predictors of VF in patients having myocardial infarction is an early repolarisation pattern and this early repolarisation has been linked to mutation in K_{ATP} channel. These clinical findings are interesting in relation to my current work.

Future work

- 1) Examine the molecular basis for the distribution of QT interval in the rabbit. This would address the hypothesis that the shorter action potential duration in the apical region of the LV is due to a change in ion channel expression that may underlie the predisposition to VF. For example, if the shorter QT is due to expression of I_{KATP} channels with a lower than normal sensitivity to ATP, this may explain the linkage between pre-occlusion electrophysiology and predisposition to VF.
- 2) Increase the size of the *in vivo* study to at least $n=24$ to determine whether occlusion of the coronary artery results in a similar 50:50 distribution between no-VF and VF groups.
- 3) In a wider context and beyond the realm of experimental study, information on how early repolarisation relates to VF incidence would be gained by clinical/epidemiological studies examining the link between early repolarisation and K_{ATP} channelopathy.

References

Cardiovascular disease statistics. British Heart Foundation . 4-12-2013a.

Ref Type: Online Source

Coronary heart disease. British Heart Foundation . 4-12-2013b.

Ref Type: Online Source

Agarwal, A., Jing, L., & Patwardhan, A. 2012. Effect of rapid delayed rectifier current on hysteresis in restitution of action potential duration in swine. *Conf.Proc.IEEE Eng Med Biol.Soc.*, 2012, 673-676.

Akar, F.G., Roth, B.J., & Rosenbaum, D.S. 2001. Optical measurement of cell-to-cell coupling in intact heart using subthreshold electrical stimulation. *Am.J Physiol Heart Circ.Physiol*, 281, (2) H533-H542.

Allingham, J.S., Smith, R., & Rayment, I. 2005. The structural basis of blebbistatin inhibition and specificity for myosin II. *Nat Struct.Mol.Biol.*, 12, (4) 378-379.

Anderson, C.L., Delisle, B.P., Anson, B.D., Kilby, J.A., Will, M.L., Tester, D.J., Gong, Q., Zhou, Z., Ackerman, M.J., & January, C.T. 2006. Most LQT2 mutations reduce Kv11.1 (hERG) current by a class 2 (trafficking-deficient) mechanism. *Circulation*, 113, (3) 365-373.

Antzelevitch, C., Pollevick, G.D., Cordeiro, J.M., Casis, O., Sanguinetti, M.C., Aizawa, Y., Guerchicoff, A., Pfeiffer, R., Oliva, A., Wollnik, B., Gelber, P., Bonaros, E.P., Jr., Burashnikov, E., Wu, Y., Sargent, J.D., Schickel, S., Oberheiden, R., Bhatia, A., Hsu, L.F., Haissaguerre, M., Schimpf, R., Borggrefe, M., & Wolpert, C. 2007. Loss-of-function mutations in the cardiac calcium channel underlie a new clinical entity characterized by ST-segment elevation, short QT intervals, and sudden cardiac death. *Circulation*, 115, (4) 442-449.

Armoundas, A.A., Nanke, T., & Cohen, R.J. 2000. Images in cardiovascular medicine. T-wave alternans preceding torsade de pointes ventricular tachycardia. *Circulation*, 101, (21) 2550.

Ataklte, F., Erqou, S., Laukkanen, J., & Kaptoge, S. 2013. Meta-analysis of ventricular premature complexes and their relation to cardiac mortality in general populations. *Am.J Cardiol.*, 112, (8) 1263-1270.

Avitall, B. 1979. Computer simulation of ventricular tachyarrhythmias during coronary artery ligation and release. *J Electrocardiol.*, 12, (1) 17-22.

Bayes de Luna, L.A., Coumel, P., & Leclercq, J.F. 1989. Ambulatory sudden cardiac death: mechanisms of production of fatal arrhythmia on the basis of data from 157 cases. *Am.Heart J*, 117, (1) 151-159.

Beach, J.M., McGahren, E.D., Xia, J., & Duling, B.R. 1996. Ratiometric measurement of endothelial depolarization in arterioles with a potential-sensitive dye. *Am.J Physiol*, 270, (6 Pt 2) H2216-H2227.

- Behrens, S., Li, C., & Franz, M.R. 1997. Effects of myocardial ischemia on ventricular fibrillation inducibility and defibrillation efficacy. *J Am.Coll.Cardiol.*, 29, (4) 817-824.
- Belloq, C., van Ginneken, A.C., Bezzina, C.R., Alders, M., Escande, D., Mannens, M.M., Baro, I., & Wilde, A.A. 2004. Mutation in the KCNQ1 gene leading to the short QT-interval syndrome. *Circulation*, 109, (20) 2394-2397.
- Bernier, M., Curtis, M.J., & Hearse, D.J. 1989. Ischemia-induced and reperfusion-induced arrhythmias: importance of heart rate. *Am.J Physiol*, 256, (1 Pt 2) H21-H31.
- Bigger, J.T., Jr., Dresdale, F.J., Heissenbuttel, R.H., Weld, F.M., & Wit, A.L. 1977. Ventricular arrhythmias in ischemic heart disease: mechanism, prevalence, significance, and management. *Prog.Cardiovasc Dis.*, 19, (4) 255-300.
- Bijl, M. & Verheugt, F.W. 1992. Extreme QT prolongation solely due to reversible myocardial ischemia in single-vessel coronary disease. *Am.Heart J*, 123, (2) 524-526.
- Billman, G.E. 1994. Role of ATP sensitive potassium channel in extracellular potassium accumulation and cardiac arrhythmias during myocardial ischaemia. *Cardiovasc Res*, 28, (6) 762-769.
- Bjerregaard, P., Jahangir, A., & Gussak, I. 2006. Targeted therapy for short QT syndrome. *Expert.Opin.Ther.Targets.*, 10, (3) 393-400.
- Boineau, J.P. & Cox, J.L. 1973. Slow ventricular activation in acute myocardial infarction. A source of re-entrant premature ventricular contractions. *Circulation*, 48, (4) 702-713.
- Botting, J.H., Curtis, M.J., & Walker, M.J. 1985. Arrhythmias associated with myocardial ischaemia and infarction. *Mol.Aspects Med*, 8, (4) 307-422.
- Bourgeois, E.B., Reeves, H.D., Walcott, G.P., & Rogers, J.M. 2012. Panoramic optical mapping shows wavebreak at a consistent anatomical site at the onset of ventricular fibrillation. *Cardiovasc Res*, 93, (2) 272-279.
- Brack, K.E., Coote, J.H., & Ng, G.A. 2010. Vagus nerve stimulation inhibits the increase in Ca²⁺ transient and left ventricular force caused by sympathetic nerve stimulation but has no direct effects alone--epicardial Ca²⁺ fluorescence studies using fura-2 AM in the isolated innervated beating rabbit heart. *Exp.Physiol*, 95, (1) 80-92.
- Brahmajothi, M.V., Morales, M.J., Reimer, K.A., & Strauss, H.C. 1997. Regional localization of ERG, the channel protein responsible for the rapid component of the delayed rectifier, K⁺ current in the ferret heart. *Circ.Res*, 81, (1) 128-135.
- Bricknell, O.L. & Opie, L.H. 1978. Effects of substrates on tissue metabolic changes in the isolated rat heart during underperfusion and on release of lactate dehydrogenase and arrhythmias during reperfusion. *Circ.Res*, 43, (1) 102-115.

- Bril, A., Forest, M.C., & Gout, B. 1991. Ischemia and reperfusion-induced arrhythmias in rabbits with chronic heart failure. *Am.J Physiol*, 261, (2 Pt 2) H301-H307.
- Brown, B.G., Lin, J.T., Kelsey, S., Passamani, E.R., Levy, R.I., Dodge, H.T., & Detre, K.M. 1989. Progression of coronary atherosclerosis in patients with probable familial hypercholesterolemia. Quantitative arteriographic assessment of patients in NHLBI type II study. *Arteriosclerosis*, 9, (1 Suppl) I81-I90.
- Brugada, R., Hong, K., Dumaine, R., Cordeiro, J., Gaita, F., Borggrefe, M., Menendez, T.M., Brugada, J., Pollevick, G.D., Wolpert, C., Burashnikov, E., Matsuo, K., Wu, Y.S., Guerchicoff, A., Bianchi, F., Giustetto, C., Schimpf, R., Brugada, P., & Antzelevitch, C. 2004. Sudden death associated with short-QT syndrome linked to mutations in HERG. *Circulation*, 109, (1) 30-35.
- Brunner, M., Peng, X., Liu, G.X., Ren, X.Q., Ziv, O., Choi, B.R., Mathur, R., Hajjiri, M., Odening, K.E., Steinberg, E., Folco, E.J., Pringa, E., Centracchio, J., Macharzina, R.R., Donahay, T., Schofield, L., Rana, N., Kirk, M., Mitchell, G.F., Poppas, A., Zehender, M., & Koren, G. 2008. Mechanisms of cardiac arrhythmias and sudden death in transgenic rabbits with long QT syndrome. *J Clin Invest*, 118, (6) 2246-2259.
- Bryant, S.M., Shipsey, S.J., & Hart, G. 1997. Regional differences in electrical and mechanical properties of myocytes from guinea-pig hearts with mild left ventricular hypertrophy. *Cardiovasc Res*, 35, (2) 315-323.
- Bryant, S.M., Shipsey, S.J., & Hart, G. 1999. Normal regional distribution of membrane current density in rat left ventricle is altered in catecholamine-induced hypertrophy. *Cardiovasc Res*, 42, (2) 391-401.
- Bullen, A., Patel, S.S., & Saggau, P. 1997. High-speed, random-access fluorescence microscopy: I. High-resolution optical recording with voltage-sensitive dyes and ion indicators. *Biophys.J*, 73, (1) 477-491.
- Burton, F.L. & Cobbe, S.M. 2001. Dispersion of ventricular repolarization and refractory period. *Cardiovasc Res*, 50, (1) 10-23.
- Cantillon, D.J. 2013. Evaluation and management of premature ventricular complexes. *Cleve.Clin J Med*, 80, (6) 377-387.
- Carlsson, L., Amos, G.J., Andersson, B., Drews, L., Duker, G., & Wadstedt, G. 1997. Electrophysiological characterization of the prokinetic agents cisapride and mosapride in vivo and in vitro: implications for proarrhythmic potential? *J Pharmacol.Exp.Ther.*, 282, (1) 220-227.
- Carmeliet, E. 1985. Electrophysiologic and voltage clamp analysis of the effects of sotalol on isolated cardiac muscle and Purkinje fibers. *J Pharmacol.Exp.Ther.*, 232, (3) 817-825.
- Carmeliet, E. 1999. Cardiac ionic currents and acute ischemia: from channels to arrhythmias. *Physiol Rev.*, 79, (3) 917-1017.

Carmeliet, E. & Vereecke, J. 2002, "Ionic Currents and Action Potentials," *In Cardiac Cellular Electrophysiology*, Dordrecht: Kluwer Academic Publishers, pp. 95-177.

Cheng, J., Kamiya, K., Liu, W., Tsuji, Y., Toyama, J., & Kodama, I. 1999. Heterogeneous distribution of the two components of delayed rectifier K⁺ current: a potential mechanism of the proarrhythmic effects of methanesulfonanilideclass III agents. *Cardiovasc Res*, 43, (1) 135-147.

Chou, C.C., Zhou, S., Hayashi, H., Nihei, M., Liu, Y.B., Wen, M.S., Yeh, S.J., Fishbein, M.C., Weiss, J.N., Lin, S.F., Wu, D., & Chen, P.S. 2007. Remodelling of action potential and intracellular calcium cycling dynamics during subacute myocardial infarction promotes ventricular arrhythmias in Langendorff-perfused rabbit hearts. *J Physiol*, 580, (Pt.3) 895-906.

Coromilas, J., Costeas, C., Deruyter, B., Dillon, S.M., Peters, N.S., & Wit, A.L. 2002. Effects of pinacidil on electrophysiological properties of epicardial border zone of healing canine infarcts: possible effects of K(ATP) channel activation. *Circulation*, 105, (19) 2309-2317.

Coronel, R. 2002. Repolarization abnormalities in heart failure. *Cardiovasc Res*, 54, (1) 11-12.

Curtis, M.J. 1998. Characterisation, utilisation and clinical relevance of isolated perfused heart models of ischaemia-induced ventricular fibrillation. *Cardiovasc Res*, 39, (1) 194-215.

Curtis, M.J. & Hearse, D.J. 1989. Ischaemia-induced and reperfusion-induced arrhythmias differ in their sensitivity to potassium: implications for mechanisms of initiation and maintenance of ventricular fibrillation. *J Mol.Cell Cardiol.*, 21, (1) 21-40.

Czarnecka, M., Lewartowski, B., & Prokopczuk, A. 1973. Intracellular recording from the in situ working dog heart in physiological conditions and during acute ischemia and fibrillation. *Acta Physiol Pol.*, 24, (2) 331-337.

D'Alonzo, A.J., Darbenzio, R.B., Hess, T.A., Sewter, J.C., Sleph, P.G., & Grover, G.J. 1994. Effect of potassium on the action of the KATP modulators cromakalim, pinacidil, or glibenclamide on arrhythmias in isolated perfused rat heart subjected to regional ischaemia. *Cardiovasc Res*, 28, (6) 881-887.

de Bakker, J.M. & Opthof, T. 2002. Is the apico-basal gradient larger than the transmural gradient? *J Cardiovasc Pharmacol.*, 39, (3) 328-331.

De Groot, J.R. & Coronel, R. 2004. Acute ischemia-induced gap junctional uncoupling and arrhythmogenesis. *Cardiovasc Res*, 62, (2) 323-334.

De, A.L. & Corlan, A.D. 2007. Clinical use of body surface potential mapping in cardiac arrhythmias. *Anadolu.Kardiyol.Derg.*, 7 Suppl 1, 8-10.

Dekker, L.R., Bezzina, C.R., Henriques, J.P., Tanck, M.W., Koch, K.T., Alings, M.W., Arnold, A.E., de Boer, M.J., Gorgels, A.P., Michels, H.R., Verkerk, A., Verheugt, F.W., Zijlstra, F., & Wilde, A.A. 2006. Familial sudden death is an

important risk factor for primary ventricular fibrillation: a case-control study in acute myocardial infarction patients. *Circulation*, 114, (11) 1140-1145.

Dixit, S. & Callans, D.J. 2002. Mapping for ventricular tachycardia. *Card Electrophysiol.Rev.*, 6, (4) 436-441.

Doroghazi, R.M. & Childers, R. 1978. Time-related changes in the Q-T interval in acute myocardial infarction: possible relation to local hypocalcemia. *Am.J Cardiol.*, 41, (4) 684-688.

Downar, E., Janse, M.J., & Durrer, D. 1977. The effect of acute coronary artery occlusion on subepicardial transmembrane potentials in the intact porcine heart. *Circulation*, 56, (2) 217-224.

Drouin, E., Charpentier, F., Gauthier, C., Laurent, K., & Le, M.H. 1995. Electrophysiologic characteristics of cells spanning the left ventricular wall of human heart: evidence for presence of M cells. *J Am.Coll.Cardiol.*, 26, (1) 185-192.

Durrer, D., van Dam, R.T., Freud, G.E., Janse, M.J., Meijler, F.L., & Arzbaecher, R.C. 1970. Total excitation of the isolated human heart. *Circulation*, 41, (6) 899-912.

Efimov, I.R., Nikolski, V.P., & Salama, G. 2004. Optical imaging of the heart. *Circ.Res*, 95, (1) 21-33.

Eldar, M., Sievner, Z., Goldbourt, U., Reicher-Reiss, H., Kaplinsky, E., & Behar, S. 1992. Primary ventricular tachycardia in acute myocardial infarction: clinical characteristics and mortality. The SPRINT Study Group. *Ann.Intern.Med*, 117, (1) 31-36.

Elharrar, V. & Surawicz, B. 1983. Cycle length effect on restitution of action potential duration in dog cardiac fibers. *Am.J Physiol*, 244, (6) H782-H792.

Elliott, A.C., Smith, G.L., Eisner, D.A., & Allen, D.G. 1992. Metabolic changes during ischaemia and their role in contractile failure in isolated ferret hearts. *J Physiol*, 454, 467-490.

Engblom, H., Hedstrom, E., Heiberg, E., Wagner, G.S., Pahlm, O., & Arheden, H. 2005. Size and transmural extent of first-time reperfused myocardial infarction assessed by cardiac magnetic resonance can be estimated by 12-lead electrocardiogram. *Am.Heart J*, 150, (5) 920.

Engels, W., Reijters, P.H., Daemen, M.J., Smits, J.F., & van der Vusse, G.J. 1995. Transmural changes in mast cell density in rat heart after infarct induction in vivo. *J Pathol.*, 177, (4) 423-429.

Estes, E.H., Jr., Entman, M.L., Dixon, H.B., & Hackel, D.B. 1966. The vascular supply of the left ventricular wall. Anatomic observations, plus a hypothesis regarding acute events in coronary artery disease. *Am.Heart J*, 71, (1) 58-67.

Ettinger, P.O., Regan, T.J., Oldewurtel, H.A., & Khan, M.I. 1973. Ventricular conduction delay and arrhythmias during regional hyperkalemia in the dog. Electrical and myocardial ion alterations. *Circ.Res*, 33, (5) 521-531.

- Extramiana, F. & Antzelevitch, C. 2004. Amplified transmural dispersion of repolarization as the basis for arrhythmogenesis in a canine ventricular-wedge model of short-QT syndrome. *Circulation*, 110, (24) 3661-3666.
- Fedida, D. & Giles, W.R. 1991. Regional variations in action potentials and transient outward current in myocytes isolated from rabbit left ventricle. *J Physiol*, 442, 191-209.
- Fedor, J.M., McIntosh, D.M., Rembert, J.C., & Greenfield, J.C., Jr. 1978. Coronary and transmural myocardial blood flow responses in awake domestic pigs. *Am.J Physiol*, 235, (4) H435-H444.
- Fedorov, V.V., Lozinsky, I.T., Sosunov, E.A., Anyukhovskiy, E.P., Rosen, M.R., Balke, C.W., & Efimov, I.R. 2007. Application of blebbistatin as an excitation-contraction uncoupler for electrophysiologic study of rat and rabbit hearts. *Heart Rhythm*, 4, (5) 619-626.
- Feng, J., Xu, D., Wang, Z., & Nattel, S. 1998. Ultrarapid delayed rectifier current inactivation in human atrial myocytes: properties and consequences. *Am.J Physiol*, 275, (5 Pt 2) H1717-H1725.
- Ferrero, J.M., Jr., Saiz, J., Ferrero, J.M., & Thakor, N.V. 1996. Simulation of action potentials from metabolically impaired cardiac myocytes. Role of ATP-sensitive K⁺ current. *Circ.Res*, 79, (2) 208-221.
- Fishman, G.I., Chugh, S.S., Dimarco, J.P., Albert, C.M., Anderson, M.E., Bonow, R.O., Buxton, A.E., Chen, P.S., Estes, M., Jouven, X., Kwong, R., Lathrop, D.A., Mascette, A.M., Nerbonne, J.M., O'Rourke, B., Page, R.L., Roden, D.M., Rosenbaum, D.S., Sotoodehnia, N., Trayanova, N.A., & Zheng, Z.J. 2010. Sudden cardiac death prediction and prevention: report from a National Heart, Lung, and Blood Institute and Heart Rhythm Society Workshop. *Circulation*, 122, (22) 2335-2348.
- Fleet, W.F., Johnson, T.A., Cascio, W.E., Shen, J., Engle, C.L., Martin, D.G., & Gettes, L.S. 1994. Marked activation delay caused by ischemia initiated after regional K⁺ elevation in in situ pig hearts. *Circulation*, 90, (6) 3009-3017.
- Follmer, C.H. & Colatsky, T.J. 1990. Block of delayed rectifier potassium current, I_K, by flecainide and E-4031 in cat ventricular myocytes. *Circulation*, 82, (1) 289-293.
- Franz, M.R. 2003. The electrical restitution curve revisited: steep or flat slope--which is better? *J Cardiovasc Electrophysiol*, 14, (10 Suppl) S140-S147.
- Friedman, P.A. 2002. Novel mapping techniques for cardiac electrophysiology. *Heart*, 87, (6) 575-582.
- Fujiki, A., Tani, M., Mizumaki, K., Shimono, M., & Inoue, H. 1994. Electrophysiologic effects of intravenous E-4031, a novel class III antiarrhythmic agent, in patients with supraventricular tachyarrhythmias. *J Cardiovasc Pharmacol*, 23, (3) 374-378.
- Furukawa, T., Moroe, K., Mayrovitz, H.N., Sampsel, R., Furukawa, N., & Myerburg, R.J. 1991. Arrhythmogenic effects of graded coronary blood flow

- reductions superimposed on prior myocardial infarction in dogs. *Circulation*, 84, (1) 368-377.
- Gerlach, A.C., Stoehr, S.J., & Castle, N.A. 2010. Pharmacological removal of human ether-a-go-go-related gene potassium channel inactivation by 3-nitro-N-(4-phenoxyphenyl) benzamide (ICA-105574). *Molecular Pharmacology*, 77, (1) 58-68.
- Ghuran, A.V. & Camm, A.J. 2001. Ischaemic heart disease presenting as arrhythmias. *Br.Med Bull.*, 59, 193-210.
- Gilmour, R.F., Jr. & Zipes, D.P. 1985. Slow inward current and cardiac arrhythmias. *Am.J Cardiol.*, 55, (3) 89B-101B.
- Gintant, G.A. 2000. Characterization and functional consequences of delayed rectifier current transient in ventricular repolarization. *Am.J Physiol Heart Circ.Physiol*, 278, (3) H806-H817.
- Giustetto, C., Di, M.F., Wolpert, C., Borggrefe, M., Schimpf, R., Sbragia, P., Leone, G., Maury, P., Anttonen, O., Haissaguerre, M., & Gaita, F. 2006. Short QT syndrome: clinical findings and diagnostic-therapeutic implications. *Eur.Heart J*, 27, (20) 2440-2447.
- Giustetto, C., Schimpf, R., Mazzanti, A., Scrocco, C., Maury, P., Anttonen, O., Probst, V., Blanc, J.J., Sbragia, P., Dalmasso, P., Borggrefe, M., & Gaita, F. 2011. Long-term follow-up of patients with short QT syndrome. *J Am.Coll.Cardiol.*, 58, (6) 587-595.
- Gollob, M.H., Redpath, C.J., & Roberts, J.D. 2011. The short QT syndrome: proposed diagnostic criteria. *J Am.Coll.Cardiol.*, 57, (7) 802-812.
- Gussak, I., Brugada, P., Brugada, J., Antzelevitch, C., Osbakken, M., & Bjerregaard, P. 2002. ECG phenomenon of idiopathic and paradoxical short QT intervals. *Card Electrophysiol.Rev.*, 6, (1-2) 49-53.
- Gussak, I., Brugada, P., Brugada, J., Wright, R.S., Kopecky, S.L., Chaitman, B.R., & Bjerregaard, P. 2000. Idiopathic short QT interval: a new clinical syndrome? *Cardiology*, 94, (2) 99-102.
- Guzman, S.V., Deleon, A.C., Jr., West, J.W., & Bellet, S. 1959. Cardiac effects of isoproterenol, norepinephrine and epinephrine in complete A-V heart block during experimental acidosis and hyperkalemia. *Circ.Res*, 7, (4) 666-672.
- Haissaguerre, M., Chatel, S., Sacher, F., Weerasooriya, R., Probst, V., Loussouarn, G., Horlitz, M., Liersch, R., Schulze-Bahr, E., Wilde, A., Kaab, S., Koster, J., Rudy, Y., Le, M.H., & Schott, J.J. 2009. Ventricular fibrillation with prominent early repolarization associated with a rare variant of KCNJ8/KATP channel. *J Cardiovasc Electrophysiol.*, 20, (1) 93-98.
- Han, J. & Moe, G.K. 1964. Nonuniform recovery of excitability in ventricular muscle. *Circ.Res*, 14, 44-60.
- Harris, A.S. 1950. Delayed development of ventricular ectopic rhythms following experimental coronary occlusion. *Circulation*, 1, (6) 1318-1328.

- Harris, A.S., Bisteni, A., Russell, R.A., Brigham, J.C., & Firestone, J.E. 1954. Excitatory factors in ventricular tachycardia resulting from myocardial ischemia; potassium a major excitant. *Science*, 119, (3085) 200-203.
- Harvey, R.D., Clark, C.D., & Hume, J.R. 1990. Chloride current in mammalian cardiac myocytes. Novel mechanism for autonomic regulation of action potential duration and resting membrane potential. *J Gen.Physiol*, 95, (6) 1077-1102.
- Hasenfuss, G. 1998. Animal models of human cardiovascular disease, heart failure and hypertrophy. *Cardiovasc Res*, 39, (1) 60-76.
- Hattori, T., Makiyama, T., Akao, M., Ehara, E., Ohno, S., Iguchi, M., Nishio, Y., Sasaki, K., Itoh, H., Yokode, M., Kita, T., Horie, M., & Kimura, T. 2012. A novel gain-of-function KCNJ2 mutation associated with short-QT syndrome impairs inward rectification of Kir2.1 currents. *Cardiovasc Res*, 93, (4) 666-673.
- Hayashi, H., Miyauchi, Y., Chou, C.C., Karagueuzian, H.S., Chen, P.S., & Lin, S.F. 2003. Effects of cytochalasin D on electrical restitution and the dynamics of ventricular fibrillation in isolated rabbit heart. *J Cardiovasc Electrophysiol.*, 14, (10) 1077-1084.
- Hearse, D.J. 1994. Myocardial ischaemia: can we agree on a definition for the 21st century? *Cardiovasc Res*, 28, (12) 1737-1744.
- Herzberg, I.M., Trudeau, M.C., & Robertson, G.A. 1998. Transfer of rapid inactivation and sensitivity to the class III antiarrhythmic drug E-4031 from HERG to M-eag channels. *J Physiol*, 511 (Pt 1), 3-14.
- Hill, J.L. & Gettes, L.S. 1980. Effect of acute coronary artery occlusion on local myocardial extracellular K⁺ activity in swine. *Circulation*, 61, (4) 768-778.
- Hirche, H., Franz, C., Bos, L., Bissig, R., Lang, R., & Schramm, M. 1980. Myocardial extracellular K⁺ and H⁺ increase and noradrenaline release as possible cause of early arrhythmias following acute coronary artery occlusion in pigs. *J Mol.Cell Cardiol.*, 12, (6) 579-593.
- Holahan, M.A., Stranieri, M.T., Stabilito, I.I., & Lynch, J.J., Jr. 1992. Effect of E-4031, a class III antiarrhythmic agent, on experimental infarct size in a canine model of myocardial ischemia-reperfusion injury. *J Cardiovasc Pharmacol.*, 19, (6) 892-898.
- Holubarsch, C., Hasenfuss, G., Thierfelder, L., Pieske, B., & Just, H. 1991. The heart in heart failure. Ventricular and myocardial alterations. *Eur.Heart J*, 12 Suppl C, 8-13.
- Hong, K., Bjerregaard, P., Gussak, I., & Brugada, R. 2005a. Short QT syndrome and atrial fibrillation caused by mutation in KCNH2. *J Cardiovasc Electrophysiol.*, 16, (4) 394-396.
- Hong, K., Piper, D.R., Diaz-Valdecantos, A., Brugada, J., Oliva, A., Burashnikov, E., Santos-de-Soto, J., Grueso-Montero, J., Diaz-Enfante, E., Brugada, P., Sachse, F., Sanguinetti, M.C., & Brugada, R. 2005b. De novo KCNQ1 mutation responsible for atrial fibrillation and short QT syndrome in utero. *Cardiovasc Res*, 68, (3) 433-440.

Hua, F. & Gilmour, R.F., Jr. 2004. Contribution of IKr to rate-dependent action potential dynamics in canine endocardium. *Circ.Res*, 94, (6) 810-819.

Huikuri, H.V., Castellanos, A., & Myerburg, R.J. 2001. Sudden death due to cardiac arrhythmias. *N Engl J Med*, 345, (20) 1473-1482.

Ideker, R.E., Smith, W.M., & Wolf, P.D. 1989. Cardiac mapping at Duke Medical Center. *Am.J Cardiol.*, 63 Suppl, 17F-30F.

Janse, M.J., van Capelle, F.J., Morsink, H., Kleber, A.G., Wilms-Schopman, F., Cardinal, R., d'Alnoncourt, C.N., & Durrer, D. 1980. Flow of "injury" current and patterns of excitation during early ventricular arrhythmias in acute regional myocardial ischemia in isolated porcine and canine hearts. Evidence for two different arrhythmogenic mechanisms. *Circ.Res*, 47, (2) 151-165.

Janse, M.J. & Wit, A.L. 1989. Electrophysiological mechanisms of ventricular arrhythmias resulting from myocardial ischemia and infarction. *Physiol Rev.*, 69, (4) 1049-1169.

Jonsson, M.K., Duker, G., Tropp, C., Andersson, B., Sartipy, P., Vos, M.A., & van Veen, T.A. 2010. Quantified proarrhythmic potential of selected human embryonic stem cell-derived cardiomyocytes. *Stem Cell Res*, 4, (3) 189-200.

Jugdutt, B.I., Becker, L.C., & Hutchins, G.M. 1979. Early changes in collateral blood flow during myocardial infarction in conscious dogs. *Am.J Physiol*, 237, (3) H371-H380.

Kagiyama, Y., Hill, J.L., & Gettes, L.S. 1982. Interaction of acidosis and increased extracellular potassium on action potential characteristics and conduction in guinea pig ventricular muscle. *Circ.Res*, 51, (5) 614-623.

Kannengiesser, G.J., Lubbe, W.F., & Opie, L.H. 1975. Experimental myocardial infarction with left ventricular failure in the isolated perfused rat heart. Effects of isoproterenol and pacing. *J Mol.Cell Cardiol.*, 7, (2) 135-151.

Kantor, P.F., Coetzee, W.A., Carmeliet, E.E., Dennis, S.C., & Opie, L.H. 1990. Reduction of ischemic K⁺ loss and arrhythmias in rat hearts. Effect of glibenclamide, a sulfonylurea. *Circ.Res*, 66, (2) 478-485.

Kaplinsky, E., Ogawa, S., Balke, C.W., & Dreifus, L.S. 1979a. Two periods of early ventricular arrhythmia in the canine acute myocardial infarction model. *Circulation*, 60, (2) 397-403.

Kaplinsky, E., Ogawa, S., Balke, W., & Dreifus, L.S. 1979b. Role of endocardial activation in malignant ventricular arrhythmias associated with acute ischemia. *J Electrocardiol.*, 12, (3) 299-306.

Kardesch, M., Hogancamp, C.E., & Bing, R.J. 1958. The effect of complete ischemia on the intracellular electrical activity of the whole mammalian heart. *Circ.Res*, 6, (6) 715-720.

Kishida, H., Surawicz, B., & Fu, L.T. 1979. Effects of K⁺ and K⁺-induced polarization on (dV/dt)_{max}, threshold potential, and membrane input resistance in guinea pig and cat ventricular myocardium. *Circ.Res*, 44, (6) 800-814.

Klabunde, R. E. 2005, "Electrical Activity of the Heart," *In Cardiovascular Physiology Concepts*, Philadelphia: Lippincott Williams & Wilkins, pp. 9-40.

Kleber, A.G., Janse, M.J., van Capelle, F.J., & Durrer, D. 1978. Mechanism and time course of S-T and T-Q segment changes during acute regional myocardial ischemia in the pig heart determined by extracellular and intracellular recordings. *Circ.Res*, 42, (5) 603-613.

Kleinfeld, M.J. & Rozanski, J.J. 1977. Alternans of the ST segment in Prinzmetal's angina. *Circulation*, 55, (4) 574-577.

Knisley, S.B., Justice, R.K., Kong, W., & Johnson, P.L. 2000. Ratiometry of transmembrane voltage-sensitive fluorescent dye emission in hearts. *Am.J Physiol Heart Circ.Physiol*, 279, (3) H1421-H1433.

Kuo, C.S., Munakata, K., Reddy, C.P., & Surawicz, B. 1983. Characteristics and possible mechanism of ventricular arrhythmia dependent on the dispersion of action potential durations. *Circulation*, 67, (6) 1356-1367.

Lazzara, R., El-Sherif, N., & Scherlag, B.J. 1975. Disorders of cellular electrophysiology produced by ischemia of the canine His bundle. *Circ.Res*, 36, (3) 444-454.

Lederer, W.J., Nichols, C.G., & Smith, G.L. 1989. The mechanism of early contractile failure of isolated rat ventricular myocytes subjected to complete metabolic inhibition. *J Physiol*, 413, 329-349.

Lee, B.H., Kim, W.H., Choi, M.J., Rho, J.R., & Kim, W.G. 2002. Chronic heart failure model in rabbits based on the concept of the bifurcation/trifurcation coronary artery branching pattern. *Artificial Organs*, 26, (4) 360-365.

Lee, P., Klos, M., Bollensdorff, C., Hou, L., Ewart, P., Kamp, T.J., Zhang, J., Bizy, A., Guerrero-Serna, G., Kohl, P., Jalife, J., & Herron, T.J. 2012. Simultaneous voltage and calcium mapping of genetically purified human induced pluripotent stem cell-derived cardiac myocyte monolayers. *Circ.Res*, 110, (12) 1556-1563.

Lenz, T.L. & Hilleman, D.E. 2000. Dofetilide, a new class III antiarrhythmic agent. *Pharmacotherapy*, 20, (7) 776-786.

Levick R.J 2010. *An Introduction to Cardiovascular Physiology*, 5 ed. Oxford University Press.

Lichtman, J.W. & Conchello, J.A. 2005. Fluorescence microscopy. *Nat Methods*, 2, (12) 910-919.

Loew, L. M. 2001, "Mechanisms and Principles of Voltage-Sensitive," *In Optical Mapping of Cardiac Excitation and Arrhythmias*, D. S. Rosenbaum & J. Jalife, eds., Armonk, New York: Futura Publishing Company, Inc., pp. 33-46.

Loew, L. M. 2010, "Design and Use of Organic Voltage Sensitive Dyes," *In Membrane Potential Imaging in the Nervous System: Methods and Applications*, M. Canepari & D. Zecevic, eds., New York, USA: Springer, pp. 13-23.

- Loew, L.M., Cohen, L.B., Salzberg, B.M., Obaid, A.L., & Bezanilla, F. 1985. Charge-shift probes of membrane potential. Characterization of aminostyrylpyridinium dyes on the squid giant axon. *Biophys.J*, 47, (1) 71-77.
- Lord, B., Boswood, A., & Petrie, A. 2010. Electrocardiography of the normal domestic pet rabbit. *Veterinary Record*, 167, (25) 961-965.
- Lou, Q., Ripplinger, C.M., Bayly, P.V., & Efimov, I.R. 2008. Quantitative panoramic imaging of epicardial electrical activity. *Ann.Biomed.Eng*, 36, (10) 1649-1658.
- Luqman, N., Sung, R.J., Wang, C.L., & Kuo, C.T. 2007. Myocardial ischemia and ventricular fibrillation: pathophysiology and clinical implications. *Int.J Cardiol.*, 119, (3) 283-290.
- Maciver, R.H., Stewart, R.D., Backer, C.L., Tsao, S., Harrington, D.A., & Mavroudis, C. 2010. An improved in vivo method for atrioventricular node ablation via thoracotomy. *Braz.J Med Biol.Res*, 43, (2) 206-210.
- Man, R.Y. & Bril, A. 1991. Effects of class I anti-arrhythmic drugs in infarcted tissue. *Clin Invest Med*, 14, (5) 466-475.
- Marcus, F.I., Cobb, L.A., Edwards, J.E., Kuller, L., Moss, A.J., Bigger, J.T., Jr., Fleiss, J.L., Rolnitzky, L., & Serokman, R. 1988. Mechanism of death and prevalence of myocardial ischemic symptoms in the terminal event after acute myocardial infarction. *Am.J Cardiol.*, 61, (1) 8-15.
- Maury, P., Extramiana, F., Sbragia, P., Giustetto, C., Schimpf, R., Duparc, A., Wolpert, C., Denjoy, I., Delay, M., Borggreffe, M., & Gaita, F. 2008. Short QT syndrome. Update on a recent entity. *Arch.Cardiovasc Dis.*, 101, (11-12) 779-786.
- Maxwell, M.P., Hearse, D.J., & Yellon, D.M. 1987. Species variation in the coronary collateral circulation during regional myocardial ischaemia: a critical determinant of the rate of evolution and extent of myocardial infarction. *Cardiovasc Res*, 21, (10) 737-746.
- McIntosh, M.A., Cobbe, S.M., & Smith, G.L. 2000. Heterogeneous changes in action potential and intracellular Ca²⁺ in left ventricular myocyte sub-types from rabbits with heart failure. *Cardiovasc Res*, 45, (2) 397-409.
- McPate, M.J., Witchel, H.J., & Hancox, J.C. 2006. Short QT syndrome. *Future.Cardiol.*, 2, (3) 293-301.
- Mines, G.R. 1913. On dynamic equilibrium in the heart. *J Physiol*, 46, (4-5) 349-383.
- Miura, T., Downey, J.M., Ooiwa, H., Ogawa, S., Adachi, T., Noto, T., Shizukuda, Y., & Iimura, O. 1989. Progression of myocardial infarction in a collateral flow deficient species. *Jpn.Heart J*, 30, (5) 695-708.
- Modell, S.M. & Lehmann, M.H. 2006. The long QT syndrome family of cardiac ion channelopathies: a HuGE review. *Genet.Med*, 8, (3) 143-155.

- Montana, V., Farkas, D.L., & Loew, L.M. 1989. Dual-wavelength ratiometric fluorescence measurements of membrane potential. *Biochemistry*, 28, (11) 4536-4539.
- Morad, M. & Salama, G. 1979. Optical probes of membrane potential in heart muscle. *J Physiol*, 292, 267-295.
- Morgan, J.M., Cunningham, D., & Rowland, E. 1992. Electrical restitution in the endocardium of the intact human right ventricle. *Br.Heart J*, 67, (1) 42-46.
- Naik, H., Sabatine, M. S., & Lilly, L. S. 2007, "Ischemic Heart Disease," In *Pathophysiology of Heart Disease*, 4th ed. ed. L. S. Lilly, ed., Philadelphia, PA, USA: Lippincott Williams & Wilkins, pp. 141-167.
- Nalos, L., Varkevisser, R., Jonsson, M.K., Houtman, M.J., Beekman, J.D., van der Nagel, R., Thomsen, M.B., Duker, G., Sartipy, P., de Boer, T.P., Peschar, M., Rook, M.B., van Veen, T.A., van der Heyden, M.A., & Vos, M.A. 2012. Comparison of the IKr blockers moxifloxacin, dofetilide and E-4031 in five screening models of pro-arrhythmia reveals lack of specificity of isolated cardiomyocytes. *Br.J Pharmacol.*, 165, (2) 467-478.
- Narayan, S.M. 2006. T-wave alternans and the susceptibility to ventricular arrhythmias. *J Am.Coll.Cardiol.*, 47, (2) 269-281.
- Narayan, S.M., Lindsay, B.D., & Smith, J.M. 1999. Demonstration of the proarrhythmic preconditioning of single premature extrastimuli by use of the magnitude, phase, and distribution of repolarization alternans. *Circulation*, 100, (18) 1887-1893.
- Narayan, S.M. & Smith, J.M. 2000. Exploiting rate-related hysteresis in repolarization alternans to improve risk stratification for ventricular tachycardia. *J Am.Coll.Cardiol.*, 35, (6) 1485-1492.
- Neely, J.R., Whitmer, J.T., & Rovetto, M.J. 1975. Inhibition of glycolysis in hearts during ischemic perfusion. *Recent Adv.Stud.Cardiac.Struct.Metab*, 7, 243-248.
- Nerbonne, J.M. 2000. Molecular basis of functional voltage-gated K⁺ channel diversity in the mammalian myocardium. *J Physiol*, 525 Pt 2, 285-298.
- Newby, K.H., Thompson, T., Stebbins, A., Topol, E.J., Califf, R.M., & Natale, A. 1998. Sustained ventricular arrhythmias in patients receiving thrombolytic therapy: incidence and outcomes. The GUSTO Investigators. *Circulation*, 98, (23) 2567-2573.
- Ng, G.A., Brack, K.E., Patel, V.H., & Coote, J.H. 2007. Autonomic modulation of electrical restitution, alternans and ventricular fibrillation initiation in the isolated heart. *Cardiovasc Res*, 73, (4) 750-760.
- Nolasco, J.B. & Dahlen, R.W. 1968. A graphic method for the study of alternation in cardiac action potentials. *J Appl.Physiol*, 25, (2) 191-196.
- Nordrehaug, J.E. 1985. Hypokalemia, arrhythmias and early prognosis in acute myocardial infarction. *Acta Med Scand.*, 217, (3) 299-306.

- Nordrehaug, J.E., Johannessen, K.A., & von der, L.G. 1985. Serum potassium concentration as a risk factor of ventricular arrhythmias early in acute myocardial infarction. *Circulation*, 71, (4) 645-649.
- Nouchi, H., Kiryu, N., Kimata, M., Tsuneoka, Y., Hamaguchi, S., Namekata, I., Takahara, A., Shigenobu, K., & Tanaka, H. 2011. Developmental changes in action potential prolongation by K⁺-channel blockers in chick myocardium. *J Pharmacol.Sci.*, 115, (2) 235-238.
- Oinuma, H., Miyake, K., Yamanaka, M., Nomoto, K., Katoh, H., Sawada, K., Shino, M., & Hamano, S. 1990. 4'-[(4-Piperidyl)carbonyl]methanesulfonanilides as potent, selective, bioavailable class III antiarrhythmic agents. *J Med Chem.*, 33, (3) 903-905.
- Oostendorp, T.F. & van, O.A. 2004. ECGSIM: an interactive tool for the study of the relation between the electric activity of the heart and the QRST waveforms at the body surface. *Conf.Proc.IEEE Eng Med Biol.Soc.*, 5, 3559-3562.
- Opthof, T., Coronel, R., Vermeulen, J.T., Verberne, H.J., van Capelle, F.J., & Janse, M.J. 1993. Dispersion of refractoriness in normal and ischaemic canine ventricle: effects of sympathetic stimulation. *Cardiovasc Res*, 27, (11) 1954-1960.
- Oster, H.S., Taccardi, B., Lux, R.L., Ershler, P.R., & Rudy, Y. 1998. Electrocardiographic imaging: Noninvasive characterization of intramural myocardial activation from inverse-reconstructed epicardial potentials and electrograms. *Circulation*, 97, (15) 1496-1507.
- Padrini, R., Bova, S., Cargnelli, G., Piovan, D., & Ferrari, M. 1992. Effects of pinacidil on guinea-pig isolated perfused heart with particular reference to the proarrhythmic effect. *Br.J Pharmacol.*, 105, (3) 715-719.
- Pastore, J.M., Girouard, S.D., Laurita, K.R., Akar, F.G., & Rosenbaum, D.S. 1999. Mechanism linking T-wave alternans to the genesis of cardiac fibrillation. *Circulation*, 99, (10) 1385-1394.
- Patberg, K.W., Shvilkin, A., Plotnikov, A.N., Chandra, P., Josephson, M.E., & Rosen, M.R. 2005. Cardiac memory: mechanisms and clinical implications. *Heart Rhythm.*, 2, (12) 1376-1382.
- Perrin, M.J., Subbiah, R.N., Vandenberg, J.I., & Hill, A.P. 2008. Human ether-a-go-go related gene (hERG) K⁺ channels: function and dysfunction. *Progress in Biophysics and Molecular Biology*, 98, (2-3) 137-148.
- Petchdee, S. 2009. *Arrhythmia mechanisms in acute ischaemia and chronic infarction in rabbit heart*. University of Glasgow.
- Podesser, B., Wollenek, G., Seitelberger, R., Siegel, H., Wolner, E., Firbas, W., & Tschabitscher, M. 1997. Epicardial branches of the coronary arteries and their distribution in the rabbit heart: the rabbit heart as a model of regional ischemia. *Anatomical Record*, 247, (4) 521-527.

- Pogwizd, S.M. & Corr, P.B. 1987a. Electrophysiologic mechanisms underlying arrhythmias due to reperfusion of ischemic myocardium. *Circulation*, 76, (2) 404-426.
- Pogwizd, S.M. & Corr, P.B. 1987b. Reentrant and nonreentrant mechanisms contribute to arrhythmogenesis during early myocardial ischemia: results using three-dimensional mapping. *Circ.Res*, 61, (3) 352-371.
- Pogwizd, S.M., Schlotthauer, K., Li, L., Yuan, W., & Bers, D.M. 2001. Arrhythmogenesis and contractile dysfunction in heart failure: Roles of sodium-calcium exchange, inward rectifier potassium current, and residual beta-adrenergic responsiveness. *Circ.Res*, 88, (11) 1159-1167.
- Ponte, M.L., Keller, G.A., & Di, G.G. 2010. Mechanisms of drug induced QT interval prolongation. *Curr.Drug Saf*, 5, (1) 44-53.
- Prinzmetal, M., Toyoshima, H., Ekmekci, A., Mizuno, Y., & Nagaya, T. 1961. Myocardial ischemia. Nature of ischemic electrocardiographic patterns in the mammalian ventricles as determined by intracellular electrographic and metabolic changes. *Am.J Cardiol.*, 8, 493-503.
- Priori, S.G., Aliot, E., Blomstrom-Lundqvist, C., Bossaert, L., Breithardt, G., Brugada, P., Camm, A.J., Cappato, R., Cobbe, S.M., Di, M.C., Maron, B.J., McKenna, W.J., Pedersen, A.K., Ravens, U., Schwartz, P.J., Trusz-Gluza, M., Vardas, P., Wellens, H.J., & Zipes, D.P. 2001. Task Force on Sudden Cardiac Death of the European Society of Cardiology. *Eur.Heart J*, 22, (16) 1374-1450.
- Priori, S.G., Pandit, S.V., Rivolta, I., Berenfeld, O., Ronchetti, E., Dhamoon, A., Napolitano, C., Anumonwo, J., di Barletta, M.R., Gudapakkam, S., Bosi, G., Stramba-Badiale, M., & Jalife, J. 2005. A novel form of short QT syndrome (SQT3) is caused by a mutation in the KCNJ2 gene. *Circ.Res*, 96, (7) 800-807.
- Prystowsky, E.N. 2004. Primary prevention of sudden cardiac death: the time of your life. *Circulation*, 109, (9) 1073-1075.
- Qu, F., Ripplinger, C.M., Nikolski, V.P., Grimm, C., & Efimov, I.R. 2007. Three-dimensional panoramic imaging of cardiac arrhythmias in rabbit heart. *J Biomed.Opt.*, 12, (4) 044019.
- Qu, Z., Garfinkel, A., Chen, P.S., & Weiss, J.N. 2000. Mechanisms of discordant alternans and induction of reentry in simulated cardiac tissue. *Circulation*, 102, (14) 1664-1670.
- Raeder, E.A., Rosenbaum, D.S., Bhasin, R., & Cohen, R.J. 1992. Alternating morphology of the QRST complex preceding sudden death. *N Engl J Med*, 326, (4) 271-272.
- Ridley, P.D., Yacoub, M.H., & Curtis, M.J. 1992. A modified model of global ischaemia: application to the study of syncytial mechanisms of arrhythmogenesis. *Cardiovasc Res*, 26, (4) 309-315.
- Ripplinger, C.M., Lou, Q., Li, W., Hadley, J., & Efimov, I.R. 2009. Panoramic imaging reveals basic mechanisms of induction and termination of ventricular

tachycardia in rabbit heart with chronic infarction: implications for low-voltage cardioversion. *Heart Rhythm.*, 6, (1) 87-97.

Roden, D.M., Lazzara, R., Rosen, M., Schwartz, P.J., Towbin, J., & Vincent, G.M. 1996. Multiple mechanisms in the long-QT syndrome. Current knowledge, gaps, and future directions. The SADS Foundation Task Force on LQTS. *Circulation*, 94, (8) 1996-2012.

Romero, L., Pueyo, E., Fink, M., & Rodriguez, B. 2009. Impact of ionic current variability on human ventricular cellular electrophysiology. *Am.J Physiol Heart Circ.Physiol*, 297, (4) H1436-H1445.

Rosenbaum, D. S. 2001, "Introduction: Optical Mapping of Cardiac Excitation and Arrhythmias: A Primer," *In Optical Mapping of Cardiac Excitation and Arrhythmias*, D. S. Rosenbaum & J. Jalife, eds., Armonk, New York: Futura Publishing Company, Inc, pp. 2-7.

Rosenbaum, D.S., Jackson, L.E., Smith, J.M., Garan, H., Ruskin, J.N., & Cohen, R.J. 1994. Electrical alternans and vulnerability to ventricular arrhythmias. *N Engl J Med*, 330, (4) 235-241.

Rosenbaum, D.S. & Jalife, J. 2001. *Optical Mapping of Cardiac Excitation and Arrhythmias* Armonk, New York, Futura Publishing Company, Inc.

Russell, J.C. & Proctor, S.D. 2006. Small animal models of cardiovascular disease: tools for the study of the roles of metabolic syndrome, dyslipidemia, and atherosclerosis. *Cardiovasc Pathol.*, 15, (6) 318-330.

Ryan, T.J., Anderson, J.L., Antman, E.M., Braniff, B.A., Brooks, N.H., Califf, R.M., Hillis, L.D., Hiratzka, L.F., Rapaport, E., Riegel, B.J., Russell, R.O., Smith, E.E., III, & Weaver, W.D. 1996. ACC/AHA guidelines for the management of patients with acute myocardial infarction: executive summary. A report of the American College of Cardiology/American Heart Association Task Force on Practice Guidelines (Committee on Management of Acute Myocardial Infarction). *Circulation*, 94, (9) 2341-2350.

Samson, W.E. & Scher, A.M. 1960. Mechanism of S-T segment alteration during acute myocardial injury. *Circ.Res*, 8, 780-787.

Sanguinetti, M.C., Jurkiewicz, N.K., Scott, A., & Siegl, P.K. 1991. Isoproterenol antagonizes prolongation of refractory period by the class III antiarrhythmic agent E-4031 in guinea pig myocytes. Mechanism of action. *Circ.Res*, 68, (1) 77-84.

Sanguinetti, M.C. & Mitcheson, J.S. 2005. Predicting drug-hERG channel interactions that cause acquired long QT syndrome. *Trends in Pharmacological Sciences*, 26, (3) 119-124.

Schaper, W. 1986. [Pathophysiology of reperfusion]. *Zeitschrift fur Kardiologie*, 75 Suppl 5, 73-75.

Schaper, W., Jageneau, A., & Xhonneux, R. 1967. The development of collateral circulation in the pig and dog heart. *Cardiologia*, 51, (6) 321-335.

- Scheler, S., Motz, W., & Strauer, B.E. 1994. Mechanism of angina pectoris in patients with systemic hypertension and normal epicardial coronary arteries by arteriogram. *Am.J Cardiol.*, 73, (7) 478-482.
- Scherlag, B.J., El-Sherif, N., Hope, R., & Lazzara, R. 1974. Characterization and localization of ventricular arrhythmias resulting from myocardial ischemia and infarction. *Circ.Res*, 35, (3) 372-383.
- Schimpf, R., Wolpert, C., Gaita, F., Giustetto, C., & Borggrefe, M. 2005. Short QT syndrome. *Cardiovasc Res*, 67, (3) 357-366.
- Sicouri, S. & Antzelevitch, C. 1991. A subpopulation of cells with unique electrophysiological properties in the deep subepicardium of the canine ventricle. The M cell. *Circ.Res*, 68, (6) 1729-1741.
- Sicouri, S., Quist, M., & Antzelevitch, C. 1996. Evidence for the presence of M cells in the guinea pig ventricle. *J Cardiovasc Electrophysiol.*, 7, (6) 503-511.
- Singh, B.N. & Vaughan Williams, E.M. 1970. A third class of anti-arrhythmic action. Effects on atrial and ventricular intracellular potentials, and other pharmacological actions on cardiac muscle, of MJ 1999 and AH 3474. *Br.J Pharmacol.*, 39, (4) 675-687.
- Smeets, J.L., Allessie, M.A., Lammers, W.J., Bonke, F.I., & Hollen, J. 1986. The wavelength of the cardiac impulse and reentrant arrhythmias in isolated rabbit atrium. The role of heart rate, autonomic transmitters, temperature, and potassium. *Circ.Res*, 58, (1) 96-108.
- Smith, J.M. & Cohen, R.J. 1984. Simple finite-element model accounts for wide range of cardiac dysrhythmias. *Proc.Natl.Acad.Sci.U.S.A*, 81, (1) 233-237.
- Solomon, S.D., Zelenkofske, S., McMurray, J.J., Finn, P.V., Velazquez, E., Ertl, G., Harsanyi, A., Rouleau, J.L., Maggioni, A., Kober, L., White, H., Van de Werf, F., Pieper, K., Califf, R.M., & Pfeffer, M.A. 2005. Sudden death in patients with myocardial infarction and left ventricular dysfunction, heart failure, or both. *N Engl J Med*, 352, (25) 2581-2588.
- Stankovicova, T., Szilard, M., De, S., I, & Sipido, K.R. 2000. M cells and transmural heterogeneity of action potential configuration in myocytes from the left ventricular wall of the pig heart. *Cardiovasc Res*, 45, (4) 952-960.
- Straight, A.F., Cheung, A., Limouze, J., Chen, I., Westwood, N.J., Sellers, J.R., & Mitchison, T.J. 2003. Dissecting temporal and spatial control of cytokinesis with a myosin II Inhibitor. *Science*, 299, (5613) 1743-1747.
- Sun, Y., Quan, X.Q., Fromme, S., Cox, R.H., Zhang, P., Zhang, L., Guo, D., Guo, J., Patel, C., Kowey, P.R., & Yan, G.X. 2011. A novel mutation in the KCNH2 gene associated with short QT syndrome. *J Mol.Cell Cardiol.*, 50, (3) 433-441.
- Sutton, P.M., Taggart, P., Opthof, T., Coronel, R., Trimlett, R., Pugsley, W., & Kallis, P. 2000. Repolarisation and refractoriness during early ischaemia in humans. *Heart*, 84, (4) 365-369.

Szentadrassy, N., Banyasz, T., Biro, T., Szabo, G., Toth, B.I., Magyar, J., Lazar, J., Varro, A., Kovacs, L., & Nanasi, P.P. 2005. Apico-basal inhomogeneity in distribution of ion channels in canine and human ventricular myocardium. *Cardiovasc Res*, 65, (4) 851-860.

Templin, C., Ghadri, J.R., Rougier, J.S., Baumer, A., Kaplan, V., Albesa, M., Sticht, H., Rauch, A., Puleo, C., Hu, D., Barajas-Martinez, H., Antzelevitch, C., Luscher, T.F., Abriel, H., & Duru, F. 2011. Identification of a novel loss-of-function calcium channel gene mutation in short QT syndrome (SQTS6). *Eur.Heart J*, 32, (9) 1077-1088.

Thomas, D., Karle, C.A., & Kiehn, J. 2006. The cardiac hERG/IKr potassium channel as pharmacological target: structure, function, regulation, and clinical applications. *Curr.Pharm.Des*, 12, (18) 2271-2283.

Thygesen, K., Alpert, J.S., Jaffe, A.S., Simoons, M.L., Chaitman, B.R., White, H.D., Thygesen, K., Alpert, J.S., White, H.D., Jaffe, A.S., Katus, H.A., Apple, F.S., Lindahl, B., Morrow, D.A., Chaitman, B.R., Clemmensen, P.M., Johanson, P., Hod, H., Underwood, R., Bax, J.J., Bonow, J.J., Pinto, F., Gibbons, R.J., Fox, K.A., Atar, D., Newby, L.K., Galvani, M., Hamm, C.W., Uretsky, B.F., Steg, P.G., Wijns, W., Bassand, J.P., Menasche, P., Ravkilde, J., Ohman, E.M., Antman, E.M., Wallentin, L.C., Armstrong, P.W., Simoons, M.L., Januzzi, J.L., Nieminen, M.S., Gheorghiade, M., Filippatos, G., Luepker, R.V., Fortmann, S.P., Rosamond, W.D., Levy, D., Wood, D., Smith, S.C., Hu, D., Lopez-Sendon, J.L., Robertson, R.M., Weaver, D., Tendera, M., Bove, A.A., Parkhomenko, A.N., Vasilieva, E.J., Mendis, S., Bax, J.J., Baumgartner, H., Ceconi, C., Dean, V., Deaton, C., Fagard, R., Funck-Brentano, C., Hasdai, D., Hoes, A., Kirchhof, P., Knuuti, J., Kolh, P., McDonagh, T., Moulin, C., Popescu, B.A., Reiner, Z., Sechtem, U., Sirnes, P.A., Tendera, M., Torbicki, A., Vahanian, A., Windecker, S., Morais, J., Aguiar, C., Almahmeed, W., Arnar, D.O., Barili, F., Bloch, K.D., Bolger, A.F., Botker, H.E., Bozkurt, B., Bugiardini, R., Cannon, C., de, L.J., Eberli, F.R., Escobar, E., Hlatky, M., James, S., Kern, K.B., Moliterno, D.J., Mueller, C., Neskovic, A.N., Pieske, B.M., Schulman, S.P., Storey, R.F., Taubert, K.A., Vranckx, P., & Wagner, D.R. 2012. Third universal definition of myocardial infarction. *J Am.Coll.Cardiol.*, 60, (16) 1581-1598.

Tikkanen, J.T., Wichmann, V., Junttila, M.J., Rainio, M., Hookana, E., Lappi, O.P., Kortelainen, M.L., Anttonen, O., & Huikuri, H.V. 2012. Association of early repolarization and sudden cardiac death during an acute coronary event. *Circ.Arrhythm.Electrophysiol.*, 5, (4) 714-718.

Uchida, T., Yashima, M., Gotoh, M., Qu, Z., Garfinkel, A., Weiss, J.N., Fishbein, M.C., Mandel, W.J., Chen, P.S., & Karagueuzian, H.S. 1999. Mechanism of acceleration of functional reentry in the ventricle: effects of ATP-sensitive potassium channel opener. *Circulation*, 99, (5) 704-712.

Vanheel, B. & de, H.A. 1992. Influence of KATP channel modulation on net potassium efflux from ischaemic mammalian cardiac tissue. *Cardiovasc Res*, 26, (11) 1030-1039.

Venkatesh, N., Lamp, S.T., & Weiss, J.N. 1991. Sulfonylureas, ATP-sensitive K⁺ channels, and cellular K⁺ loss during hypoxia, ischemia, and metabolic inhibition in mammalian ventricle. *Circ.Res*, 69, (3) 623-637.

- Verdouw, P.D., van den Doel, M.A., de, Z.S., & Duncker, D.J. 1998. Animal models in the study of myocardial ischaemia and ischaemic syndromes. *Cardiovasc Res*, 39, (1) 121-135.
- Verdouw, P.D., Wolffenbuttel, B.H., & van der Giessen, W.J. 1983. Domestic pigs in the study of myocardial ischemia. *Eur.Heart J*, 4 Suppl C, 61-67.
- Verrier, R.L., Nearing, B.D., La Rovere, M.T., Pinna, G.D., Mittleman, M.A., Bigger, J.T., Jr., & Schwartz, P.J. 2003. Ambulatory electrocardiogram-based tracking of T wave alternans in postmyocardial infarction patients to assess risk of cardiac arrest or arrhythmic death. *J Cardiovasc Electrophysiol.*, 14, (7) 705-711.
- Villafane, J., Atallah, J., Gollob, M.H., Maury, P., Wolpert, C., Gebauer, R., Watanabe, H., Horie, M., Anttonen, O., Kannankeril, P., Faulknier, B., Bleiz, J., Makiyama, T., Shimizu, W., Hamilton, R.M., & Young, M.L. 2013. Long-term follow-up of a pediatric cohort with short QT syndrome. *J Am.Coll.Cardiol.*, 61, (11) 1183-1191.
- Volders, P.G., Stengl, M., van Opstal, J.M., Gerlach, U., Spatjens, R.L., Beekman, J.D., Sipido, K.R., & Vos, M.A. 2003. Probing the contribution of IKs to canine ventricular repolarization: key role for beta-adrenergic receptor stimulation. *Circulation*, 107, (21) 2753-2760.
- Wallace, A.A., Stupienski, R.F., III, Brookes, L.M., Selnick, H.G., Claremon, D.A., & Lynch, J.J., Jr. 1991. Cardiac electrophysiologic and inotropic actions of new and potent methanesulfonanilide class III antiarrhythmic agents in anesthetized dogs. *J Cardiovasc Pharmacol.*, 18, (5) 687-695.
- Wallbridge, D.R. & Cobbe, S.M. 1996. Coronary haemodynamics in left ventricular hypertrophy. *Heart*, 75, (4) 369-376.
- Waller, A.D. 1887. A Demonstration on Man of Electromotive Changes accompanying the Heart's Beat. *J Physiol*, 8, (5) 229-234.
- Wang, Z., Fermini, B., & Nattel, S. 1993. Sustained depolarization-induced outward current in human atrial myocytes. Evidence for a novel delayed rectifier K⁺ current similar to Kv1.5 cloned channel currents. *Circ.Res*, 73, (6) 1061-1076.
- Warltier, D.C., Zyvoloski, M.G., Gross, G.J., & Brooks, H.L. 1982. Subendocardial versus transmural myocardial infarction: relationship to the collateral circulation in canine and porcine hearts. *Can.J Physiol Pharmacol.*, 60, (12) 1700-1706.
- Watanabe, T., Yamaki, M., Yamauchi, S., Minamihaba, O., Miyashita, T., Kubota, I., & Tomoike, H. 2002. Regional prolongation of ARI and altered restitution properties cause ventricular arrhythmia in heart failure. *Am.J Physiol Heart Circ.Physiol*, 282, (1) H212-H218.
- Weber, K.T., Brilla, C.G., Campbell, S.E., Guarda, E., Zhou, G., & Sriram, K. 1993. Myocardial fibrosis: role of angiotensin II and aldosterone. *Basic Res Cardiol.*, 88 Suppl 1, 107-124.
- Weiss, J. & Shine, K.I. 1982. Extracellular K⁺ accumulation during myocardial ischemia in isolated rabbit heart. *Am.J Physiol*, 242, (4) H619-H628.

Weiss, J.N., Garfinkel, A., Karagueuzian, H.S., Qu, Z., & Chen, P.S. 1999. Chaos and the transition to ventricular fibrillation: a new approach to antiarrhythmic drug evaluation. *Circulation*, 99, (21) 2819-2826.

Weiss, J.N., Venkatesh, N., & Lamp, S.T. 1992. ATP-sensitive K⁺ channels and cellular K⁺ loss in hypoxic and ischaemic mammalian ventricle. *J Physiol*, 447, 649-673.

Wettwer, E., Scholtysik, G., Schaad, A., Himmel, H., & Ravens, U. 1991. Effects of the new class III antiarrhythmic drug E-4031 on myocardial contractility and electrophysiological parameters. *J Cardiovasc Pharmacol.*, 17, (3) 480-487.

Widimsky, P., Gregor, P., Cervenka, V., & Visek, V. 1984. Two-dimensional echocardiography in acute transmural and non-transmural myocardial infarction. *Cor et Vasa*, 26, (1) 12-19.

Wolleben, C.D., Sanguinetti, M.C., & Siegl, P.K. 1989. Influence of ATP-sensitive potassium channel modulators on ischemia-induced fibrillation in isolated rat hearts. *J Mol.Cell Cardiol.*, 21, (8) 783-788.

Yan, G.X. & Antzelevitch, C. 1998. Cellular basis for the normal T wave and the electrocardiographic manifestations of the long-QT syndrome. *Circulation*, 98, (18) 1928-1936.

Yan, G.X., Joshi, A., Guo, D., Hlaing, T., Martin, J., Xu, X., & Kowey, P.R. 2004. Phase 2 reentry as a trigger to initiate ventricular fibrillation during early acute myocardial ischemia. *Circulation*, 110, (9) 1036-1041.

Zipes, D.P. & Rubart, M. 2006. Neural modulation of cardiac arrhythmias and sudden cardiac death. *Heart Rhythm.*, 3, (1) 108-113.